The Proton Translocation Mechanisms of the Cytochrome bo_3-type Ubiquinol Oxidase Complex and the Mitochondrial Cytochrome *c* Oxidase Complex

Thesis by

Siegfried M. Musser

In Partial Fulfillment of the Requirements

for the Degree of

Doctor of Philosophy

California Institute of Technology

Pasadena, California

1996

(submitted May 10, 1996)

Acknowledgements

Over the past six years, I have had the good fortune to interact with a number of intellectually and experimentally talented individuals. First and foremost has been my advisor, **Sunney Chan**, who has often revealed his brilliance in the shortest of verbal exchanges, in the classroom, and through lengthy discussions in his office or over lunch or dinner. The development of the thermodynamic model of redox linkage discussed in Chapter 2 was a fascinating intellectual and collaborative exercise that shall always remain a cherished memory. I am equally grateful for his patience, integrity, kind heart, and the respect with which he treats his students. I know that I have grown tremendously during my stay here at Caltech on a professional as well as a personal level and it is **Sunney** who has been the major driving force behind this development. He has been, and continues to be, my mentor in the truest sense of the word.

During my time here, the Chan group has always consisted of an interesting and diverse bunch of individuals. **Randy Larsen** introduced me to the complexities of the cytochrome *c* oxidase (CcO) complex and helped me begin work on this fascinating molecular machine. **Ted DiMagno** and **Brian Schultz** were great to have around to bounce ideas off of and to discuss the intricacies of CcO turnover. **John Evans** astounded me with his boundless energy and quick wit and exuberantly informed me of the value of molecular dynamics calculations. **Sean Elliot** kept me abreast of the progress in the particulate methane monooxygenase subgroup. **Reggie Waldeck** opened my eyes to the complicated nature of succinate dehydrogenase turnover. **Ron Rock** has been a wonderful friend both in and out of lab and helped me recognize the complexity of the protein folding problem. It is difficult to say enough about **Michael Stowell**. To be concise, though, I shall just say that it has been fascinating to observe a brilliant mind at work. I could not have carried out the work on the cytochrome bo_3 complex were it not for his synthesis and purification of ubiquinone-1 and ubiquinone-2, his synthetic expertise for UHDBT synthesis, and his help with enzyme isolation. There have been

many other Chan group members over the past six years: **Scott**, **Pan**, **Qizhi**, **Jian**, **Silvia**, **Gary**, **Hoa**, **Hung Kay**, **Dorothy**, **Ruth Ann**, **Dennis**, **Shuguang**, and **Zhuyin**. I have learned from all of you.

There are a number of collaborators without whom this work could not have been completed. **Brian Hoffman**, **Richard Gurbriel**, and **Yang Fann** from Northwestern University obtained the ENDOR data and taught me the power, as well as the limitations, of this technique. The work on the cytochrome bo_3 complex required enzyme and cells from and constant communication with **Robert Gennis**, **John Rumbley** and **Jeff Osborne** at the University of Illinois (Urbana). **Bernard Trumpower** from Dartmouth Medical School kindly provided me with the inhibitor 2-*n*-nonyl-4-hydroxyquinoline-N-oxide (NQNO) for binding studies on the cytochrome bo_3 complex. Special thanks to **Mårten Wikström** from the University of Helsinki for sharing manuscripts before publication and for a number of interesting discussions.

And then there were the breaks from science: the games of Risk with **Randy**; Tetris, Movod, and Falcon with **Ron**; chess with **Brian**, **Mike**, and **Ron**; fly-fishing and backpacking with **Ron**; flying with **Kevin**; beer-drinking with **Mike**; and, of course, poker with the "core", **Dan**, **Bruce**, **Kevin**, and **Ron**. You guys helped me keep my sanity.

A special thanks to my family for their support since Day 1, especially to **Mom** who has demonstrated time and time again that love knows no bounds.

This work was supported by funding from the NIH.

Thanks guys!

Abstract

Every organism contains a respiratory chain that enables it to convert the energy obtained from food molecules into adenosine triphosphate (ATP), the universal energy currency which drives a multitude of life-giving biochemical reactions. A typical respiratory chain contains a series of integral membrane protein complexes that produce a transmembrane proton gradient as a result of sequential electron transfers through these complexes. The energy stored in this proton gradient, a biological battery, is utilized to synthesize ATP. In the oxygenic respiratory process functioning in mitochondria, dioxygen is fully reduced to water by the cytochrome *c* oxidase (CcO) complex. This molecular machine couples the highly exergonic reduction of dioxygen to the pumping of protons against a transmembrane electrochemical gradient. Another structurally similar enzyme, the cytochrome bo_3 complex from *Escherichia coli*, catalyzes the reduction of dioxygen to water using the same heme-copper dioxygen activating site and also catalyzes the translocation of protons. However, whereas the electron donor for the CcO complex is the water-soluble one-electron carrier cytochrome *c*, two-electron-donating ubiquinol molecules within the lipid bilayer input electrons into the cytochrome bo_3 complex. The dramatically different electron input mechanisms dictated by these electron-donating substrates led to the hypothesis that the proton translocation machineries for these two terminal oxidases are completely disparate. Based on the available data, it is concluded that the cytochrome bo_3 complex translocates protons via a quinone(quinol)-loop ($Q(H_2)$-loop) mechanism. In a $Q(H_2)$-loop proton translocation mechanism, proton uptake/release follows electron input to/output from two $Q(H_2)$ binding sites and protein conformational cycling is not required. On the other hand, the more complicated redox-linked proton pump of the CcO complex functions by forcing protons through the protein matrix as a result of a series of conformational rearrangements and is successful only through careful control of both electron and proton transfer reactions. This thesis focuses on deciphering the proton translocation capabilities

of these two enzymes and contrasts the simplicity of a Q(H_2)-loop mechanism with the more evolutionarily advanced CcO proton pump.

Contents

Abbreviations and Nomenclature

A_N	hyperfine coupling constant
ATP	adenosine triphosphate
ADP	adenosine diphosphate
B	magnetic field strength
Brij-35	polyoxyethylene 23 lauryl ether
CCCP	carbonyl cyanide, *m*-chlorophenyl hydrozone
CcO	cytochrome *c* oxidase, specifically the mitochondrial aa_3-type enzyme
CL	cardiolipin
COVs	CcO vesicles
CW	continuous-wave
DCCD	dicyclohexylcarbodiimide
DDM	*n*-dodecyl-β-D-maltoside
DMF	dimethylformamide
DOXYL-	4,4-dimethyl-3-oxazolinyloxy-
DTT	dithiothreitol
EDTA	ethylenediaminetetraacetate
ENDOR	electron nuclear double resonance
EPR	electron paramagnetic resonance
ET	electron transfer
EXAFS	extended X-ray absorption fine structure
FR	fully-reduced
g_N	nuclear *g*-value
HQNO	2-*n*-heptyl-4-hydroxyquinoline-N-oxide
h	Planck's constant
I	nuclear spin
K-phos	K_2HPO_4/KH_2PO_4 buffer

MCD	magnetic circular dichroism
Me-UHDBT	5-*n*-undecyl-6-methoxy-4,7-dioxobenzothiazole
MV_2	two-electron reduced mixed-valence
MW	molecular weight
NAD^+	nicotinamide adenine dinucleotide (oxidized)
NADH	nicotinamide adenine dinucleotide (reduced)
$NADP^+$	nicotinamide adenine dinucleotide phosphate (oxidized)
NADPH	nicotinamide adenine dinucleotide phosphate (reduced)
Na-phos	Na_2HPO_4/NaH_2PO_4 buffer
NCCD	N-(2,2,6,6-tetramethylpiperidyl-1-oxyl)-N'-cyclohexylcarbodiimide
NCD-4	N-cyclohexyl-N'-(4-dimethylamino-α-napthyl)carbodiimide
NCD-4-CcO	NCD-4 labeled CcO
NCD-4-COVs	NCD-4-CcO vesicles
NCET	nuclear coordinate associated with electron transfer
NCPP	nuclear coordinate associated with the proton pump
NMR	nuclear magnetic resonance
NOR	nitric oxide reductase
N_2OR	nitrous oxide reductase
NQNO	2-*n*-nonyl-4-hydroxyquinoline-N-oxide
PC	L-α-phosphatidylcholine
PE	L-α-phosphatidylethanolamine
P_i	inorganic phosphate
P_N	quadrupole coupling constant
PP_i	inorganic pyrophosphate
p-HMB	*p*-(hydroxymercuri)benzoate
pmf	proton motive force
RCR	respiratory control ratio

RR	resonance Raman
TEMPO	2,2,6,6-tetramethyl-1-piperidine-N-oxyl
TR3	time-resolved resonance Raman
SB-12	sulfobetaine 12
SDS	sodium dodecyl sulfate
SDS-PAGE	sodium dodecyl sulfate-polyacrylamide gel electrophoresis
Tris	tris(hydroxymethyl)aminomethane
Tris-HCl	tris(hydroxymethyl)aminomethane hydrochloride
UHDBT	5-*n*-undecyl-6-hydroxy-4,7-dioxobenzothiazole
$UQ_n(H_2)$	ubiquinone(ol)-n
UQ_n	ubiquinone-n
UQ_nH_2	ubiquinol-n
UQO	ubiquinol oxidase, specifically the cytochrome *bo*$_3$ complex from *Escherichia coli*
β_N	nuclear magneton
$\Delta\psi$	transmembrane electric potential
ν_N	nuclear Larmor frequency

Chapter 1

The Superfamily of Ubiquinol and Cytochrome *c* Terminal Oxidase Complexes

Every organism requires energy to drive its life-giving processes. The controlled breakdown of food molecules through multiple biochemical pathways into simpler, less energy-rich molecules is thus common to the simplest bacterium as well as to the multitude of evolutionarily advanced eukaryotes that inhabit our planet. In some situations, adenosine triphosphate (ATP), the most prevalent ubiquitous cellular energy currency, is directly produced from biochemical degradation reactions. In other cases, energy is stored in the strong reducing agents nicotinamide adenine dinucleotide (NADH) or nicotinamide adenine dinucleotide phosphate (NADPH). A currency exchange mechanism converts most of the NADH molecules produced into ATP for use in the cell's many energy-requiring reactions. On the other hand, NADPH serves almost exclusively as an electron donor (hydride ion donor) in reductive biosyntheses. Interestingly, the exchange-rate of the NADH currency exchange is not the same in all organisms. In fact, in some bacteria, the exchange-rate can vary during the organism's life-time depending on a number of environmental factors. However, the currency exchange process is basically identical throughout the living world: a series of integral membrane protein complexes convert energy stored in NADH molecules into a transmembrane proton gradient. Another protein complex in the same membrane couples the collapse of this proton gradient to the synthesis of ATP.[1,2] This thesis focuses on a few of the enzyme complexes which generate this proton gradient.

The mitochondria of eukaryotic cells are ATP-generating factories. The outer membrane of mitochondria is quite permeable to small molecules due to the presence of porin, a transmembrane protein with a large pore that allows passage of solute molecules up to about 10 kDa. The inner membrane, however, is quite impermeable and is able to support a proton gradient in which the interior of the mitochondrium (matrix) is about one pH unit higher than the outside cytosolic medium. This proton gradient results from the turnover chemistry of three integral membrane protein complexes: the NADH dehydrogenase complex, the cytochrome bc_1 (ubiquinol:cytochrome c oxidoreductase)

complex and the cytochrome *c* oxidase (cytochrome aa_3) complex. The F_0F_1-ATPase complex controls the collapse of this proton gradient and uses the free energy released by this process to synthesize ATP from adenosine diphosphate (ADP) and inorganic phosphate (P_i). Electrons from the succinate → fumarate step of the citric acid cycle enter the respiratory chain through the succinate:ubiquinone oxidoreductase complex and therefore also contribute to proton gradient formation. This series of enzyme complexes is termed the respiratory chain and the process of energy conversion is termed oxidative phosphorylation (Figure 1.1). In general, bacteria contain simpler versions of these enzyme complexes. However, bacteria do not have mitochondria. Instead, the respiratory protein complexes are found in the plasma (inner) membrane and protons are pumped out of the bacterial cytoplasm. In fact, the first mitochondrium is thought to have arisen when one bacterium enveloped another and a symbiotic relationship

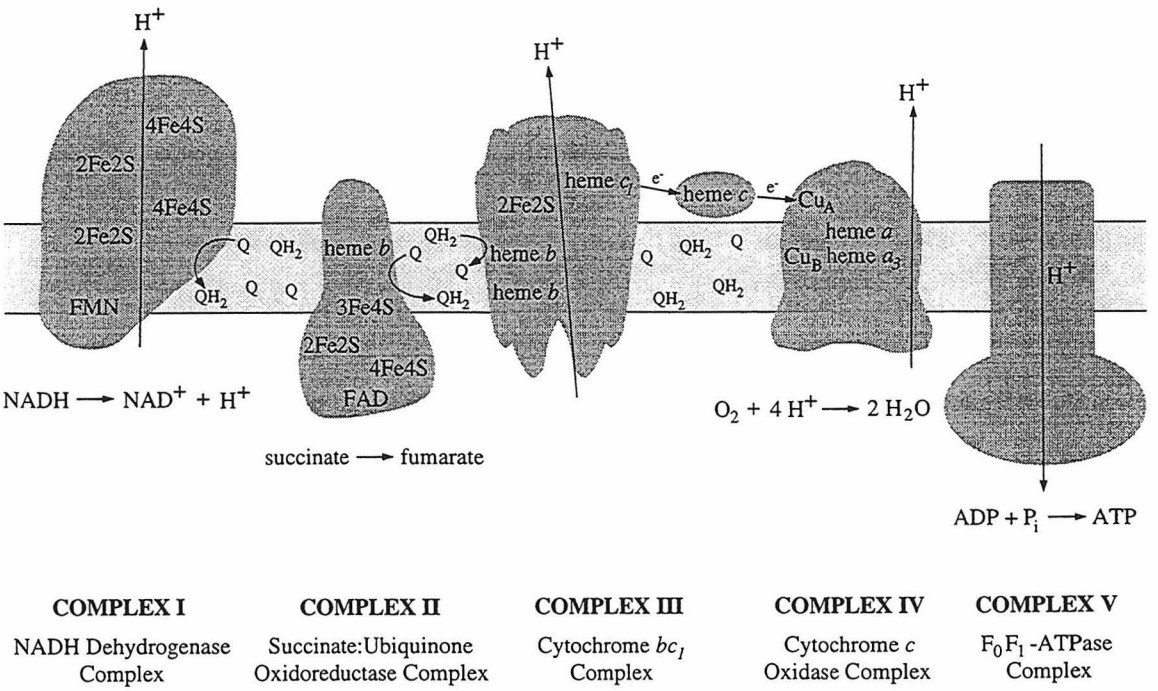

Figure 1.1 Schematic of the electron transport chain of oxidative phosphorylation located in the inner membrane of mitochondria. Electrons enter (from NADH and succinate) and exit (donated to dioxygen) the chain on the matrix side of the membrane. Complexes I, III, and IV produce the proton gradient used by complex V to synthesize ATP.

developed. Bacteria have a dizzying number of variations on the respiratory chain theme. Some variations are minor, e.g. a slightly different prosthetic group in one of the protein complexes. Other differences are major, e.g. the oxidation-reduction chemistry carried out by two eukaryotic protein complexes may be accomplished by a single bacterial enzyme. In fact, the overall chemistry itself may be different. Typically, the high-energy electrons found on NADH are transported through the respiratory chain and ultimately end up reducing dioxygen to water. But a number of bacteria have modified respiratory chains and can grow anaerobically using nitrate or elemental sulfur as the terminal electron acceptor.[3,4] There is usually a clear structural relatedness amongst the proteins of the many different bacterial respiratory chains investigated thus far. Yet the details of enzyme function are not so easily compared since deciphering the complicated turnover mechanisms of these enzymes has proved to be quite a challenging endeavor. The work described here investigates the details of the proton translocation mechanisms of two structurally related families of terminal oxidase complexes.

The Cytochrome c *Oxidase Complex*

The aa_3-type cytochrome *c* oxidase (CcO) complex, the terminal electron transport protein complex of the respiratory chain in eukaryotes and some prokaryotes, catalyzes the reduction of dioxygen to water using electrons input from ferrocytochrome *c*. This enzyme is a complicated integral membrane protein, both structurally and functionally. Its subunit composition has been found to vary from only two or three subunits in bacteria to as many as 13 different subunits in mammals. Three redox active metal centers are found in this metalloprotein: cytochrome *a* and the binuclear Cu_A center (both one-electron acceptors) mediate electron transfer (ET) to the heme a_3-Cu_B binuclear site (a two-electron acceptor) where dioxygen is activated and reduced. The heme A chromophore (Figure 1.2) of cytochromes *a* and a_3 are unusual in biological systems as it is only found in terminal oxidase complexes. It is not understood why

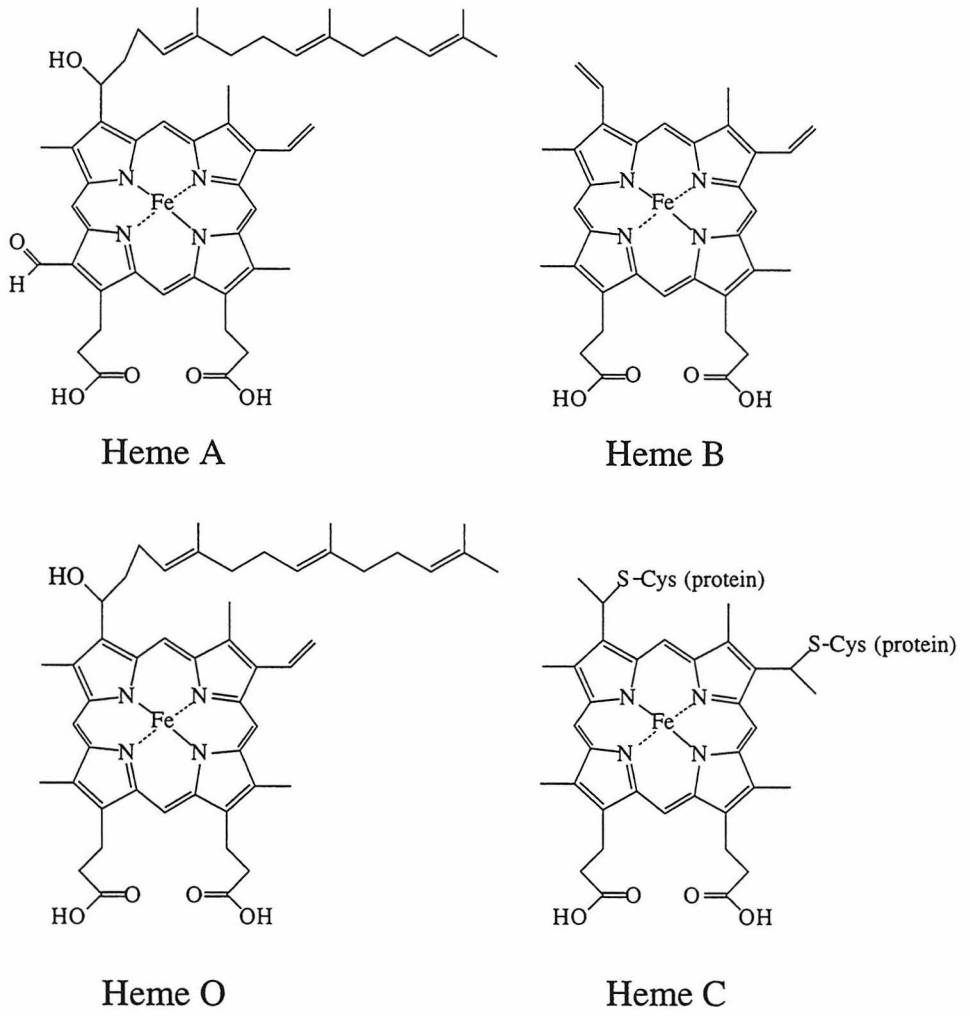

Figure 1.2 A comparison of the four hemes discussed in this thesis. Note that variations in the heme A and heme O hydroxyethylfarnesyl substituent have been found in various bacterial species.[5] Isolated heme structures are indicated by upper-case letters (hemes A, B, C, O), whereas when the corresponding hemes are within their natural proteinaceous surroundings, the term cytochrome is applied and italic lower-case letters are used (cytochromes *a*, *b*, *c*, *o*). A further distinction is sometimes necessary when only the heme macrocycle of a particular cytochrome is under discussion. Hence, whereas the term cytochrome encompasses the heme and immediate surrounding protein matrix thus identifying a general region of the protein (e.g., reduction potential of cytochrome *a*), the term heme and italic lower-case letters (hemes *a*, *b*, *c*, *o*) are used when the heme macrocycle is being referred to (e.g., the ligation of heme *a*). In addition, the low-spin heme, which is unreactive towards extraneous ligands, is denoted without subscript, yet following the classical terminology of the mitochondrial CcO complex, the dioxygen-binding heme is denoted with the subscript 3 (hemes a_3 and o_3).[6]

nature uses this heme moiety.[7] Non-redox active metal ions have also been found (e.g. Mg and Zn) but their role is largely uncertain. Under physiological conditions, the mammalian enzyme is thought to be a dimer and has a maximum molecular weight of

approximately 400 kDa, although *in vitro* both the dimer and the monomer are competent in mediating ET and O_2 reduction. The many additional subunits of the mammalian enzyme do not serve any obvious purpose and are usually assigned a regulatory and/or assembly role. While these additional subunits may also contribute to the structural integrity of the enzyme, there is no evidence that the bacterial enzymes are any less stable than their mammalian counterparts.[6,8-12]

Two crystal structures of the CcO complex were recently reported simultaneously in *Nature* and *Science*. In one case, the four-subunit *Paracoccus denitrificans* enzyme was cocrystallized with an antibody F_v fragment.[13] Astonishingly, Yoshikawa and coworkers were able obtain well-diffracting crystals of the entire 13-subunit bovine enzyme.[14] Both structures are reported to a resolution of 2.8 Å. A low resolution map of the bovine enzyme showing the approximate location of the lipid bilayer is shown in Figure 1.3. A close-up view showing the orientation of the redox centers without interference from the polypeptide matrix is shown in Figure 1.4. While the structures in and of themselves are major accomplishments due to the

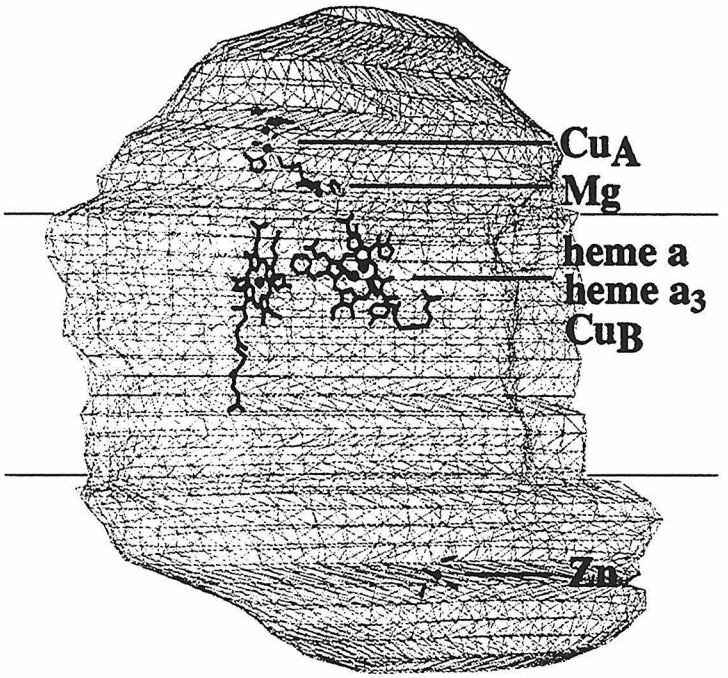

Figure 1.3 A schematic representation of metal site location in the beef heart cytochrome *c* oxidase complex. The molecular surface is defined with the electron density map at 5 Å resolution. The transmembrane portion has an approximate thickness of 48 Å whereas the protrusions into the cytosolic (top) and matrix (bottom) side hydrophilic phases are 32 and 37 Å, respectively. The three metals, Fe_a, Fe_{a3} and Cu_B, are located at the same level, 13 Å below the cytosolic membrane surface. The Cu_A center is 8 Å above this membrane surface level, whereas the Mg ion is approximately at this membrane surface level. The distances of Cu_A-Fe_a, Cu_A-Fe_{a3}, Cu_A-Mg, Fe_{a3}-Fe_a, and Fe_{a3}-Mg are 19, 22, 9, 14 and 15 Å respectively. Reproduced from Tsukihara and coworkers[14] with minor modifications.

fact that the structure of very few membrane proteins have been determined and since, especially in the case of the bovine enzyme, the structures are quite complex, the predictions from biophysical studies have been surprisingly accurate.

Subunit I, the largest subunit of the CcO complex, contains two of the three redox active metal centers, namely, cytochrome *a* and the heme a_3-Cu_B binuclear site. By assuming a purely dipolar interaction between nitrosylferrocytochrome a_3 and Cu_B^{2+} spin centers, the distance between the two metallic centers of the binuclear site was estimated as 3-5 Å from electron paramagnetic resonance (EPR) studies.[15,16] This distance was determined to be 3-4 Å by extended X-ray absorption fine structure (EXAFS) spectroscopy.[17-20] For comparison, the X-ray diffraction determined distance is 4.5-5.2 Å. The close physical relationship between the two metal ions of the heme a_3-Cu_B binuclear site results in strong exchange and dipolar interactions as well as modulation of the axial and rhombic zero-field splittings of the heme in the oxidized enzyme.[21] As the reduction of dioxygen occurs at this binuclear site, it is thought that the proximity of the two metallic centers is important for the productive activation of dioxygen and the subsequent catalyzed reduction. In other EPR studies, the distance between heme *a* and the heme a_3-Cu_B binuclear center was estimated to be about 14 Å,[22-26] whereas the heme *a* – Cu_A distance was found to be about 10 Å.[15,27,28] The heme *a* – binuclear center distance prediction was very accurate,

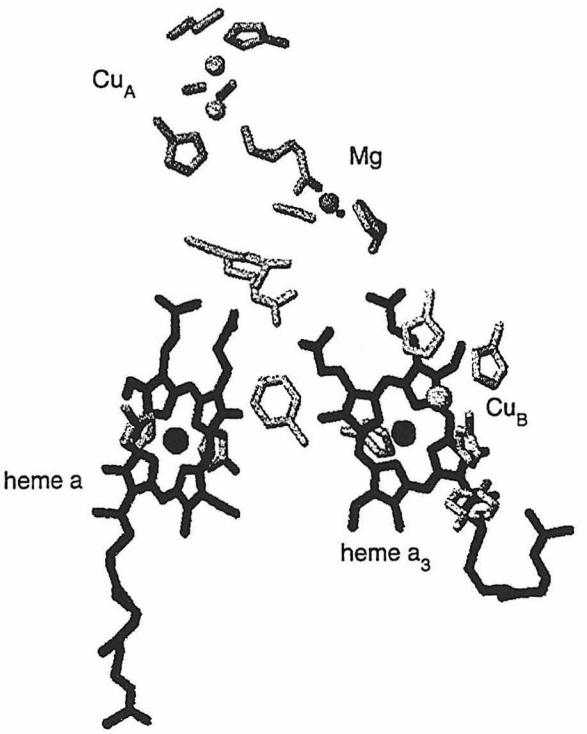

Figure 1.4 Redox centers and the magnesium ion in the cytochrome *c* oxidase complex. Reproduced from Tsukihara and coworkers.[14]

yet the EPR determined heme *a* – Cu_A distance is inaccurate (19 Å in the crystal structures). The discrepancy arises from the mononuclear Cu_A structure assumed, and hence, the neglect of electron exchange in the mixed-valence binuclear Cu_A center when interpreting the EPR data. It was not known at the time of the EPR experiments that the Cu_A center was actually a binuclear copper center.

Resonance Raman (RR), EPR, electron nuclear double resonance (ENDOR), magnetic circular dichroism (MCD), Mössbauer and EXAFS spectroscopies have all been applied to the study of the redox centers in the CcO complex. The data revealed that heme *a* is six-coordinate, low-spin and heme a_3 is predominently five-coordinate, high-spin in the oxidized enzyme. However, there is at least some heterogeneity in coordination number and spin state assignment in the case of heme a_3.[29,30] Two histidines were assigned as the fifth and sixth ligands of heme *a* and another histidine as the fifth ligand of heme a_3.[31-35] The Cu_B ion was predicted to be coordinated by at least three histidine ligands.[17,19,20,36,37] A comparison of cytochrome aa_3-type subunit I sequences from over 30 species reveals that there are seven strictly conserved histidine residues. Hydrophobicity calculations placed six of these histidines in transmembrane helices yet located in the outer leaflet of the membrane bilayer. This location of these histidines was somewhat surprising as, historically, the heme a_3-Cu_B binuclear center was assumed to be close to the interior side of the membrane since the protons involved in the dioxygen reduction process are derived from the inner aqueous phase. These hydrophobicity calculations and sequence comparisons lead investigators to isolate histidine mutants of the *Rhodobacter sphaeroides* cytochrome *c* oxidase complex. Fourier-transform infra-red (FTIR), RR and optical absorption spectroscopy indicated that His^{61} and His^{378} (bovine numbering) ligate to the low-spin heme, His^{376} ligates to the high-spin heme, and His^{240}, His^{290}, and His^{291} coordinate to Cu_B.[38,39] All of these ligand assignments were confirmed as accurate by the recent crystal structures. The use of a consensus sequence from the many sequences known for subunits I, II and III for

transmembrane helix prediction proved to be highly accurate in positioning the helices.[6,13]

Subunit II contains the third redox active metal center, the Cu_A site, which, like cytochrome *a*, mediates electron flow from ferrocytochrome *c* to the heme a_3-Cu_B binuclear center. This copper center gives rise to an unusual EPR signal in that both the copper hyperfine splittings and the *g*-values are quite small; thus, its ligand structure has been the subject of intense study and speculation for a number of years. MCD experiments revealed a metal-ligand charge transfer transition that can only arise from a coordinated cysteine thiol[40] and ENDOR experiments indicated that at least two histidines and one cysteine are ligands to Cu_A.[41,42] In fact, ENDOR spectroscopy suggested that two cysteines are involved in copper coordination in a highly symmetric ligation structure.[43] Experiments using EXAFS spectroscopy suggested two (N, O)-type ligands and two (S, Cl)-type ligands for the Cu_A site.[36] Of subunits I, II, and III, the core subunits, the only conserved cysteines are in subunit II. A comparison of cytochrome aa_3-type subunit II sequences from over 50 species reveals that there are only two strictly conserved cysteines (Cys^{196} and Cys^{200}). In addition, His^{161} and His^{204} are the only two strictly conserved histidines.[6] Thus, for a long time, the Cu_A center was modeled as a single copper ion coordinated by two histidines and two cysteines.[44] The "extra" copper typically found in CcO preparations had bothered investigators for a long time, however. Kroneck and coworkers' hypothesis that the Cu_A site actually is a mixed-valence, binuclear copper center[45] provided a solution to this problem. This hypothesis therefore quickly lead to a number of experiments designed to distinguish between a mononuclear or binuclear structure. It turned out that a binuclear structure is more consistent with the data.[45-54] Almost identical Cu-(N, O) and Cu-(S, Cl) bond distances for both the CcO and *Pseudomonas stutzeri* nitrous oxide reductase (N_2OR) complexes are obtained from EXAFS spectroscopy.[46] In addition, the Cu_A binding region of CcO subunit II is similar to a stretch of sequence in the N_2OR complex (CXXXCXXXHXXM).[52] The two

enzymes have absorption peaks in the near IR: the N_2OR complex at about 800 nm[46] and the CcO complex at about 830 nm (attributed to the Cu_A site).[55] Finally, the MCD[46,53] and EPR[47,54] spectra for the two enzymes are surprisingly similar. Since four ligands (the two Cys and two His residues discussed above) are insufficient to stably ligate two copper ions, investigators postulated that the highly conserved Met^{207} of subunit II is a copper ligand in a number of proposed structures for the Cu_A site.[56-58] The actual X-ray determined structure of the Cu_A center (Figure 1.5) turned out to be a combination of these proposed models and the five ligand predictions (two Cys, two His, and Met) all were accurate (there is an additional ligand in the crystal structure - a backbone carbonyl). Electron spin echo envelope modulation (ESEEM) studies[59] indicated that the minimum distance between the Cu_A center and the protein-aqueous interface is about 5 Å also in agreement with the crystal structure.

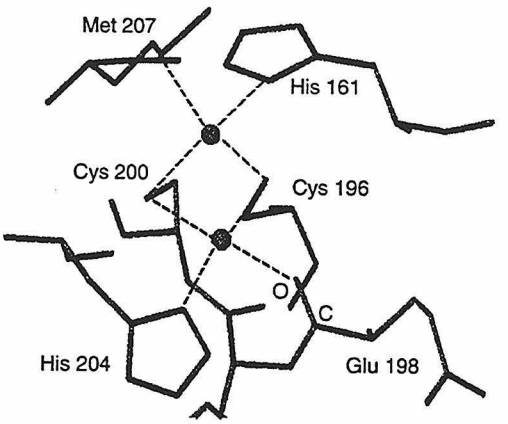

Figure 1.5 Crystal structure of the Cu_A site. Reproduced from Tsukihara and coworkers.[14]

Studies with monoclonal antibodies have indicated that subunit II provides a major contribution to the cytochrome *c* binding site.[60] Cytochrome *c* crosslinking experiments have demonstrated that carboxylic acid residues on the CcO complex mediate the cytochrome *c*-CcO transient complex formation through electrostatic attraction to lysines on the surface of cytochrome *c*.[61-64] These data suggested that the Cu_A center is the initial acceptor of electrons from ferrocytochrome *c*, a conclusion that has been confirmed by transient ET studies (see below).

A big surprise of the bovine crystal structure is the presence of the Mg binding site in the middle of all the action, i.e. very near the redox centers. The prevailing view had been that the Mg was bound to subunit IV and was required for regulatory binding of

ATP.[65-67] Instead, the Mg is bound at the interface of subunits I and II. Its purpose is still a mystery, but it may play an important role in conformational communication.

Dioxygen Chemistry

Details of the four-electron reduction of dioxygen catalyzed by the CcO complex are of particular interest because the electrons involved in the reduction process are donated individually to the enzyme and are transferred in a precisely controlled manner to the dioxygen molecule without the release of highly reactive and toxic intermediates. The electronic structure of the various intermediates formed during the catalytic cycle have been characterized by a wide variety of spectroscopic techniques including RR, EPR, EXAFS, Mössbauer, and optical absorption spectroscopy.[68-71]

The current consensus on the dioxygen reduction mechanism is shown in Figure 1.6. Electrons from two molecules of ferrocytochrome *c* fully reduce the heme a_3-Cu_B binuclear center before dioxygen binds to the protein to form compound A. Redistribution of the electron density in this hemoglobin-like dioxygen adduct results in formation of a peroxidic adduct, compound C. In the hands of some investigators, compound C is stable for over an hour at pH 8.8-9.0 in the absence of additional reducing equivalents.[72] Under physiological conditions, however, a third electron results in formation of a cupric hydroperoxide species.[73] Immediate cleavage of the O-O bond follows and electron redistribution occurs yielding a fairly stable species that has been assigned an oxyferryl heme a_3/cupric Cu_B structure on the basis of a wealth of spectroscopic data (EPR,[74,75] RR,[76-79] Mössbauer,[80] and EXAFS[20,81]). Further reduction by the fourth electron results in the "pulsed" enzyme and the complete reduction of molecular oxygen to water. All of the protons necessary for this dioxygen reduction process originate on the matrix side of the membrane.[82] The role of Cu_B in the dioxygen chemistry is still not completely clear. Although one of the oxygen atoms must become a ligand to Cu_B upon formation of the cupric hydroperoxide intermediate, it is likely that

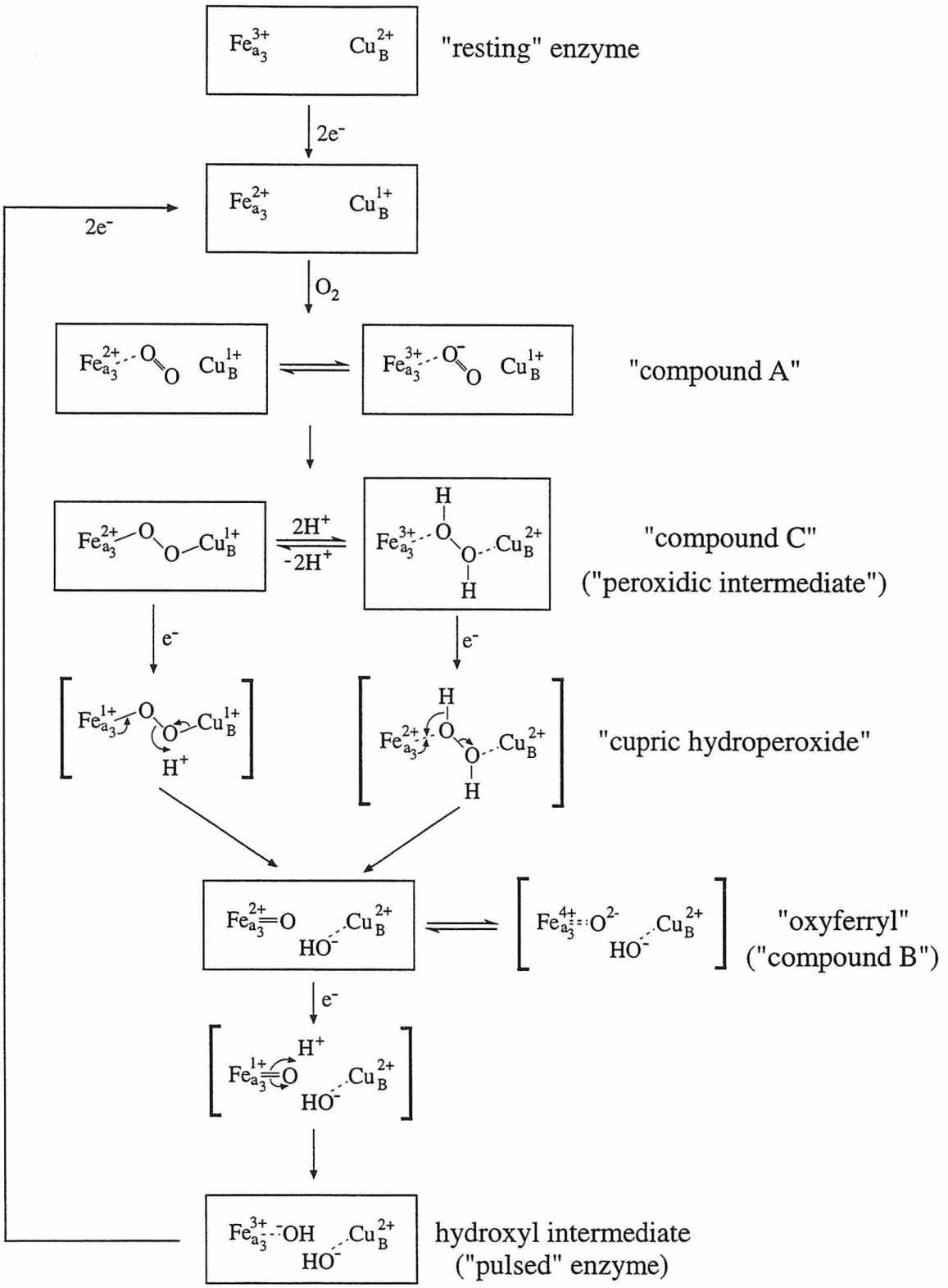

Figure 1.6 Current view of the dioxygen chemistry catalyzed by the CcO complex.

Cu_B interacts with other intermediates (e.g. the peroxidic intermediate) in some fashion due to its proximity to the dioxygen binding heme; however, the extent of such interactions is still unresolved.

A few of these intermediates can also be formed by the reaction of the enzyme with H_2O_2. Incubation of the enzyme with stoichiometric amounts (or a slight excess) of H_2O_2 yields compound C. Under conditions of excess peroxide, compound C is reduced by H_2O_2 resulting in the formation of the superoxide radical anion ($O_2^{\bullet -}$) and the oxyferryl adduct.[83] Both of these intermediates are easily characterized by optical difference spectroscopy.[72,84] In addition, it has been shown that the catalytic cycle of the CcO complex can be partially reversed by poising mitochondria in a highly oxidizing environment and adding high concentrations of ATP. Two species are formed, dubbed P and F, which are spectroscopically indistinguishable from the compound C and oxyferryl intermediates, respectively, resulting from reaction of the enzyme with H_2O_2. These data provide strong confirming evidence for the intermediates involved in the dioxygen reduction cycle.[85-88]

Although much of the dioxygen chemistry has been worked out by low temperature trapping of the intermediates and through study of fairly homogeneous populations of the various intermediates, many of these intermediates have also been observed transiently under physiological conditions. By utilizing flow-flash technology in combination with RR or optical absorption instrumentation, various groups have recently been able to monitor the partial or full turnover cycle of the enzyme as well as specifically observing how one intermediate evolves into the next under ambient conditions (see next section). In general, in these experiments, the enzyme is initially partially- or fully-reduced and carbon monoxide is bound to heme a_3 to inhibit turnover in the presence of molecular oxygen. The reaction is then initiated by photolysis of the CO ligand from the enzyme and the reaction of dioxygen with the enzyme is monitored spectroscopically. In this manner, optical absorption and RR spectroscopies have been used to confirm the

presence of the compound A,[76,89-98] compound C,[78,97] oxyferryl,[76-79] and hydroxyl[79] intermediates during the reduction of dioxygen.

Transient RR experiments indicate that compound A has characteristic Fe-O_2 stretching modes similar to oxyhemoglobin and oxymyoglobin indicating, in fact, that there is little interaction with Cu_B.[90] Furthermore, there is little change in the RR spectrum upon conversion from compound A to compound C suggesting that compound A is best described as a ferric-superoxide complex rather than as a ferrous-dioxygen complex.[97] In this scenario, then, compound C is *not* formed via a concerted two-electron reduction of dioxygen; rather, compound A evolves into compound C upon transfer of one electron to the ferric heme a_3-superoxide adduct. Little is known about the stability of compound A in the absence of additional reducing equivalents. However, continuing the analogy with oxyhemoglobin and oxymyoglobin, which are necessarily stable due to their dioxygen transport function, it is not expected that significant release of the toxic superoxide anion occurs from compound A. On the other hand, since the CcO complex catalyzes the reduction of dioxgen to water, a decidedly different function from that of the dioxygen transport proteins, alternative chemistry may be utilized to prevent release of superoxide anion from compound A.[6]

Electron Transfer Kinetics

The dioxygen reduction chemistry of the CcO complex is only one aspect of the enzyme's complexity. The highly exergonic dioxygen reduction reactions are coupled to the translocation of protons against both a transmembrane electrical and pH gradient. To understand the manner in which the dioxygen chemistry is linked to the proton pumping function of the enzyme, it is essential to know the details of both the intermolecular ET from cytochrome *c* to the enzyme as well as the intramolecular ET from the various redox centers of the protein to dioxygen. It has been known for a long time that electrons from ferrocytochrome *c* enter the CcO complex at cytochrome *a* and

Cu_A and are subsequently transferred to the heme a_3-Cu_B binuclear site where the dioxygen chemistry takes place. Recent extensive effort has been put forward by a number of groups to understand the details of these electron transfers.

The first step in enzyme turnover has been studied using several types of photo-initiated reduction systems and it has been found that the initial ET from ferrocytochrome *c* to cytochrome *a* in the fully-oxidized CcO complex obeys Michaelis-Menten kinetics:[99-101]

$$\text{Cyt } c^{2+} + (\text{CcO})_{ox} \underset{k_{-1}}{\overset{k_1}{\rightleftharpoons}} \text{Cyt } c^{2+}{:}(\text{CcO})_{ox} \qquad (1.1)$$

$$\text{Cyt } c^{2+}{:}(\text{CcO})_{ox} \xrightarrow{k_{cat}} \text{Cyt } c^{3+} + (\text{CcO})_{red} \qquad (1.2)$$

By the nature of these transient experiments (~ 2-3% of ferrocytochrome *c* is transiently reduced), the second reaction becomes rate-limiting as $[CcO]_{ox}$ is increased. Thus, the kinetics are adequately described by:

$$k_{obs} = \frac{k_{cat}[CcO]_{ox}}{K_m + [CcO]_{ox}} \qquad (1.3)$$

where K_m is the Michaelis constant, $\frac{k_{-1} + k_{cat}}{k_1}$. In these experiments, K_m is found to be 9-19 μM,[99-101] in reasonable agreement with values determined from steady-state experiments.[102,103] In addition, k_{cat} is reported as 1500-2600 s^{-1}; that is, inter-protein ET within the ferrocytochrome *c*-CcO complex occurs in 380-670 μs.[99-101] These values of k_{cat} and K_m indicate that k_1 is at least 1×10^8 M^{-1} s^{-1}. The majority of transient experiments have emphasized electron input to the fully-oxidized enzyme.

It was initially thought that the immediate electron acceptor from ferrocytochrome *c* was cytochrome *a*.[70,99,104-107] Studies performed on the Cu_A-depleted enzyme show a significantly decreased electron input rate (k_{cat} = 740 s^{-1}) but similar K_m (20 μM),

however, and implicate Cu_A as the immediate electron acceptor from cytochrome *c*.[101] Studies on the CO-photolyzed fully-reduced mammalian enzyme[108-111] and on the *P. denitrificans* resting enzyme[112] also favor Cu_A as the initial electron acceptor from cytochrome *c*. These results make sense in light of the recently determined crystal structures. The Cu_A center is located within about 10 Å of the protein-aqueous interface in an extramembranous domain, whereas the other redox centers are more deeply buried within the protein's interior. Thus, the Cu_A center serves as a rapid ET conduit to the hydrophobic recesses of the protein.

After input of the first electron from cytochrome *c* to Cu_A, there is a rapid electron equilibration between cytochrome *a* and Cu_A. This equilibration has been reported to occur within 50-170 μs.[109,113-116] At the one-electron reduced state of the enzyme, further ET from cytochrome *a* to the heme a_3-Cu_B binuclear center does not occur or occurs at a very slow rate (~ 1 s), as demonstrated by transient kinetic studies.[117,118]

Stopped-flow and steady-state experiments provide evidence that the input of a second electron into the CcO complex triggers a conformational transition, which allows rapid two-electron reduction of the heme a_3-Cu_B binuclear center. While little is known about the two-electron transfer from cytochrome *a* and Cu_A to the dioxygen binding site upon input of a second electron to the enzyme, there is some evidence that although the ET is not concerted, both ETs occur in rapid succession.[119] Upon reduction of both cytochrome *a* and Cu_A, the enzyme converts from the "closed" (slow cyanide binding form) to the "open" (rapid cyanide binding form) conformation;[120,121] this conformational transition is postulated to be mechanistically coupled to the proton pump function of the enzyme.[122] In addition, the argument has been made that reduction of both cytochrome *a* and Cu_A results in the removal (or reduction) of the reorganizational barrier to ET thus promoting fast ET to the heme a_3-Cu_B binuclear site.[123] This rapid internal ET to the dioxygen binding site triggered by a two-electron reduction of the CcO complex is thought to occur in both the "resting" and "pulsed" conformations[117] and may be

important physiologically. Since two electrons are simultaneously available for dioxygen reduction, the dioxygen molecule can be trapped as a peroxy adduct (compound C) thereby minimizing the release of the toxic superoxide anion from the compound A intermediate. Note, however, that the conclusion that the "closed" to "open" conversion occurs after two-electron reduction of the enzyme has recently been challenged; Wilson and coworkers[124] find that the "closed" to "open" conversion occurs after only a one-electron reduction of the enzyme.

Time-resolved resonance Raman (TR3) spectroscopy has been used to study the reaction of dioxygen with the heme a_3-Cu_B binuclear center in real time by observing the CO-photolyzed MV_2 (two-electron reduced mixed-valence) and FR (fully-reduced) enzyme in the presence of dioxygen. In both cases, there is clear evidence for the compound A intermediate about 10 μs after photolysis of CO.[95,98] These data agree with stopped-flow flash photolysis studies on the CO-photolyzed enzyme which found that the primary oxygen intermediate forms with a second order rate constant of about 1×10^8 $M^{-1}\,s^{-1}$.[91,96,125] Later oxygen intermediates have also been detected by TR3 studies of the reaction of CO-photolyzed MV_2 or FR enzyme with dioxygen. For the MV_2 enzyme, compound A disappears in about 220-290 μs[93,97,98] whereas for the FR enzyme, this decay occurs in about 30 μs.[95] When beginning with the MV_2 enzyme, compound C is as far as dioxygen reduction can proceed, and thus, this intermediate lives for a long time (~ 150 s).[97] For the CO-photolyzed FR enzyme, however, the oxyferryl intermediate appears in 500-800 μs (estimated)[77,79] and full oxidation occurs in 1-2 ms (estimated).[79]

In addition to the above Raman experiments, the outcome of photolysis of the CO-bound CcO complex has been studied by transient absorption spectroscopy. Whereas in Raman spectroscopy, the dioxygen intermediates are recognized by diagnostic resonance frequencies, interpreting optical data is more complex because the optical transitions are less defined and result in overlapping signals. On the other hand, one is able to monitor the oxidation state of three of the four redox centers (all but Cu_B),

therefore allowing more explicit interpretion of the ET reactions. The transient absorption studies on the CO-photolyzed enzyme indicate that compound A forms in about 10 μs, compound C in 30-50 μs (FR)/100-170 μs (MV_2), the oxyferryl in 100-170 μs, and full oxidation of the CcO complex occurs in 1-1.3 ms.[91,96,116,125-127] In general, these results agree with the Raman data with the exception of the decay of compound C (500-800 μs vs. 100-170 μs). One explanation is that the transient absorption measurements monitor the oxidation of heme *a* in the compound C intermediate (100-170 μs) whereas the electronic, structural and/or nuclear rearrangement of the reduced peroxy adduct to form the oxyferryl is observed in the TR3 experiments (500-800 μs).

There is some concern over the physiological relevance of the CO-photolyzed FR enzyme and the subsequent ET reactions. For example, the binding of CO to Cu_B^+ can potentially interfere with the binding of dioxygen to heme a_3^{2+}.[128-132] In addition, there is concern over the physiological relevance of the FR enzyme itself, i.e. it is *not* expected that the enzyme becomes fully-reduced before reaction with dioxygen to form compound A under physiological conditions. It has been found that reaction of the FR enzyme with dioxygen in a stopped-flow apparatus and reaction of the FR enzyme with dioxygen after CO photolysis do not yield identical conformers.[133-135] The difference in the two methods are not apparent in the first 120 μs after reaction initiation, however.[136] These issues are discussed more fully by Musser and coworkers.[6] It is clear, however, that there are problems with the CO-flash technique and the ET events observed have to be interpreted cautiously.

The Cytochrome bo_3 *Complex*

The cytochrome bo_3 (abbreviated "UQO" for "ubiquinol oxidase") complex, a terminal oxidase found in *Escherichia coli*, catalyzes the two-electron oxidation of ubiquinol-8 and the four-electron reduction of dioxygen to water.[137-139] In addition, it

has been shown that part of the free energy of dioxygen reduction is stored by UQO-mediated translocation of protons across the cytoplasmic membrane.[140,141] Functionally, the UQO complex combines the chemistry mediated by the cytochrome bc_1 and CcO complexes (Figure 1.7); structurally, however, this enzyme more closely resembles the CcO complex. To summarize, similarities between the UQO and CcO complexes include: (1) subunit sequence similarity;[139] (2) the presence of one low-spin (six-coordinate) and one high-spin (five-coordinate) heme;[142,143] (3) exchange coupling between the high-spin heme and a copper ion (heme-copper binuclear site) in the resting enzyme; (4) heme-heme interaction and alignment of these hemes with respect to the bilayer normal;[144-146] and (5) the capability to couple dioxygen reduction to the translocation of protons across a membrane.[140,141] The major differences include: (1) one heme B and one heme O (bo_3) versus two hemes A (aa_3) (note that it has been found that the low-spin heme B of the UQO complex can be replaced by a heme O with little effect on the activity of the enzyme);[147] (2) one copper site (bo_3) versus two copper sites (aa_3) (the UQO complex lacks the unusual $g = 2$ EPR signal arising from the Cu_A site of the CcO complexes); and (3) the different physiological substrates, ubiquinol-8 (bo_3)[138] versus ferrocytochrome c (aa_3).

The purified UQO complex contains stoichiometric amounts of four polypeptides which are encoded by the *cyoABCDE* operon.[148] The *cyoB* gene product is homologous to subunit I of the cytochrome *c* oxidase complexes; there exists 37% sequence identity between the subunits I of the cytochrome bo_3 and the *Paracoccus denitrificans* cytochrome aa_3 complexes.[139] The six histidines responsible for redox center ligation in the cytochrome *c* oxidase complexes are positionally conserved in the UQO complex. Site-directed mutagenesis has revealed that these histidines ligate the corresponding redox centers in the UQO complex.[39,149-151] In addition, the amino acid sequence around the ligands of the binuclear site is highly conserved.[152,153] In conjunction with the biophysical studies noted above, it appears that the three-dimensional structures of

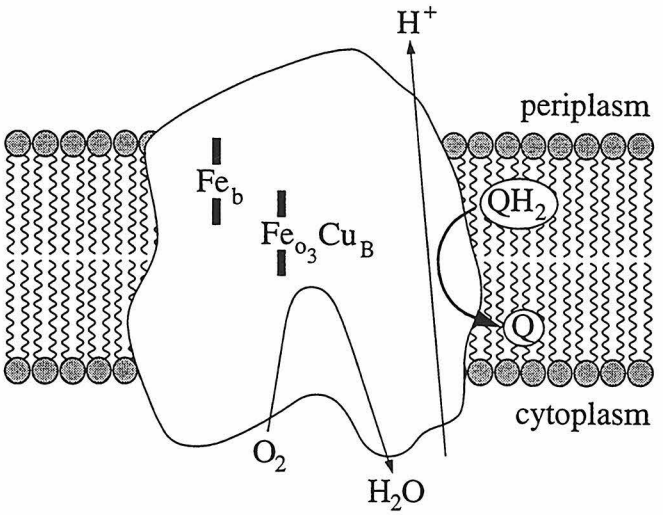

cytochrome bo_3 complex

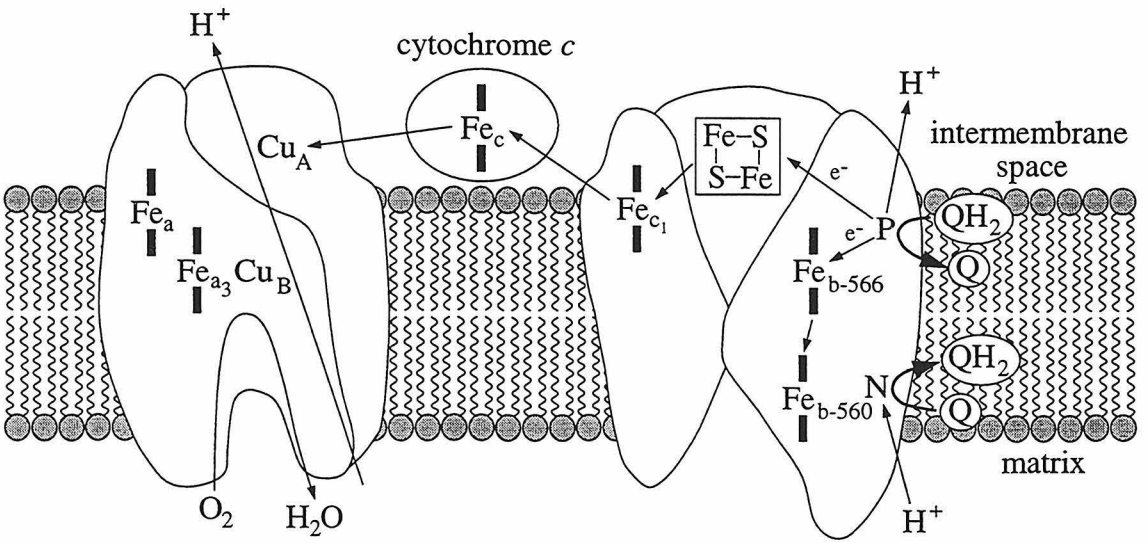

cytochrome aa_3 complex cytochrome bc_1 complex

Figure 1.7 Schematic of the chemistry catalyzed by the cytochrome bo_3, bc_1 and aa_3 complexes. Both ubiquinol-8 (QH_2) and ubiquinone-8 (Q) are extremely hydrophobic and therefore remain in the lipid bilayer.

subunit I of the two oxidases are quite similar. As a result, it is generally agreed that the dioxygen chemistry of the two enzymes is very similar if not identical (recent data reveal different proton transfer characteristics during dioxygen reduction for the two enzymes, however[154]). In essence, the "catalytic core" (i.e. subunit I and its associated redox centers) is a highly conserved motif for dioxygen activation and reduction.

The similarity between the other subunits of these terminal oxidase complexes is not nearly as high as that for their respective subunit I sequences. Subunit II (the *cyoA* gene product) of the UQO complex lacks the two histidines and two cysteines which are ligands for the Cu_A site in cytochrome aa_3 complexes, but otherwise has a similar hydropathy profile. Not surprisingly, conserved residues which have been implicated in the binding of cytochrome *c* to the cytochrome *c* oxidase complexes (Asp^{158}, Glu^{198} - bovine numbering) are absent in the subunit II sequence of the UQO complex. Sequence identity between subunit II of the *P. denitrificans* cytochrome aa_3 and cytochrome bo_3 complexes is only 10%. The *cyoC* gene product (subunit III) shows slightly greater sequence identity with subunit III of the *P. denitrificans* cytochrome aa_3 complex (23%) yet two transmembrane helices found at the N-terminus of subunit III of the cytochrome *c* oxidase complexes are missing in subunit III of the UQO complex. These missing helices are found at the C-terminus of subunit I of the UQO complex.[139,155]

Due to the similarities between the ubiquinol and cytochrome *c* terminal oxidase complexes, some investigators have mutated up to six residues in a fragment of subunit II from the UQO complex in an attempt to create a Cu_A site[50,51] and thus more easily study this unusual copper site. Specifically, the two cysteines and two histidines ligating the Cu_A site in the cytochrome *c* oxidase complexes but missing from the analogous positions in subunit II of the UQO complex were introduced into the appropriate positions of the cloned fragment. A soluble fragment of subunit II from the *P. denitrificans* CcO complex has been expressed in *E. coli*.[49] The Cu_A-like EPR spectra obtained in these experiments suggest that the polypeptide folding of the soluble portion

of subunit II for the ubiquinol and cytochrome *c* oxidase complexes are similar.

An Oxidase Superfamily

The many similarities between the *E. coli* cytochrome bo_3 complex and the aa_3-type cytochrome *c* oxidase complexes led to the recognition of a superfamily of terminal oxidase complexes related in structure and function (Table 1.1). This superfamily is divided into two families: the ubiquinol oxidase complexes and the cytochrome *c* oxidase complexes. The variations within the families are mainly in the number and type of hemes present in the various enzymes. In general, all members of this superfamily of terminal oxidase complexes are thought to translocate protons against a transmembrane potential gradient (although this has not been proven in all cases) and all appear to catalyze dioxygen activation and reduction at a heme-copper binuclear center.

As discussed above, electrons are input to the cytochrome *c* oxidase complexes at the Cu_A site. This redox site is located in the cytoplasmic domain of the enzyme complex. Additionally, it is noteworthy, that Cu_A is the only redox site found in subunit II and cytochrome *c* binding residues have been localized on this subunit. Thus, Cu_A is appropriately situated to act as an intermediary acceptor of electrons from aqueous ferrocytochrome *c*, subsequently donating electrons to the hemes and Cu_B in the more hydrophobic recesses of the enzyme in the membrane. In contrast, ubiquinol-8 (UQ_8H_2) is localized in the hydrophobic interior of the membrane bilayer. Thus, the binding domain for UQ_8H_2 is expected to be in a different three-dimensional location on the enzyme complex relative to the binding domain for ferrocytochrome *c*. The structural differences needed to accommodate these different substrate binding sites can be easily satisfied by appropriate sequence changes. This analysis implies that the Cu_A site serves merely to funnel electrons into the "catalytic core." Since UQ_8H_2 can approach closer to the hemes and Cu_B in subunit I, the intermediary electron acceptor, Cu_A, is unnecessary and therefore is absent from the ubiquinol oxidase complexes.

Table 1.1 The Superfamily of Ubiquinol and Cytochrome *c* Terminal Oxidase Complexes*

Type	Cu_A present?[a]	Translocates protons?	hemes *c*	Species	Reference(s)
Ubiquinol Oxidase Complexes					
bo_3[b]	no	yes	no	*E. coli*	139-141,148
ba_3	no	no	no	*Acetobacter aceti*	156,157
ba_3/bb_3	no	yes	no	*P. denitrificans*	158,159
aa_3	no	yes	no	*Bacillus subtilis*	160,161
	no	ND[c]	no	*Sulfolobus acidocaldarius*	162-165
Cytochrome *c* Oxidase Complexes					
aa_3[d]	yes	yes	no		
ba_3	yes	ND	no	*Thermus thermophilus*	166
caa_3	yes	yes	1	*T. thermophilus*	80,152,167
	ND	yes	1	*Bacillus stearothermophilis*	168,169
	yes	yes	1	thermophilic Bacillus PS3[e]	170-173
	yes	ND	1	*B. subtilis*	160,174,175
cbb_3	no	ND	3	*Rhodobacter capsulatus*	176,177
	no	ND	3	*Rhodobacter sphaeroides*	178

* This table includes the more well-characterized heme-copper oxidase complexes. See García-Horsman and coworkers[179] for a more expanded listing.

[a] The presence or absence of a Cu_A site has not been definitively confirmed in all cases. A best guess is made based on the present literature.

[b] This enzyme is expressed as a cytochrome oo_3 complex with little difference in activity in various overexpressing strains.[147]

[c] not determined.

[d] The aa_3-type cytochrome *c* oxidase complex has been isolated from many organisms, from bacteria to mammals. See Musser and coworkers[6] and García-Horsman and coworkers[179] for reviews.

[e] The PS3 enzyme is expressed as a cytochrome cao_3 complex under air-limited conditions.[180,181]

The ubiquinol and cytochrome *c* oxidase complexes are clearly similar in both overall structure and function. However, it has not been settled yet whether the differences between the two enzymes are minor or whether they give rise to substantially different mechanisms of ET and proton translocation. Although the dioxygen chemistry of the two families of enzymes is virtually identical, the electron input mechanisms are necessarily different as pointed out by Musser and coworkers.[182] The physiological substrate for the cytochrome *c* oxidase complexes is the redox protein ferrocytochrome *c* (MW ~ 12 kDa), a water-soluble one-electron donor whereas that for the ubiquinol oxidases is the small, membrane-associated electron carrier ubiquinol-8 (MW < 1 kDa), a very hydrophobic two-electron donor. As the low-spin heme ET site in these enzymes is a one-electron acceptor, the ubiquinol oxidase complexes must stabilize the highly reactive ubisemiquinone intermediate through strong interaction with the enzyme complex. In contrast, the electron input from ferrocytochrome *c* can occur through a simple outer-sphere process.

Quinone(ol) binding proteins often have two binding sites for the quinone(ol) substrate. For example, photosynthetic reaction centers have a Q_A site and a Q_B site. A tightly-bound plastoquinone at the Q_A site passes electrons sequentially to the Q_B site where a plastoquinone molecule is fully reduced and subsequently diffuses away. The cytochrome bc_1 complex utilizes two ubiquinone(ol) ($UQ(H_2)$) binding sites in a very different manner. Ubiquinol oxidation occurs at the Q_P site. The electrons from this ubiquinol molecule follow two different pathways; one electron eventually reduces cytochrome *c* and the other electron is transferred to a ubiquinone molecule bound at the Q_N site. A second cycle of ubiquinol oxidation at the Q_P site results in reduction of the ubisemiquinone now present (and strongly bound) at the Q_N site. As the protons released from the Q_P site upon ubiquinol oxidation are released on one side of the membrane and the protons taken up upon ubiquinone reduction at the Q_N site originate from the other side of the membrane, the cytochrome bc_1 complex is able to catalyze the formation of a

proton gradient across the membrane in which it resides. This mechanism of proton translocation is termed a "$Q(H_2)$-loop" (Figure 1.6).[183] The NADH dehydrogenase and succinate:ubiquinone oxidoreductase complexes also appear to contain two $UQ(H_2)$ binding sites although it is still not clear what functional purpose these binding sites serve on their respective enzymes.[184-187]

The presence of two $UQ(H_2)$ binding sites can profoundly influence enzyme turnover and function. It is thus important to establish the number of $UQ(H_2)$ binding sites on the ubiquinol terminal oxidase complexes. Musser and coworkers[182] first suggested the possibility that there are two $UQ(H_2)$ binding sites on these enzymes. In fact, these investigators postulated that a $Q(H_2)$-loop might be utilized by the ubiquinol oxidase complexes in order to catalyze proton translocation. Since the ubiquinol terminal oxidase complexes combine, in effect, the ET chemistry of both the cytochrome bc_1 and cytochrome *c* oxidase complexes, it would not be surprising if the ubiquinol oxidase complexes shared turnover mechanisms with both of these enzymes. Sato-Watanabe and coworkers[188] found a strongly bound ubiquinone-8 (UQ_8) molecule in the as-isolated UQO complex which could not be easily removed with substrate or inhibitors thereby confirming the two $UQ(H_2)$ binding site hypothesis of Musser and coworkers.[182] These investigators concluded, however, that the UQO complex contains a UQ_8 molecule that remains strongly bound to the enzyme during the entire turnover cycle. According to their interpretation, the strongly bound ubiquinone behaves like the Q_A in photosynthetic reaction centers as a transient electron acceptor. Clearly, the function of the two $UQ(H_2)$ binding sites is crucial to understanding the UQO complex as a whole and critically influences possible proton translocation models.

Thesis Focus

The high structural similarity between the ubiquinol and cytochrome *c* terminal oxidase complexes makes it tempting to search for common motifs in the two families of

enzymes in order to decipher the nuances of their function. This approach inhibits investigation of differences between the protein complexes that may in fact be crucial for understanding their respective functions. In the work described here, it is recognized that the ubiquinol and cytochrome *c* terminal oxidase complexes are similar structurally, but they are different enzymes and their functions must be investigated independently. Throughout this discussion, the *E. coli* cytochrome bo_3 and the (bovine) mitochondrial cytochrome aa_3 complexes are considered representative members from the families of ubiquinol and cytochrome *c* oxidase complexes. The central theme in these investigations is the proton translocation capabilities of the two enzymes. In Chapter 2, a thermodynamic model of the protein conformational rearrangments required to effect proton pumping in the cytochrome *c* oxidase complexes is developed. This model provides an important understanding of the proton pumping reactions on a theoretical basis that is crucial to understanding chemical models of proton translocation. The following chapter probes the mode of action of the ubiquinone analogues UHDBT and NQNO on the steady-state turnover kinetics of the cytochrome bo_3 complex and contrasts the complexity of the cytochrome *c* oxidase proton pump with a simpler $Q(H_2)$-loop proton translocation mechanism. Chapter 4 focuses on the stability of the Cu_A center in the CcO complex under various conditions and the implications of this stability on a possibile role for this redox site in the coupling of redox energy to the endergonic proton pumping reactions. Experiments using a fluorescence analog of the CcO proton pump inhibitor dicyclohexylcarbodiimide (DCCD) are described in Chapter 5 and the possible role of subunit III in enzyme function is discussed. In Chapter 6, the thermodynamic model of redox linkage introduced in Chapter 2 is further developed in order to illustrate the importance of electron and proton gating mechanisms for prevention of electron leaks and proton slips. Finally, the argument is made that a primitive ubiquinol terminal oxidase complex evolved into the more complicated cytochrome bc_1 and cytochrome *c* oxidase complexes.

Chapter 2

The Thermodynamics of Redox Linkage

The mechanism of dioxygen activation and reduction by the CcO complex is now, in large part, understood. In addition, the pathways of electron flow through the enzyme for the various conformers that exist during enzyme turnover and the rates associated with these processes are slowly becoming clear. But the physiological function of the CcO complex is much more than to dispose of electrons on dioxygen molecules. A portion of the free energy released from the highly exergonic reduction of dioxygen is used to drive the transport of protons from the matrix to the intermembrane space against a transmembrane electrochemical gradient with an average proton pump stoichiometry of $1\,H^+/e^-$ (Table 2.1). Despite steady progress on this problem over the years, the molecular mechanism of the proton pumping process has remained elusive. There is still no consensus on which ET steps are most intimately involved in coupling redox energy to the proton pump reactions. In fact, each of the four redox centers has been postulated to play a central role in the proton pump mechanism and fairly detailed models have been presented for each case.[44,129,189-192] In all scenarios, however, it is accepted on faith that the proton pumping conformational changes are linked to the transfer of redox energy to the polypeptide fold. In particular, no attempt has been made to assess the energetic requirements of the proposed conformational changes as they relate to enzyme turnover. Just such a description of the proton pump is presented in this chapter.

Before proceeding further, it is important to emphasize the distinction between a redox loop proton translocation mechanism and a redox-linked proton pump. A redox loop involves a diffusable element that can be protonated or deprotonated depending on its oxidation state. The reduction/protonation and oxidation/deprotonation reactions occur at distinct sites, the net result being the transport of protons and electrons from one site to the other. Ubiquinone(ol) ($UQ(H_2)$) is an example of such a diffusable element. In the case of the mitochondrial respiratory chain (Figure 1.1), sites of reduction/protonation occur on the NADH dehydrogenase complex (Complex I) and on the succinate dehydrogenase complex (Complex II).[193] Reduction/protonation and

Table 2.1 H^+/e^- Ratios for the Native CcO Complex

Cytochrome *c* Oxidase Sample	Approximate H^+/e^-	Reference(s)
reconstituted beef/ox heart enzyme	0.8-1.1	158,194-201
rat liver mitochondria	0.9	202
P. denitrificans enzyme (whole cells)	1.0	203

oxidation/deprotonation sites are both found on the cytochrome bc_1 complex (Complex III) and are denoted the N and P sites, respectively. The N and P sites are an integral part of the Q(H_2)-loop, which is the mechanism utilized by the cytochrome bc_1 complex to catalyze the release of two protons into the intermembrane space, instead of one, per electron transferred to cytochrome *c*, and thus achieve proton translocation via a diffusable element.[183] In this proton translocation mechanism, the two electrons from a ubiquinol molecule at the P site are split; one electron is eventually transferred to cytochrome *c* and the other is used to reduce a ubiquinone at the N site to a ubisemiquinone. The cycle repeats itself and the ubisemiquinone at the N site is reduced to ubiquinol and released from the enzyme complex. The two protons required to form this ubiquinol molecule are taken up from the matrix, whereas the two molecules of ubiquinol oxidized at the P site release all four protons into the intermembrane space (Figure 1.6). Ingenious redox loop mechanisms have been proposed for the CcO complex wherein O_2/H_2O_2 or O_2/H_2O is the diffusable element.[204] A redox loop model predicts, however, that the electron-transport and proton-translocating elements of the machinery are tightly coupled, that is, under standard turnover conditions, ET does not occur in the absence of proton translocation. For the CcO complex, however, H^+/e^- ratios have been found to vary anywhere from zero to unity (see Chapters 5 and 6 for

discussions of how this is possible) strongly arguing against a redox loop mechanism. In fact, some investigators have found that the H^+/e^- stoichiometry of the CcO complex is inversely dependent on the transmembrane potential; in contrast, the H^+/e^- ratio for the cytochrome bc_1 complex is constant.[205,206] Thus, the proton pump of the CcO complex must operate via a *different* translocation mechanism more reminiscent of ion pumps. It is envisioned that protons are forced through a well-defined channel in the protein matrix against a concentration and potential gradient by a process which is driven by the highly exergonic ET reactions within the enzyme complex. Clearly, the *coupling* between the ET and proton translocation events is critical to the successful operation of the proton pump and therefore will be the focus of the discussion to follow.

Thermodynamics of the Catalytic Cycle

In "resting" enzyme, cytochrome *a*, cytochrome a_3 and Cu_A have reduction potentials of about 340, 290 and 290 mV, respectively, at room temperature and pH 7.[207,208] The lack of spectroscopic signals for Cu_B has hindered direct experimental investigation of its redox properties, but it is generally assigned a reduction potential of about 340 mV.[209] These midpoint potentials are difficult to define since they vary during turnover as electrons are input to the enzyme (complicating the reduction potential measurements themselves) and as the heme a_3-Cu_B binuclear center is activated by dioxygen (see below). For example, some investigators estimated that the two hemes have approximately equal reduction potentials (340-360 mV) in the fully oxidized enzyme, yet when cytochrome a_3 is reduced, the reduction potential of cytochrome *a* drops to 220-250 mV.[209] Nevertheless, these potentials provide a convenient point of departure for the present discussion. The midpoint potential of cytochrome *c* is about 250 mV,[210] implying that the maximum redox free energy available upon electron input from cytochrome *c* to fully-oxidized CcO under standard conditions is about 90 mV. In respiring mitochondria, however, the electrochemical potential barrier to proton transfer

across the inner mitochondrial membrane (the proton motive force or pmf) is about 200 mV[211,212] indicating that proton pumping is unlikely to occur upon electron input to the full-oxidized CcO complex. On the other hand, the situation changes dramatically when the heme a_3-Cu_B binuclear center is activated by formation of the two- or three-electron reduced dioxygen intermediates (compound C and oxyferryl, respectively). From experiments on the reversal of the CcO catalytic cycle by high concentrations of ATP, it was estimated that these intermediates have reduction potentials of about 940 (compound C) and 800 mV (oxyferryl).[87] Recently, these estimates have been revised upwards to 1.22 V and 1.05 V, respectively.[88] In any case, the strong oxidizing ability of dioxygen substantially raises the reduction potential of the heme a_3-Cu_B binuclear site when dioxygen binds to the enzyme. As discussed in Chapter 1, dioxygen does not normally bind to the CcO complex until at least two electrons have been input to the enzyme.[117,123] Thus, proton pumping can only occur upon transfer of the third and fourth electrons to the activated dioxygen binding site during enzyme turnover. Given that the overall stoichiometry of the CcO proton pump is maximally about 1 H^+/e^- and the first two electrons of the dioxygen reduction cycle are not coupled to proton pumping, the average stoichiometry for the third and fourth electrons must then be 2 H^+/e^-. This picture in which the electrons involved in dioxygen reduction are inequivalent with respect to the proton pump has been proven experimentally by poising cytochrome *c* at a high redox potential and partially reversing the catalytic cycle of the CcO complex in rat liver mitochondria.[87,88,213]

At pH 7, 35°C and 0.05 atm O_2 (approximate physiological conditions in muscle[214]), the O_2/H_2O and O_2/H_2O_2 redox couples have potentials of about 780 mV and 210 mV ($[H_2O_2]$ = 1 M), respectively, in aqueous solution. Since the reduction potentials of the redox centers of the fully oxidized CcO complex are greater than or equal to about 290 mV, it is clear that the O_2/H_2O_2 redox couple involved in CcO turnover must function at a higher potential in order for efficient formation of compound C. In fully energized

mitochondria, the transmembrane electric potential ($\Delta\psi$) is about 150 mV.[211] Therefore, since two charge-equivalents traverse the inner mitochondrial membrane during the first half of the dioxygen reduction process,* the O_2/H_2O_2 couple must minimally function at about 290 mV + 150 mV = 440 mV. In order to drive the forward reactions and prevent reversibility, an additional 50-100 meV of redox free energy is likely required. Thus, the O_2/H_2O_2 couple probably functions at greater than or equal to 500 mV. The low physiological concentration of H_2O_2 (micromolar range) and the increased stability of the H_2O_2-protein adduct (relative to free H_2O_2) are both expected to contribute to increasing the O_2/H_2O_2 potential to this level. The necessary consequence of this analysis is that the H_2O_2/H_2O couple must function at $2 \times (\sim 780\ mV) - 500\ mV = \sim 1060\ mV$ $[2 \times E^{red}(O_2/H_2O) - E^{red}(O_2/H_2O_2) = E^{red}(H_2O_2/H_2O)]$ which agrees well with the estimates from Wikström's laboratory.[87,88] This result implies that an average of 1060 meV – 290 meV = 770 meV of free energy is available for the translocation of two protons and one electron across the fully-charged mitochondrial membrane for each of the last two electrons of the catalytic cycle. Since the net electron and proton transfer reactions occur in opposite directions across the membrane, both reactions are endergonic in the presence of a pmf. As a result, the transfer of a negative charge-equivalent across a fully charged mitochondrial membrane requires about 150 meV of free energy ($\Delta\psi = \sim 150$ mV)† and the transfer of two protons against the proton motive force ($pmf = \Delta\psi - 2.303(RT/F)\Delta pH$) requires $2 \times \sim 200\ meV = \sim 400\ meV$ of free energy.[211,212] Under conditions of maximum pmf, then, a *thermodynamic* requirement of about 550 meV of free energy is required to pump two protons. The redox energy

---

* The electrons donated from cytochrome *c* do not traverse the entire membrane during the dioxygen reduction process; however, it is generally assumed that two protons are taken up by the heme a_3-Cu_B binuclear center from the matrix upon formation of compound C. If this is so, the overall process is energetically equivalent to the inward transfer of two negative charge-equivalents across the inner mitochondrial membrane.

† Again, the electrons do not traverse the entire membrane during the dioxygen reduction process; however, proton uptake from the matrix is required as part of the dioxygen chemistry. This overall process is energetically equivalent to the inward transfer of a negative charge-equivalent across the inner mitochondrial membrane.

available to *drive* the ET steps and the conformational dynamics of the proton pump is therefore 770 meV – 550 meV = 220 meV, on average, for the third and fourth electrons of the catalytic cycle. Note that the $H_2O_2/H_2O_2^-$ and $H_2O_2^-/H_2O$ redox couples are expected to function at slightly different reduction potentials with the former functioning at the higher reduction potential.[87,88]

Requirements of a Redox-Linked Proton Pump

The energy released during the highly exergonic reduction of dioxygen must be transferred from the energetic electron to the protein matrix through a process which necessarily involves communication between *at least one* of the enzyme's redox centers and the proton translocating elements. This process is termed redox linkage, and the redox center(s) involved in this transfer of energy to the polypeptide is (are) referred to as the site(s) of linkage. There are two distinct electronic states of a linkage site (oxidized and reduced). In addition, a number of distinct conformational substates (≥ 2) must exist for each of these electronic states; the appropriate cyclic conversion between these conformational states results in proton pumping. The efficacy of the proton pump relies heavily on electron and proton gating mechanisms. Electron gating refers to the requirement that the electron enters the linkage site in a different protein conformation than when it is transferred from this site. Similarly, proton gating implies that protons are input to a different conformation of the proton pump machinery than that from which they are ejected.[215] These conformational changes are necessary to prevent reverse electron and proton transfers (according to the law of microscopic reversibility) as well as for dictating when subsequent reactions should occur. Thus, there are four requirements for a redox-linked proton pump: 1) a sufficiently exergonic ET; 2) redox linkage; 3) electron gating; and 4) proton gating. Clearly, the regulation of rates of ET and proton flow so that uncoupling reactions do not occur is fundamental to the efficiency of the proton pump. In fact, the most likely way that the enzyme can control the coupling of ET

events to proton pumping is through kinetic control of ET pathways.

Energetics of Redox Linkage

There are several ways in which redox linkage could be achieved once the proton pump is engaged. In all scenarios, the linkage site exists in at least two stable conformations, a stable oxidized configuration and a stable reduced configuration. The conversion between these two ligation structures results from oxidation/reduction of the site, and this conformational change is linked to conformational changes of the proton translocating elements (redox linkage). Note that for the majority of redox sites in proteins, the protein fold is so strong that minimal ligand rearrangement occurs upon a change in oxidation state, a condition that is ideal for efficient ET as a result of the low reorganizational energy.[216] For blue copper proteins (such as azurin), whose purpose is to act as electron carriers, the ligand configuration is intermediate between that preferred by Cu(II) and Cu(I). The protein fold is so strong ("rack" energy) that very little structural rearrangement occurs upon oxidation or reduction.[217] The linkage site of the CcO complex, then, represents an exception to this general characteristic of electron transport proteins; in fact, ligand rearrangement is required for proton pumping to be feasible. Initially, oxidation/reduction of the linkage site results in a thermally unstable conformation of the protein; subsequent thermal relaxation allows the linkage site to adopt the more stable conformation. Clearly, the unstable and stable conformations of the oxidized/reduced linkage site are of different total energy. These conformational states of the enzyme can be represented by multidimensional vibronic potential energy wells. Since the conformational coupling between a thermally unstable conformation and its associated stable conformation must be strong for an efficient proton pump (strong coupling is synonymous with efficient redox linkage), these two states can be represented by a single vibrational energy curve with two minima of different energies. The specific vibrational curve describing the energy state of the enzyme depends, of course, on the

redox state of the linkage site. An exergonic ET from the linkage site is the process whereby the description of the enzyme's energy profile changes from one vibronic potential curve to the other.

Figure 2.1 illustrates various types of redox linkage for the case where there is no pmf. Electrons are input to the linkage site from an electron donor (cytochrome *c* is used for simplicity) resulting in a thermally unstable conformation, $(cD^-A)_1$. Upon thermal relaxation, the enzyme achieves a lower energy conformational state, $(cD^-A)_2$. ET from $(cD^-A)_2$ to the activated dioxygen binding site results in a different electronic state of lower energy, $(cDA^-)_2$. This state has an alternative nuclear configuration than $(cD^-A)_2$ since the dioxygen intermediate present at the heme a_3-Cu_B binuclear site is now one-electron reduced. Again, the enzyme's conformation is described by a higher vibrational energy well; conformational relaxation allows the enzyme to achieve a nuclear configuration similar to the original electron input conformation, $(cDA^-)_1$. The conformational relaxations that occur when the linkage site is reduced or oxidized are described by the energy differences α_0 and β_0, respectively (both are negative quantities as defined here). The sum $|\alpha_0 + \beta_0|$ is the energy available to drive the proton pump; this energy is lost mostly as heat in the absence of a pmf. If redox linkage were non-existent, the ET reaction would be described by ΔG°_{ET} (< 0); however, due to coupling to the proton pump, the ET is described by $\Delta G_{ET} = \Delta G^\circ_{ET} - (\alpha_0 + \beta_0)$. This analysis implies that the internal ET is governed by only a fraction of the driving force available, and thus, it is not necessary to invoke ET in the inverted region for the highly exergonic reduction of dioxygen.

The magnitude of the α_0-term represents the free energy available to "prime the proton pump," that is, the energy the protein can access to achieve a conformation where ejection of a proton across the chemiosmotic barrier is imminent. The magnitude of the β_0-term represents the free energy available to "replenish the proton pump," that is, the energy the protein can utilize to take up a proton from the matrix and fill the hole created

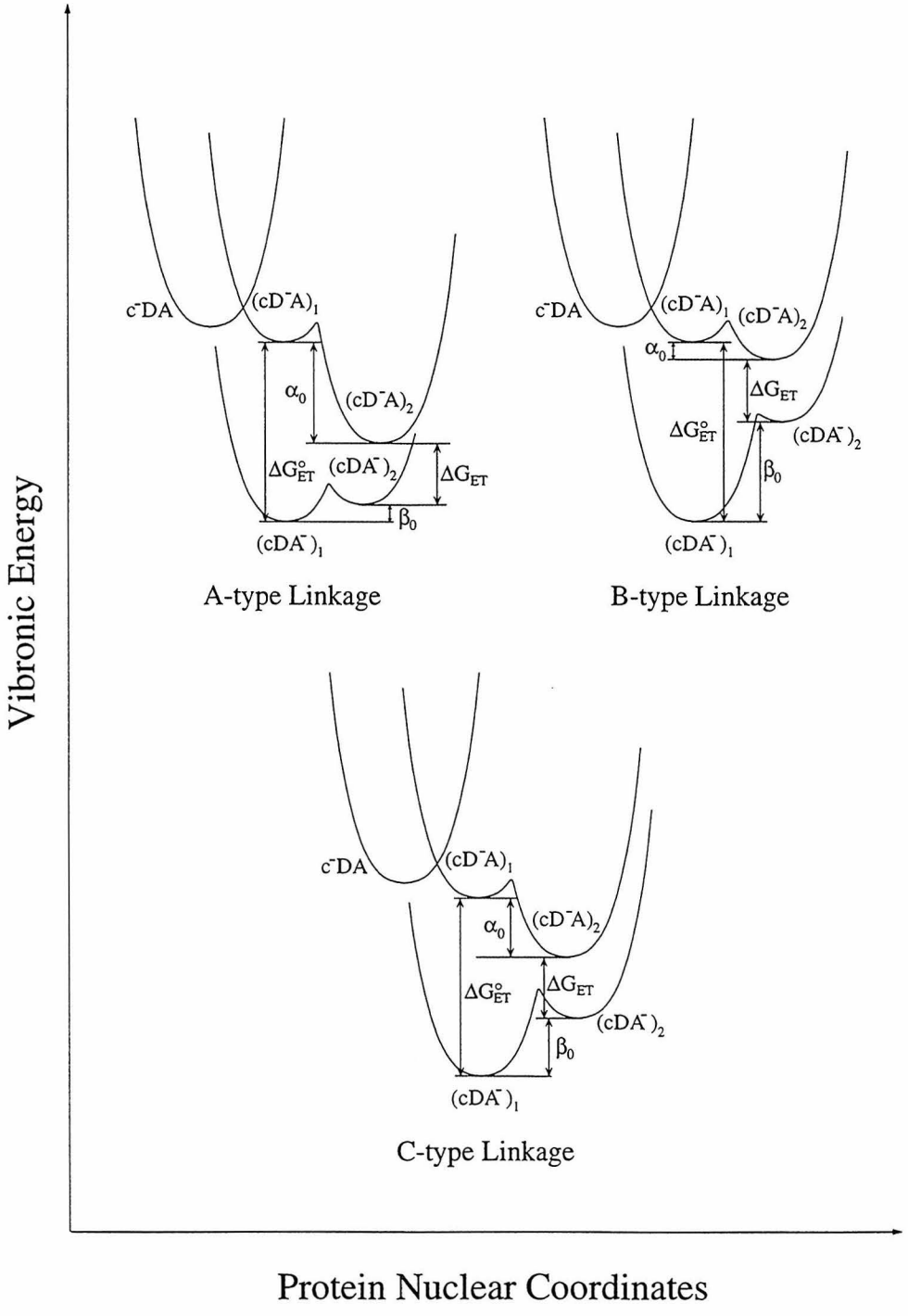

Figure 2.1 Schematics of A-, B- and C-type redox linkage in the absence of a transmembrane potential. The primary electron donor to the linkage site (e.g. cytochrome *c*) is denoted by c, D denotes the electron donor for the ET coupled to the proton pump (i.e. the linkage site), and A represents the peroxidic or oxyferryl dioxygen intermediate (electron acceptor). These symbols are used in unison (e.g. $c^{-}DA$) to denote a specific redox and conformational state of the CcO complex. Plotted along the ordinate is the total vibronic energy of the enzyme complex, the electron donating cytochrome *c* and the protons involved in the dioxygen chemistry and the proton pumping process. See text for further details. Reproduced from Musser and Chan.[218]

by the ejection of a proton into the intermembrane space. Both of these functions are required for any proton pump, but the relative magnitudes of α_0 and β_0 can vary significantly depending on the energetic requirements of the chemical mechanism. For clarity, three cases are considered here: 1) $|\alpha_0| > |\beta_0|$ will be referred to as A-type linkage; 2) $|\alpha_0| < |\beta_0|$ will be referred to as B-type linkage; and 3) $|\alpha_0| \approx |\beta_0|$ will be referred to as C-type linkage (Figure 2.1). Note that both α_0 and β_0 must be less than zero; in fact, for an efficient proton pump, $|\alpha_0|$ and $|\beta_0|$ must be large enough to drive the conformational changes irreversibly in a kinetically facile manner.

In addition, $\alpha_0 < 0$ implies that the effective reduction potential of D *increases* upon conversion from the $(cD^-A)_1$ state to the $(cD^-A)_2$ state; similarly, $\beta_0 < 0$ implies that the effective reduction potential of A *increases* upon conversion from the $(cDA^-)_2$ state to the $(cDA^-)_1$ state. These changes in reduction potential could occur by ligand rearrangements or ligand exchange reactions. Note that the D site must communicate with A (the compound C or oxyferryl dioxygen intermediate) so that upon reduction of D, the reduction potential of A *decreases*. Perhaps the simplest manner in which the reduction potential of A can be influenced is through the introduction of strain in the Fe_{a3}-His bond; however, polypepetide interactions with the bound dioxygen intermediate or perturbations to the heme macrocycle are also possible. Relaxation of A back to a conformation of higher reduction potential results upon ET from D to A. This discussion makes it clear that a given redox center is not "the proton pump;" rather, the whole protein is the proton pump. Thus, it may be difficult to identify the site of linkage by the simple observation of a conformational change at a given redox center; instead, cause and effect must be determined. The energetics of *all* conformational changes must be estimated for an accurate conclusion regarding the *type* of linkage.

In Figure 2.2, a more complete representation of C-type linkage is depicted. This type of redox linkage is considered to be the most general. To clarify the schematics, the description of the protein's conformational space has been expanded into two dimensions

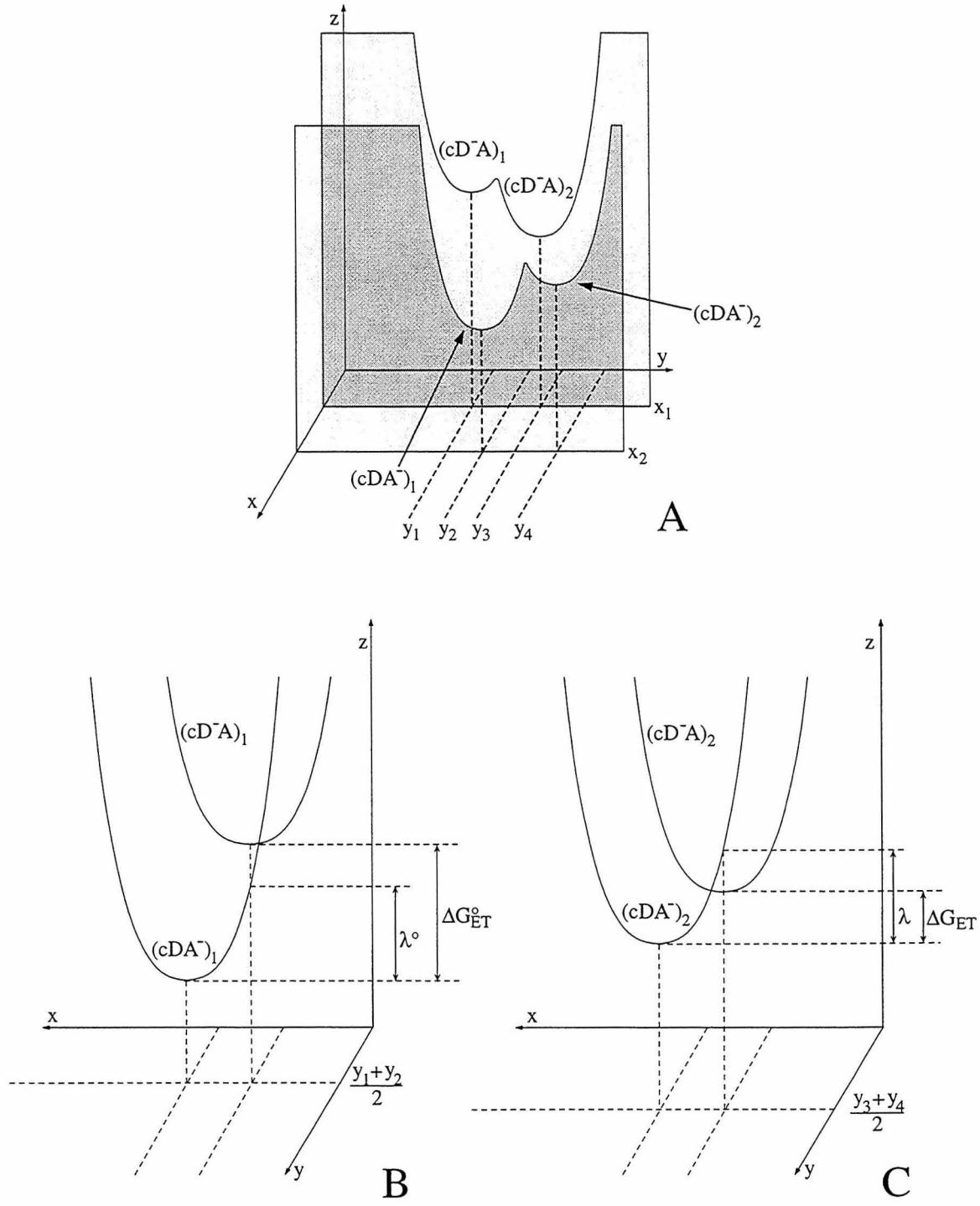

Figure 2.2 A model of C-type redox linkage in the absence of a transmembrane potential explicitly showing the NCET (x) and the NCPP (y) of the protein's vibrational energy surface. Vibronic energy is plotted along the z-direction. Reproduced from Musser and Chan.[218]

(instead of one as in Figure 2.1). The vibronic energy is plotted along the z-direction whereas the x- and y-coordinates can be thought of as the nuclear coordinate associated with electron transfer (NCET) and the nuclear coordinate associated with the conformational elements of the proton pump (NCPP), respectively. In Figure 2.2A, the intersections of two planes ($x = x_1$ and $x = x_2$) with the protein's vibronic energy surface are shown. Each of these intersections is a two-dimensional potential energy curve with two wells labeled using the nomenclature introduced earlier. Potential energy curves along the x-dimension are shown in Figures 2.2B and 2.2C. While the potential energy curves are assumed to be parabolic along both the NCET and the NCPP, the coupling between the vibronic (conformational) states is of a different type and strength. Along the NCET, the coupling between the wavefunctions of the different electronic states is relatively weak and is governed by the electronic coupling matrix element, $[H_{ab}]$, according to the traditional theory of long-distance ET in proteins.[219,220] In contrast, the coupling between nuclear configurations must be strong along the NCPP (required for efficient redox linkage), and therefore, in this dimension, the conformational space is best described by an adiabatic surface with two minima. Thus, along the NCET, the full parabolic nature of the two vibronic states is shown, whereas along the NCPP, vibronic energy curves with two parabolic minima are depicted. This rationale explains the two-dimensional representations of redox linkage shown in Figure 2.1, where the weak electronic coupling between c^-DA and $(cD^-A)_1$ is explicitly depicted. It should be noted that the minimum energy of each vibronic state likely does not have an x- or y-coordinate in common with any other state. Thus, the minima depicted may not necessarily represent the true minima of the vibronic/conformational states represented. Nevertheless, it is useful to assume that the minima represented are the true minima in order to more accurately visualize free energy differences in these types of figures.

Concluding Remarks

This discussion has focused on the idea that the loss of redox energy by the incoming electrons occurs in a stepwise fashion thus providing the directionality and irreversibility required for an efficient proton pump. The proton pumping reactions occur as the protein changes its conformation to accommodate different states of varying redox energy. In other words, the change in the nuclear coordinates associated with the pumping reactions occur *subsequent to* the ET reactions *not* concurrent with them. It is for this reason that the ET and proton pumping coordinates are separable. Note that the conformational rearrangements associated with the proton pumping reactions are to be distinguished from the nuclear reorganizations that accompany the ET steps; the latter are small and localized at the donor and acceptor sites. Here, it is assumed that the coupling between the donor and acceptor sites is sufficiently weak that the ET falls within the non-adiabatic weak coupling limit of Marcus' theory.[220] On the other hand, the major conformational rearrangements of the enzyme which necessarily occur globally over large distances must follow *after* the coupled ET reactions are completed. This is analogous to the slow conformational relaxation process that follows the rapid photoexcitation of the retinal chromophore in bacteriorhodopsin.

The proximity of heme a_3 and Cu_B in the dioxygen binding site (3-5 Å) indicates that electron delocalization over these redox centers and any dioxygen intermediate present should be extremely fast. It is difficult to imagine that ET over the short distance from heme a_3 or Cu_B to the dioxygen intermediate requires more than a few nanoseconds. In contrast, the long-range conformational relaxations implicated in this thermodynamic model are expected to occur on a much slower time scale (microseconds to milliseconds). Thus, the conformational changes associated with the proton pump cannot compete effectively with ET from cytochrome a_3 or Cu_B to the dioxygen intermediates (the result is uncoupling of the proton pump). Any model which proposes cytochrome a_3 or Cu_B as the electron donor in the redox linkage step must also include a very efficient mechanism

to avert uncoupled ET from cytochrome a_3/Cu_B to the high potential dioxygen intermediate. None of the three models postulated to date based on the heme a_3 or Cu_B as the linkage site[190-192] has such a feature built into the model. Continuing in this vein, the ETs from cytochrome a/Cu_A to the activated dioxygen binding site are expected to be one-step rather than two-step processes, that is, the electrons spend no significant time delocalized on Fe_{a3} or Cu_B. In essence, the electronic coupling between the bound dioxygen and the heme macrocycle is likely to be so large as to effectively yield a single electronic state (adiabatic limit). These arguments indicate that it is impossible for cytochrome a_3 or Cu_B to be the site of linkage. Note that in the absence of a dioxygen intermediate, ET between cytochrome a_3 and Cu_B is still expected to be fast (< 1 μs); in fact, this ET is expected to be significantly faster than any other ET steps or conformational changes (other than conformational breathing) that occur during turnover. It is for this reason that the heme a_3-Cu_B binuclear center is considered a single two-electron accepting redox center.

The thermodynamic description presented here is incomplete. Any real model of the proton pump mechanism is expected to include a larger number of sequentially accessible conformational states. In addition, a pmf alters the relationship between the various energy levels quite dramatically. A more complete presentation of the thermodynamic principles discussed here will be given in Chapter 6 after a critical discussion of the possibility that the Cu_A site is D, the electron donor for the ET coupled to the proton pump (Chapter 4) and the potential role of subunit III in regulating the stoichiometry of the proton pump (Chapter 5). But first, the proton translocation mechanism of the bo_3-type ubiquinol oxidase complexes is examined.

Chapter 3

Uncompetitive Substrate Inhibition and Noncompetitive Inhibition by UHDBT and NQNO is Observed for the Cytochrome bo_3 Complex: Implications for a $Q(H_2)$-loop Proton Translocation Mechanism

The structural similarities of the CcO and UQO complexes naturally suggest that they have similar functions. They do: both enzymes catalyze the highly exergonic reduction of dioxygen to water and couple this process to the translocation of protons. The proton translocation mechanisms are usually *assumed* to be identical in the two families of enzymes based on polypeptide homology and the similar dioxygen activation and reduction mechanisms[192,221,222] but there are virtually no experimental data which address this issue. It is certainly possible that sequence differences accommodate the different electron donors and couple the dioxygen reduction reactions to similar proton translocation machineries. On the other hand, radically different proton translocation mechanisms are possible.

As discussed in Chapter 1, the different electron donors for the two enzymes, ferrocytochrome *c* and ubiquinol, dictate at least some differences in electron input mechanisms. Quinone(ol) ($Q(H_2)$) binding proteins typically have two ($Q(H_2)$) binding sites in order to facilitate the coupling of one-electron redox chemistry to a two-electron acceptor/donor. Typically, one of these binding sites is primarily responsible for stabilizing the semiquinone radical whereas the other acts as the electron input/output site. Based in part on this fact, Musser and coworkers[182] suggested that the UQO complex has two ubiquinone(ol) ($UQ(H_2)$) binding sites. Approximately a year later, Sato-Watanabe and coworkers[188] found a tightly-bound ubiquinone-8 (UQ_8) molecule in the as-isolated UQO complex that could not be removed by high concentrations of ubiquinol-1 (UQ_1H_2) or inhibitors. These investigators concluded that the UQ_8 binding site was not the ubiquinol oxidation site and that there were in fact two $UQ(H_2)$ binding sites on the UQO complex, in agreement with the proposal of Musser and coworkers. These data were interpreted to imply that the tightly-bound ubiquinone acts as an intermediate electron acceptor from ubiquinol subsequently passing electrons on to cytochrome *b*. According to this model, the electron input reactions of the UQO complex are similar to the electron output reactions of photosynthetic reaction centers. It has been

found, however, that UQ_1, UQ_6 and UQ_8 as well as 2,6-dichloro-4-nitrophenol (an inhibitor) can be reconstituted into enzyme with an empty UQ_8 binding site.[188,223] These data suggest that the UQ_8 binding site is fairly accessible from the solvent. It is possible, therefore, that this ubiquinone binding site is accessible from the $UQ(H_2)$ pool on the timescale of enzyme turnover.

Clearly, the basic biochemistry of UQO turnover must be understood in greater detail before the proton translocation mechanism of this enzyme can be comprehended. In this study, UQO activity was investigated at high concentrations of ubiquinol and it was observed that ubiquinol acts as an uncompetitive inhibitor under these conditions. Furthermore, two common $UQ(H_2)$ analogs, 2-*n*-nonyl-4-hydroxyquinoline-N-oxide (NQNO) and 5-*n*-undecyl-6-hydroxy-4,7-dioxobenzothiazole (UHDBT) (Figure 3.1), act as potent inhibitors in a noncompetitive fashion. These data indicate that there are two $UQ(H_2)$ binding sites in dynamic equilibrium with the $UQ(H_2)$ pool during enzyme turnover. One of these binding sites is clearly the ubiquinol oxidation site whereas the other site is likely to be the UQ_8 binding site found earlier.[188,223] The implications of these findings on the $Q(H_2)$-loop hypothesis initially proposed by Musser and coworkers[182] are discussed.

Experimental Procedures

Reagents

UHDBT and 5-*n*-undecyl-6-methoxy-4,7-dioxobenzothiazole (Me-UHDBT) were synthesized as described by Selwood and Jandu[224] with the aid of Michael Stowell. The synthesis and characterization (NMR, high resolution mass spectroscopy) of ubiquinone-1 (UQ_1) and ubiquinone-2 (UQ_2) was accomplished by Michael Stowell and will be described elsewhere. NQNO was kindly provided by Bernard Trumpower (Dartmouth Medical School). The detergents DDM and *n*-octyl-β-D-glucoside were purchased from Anatrace.

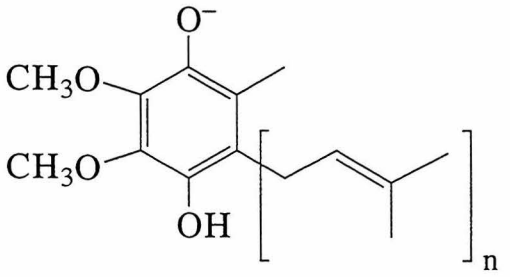

deprotonated ubiquinol (n = 1-10)

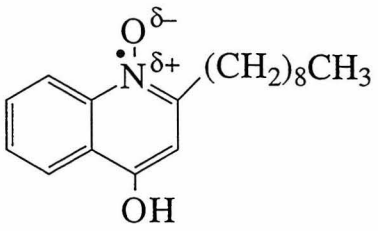

NQNO

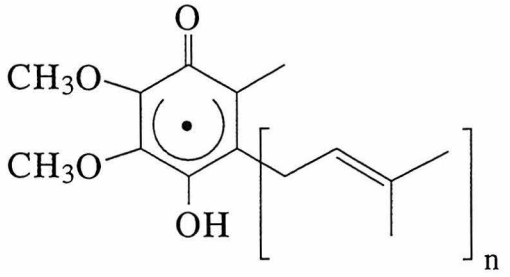

protonated ubisemiquinone

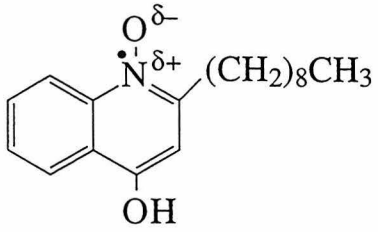

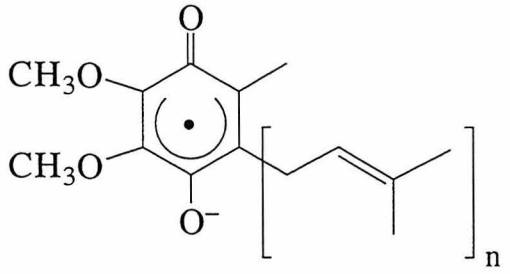

ubisemiquinone anion

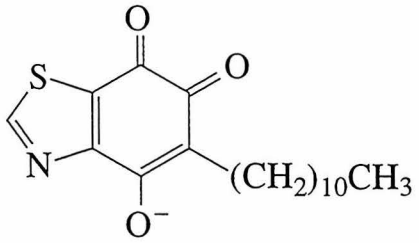

UHDBT

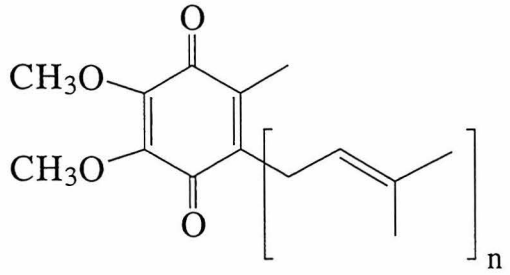

ubiquinone

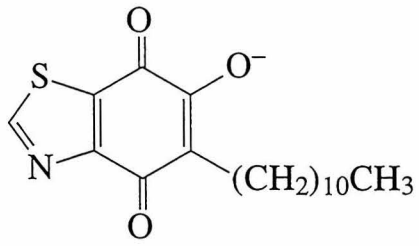

Figure 3.1 Chemical structures of ubiquinone in various redox states and of the inhibitors NQNO and UHDBT. For UQ_1 and UQ_2, n is 1 and 2, respectively. Note that UHDBT ($pK_a = 6.5$)[225] is ionized under the conditions of the turnover experiments (pH 7.4). Ubiquinol has a pK_a of about 10.[226] The phenolic oxygen on the bottom tautomer of UHDBT is esterified with a methyl group in Me-UHDBT. Thus, Me-UHDBT can act only as a ubiquinone analog.

Protein Purification

Growth of *E. coli* cells and isolation of "His-tagged" UQO complex was accomplished essentially according to Morgan and coworkers.[227] The University of Illinois (Urbana-Champaign) fermentation facility was utilized for cell growth. Cells (200 g) were treated with 0.5 g lysozyme in 2 l 200 mM Tris, 2.5 mM EDTA, pH 7.5 for 15 min and centrifuged for 1 h at 13,700 × *g*, 4°C. The pellets were suspended in 1.1 l osmotic lysis buffer (10 mM Tris, 2.5 mM EDTA, pH 7.5), stirred for 30 min and centrifuged at 30,100 × *g*, 4°C for 4 h. The membranes were resuspended with an equal volume of 100 mM NaCl, 5 mM imidazole, 25 mM Tris, pH 7.8. The UQO complex was solubilized from this suspension by addition of an eighth volume each of 10% DDM and 10% *n*-octyl-β-D-glucoside (final concentration of each detergent was 1%) followed by stirring on ice for 1 h. After ultracentrifugation at 90,700 × *g*, 4°C for 30 min, the red supernatant was diluted with an equal volume of distilled water and applied to a 100 ml Ni-NTA-agarose (Qiagen) column equilibrated with 25 mM Tris, 0.1% DDM, pH 7.8 (Buffer A). The column was washed with: 1) 200 ml Buffer A; 2) 200 ml Buffer A supplemented with 300 mM NaCl; and 3) 200 ml Buffer A supplemented with 20 mM imidazole. Pure four-subunit enzyme was eluted with Buffer A supplemented with 200 mM imidazole. Fractions containing pure enzyme were pooled and concentrated with a Filtron 100 kDa membrane. A 20-fold dilution with Buffer A and subsequent reconcentration cycle allowed removal of excess imidazole. The enzyme was aliquoted, frozen in liquid nitrogen and stored at -80°C until use.

Extinction Coefficients

UHDBT concentration was determined in 0.1 mM ethanolic NH_4OH using ε_{280} = 15.6 mM^{-1} cm^{-1}.[225] Me-UHDBT concentration was estimated in ethanol using ε_{288} = 12.2 mM^{-1} cm^{-1}, the extinction coefficient for the protonated form of UHDBT.[225] NQNO concentration was determined in 1 mM NaOH using ε_{348} = 9.45 mM^{-1} cm^{-1}.[228]

Ubiquinone (UQ_1 and UQ_2) and ubiquinol (UQ_1H_2 and UQ_2H_2) concentrations were determined in 80% ethanol using ε_{276} = 14.0 mM^{-1} cm^{-1} and ε_{288} = 4.14 mM^{-1} cm^{-1}, respectively.[229] Enzyme concentration was determined by the pyridine hemochrome method using $\varepsilon^{red\text{-}ox}_{566\text{-}588}$ = 68.4 mM^{-1} cm^{-1}.[230] The use of this value assumes that there are two hemes B in the cytochrome *bo_3* complex. While it is true that the absorption spectra of the pyridine hemochrome of hemes B and O are slightly different, the pyridine hemochrome spectra of these two hemes are sufficiently similar[231] that this extinction is an adequate approximation.

Activity Assay

Approximately 10 mg ubiquinone was solubilized in about 200 µl dimethyl-formamide (DMF) and added to an equal volume mixture of water and diethyl ether (total volume: ~ 3 ml). After the ubiquinone (yellow) was completely reduced to ubiquinol (colorless) by addition of excess solid sodium dithionite, the organic phase was washed once with an equal volume of water and evaporated completely under vacuum. The ubiquinol residue was dissolved under a nitrogen atmosphere in DMF. Enzyme catalyzed ubiquinol oxidation was monitored spectrophotometrically in freshly-made 100 mM Na-phos, 0.1% DDM, pH 7.4 using a Hewlett-Packard 8452 diode array UV/Vis spectrophotometer. Ubiquinol was added directly to the assay reaction mixture from the anaerobic DMF stock solution and the solution was allowed to stabilize (flat baseline) before addition of enzyme (~ 4 nM) to the stirred cuvette. For a given set of turnover measurements, the total DMF concentration was kept constant and was usually kept below 0.8% of the total assay volume. The oxidized minus reduced delta extinction coefficient for ubiquinone was found to vary as a function of total ubiquinone concentration in the UV region of the optical spectrum (Figure 3.2). This observation is simply explained by aggregation-induced exciton interactions between ubiquinone molecules within the detergent micelles. For example, the *delta* extinction coefficient at

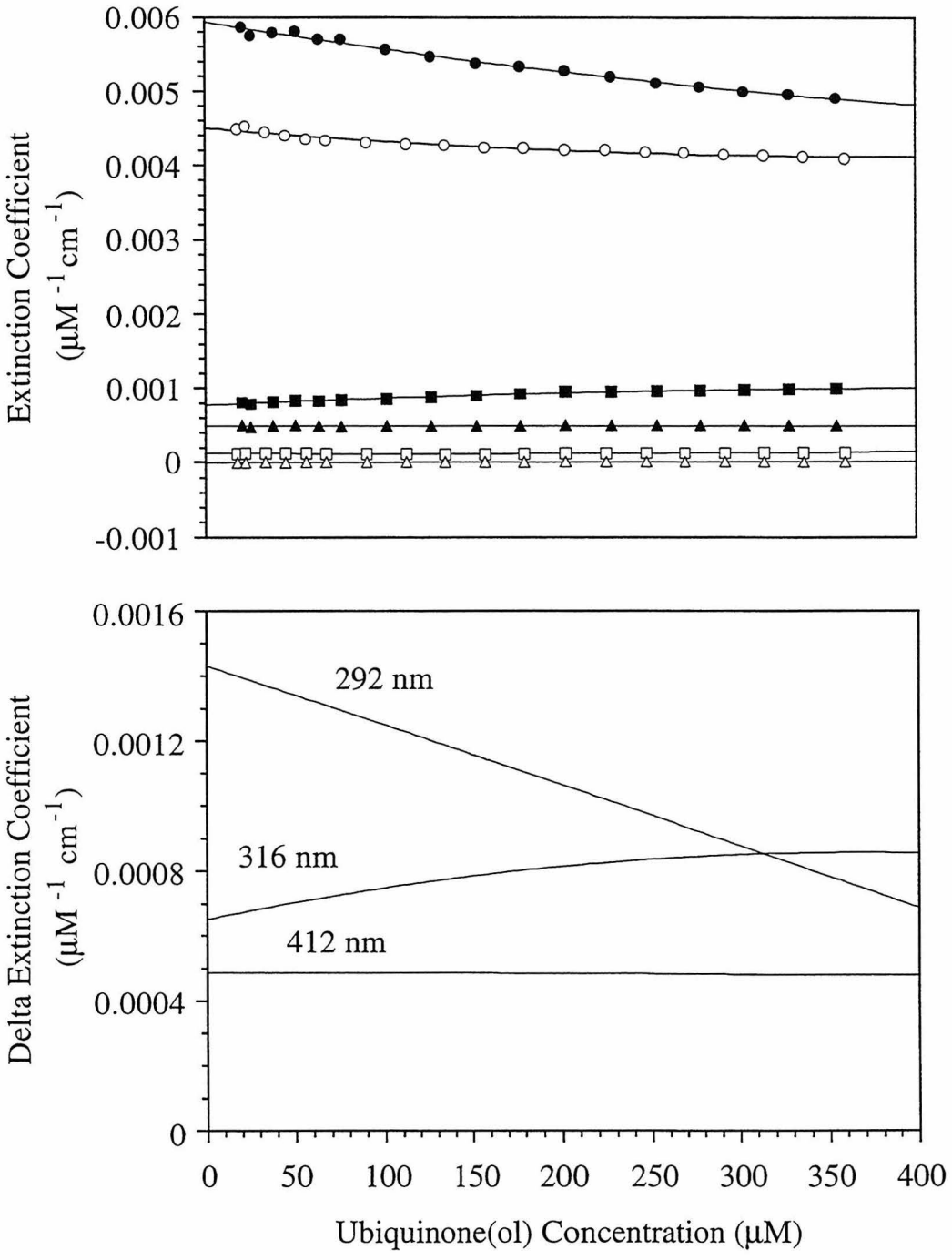

Figure 3.2 (*top*) Extinction coefficients for UQ_2 (filled symbols) and UQ_2H_2 (open symbols) as a function of concentration in 100 mM Na-phos, 0.1% DDM, pH 7.4 at 292 nm (circles), 316 nm (squares) and 412 nm (triangles). (*bottom*) Delta extinction coefficients for UQ_2 minus UQ_2H_2 at these same three wavelengths using the second degree polynomial fits shown in the top panel.

292 nm for UQ_2 minus UQ_2H_2 *decreases* by approximately a factor of two from 0 to 400 μM. Conversely, the delta extinction coefficient at 316 nm *increases* over the same concentration range. At 412 nm, however, the delta extinction coefficient remains constant and is approximately 0.49 $mM^{-1}\,cm^{-1}$ for UQ_2 minus UQ_2H_2 and 0.44 $mM^{-1}\,cm^{-1}$ for UQ_1 minus UQ_1H_2. All turnover numbers reported here were calculated by estimating the initial slope of the kinetics monitored at 412 nm.

Kinetic Model

The kinetic model and notation used in describing the observed kinetics are shown in Figure 3.3. In this kinetic scheme, the symbol EOO is used to denote the enzyme with two empty binding sites; the first "O" represents the catalytic substrate binding site whereas the second "O" is the alternate substrate binding site. Thus, ESO and EIO denote substrate and inhibitor in the catalytic substrate binding site, respectively, whereas EOS and EOI denote substrate and inhibitor in the alternate substrate binding site, respectively. Typical Michaelis-Menten analysis of $\upsilon = d[P]/dt = k_{cat}[ESO]$ and the steady-state assumption $d[ESO]/dt \approx 0$ yields the following expression of the initial rate of ubiquinol oxidation:

$$\upsilon = \frac{V_{max}[S]}{K_m\left(1+\frac{[S]}{K_{S1}}+\frac{[I]}{K_{Ic}}+\frac{[I]}{K_{Iu1}}\right)+[S]\left(1+\frac{[S]}{K_{S2}}+\frac{[I]}{K_{Iu2}}\right)} \tag{3.1}$$

where $V_{max} = k_{cat}[E_{total}]$. As there is no way to distinguish kinetically between EIO and EOI, the average binding constant $K_{ave} = \frac{K_{Ic}K_{Iu1}}{K_{Ic}+K_{Iu1}}$ is introduced to simplify the kinetic expression:

$$\upsilon = \frac{V_{max}[S]}{K_m\left(1+\frac{[S]}{K_{S1}}+\frac{[I]}{K_{ave}}\right)+[S]\left(1+\frac{[S]}{K_{S2}}+\frac{[I]}{K_{Iu2}}\right)} \tag{3.2}$$

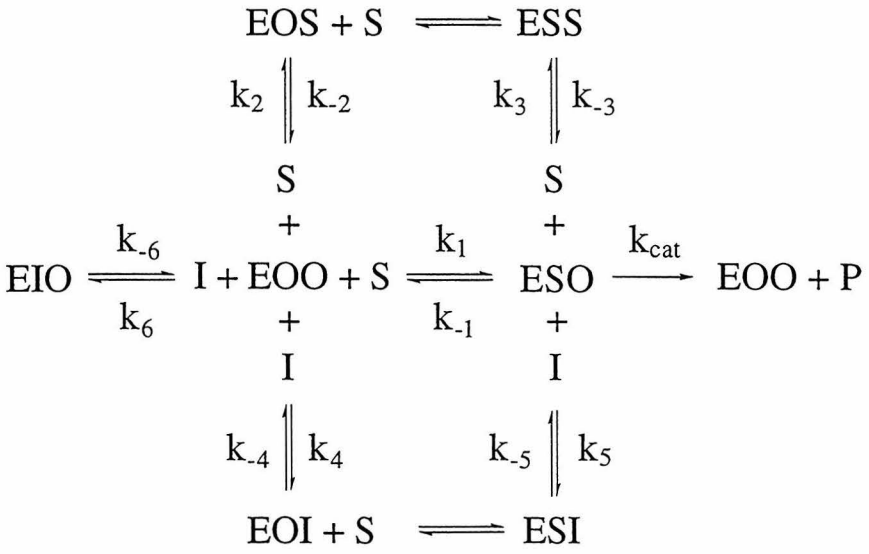

$$K_M = \frac{k_{-1} + k_{cat}}{k_1} \approx K_D = \frac{[EOO][S]}{[ESO]} = \frac{k_{-1}}{k_1}$$

$$K_{Iu1} = \frac{[EOO][I]}{[EOI]} = \frac{k_{-4}}{k_4}$$

$$K_{S1} = \frac{[EOO][S]}{[EOS]} = \frac{k_{-2}}{k_2}$$

$$K_{Iu2} = \frac{[ESO][I]}{[ESI]} = \frac{k_{-5}}{k_5}$$

$$K_{S2} = \frac{[ESO][S]}{[ESS]} = \frac{k_{-3}}{k_3}$$

$$K_{Ic} = \frac{[EOO][I]}{[EIO]} = \frac{k_{-6}}{k_6}$$

Figure 3.3 Simplified kinetic scheme used for interpretation of the steady-state turnover data. EOO denotes the free enzyme; S, ubiquinol; P, ubiquinone; and I is an inhibitor.

Also, the K_{S1} term was found to be kinetically unimportant for the UQO complex:

$$\upsilon = \frac{V_{max}[S]}{K_m\left(1 + \frac{[I]}{K_{ave}}\right) + [S]\left(1 + \frac{[S]}{K_{S2}} + \frac{[I]}{K_{Iu2}}\right)} \qquad (3.3)$$

Note that *competitive* inhibitors bind to the catalytic substrate binding site with a binding affinity described by the inhibition constant K_{Ic}. Kinetically, these inhibitors increase the effective K_m but do not affect V_{max} because the effect of the inhibitor can be obviated by high substrate concentration. *Uncompetitive* and *noncompetitive* inhibitors do not bind to the catalytic substrate binding site but rather decrease enzyme activity when bound to another site on the enzyme. Since these types of inhibitors can bind to both free enzyme,

EOO, as well as the enzyme-substrate complex, ESO, two inhibition constants are required per inhibitor in the kinetic model (K_{Iu1} and K_{Iu2} for the inhibitor, I, and K_{S1} and K_{S2} for the substrate, S). Uncompetitive inhibitors are defined as those which bind much stronger to ESO than to EOO ($K_{Iu1} >> K_{Iu2}$; $K_{S1} >> K_{S2}$) while noncompetitive inhibitors bind to both ESO and EOO with approximately equal affinity (K_{Iu1} and K_{Iu2} and comparable; K_{S1} and K_{S2} are comparable). Note that if $K_{Iu1} << K_{Iu2}$, the inhibitor behaves competitively; it must be determined by other means whether the inhibitor binds to the substrate binding site or to an alternate site. Kinetically, uncompetitive inhibitors decrease the effective V_{max} by binding to ESO and inhibiting catalysis whereas noncompetitive inhibitors increase the effective K_m as well as decrease the effective V_{max}. The number of constants required to fit the data and where they are required allows assignment of the inhibitor type for a given inhibitor. In this work, the data were fitted with Kaleidagraph™ using least squares regression.

Results and Discussion

Substrate Inhibition

Figure 3.4 shows that enzyme activity is inhibited by high concentrations of UQ_1H_2 or UQ_2H_2. For both ubiquinols, a good fit to the data was obtained using equation 3.3. When the constant K_{S1} was included in the fitting algorithm as in equation 3.2, the values obtained for this constant were highly variable and typically exceedingly large. The magnitude and high variability of K_{S1} implies that this constant is kinetically unimportant (i.e. the ubiquinol substrate acts as an uncompetitive inhibitor). The large difference between K_{S1} and K_{S2} indicates, however, that strong allosteric interactions exist between the two ubiquinol binding sites. The values for k_{cat}, K_m, and K_{S2} found in this study are tabulated in Table 3.1.

The shapes of the best-fit curves for UQ_1H_2 and UQ_2H_2 are clearly similar yet they differ dramatically in scale along the ubiquinol concentration axis. This difference results

from the difference in partition coefficients describing the distribution between the aqueous and micellar phases for the two ubiquinols due to the extra isoprene moeity of UQ_2H_2.[232] Under the conditions of the turnover experiments, the reduction rates of UQ_1 and UQ_2 by dithiothreitol (DTT) differ by about an order of magnitude (data not shown). As DTT partitions preferentially into the aqueous phase and this is where ubiquinone reduction occurs, UQ_1 clearly is more soluble in the aqueous phase. The solubility of UQ_2H_2 under the experimental conditions was found to be about 400 μM whereas that for UQ_1H_2 is greater than 2 mM. The difference in partition coefficients for the two ubiquinones also explains the difference in their oxidized minus reduced delta extinction coefficients at 412 nm (see Experimental Procedures). The more hydrophilic environment experienced on average by UQ_1 and UQ_1H_2 lowers the absorption cross section of these molecules relative to UQ_2 and UQ_2H_2, respectively.

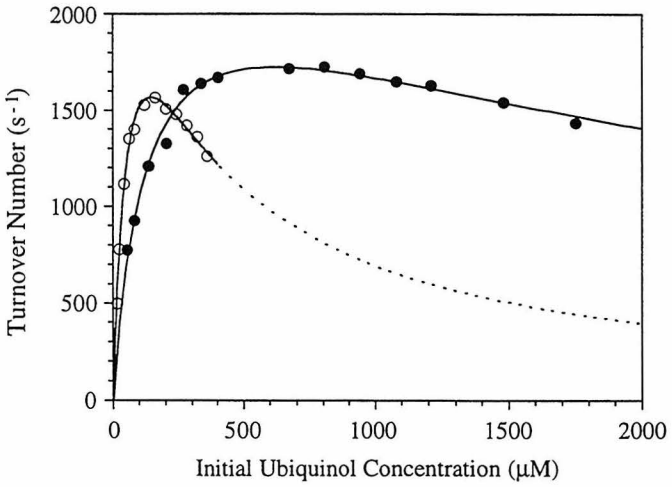

Figure 3.4 UQ_1H_2 (filled circles) and UQ_2H_2 (open circles) activity of the cytochrome *bo*$_3$ complex. The data were fitted using equation 3.3 to yield k_{cat} = 2440 s^{-1}, K_m = 128 μM and K_{S2} = 3000 μM for UQ_1H_2 and k_{cat} = 3090 s^{-1}, K_m = 70.1 μM and K_{S2} = 296 μM for UQ_2H_2. Turnover number = $\upsilon/[E_{total}]$ where υ is in units of μM e^-/s.

The high concentrations of ubiquinol used in these experiments are expected to lead to non-ideal solution behavior. It should be questioned, therefore, whether the kinetic effects observed arise at least in part from non-ideal behavior of the $UQ(H_2)$ in the detergent micelles. The hyperchromic and hypochromic interactions observed in the UV region of the optical spectrum (Figure 3.2) indicate that the $UQ(H_2)$ molecules interact electronically with each other in the detergent micelles. This interaction occurs most

likely through π-stacking of the chromophores. This π-stacking is expected to decrease the activity of the ubiquinol (activity coefficient less than unity). Thus, the effective concentration of ubiquinol in solution is expected to be less than the stoichiometric concentration. In other words, the values for K_{S2} determined here are upper limits for this constant. Since the extinction coefficients for the ubiquinones vary by at most about 20%, the activity coefficients are expected to be greater than 0.7.[233] Thus, the lower limits for the real K_{S2} constants are considered to be 70% of the values determined here.

Figure 3.5 shows the simulated Michaelis-Menten curve assuming no substrate inhibition occurs by UQ_2H_2 using the K_{cat} and K_m values determined from the equation 3.3 fit of the data in Figure 3.4. The difference between the observed and the expected enzyme activity at relatively low UQ_2H_2 concentrations (e.g. 100 μM) dramatically demonstrates that substrate inhibition occurs even at these low UQ_2H_2 concentrations. The 15-20% variation in the UQ_2 and UQ_2H_2 extinction coefficients (Figure 3.2) is insufficient to explain the approximate 2-fold difference between the observed and expected enzyme activity at high initial UQ_2H_2 concentrations (e.g. 350 μM).

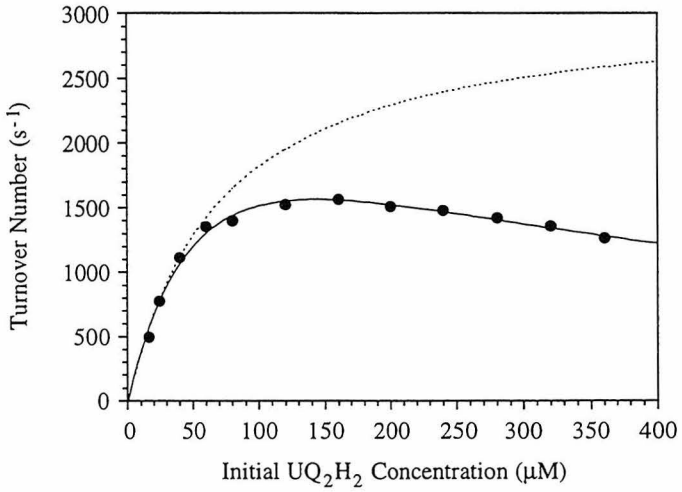

Figure 3.5 UQ_2H_2 activity of the cytochrome *bo*$_3$ complex. The dashed curve describes the expected activity assuming no substrate inhibition occurs and was simulated using k_{cat} = 3090 s^{-1} and K_m = 70.1 μM. Same data and fit (solid curve) as in Figure 3.4.

Inhibition by NQNO and UHDBT

The inhibition of UQO activity by NQNO and UHDBT is demonstrated in Figure 3.6. The kinetic constants k_{cat}, K_m, and K_{S2} determined in the absence of inhibitor were used

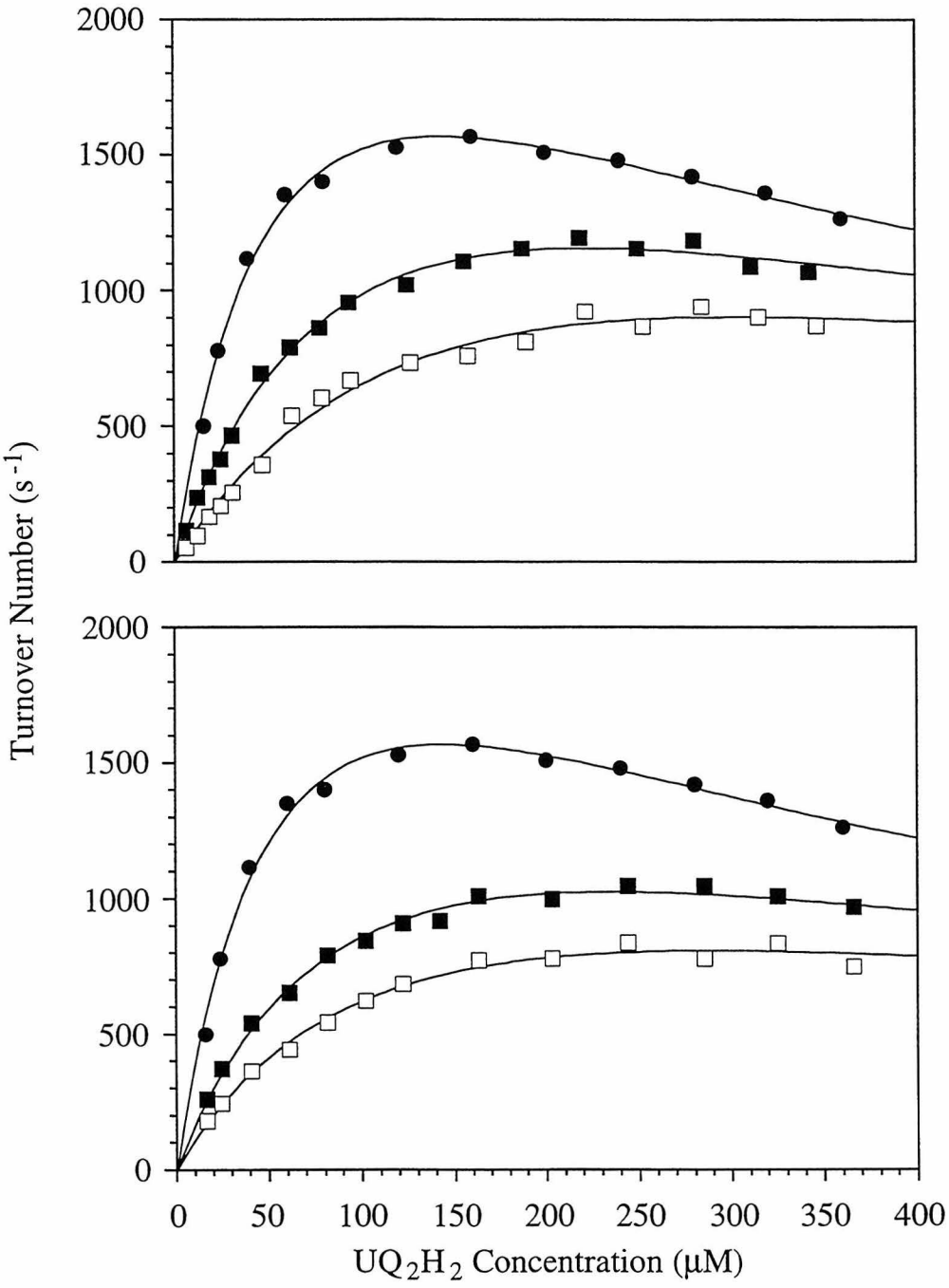

Figure 3.6 NQNO and UHDBT inhibition of UQ_2H_2 activity. (*top*) no inhibitor (filled circles), 0.5 μM NQNO (filled squares), and 1.0 μM NQNO (open squares). (*bottom*) no inhibitor (filled circles), 4.1 μM UHDBT (filled squares), and 8.2 μM UHDBT (open squares). The data were fitted using equation 3.3.

to fit the data obtained in the presence of inhibitor. Importantly, for both inhibitors, the inclusion of both K_{ave} and K_{Iu2} was required to fit the data adequately. This is dramatically shown in Figure 3.7 where the best fit to the data with either one of these constants alone is shown. The values for K_{ave} and K_{Iu2} found in this study are also tabulated in Table 3.1.

The turnover measurements conducted in the absence of an inhibitor can be considered as control experiments for the same measurements conducted in the presence of an inhibitor. The ubiquinol self-interactions present in solution are expected to be present to approximately the same extent in both situations at the low concentrations of inhibitor examined relative to the ubiquinol concentrations used here. Thus, on the off chance that there is some not yet understood phenomenon that results in what is interpreted as substrate inhibition, the inhibition constants determined here should remain valid. It should certainly be questioned whether the two inhibition constants required to fit the data for both inhibitors reflect larger concentrations of more reduced enzyme species with different inhibitor binding affinities at higher substrate concentration levels. This explanation is unlikely, however, since, even at the lowest initial substrate concentrations employed in these experiments, the ubiquinol concentration is over 1000-fold greater than the enzyme concentration.

The Ubiquinol Binding Sites

The substrate inhibition of UQO activity at high concentrations of UQ_1H_2 and UQ_2H_2 implies that ubiquinol can bind to two different locations on the enzyme complex. One of these sites is clearly the ubiquinol electron input site (high-affinity ubiquinol binding site) while the other must be a distinctly different site (low-affinity ubiquinol binding site). The fact that two inhibition constants are required to fit the inhibitor data indicates that NQNO and UHDBT are both noncompetitive inhibitors; that is, these inhibitors must bind to a site on the enzyme distinct from the ubiquinol oxidation site. Since these two

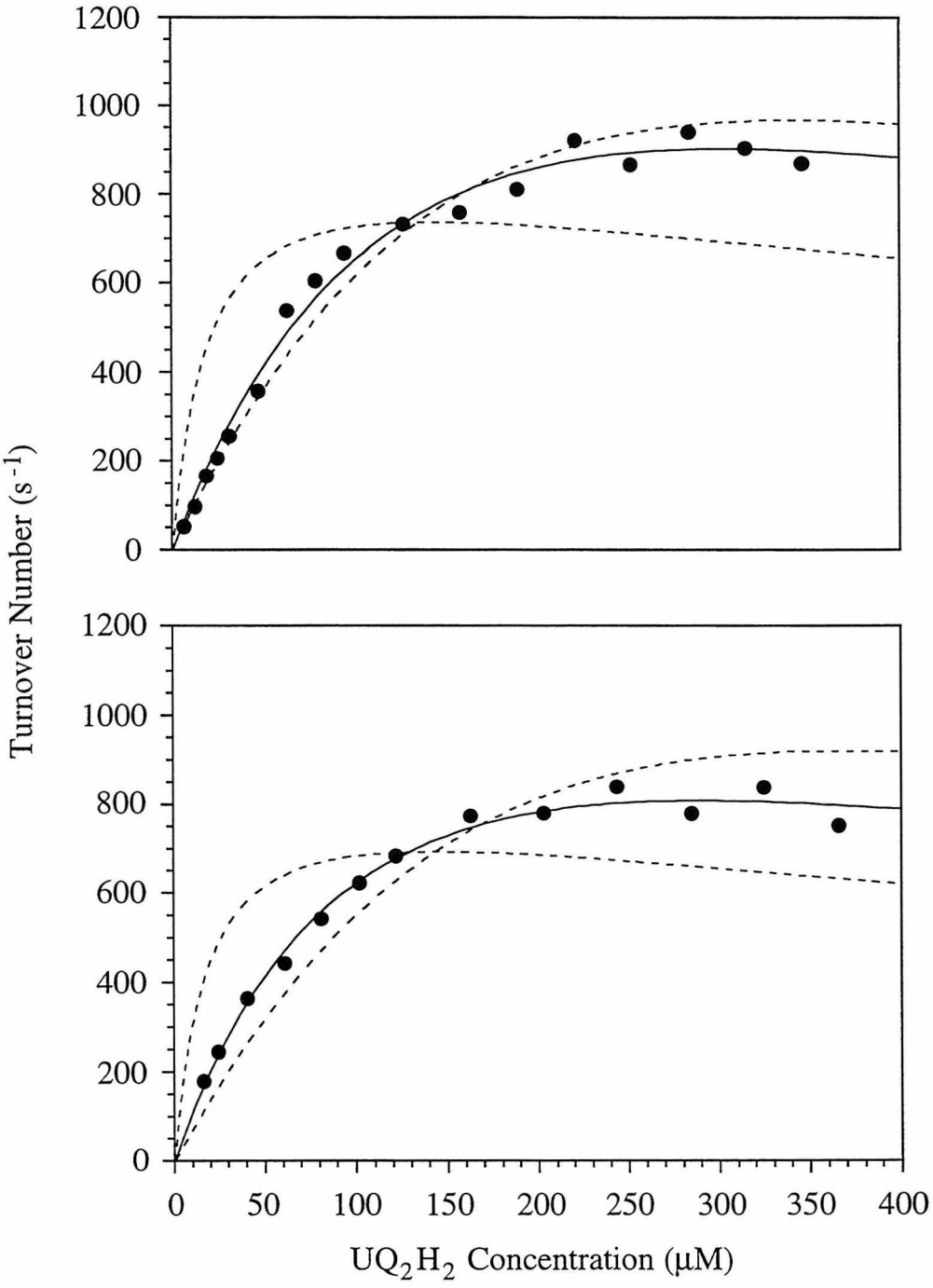

Figure 3.7 UQ_2H_2 activity in the presence of 1.0 μM NQNO (*top*) and 8.2 μM UHDBT (*bottom*). The solid lines are the best fit to equation 3.3 with both K_{ave} and K_{Iu2} included. The dotted lines are the best fits when only one of these constants is included. Same data as shown in Figure 3.6.

inhibitors are $UQ(H_2)$ analogs and, as such, are expected to bind at $UQ(H_2)$ binding sites, it is reasonable to conclude that these inhibitors bind to the low-affinity ubiquinol binding site. Sato-Watanabe and coworkers found a UQ_8 molecule strongly bound to the as-isolated wildtype UQO complex that could not be removed by either excess UQ_1H_2 or inhibitors.[188] When the UQO complex is isolated using DDM for membrane solubilization according to the procedure used in this study, the enzyme obtained contains this UQ_8 molecule.[227] If the binding site for this UQ_8 molecule corresponds to the low-affinity ubiquinol binding site, the strongly bound UQ_8 molecule exchanges with the $UQ(H_2)$ pool under turnover conditions. This explanation is reasonable since this UQ_8 binding site has been shown to be fairly accessible.[188,223] Unfortunately, at this juncture, the possibility that there are three $UQ(H_2)$ binding sites (the UQ_8 binding site plus the two sites found here under turnover conditions) cannot be ruled out. However, the simpler two-binding-site picture is the favored explanation. It is quite possible that the

Table 3.1 Summary of kinetic parameters*

	UQ_2H_2	UQ_1H_2
k_{cat}	3030 ± 370 (6)	2450 ± 260 (3)
K_m	65.4 ± 13.6 (6)	172 ± 52 (3)
K_{S2}	320 ± 132 (6)	2970 ± 790 (3)
	NQNO	UHDBT
K_{ave}	0.270 ± 0.075 (4)	2.78 ± 0.26 (4)
K_{Iu2}	1.58 ± 0.69 (4)	6.70 ± 2.26 (4)

* Values are given as average ± standard deviation (number of independent data sets). Units for k_{cat} are s^{-1}. All other values are given in units of μM. Each of the values is averaged over data from two different preparations of enzyme. The inhibitor binding constants were measured with UQ_2H_2 as the substrate.

long isoprene tail of UQ_8 is wrapped tightly around the hydrophobic transmembrane domain of the enzyme (as is found in photosynthetic reaction center structures). The head group of such a strongly-bound ubiquinone molecule could potentially move relatively freely into and out of its binding pocket but exchange between detergent micelles is expected to be severely inhibited due to the extreme hydrophobicity and large size of the UQ_8 molecule. Therefore, it is not surprising that tightly-bound UQ_8 cannot be removed from the UQO complex by simply washing the enzyme with detergent buffer.

The chemical nature of NQNO and UHDBT should offer some insight into the structural features of the low-affinity ubiquinol binding site. The chemical structures of these inhibitors and the various oxidation states of ubiquinone are shown in Figure 3.1. UHDBT has a phenolic proton with a pK_a of 6.5.[225] Therefore, under the conditions of the inhibition experiments, UHDBT is ionized and two tautomers are present in solution. One of these tautomers behaves as a ubiquinone analog and the other behaves as a ubisemiquinone anion analog. NQNO can behave as a deprotonated ubiquinol molecule or a protonated ubisemiquinone analog. According to this analysis: (1) UHDBT inhibits the binding of ubiquinone; (2) NQNO inhibits the binding of deprotonated ubiquinol (although note that the pK_a of ubiquinol[226] is about 10 and thus ubiquinol is fully protonated under the turnover conditions utilized here); and (3) both inhibitors will bind to a site that stabilizes a strongly bound ubisemiquinone intermediate. High concentrations of ubiquinone (~ 100 μM UQ_2) are required in order to inhibit UQ_2H_2 oxidation (data not shown). Further, Me-UHDBT, a form of UHDBT which can only act as a ubiquinone analog, is less than 10% as effective as UHDBT as an inhibitor (data not shown).* Thus, the UHDBT tautomer that is chemically similar to ubisemiquinone is the inhibitory form of this inhibitor. The noncompetitive nature of UHDBT inhibition

* Attempts to determine accurately the inhibition constants of UQ_2 and Me-UHDBT were unsuccessful because the high concentrations required perturb the activity coefficient of ubiquinol in an unknown manner.

indicates that UHDBT binds to the low-affinity ubiquinol binding site. Thus, the low-affinity ubiquinol binding site must stabilize ubisemiquinone. Note that the enzyme's affinity for both NQNO and UHDBT is stronger than that for the ubiquinol substrates (by at least 10-fold) and both act noncompetitively. It is quite likely, then, that NQNO is recognized by the enzyme as a ubisemiquinone analog as well.

Matsushita and coworkers[234] and Sato-Watanabe and coworkers[235] observed that HQNO (same as NQNO but with a shorter hydrocarbon tail) noncompetitively inhibits UQO turnover in agreement with the studies reported here. The latter workers tested the inhibitory effects of an extensive series of benzophenols and found that the inhibition kinetics varies dramatically. For example, changing both of the bromine substituents of 2,6-dibromo-4-dicyanovinylphenol to iodine alters the observed inhibitory mechanism from noncompetitive to competitive; changing a single bromine substituent to a methoxy group results in an uncompetitive inhibitor. All three of these benzophenol inhibitors have a pI_{50} = 4.1-4.2 (pI_{50} = log of the reciprocal of the molar concentrations of the inhibitors required to halve the full enzyme activity). Noncompetitive and uncompetitive inhibitors clearly must bind to a site different from the ubiquinol oxidation site. Also, an inhibitor can behave competitively and yet not bind to the substrate binding site (e.g. $K_{Iu1} << K_{Iu2}$); for example, 2,6-dichloro-4-nitrophenol behaves as a competitive inhibitor and yet binds to the UQ_8 binding site.[188,235] As phenols are chemically similar to ubisemiquinones, it is reasonable to assume that these benzophenol inhibitors bind to the low-affinity ubiquinol binding site found here. Thus, the three benzophenol inhibitors mentioned above likely all inhibit turnover by binding to the low-affinity ubiquinol binding site but the variation in substituents alters the relationship between K_{Iu1} and K_{Iu2} dramatically. Note that a difference in K_{Iu1} and K_{Iu2} requires allosteric interactions between the two ubiquinol binding sites.

The Mechanism of Proton Translocation

The structural similarities of the ubiquinol and cytochrome *c* oxidase complexes certainly makes it imperative to question whether both families of enzymes catalyze proton translocation via similar mechanisms. The observed overall H^+/e^- stoichiometry for the UQO complex has been found to be 2.[140] Half of the protons translocated most certainly arise from the scalar release of protons from the ubiquinol oxidation chemisty and the uptake of protons from the opposite side of the membrane to electrically balance the dioxygen reduction chemistry. A cytochrome *c* oxidase-type proton pump mechanism may account for the other protons:

$$\begin{aligned} &2\ QH_2 + 4\ H^+(\text{inside}-\text{scalar}) + O_2 + 4\ H^+(\text{inside}-\text{pump}) \\ &\quad \rightarrow 2\ Q + 4\ H^+(\text{outside}-\text{scalar}) + 2\ H_2O + 4\ H^+(\text{outside}-\text{pump}) \end{aligned} \tag{3.4}$$

While only one $UQ(H_2)$ binding site is required to satisfy the chemistry of this turnover cycle, the finding that there are two $UQ(H_2)$ binding sites on the UQO complex does not imply that this proton translocation mechanism is incorrect. For example, Sato-Watanabe and coworkers[188] postulated that a strongly bound ubiquinone molecule (at the Q_H site) mediates electron input from ubiquinol (at the Q_L site). This ubiquinone binding site could certainly, in fact is expected to, stabilize a ubisemiquinone species. However, this ubiquinone binding site is *not* expected to be in dynamic equilibrium with the $UQ(H_2)$-pool. Thus, this model does not predict uncompetitive substrate inhibition or noncompetitive inhibition by $UQ(H_2)$ analogs. A third $UQ(H_2)$ binding site could be involved in regulating enzyme turnover. Thus, there could be two $UQ(H_2)$ binding sites in dynamic equilibrium with the $UQ(H_2)$-pool in addition to the site that strongly binds ubiquinone. According to the data presented here, such a regulatory $UQ(H_2)$ binding site would have to strongly stabilize ubisemiquinone. It is difficult to accept such regulation of enzyme turnover by ubisemiquinone, however.

As mentioned in Chapter 1, Musser and coworkers[182] postulated that a $Q(H_2)$-loop

operates during turnover of the UQO complex. According to this $Q(H_2)$-loop model, the two $Q(H_2)$ binding sites are termed the Q_A site and the Q_B site (Figure 3.8). Ubiquinol oxidation occurs at the Q_A site, formed at least in part by the transmembrane segments of subunit II, by analogy with the Cu_A electron input site of the cytochrome *c* oxidase complexes. Studies with a photoreactive azidoubiquinone derivative support this hypothesis.[236] Ubiquinone reduction occurs at the Q_B site which is located near cytochrome *b*, by analogy with the Q_N site of the cytochrome bc_1 complex.[183] The blue-shift of the Soret absorption band and the perturbations to resonance Raman lines for heme *b* but not for heme o_3 upon addition of UQ_1 to the ubiquinone-free enzyme[188] support this postulate. The two ubiquinol electrons split at the Q_A site. Under steady-state conditions, one electron is transferred to the dioxygen binding and reduction site, whereas the other is donated to the cytochrome *b*/ubiquinone shunt. This model predicts that the Q_B site stabilizes a ubisemiquinone intermediate and therefore agrees well with the stable ubisemiquinone species found by a number of investigators.[237,238] In order for net proton translocation to occur during enzyme turnover, all protons released from the Q_A site must exit on the periplasmic side of the membrane whereas the protons required at the Q_B site must originate on the cytoplasmic side of the membrane. The experimentally observed 2 H^+/e^- stoichiometry[140] is thus fully accounted for by the $Q(H_2)$-loop hypothesis:

$$\begin{aligned} &4\ QH_2\,(Q_A\ \text{site}) + 4\ H^+\,(\text{scalar}) + O_2 + 4\ H^+\,(Q_B\ \text{site}) + 2\ Q(Q_B\ \text{site}) \\ &\quad \rightarrow 4\ Q(Q_A\ \text{site}) + 8\ H^+\,(Q_A\ \text{site}) + 2\ H_2O + 2\ QH_2\,(Q_B\ \text{site}) \end{aligned} \tag{3.5}$$

Both of these $UQ(H_2)$ binding sites are in dynamic equilibrium with the $UQ(H_2)$ pool and the binding of ubiquinol or inhibitors to the Q_B site are expected to perturb the oxidation kinetics of ubiquinol at the Q_A site. It is therefore unnecessary to postulate a third $UQ(H_2)$ binding site to explain the data reported here: the high-affinity ubiquinol binding site is equivalent to the Q_A site whereas the low-affinity ubiquinol binding site is

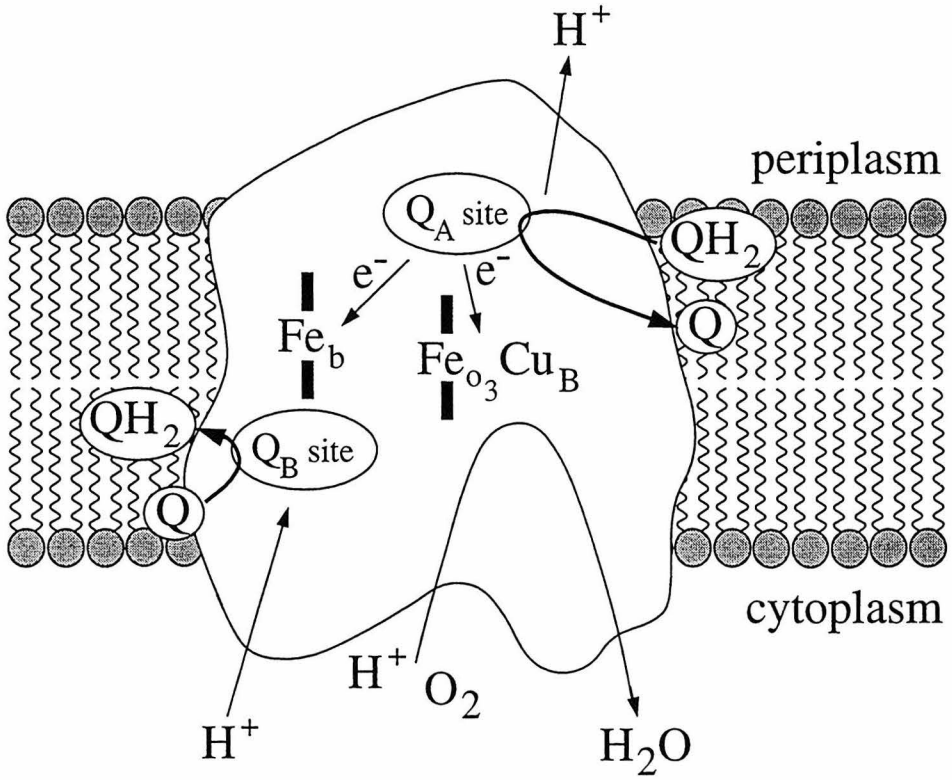

	Q_B site	Q_A site
K_D (UQ_1)	0.0025 mM[a]	> 10 mM[b]
K_D (UQ_1H_2)	2.97 mM[c]	0.172 mM[c]
location	subunit I	subunit II

Figure 3.8 Schematic of the proposed $Q(H_2)$-loop proton translocation mechanism of the cytochrome bo_3 complex. See text for details. Notes: (a) from Sato-Watanabe and coworkers.[188] This value is certainly much lower for UQ_8; (b) based on the difference in $UQ(H_2)$ binding affinities of the Q_B site and the apparent absence of ubiquinone inhibition, this value is likely to be greater than 10 mM; and (c) this work.

equivalent to the Q_B site. While it is clear that there are other turnover scenarios that can be conceptualized, this $Q(H_2)$-loop proton translocation mechanisms offers a simple model that is consistent with the experimental data.

Energetics of the Turnover Cycle

It is imperative to question whether it is thermodynamically feasible for the UQO complex to catalyze proton translocation for every electron input to the enzyme according to the above $Q(H_2)$-loop mechanism. The cytochrome *c* oxidase complexes pump protons only during the second half of the dioxygen reduction cycle [213]. This feature of cytochrome *c* oxidase activity is explained by the thermodynamics of the chemistry: the H_2O_2/H_2O redox couple is much more exergonic than the O_2/H_2O_2 redox couple ($\geq$ 1 V vs. $\geq$ 500 mV respectively) [218]. However, whereas cytochrome *c* has a reduction potential of about 250 mV [210], ubiquinone has a reduction potential of about 70 mV [229]. Assuming a similar potential for the O_2/H_2O_2 redox couple in the ubiquinol and cytochrome *c* oxidase complexes ($\geq$ 500 mV) [218], greater than 400 meV of redox free energy is available to translocate 2 H^+/e^- against a typical 200 mV proton motive force [211,212] for the first two electrons input to the UQO complex. This analysis implies that essentially all of the redox free energy would be conserved (2 $H^+ \times$ 200 meV = 400 meV) by the proton translocation reactions. Energy to *drive* this process may ensue from a high ubiquinol:ubiquinone ratio and/or from a greater functional potential of the O_2/H_2O_2 redox couple. Note that for the exergonic dioxygen reduction reactions to be coupled to the proton translocation reactions of the proposed $Q(H_2)$-loop mechanism, proton uptake at the Q_B site must occur subsequent to dioxygen binding, that is, after two-electron reduction of the heme o_3-Cu_B binuclear center. Cytochrome *b* may be utilized to temporarily store an electron so that the two-electron reduction of the Q_B site ubiquinone in the absence of proton uptake is not required. Thus, it is thermodynamically reasonable that all four electrons of the UQO dioxygen reduction cycle are coupled to proton

translocation reactions.

Since the dioxygen chemistry of the ubiquinol and cytochrome *c* oxidase complexes are so similar, it is certainly expected that the third and fourth electrons input to the UQO complex are energetic enough to drive the translocation of 3 H^+/e^- (one of which is a scalar proton; the other two could arise from a cytochrome *c* oxidase-type proton pump mechanism). This is the electron-dependent stoichiometry inherent in equation 3.4. If it is assumed that a cytochrome *c* oxidase-type proton pump mechanism is responsible for the translocation of 2 H^+/e^- for the third and fourth electrons input to the UQO complex, there is no thermodynamic reason why 1 H^+/e^- cannot be pumped for the first two electrons via partially uncoupling the same translocation mechanism. If protons are pumped for the first two electrons of the catalytic cycle in this manner, the overall number of protons released on the periplasmic side of the membrane would be 10 $H^+/4\ e^-$ (4 scalar protons; 6 pumped protons - two for the first two electrons, four for the last two electrons). The fact that the cytochrome bc_1 and cytochrome *c* oxidase complexes acting in tandem translocate 12 $H^+/4\ e^-$ indicates that from a *thermodynamic* standpoint the UQO complex could certainly translocate the same number of protons. However, the observed stoichiometry is 8 $H^+/4\ e^-$.[140] The proton translocation efficiency of the proposed $Q(H_2)$-loop cannot be increased for the more energetic third and fourth electrons. Thus, this $Q(H_2)$-loop proton translocation mechanism rationally explains why the UQO complex translocates 8 $H^+/4\ e^-$ despite the thermodynamic possibility of translocating 10 $H^+/4\ e^-$ or even 12 H^+/e^-.

Concluding Remarks

The kinetics of the cytochrome bo_3 complex are clearly more complicated than originally envisioned. The k_{cat} and K_m determined from the experimental data are significantly higher (2- to 3-fold) when it is recognized that substrate inhibition occurs and the data are fitted with a model that includes this fact. The inhibition of ubiquinol

oxidase activity by high concentrations of ubiquinol and by the inhibitors NQNO and UHDBT indicates that there are two $UQ(H_2)$ binding sites in dynamic equilibrium with the $UQ(H_2)$ pool during enzyme turnover. The uncompetitive nature of the observed substrate inhibition and the differences between K_{Iu1} and K_{Iu2} for a number of inhibitors indicates that there are allosteric interactions between the two $UQ(H_2)$ binding sites. Since ubiquinone inhibition is not observed (except, perhaps, at very high concentrations), it is clear that the ubiquinol oxidation site (Q_A site) has a low affinity for ubiquinone. On the other hand, the low-affinity ubiquinol binding site (Q_B site) binds UQ_2H_2 with a dissociation constant of 320 μM and UQ_1H_2 with a dissociation constant of 2970 μM (K_{S2}). The high affinity of the Q_B site for ubisemiquinone analogs indicates that this $UQ(H_2)$ binding site strongly stabilizes ubisemiquinone. A turnover cycle in which all protons are translocated via a $Q(H_2)$-loop mechanism is considered the most reasonable explanation for these data.

The simplicity of a $Q(H_2)$-loop proton translocation mechanism relative the CcO proton pump as described in Chapter 2 should be readily apparent. In a $Q(H_2)$-loop, proton uptake or release at a $UQ(H_2)$ binding site simply results from the electrostatic unbalance caused by the input or output of electronic charge to or from that site. The proton channels to these $UQ(H_2)$ binding sites are simply conduits that connect these sites with the appropriate aqueous medium; no conformational communication with the enzyme's redox sites is required during turnover. On the other hand, the proton channel of the CcO proton pump must alternate access to the internal and external aqueous phases. This access is controlled by conformational communication between the linkage site and the proton translocating elements and is initiated by electron input to or output from the linkage site. It is the exquisite control of the coupling between the ET steps and the proton pumping machinery that makes the CcO complex a sophisticated molecular machine in a class by itself.

Chapter 4

35 GHz ENDOR and 9.2 GHz EPR of the SB-12 Heat-treated Cytochrome *c* Oxidase Complex

At the end of the Chapter 2, it was argued that cytochrome a_3 or Cu_B cannot be the site of redox linkage in the cytochrome *c* oxidase complexes. Consequently, cytochrome *a* or Cu_A must be the donor for the coupled electron transfers. Babcock and Callahan found that the hydrogen bond strength of the cytochrome *a* formyl group changes upon reduction of this redox center and they postulated a proton pump mechanism based on this result.[189] This is the only experimental evidence that directly addresses the possibility that conformational changes of cytochrome *a* drive the proton pumping reactions. On the other hand, there are a number of studies that have implicated the Cu_A site as the linkage site. Incubation of the CcO complex with the thiol specific reagent *p*-(hydroxymercuri)benzoate (*p*-HMB) or heat-treatment of the enzyme in DDM or the zwitterionic detergent sulfobetaine 12 (SB-12) result in complete abolition of proton pumping activity.[239-241] A substantial increase in the transmembrane proton leak rate is observed for both of the heat-treated enzyme species. All of these modifications result in a perturbation to the EPR spectrum of the enzyme. The harshest treatments yield a type-II copper species while a type-I species is observed under milder conditions. For a long time, the interpretation has been that these modifications perturb the structure of the Cu_A site, and hence, the ability of the Cu_A site to couple ET to the conformational changes of the proton pump has been destroyed. When these experiments were performed, the Cu_A site was still thought to be mononuclear with a two His and two Cys ligation structure. Thus, Li and coworkers postulated that dissociation of one of the Cu_A cysteines yields the type-I species whereas dissociation of two cysteines and addition of at least one nitrogeneous ligand yields the type-II species (Figure 4.1). The structural lability of the Cu_A site has also been inferred from $AgNO_3$ incubation.[242,243] As Ag^+ is a thiol specific reagent, the type-II copper signal that results in these experiments has been also thought to result from modification of the Cu_A site.

As discussed in Chapter 1, however, the Cu_A site is binuclear, not mononuclear (Figure 1.5). Thus, the ligand rearrangements of the Cu_A site proposed by Li and

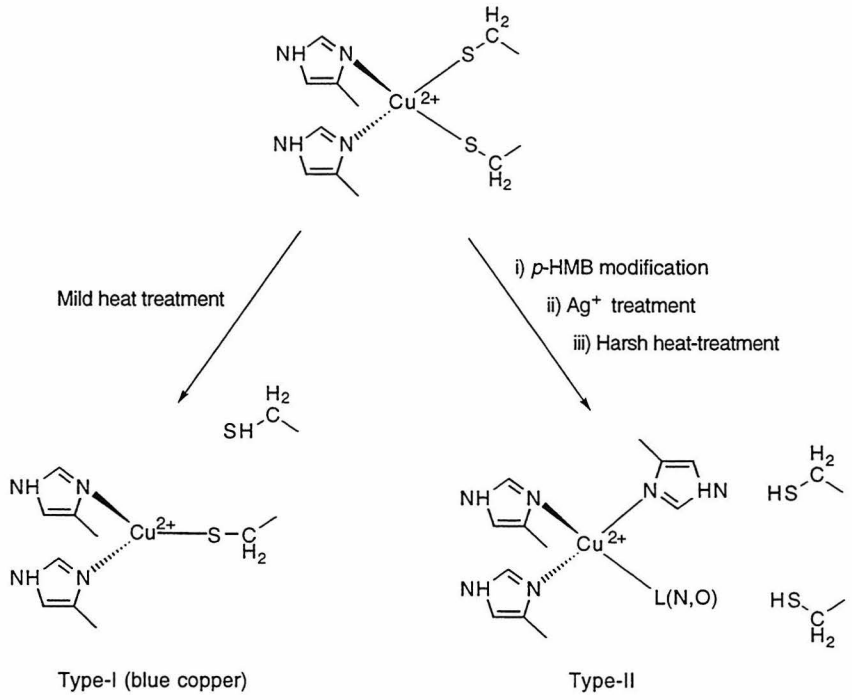

Figure 4.1 Scheme proposed by Li and coworkers explaining the appearance of type-I and type-II copper species after various treatments. Adapted from Li and coworkers.[241]

coworkers as a result of various treatments must be re-evaluated. Specifically, it must be determined if the loss in proton pumping activity of the enzyme is due to modification of the Cu_A site or actually is due to some other structural perturbation. The presence of two copper ions at the Cu_A site certainly makes the potential products of modification of this site more diverse. As type-II signals can arise from Cu_B under appropriate conditions,[37,244,245] it should be noted that it has not been demonstrated definitively which of the three copper ions in the CcO complex are EPR detectable as a result of these various modification procedures. The possibility exists that Cu_B becomes EPR detectable under one set of conditions, whereas the Cu_A site is modified under a different set of conditions. Also, perturbations to both copper sites can occur concurrently either by independent means or through allosteric interactions between the two copper sites. ENDOR spectroscopy can be used to interpret ligand rearrangement reactions much more

accurately than EPR and absorption spectroscopies. Thus, it was thought prudent to examine whether the type-II signals that appear in the above modification experiments are accompanied by loss of the strongly coupled cysteinyl protons in the ENDOR spectrum associated with the Cu_A site. A change in the nitrogen ENDOR of the Cu_A center is certainly expected as well.

To a first approximation, the ENDOR spectrum for a single orientation of a nucleus (N) of spin I consists of $2I$ transitions at frequencies given by:

$$\nu_{\pm}(m_I) = \left| A_N/2 \pm \nu_N + \tfrac{3}{2}P_N(2m_I - 1) \right| \qquad -I + 1 \leq m_I \leq I \tag{4.1}$$

where A_N and P_N are orientation dependent hyperfine and quadrupole coupling constants, respectively, which are molecular parameters and independent of the spectrometer microwave frequency, and ν_N is the nuclear Larmor frequency $h\nu_N = g_N\beta_N\mathbf{B}$.[246] For a ^{14}N nucleus ($I = 1$), equation 4.1 in principle describes a four-line pattern consisting of a Larmor-doublet centered at $A(^{14}N)/2$ split by $2\nu(^{14}N)$ and further split by the quadrupole term. Although there are no quadrupole interactions for protons ($I = 1/2$), one must be careful when predicting ^1H ENDOR spectra because β_N is so large. At both 9 and 35 GHz, $\nu(^1H)$ is typically larger than $A(^1H)/2$ and the ENDOR frequencies are predicted by:

$$\nu_{\pm}(^1H) = \left| \nu(^1H) \pm A(^1H)/2 \right| \tag{4.2}$$

At 9 GHz, the ^1H and ^{14}N ENDOR resonances from the Cu_A site overlap and the spectrum is difficult to interpret (Figure 4.2A). However, at 35 GHz, these resonances are well separated because the field dependence of ν_N shifts the ^1H resonances to higher frequencies (> 40 MHz) whereas the ^{14}N resonances remain centered about $A(^{14}N)/2$ in the 2-26 MHz frequency range (Figure 4.2B). Clearly, the ENDOR spectrum of the Cu_A site is more informative at the higher microwave frequency, and therefore, the ENDOR

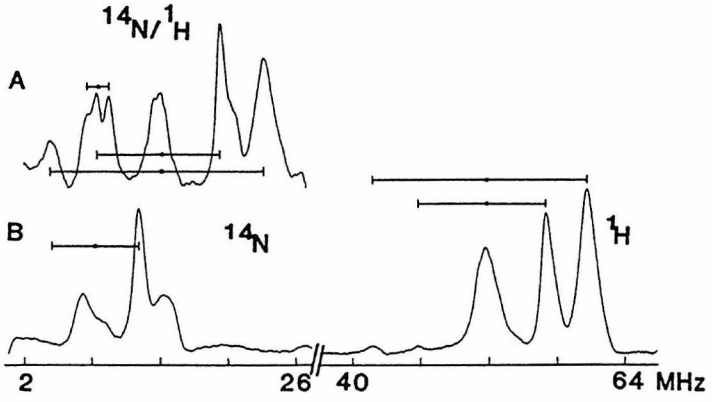

Figure 4.2 9 GHz (A) and 35 GHz (B) ENDOR spectra of the native CcO complex taken near $g = 2.04$. Reproduced from Gurbiel and coworkers.[42]

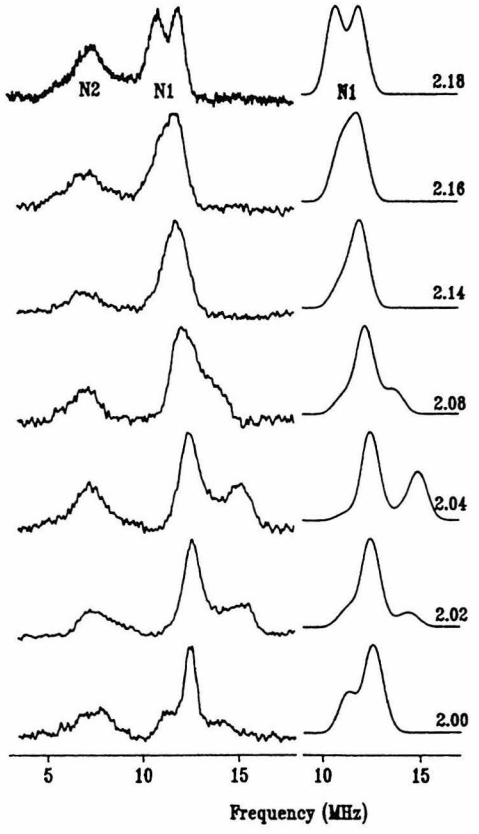

Figure 4.3 35.3 GHz ^{14}N ENDOR of the bovine CcO complex. Simulations of the ν_+ features for N1 are shown on the right. Reproduced from Gurbiel and coworkers.[42]

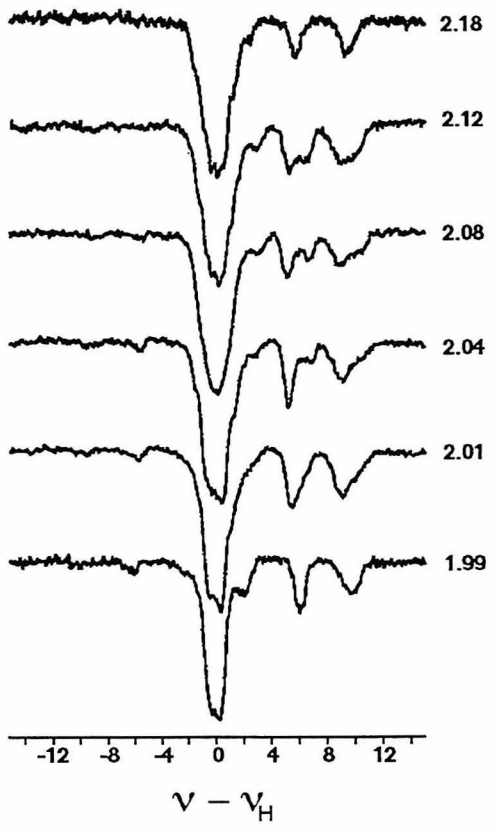

Figure 4.4 ^{1}H ENDOR of the native CcO complex at 35.3 GHz.

spectra reported here were obtained exclusively at 35 GHz.

The 35 GHz ^{14}N ENDOR of the native CcO complex as a function of g-value is shown in Figure 4.3. The observed signals are assigned to two different nitrogen ligands, N1 and N2. Gurbiel and coworkers[42] were able to simulate the N1 spectrum as shown on the right side of Figure 4.3. These two nitrogen signals most certainly arise from the two histidine ligands to the Cu_A site. The ^1H ENDOR of the native CcO complex as a function of g-value is shown in Figure 4.4. There are four strongly coupled protons observed (displaced by about 5, 6.5, 8.5 and 10 MHz from the proton Larmor frequency ($\nu_H \approx 46.3$ MHz) in the $g = 2.08$ spectrum). These four protons are most likely the four β-protons on the two cysteine ligands of the Cu_A site. There is an intermediately coupled proton signal at about 2-3 MHz from the proton Larmor frequency. It is possible that this signal arises from the methionyl protons. As the methionyl ligand of the Cu_A site is more distant from the metal ions than the cysteine ligands, the coupling of the methionyl β-protons is expected to be less than that for the cysteinyl β-protons.

Experimental Procedures

Enzyme Purification

The beef heart CcO complex was isolated essentially by the Hartzell and Beinert method.[247] Mitochondria were lysed with 2.5 g Triton X-114/g protein in TEH buffer (20 mM Tris, 10 mM EDTA, 1 mM histidine, pH 8.0) supplemented with 200 mM KCl and centrifuged at 13,700 × g for 10 h. The pellet was washed three times with TEH buffer and solubilized with 2 g K-cholate (twice recrystallized)/g protein in TEH buffer at a protein concentration of 40 mg/ml. The enzyme was precipitated with ammonium sulfate and the pellets were redissolved in 25 mM Tris, 0.1% DDM, 10 mM EDTA, pH 8.0. The enzyme was dialyzed (50 kDa membrane) against 50-100 volumes of this solubilization buffer and then 50-100 volumes 25 mM Tris, 0.1% DDM, pH 8.0. After centrifugation at 32,500 × g, 4°C for 30 min, the enzyme (150-250 μM) was aliquoted,

frozen in liquid nitrogen and stored at -80°C until use.

Growth of *E. coli* cells and isolation of "His-tagged" UQO complex was accomplished as described in Chapter 3.

Concentration and Activity Assays

Stock CcO concentrations were calculated from the reduced-minus-oxidized difference spectrum at 605 nm ($\Delta\varepsilon_{605}^{red\text{-}ox}$ = 24 mM^{-1} cm^{-1}) using sodium dithionite as the reductant. However, this method was found to be unreliable for the various modified enzyme samples, and the pyridine hemochrome method[230] was used instead. A dual wavelength extinction coefficient of 46.5 ± 1.0 mM^{-1} cm^{-1} (mean ± standard deviation) at 588-638 nm for the reduced minus oxidized pyridine hemochrome was determined from ten different determinations on five different batches of as-isolated enzyme. Turnover numbers were calculated from the initial rate of ferrocytochrome *c* (1-80 μM initial concentration) oxidation monitored optically (550 nm or 520 nm) in 100 mM Na-phos, 0.1% DDM, pH 7.4. The k_{cat} and K_m for a particular enzyme sample were obtained from Eadie-Hofstee plots.

Stock UQO concentrations and enzyme activity were calculated as described previously (Chapter 3). Also, the kinetic constants for the UQO complex used here were identical to those reported earlier (Chapter 3).

SB-12 Heat-treatment

The SB-12 heat-treated CcO complex was prepared by a modification of the procedure of Nilsson and coworkers.[240] Three parts stock enzyme was diluted with ten parts 15 mM SB-12, 100 mM Na-phos, 500 mM NaCl, pH 7.4 and incubated in a 40°C water bath for 15 min. The solution was cooled on ice for 10 min and centrifuged at 32,500 × *g*, 4°C for 30 min to remove large aggregates. After dialysis (50 kDa membrane) at 8°C against 30-40 volumes 5 mM SB-12, 10 mM Tris, pH 8.0, samples

were applied to a short (2.5-3.5 × 2.5 cm) DE-52 (Whatman) column equilibrated with 10 mM Tris, 0.1% DDM, pH 8.0. The column was then washed with 50 ml 10 mM Tris, 0.1% DDM, pH 8.0 and the enzyme was eluted with 200 mM NaCl, 25 mM Tris, 0.1% DDM, pH 8.0. The fractions containing enzyme were pooled and concentrated to greater than 150 μM using Centricon-100s (Amicon). After dialysis (50 kDa membrane) at 8°C against about 100 volumes of 25 mM Tris, 0.1% DDM, pH 8.0 for 4-10 h, the enzyme was centrifuged at 32,500 × *g*, 4°C for 30 min, frozed in liquid nitrogen and stored at -80°C until use.

Subunit III-depletion

Subunit III was removed from the CcO complex using high detergent and salt concentrations. One part stock enzyme was diluted with six parts 5% Triton X-100 (w/v), 300 mM Tris-HCl, 50 mM EDTA, pH 8.5 and incubated at room temperature for 20 h. After ten-fold dilution with distilled water, the enzyme was applied to a DE-52 column equilibrated with 10 mM Tris, 0.1% DDM, pH 8.0. The column was then washed with 100 ml 10 mM Tris, 0.1% DDM, pH 8.0 and the enzyme was eluted with 200 mM NaCl, 25 mM Tris, 0.1% DDM, pH 8.0. The fractions containing enzyme were pooled and concentrated to greater than 150 μM using Centricon-100s. After dialysis (50 kDa membrane) at 8°C against about 100 volumes of 25 mM Tris, 0.1% DDM, pH 8.0 for 4-10 h, the enzyme was centrifuged at 32,500 × *g*, 4°C for 30 min, frozed in liquid nitrogen and stored at -80°C until use.

Electrophoresis

The absence or presence of subunit III in various enzyme samples was determined by sodium dodecyl sulfate-polyacrylamide gel electrophoresis (SDS-PAGE). Enzyme samples were dissociated using 250 mM Tris-HCl, 8 M urea, 3.3% β-mercaptoethanol, 5% sodium dodecyl sulfate (SDS), 15% glycerol, pH 6.2 at room temperature for about

1 h and run on a Hoefer SE 250 vertical electrophoresis unit using a 7.2%/0.19% (acrylamide/bisacrylamide) stacking gel, a 14%/0.37% running gel, and a running buffer of 20 mM Tris, 240 mM glycine, 0.1% SDS, pH 8.4. Gels were stained with Coomassie Blue.

Instrumentation

Optical absorption spectra and kinetic measurements were obtained with Hewlett-Packard 8452 or 8453 diode array UV/Vis spectrophotometers. The X-band EPR spectra were recorded using a Varian E-109 spectrometer equipped with a Varian E-231 TE 102 rectangular cavity. The modulation frequency used was 100 kHz and temperature was controlled with a helium cryostat (Oxford Instruments) or liquid nitrogen finger dewar (Wilmad). The ENDOR spectra were recorded on a modified Varian E-109 EPR spectrometer equipped with an E-109 9 GHz microwave bridge or an E-110 35 GHz microwave bridge using 100 kHz field modulation as described previously.[248] All ENDOR spectra were obtained in the laboratory of Professor Brian Hoffman (Northwestern University, Evanston, IL) by Drs. Ryszard J. Gurbiel and Yang-Cheng Fann.

Data Analysis

Double integration of first derivative X-band EPR spectra was carried out using the baseline correction and integration capabilities of Lab Calc^{TM}. The EPR visible copper concentration was calculated by spin integration of standard solutions of $CuSO_4$ in 100 mM imidazole, pH 8.4 or in 100 mM histidine, pH 8.0 under the same experimental conditions.

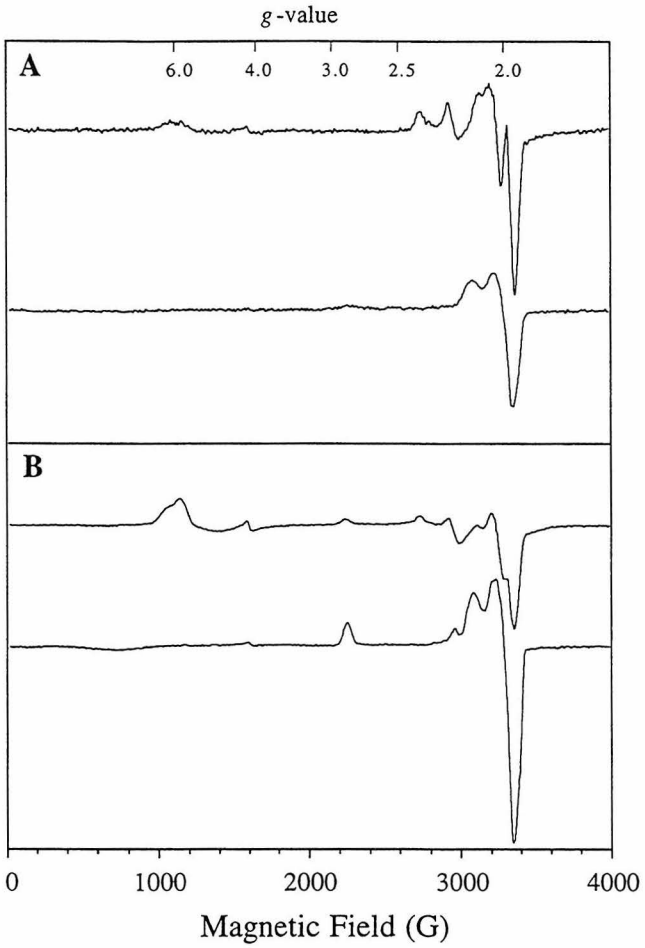

Figure 4.5 (A) The EPR spectra of the SB-12 heat-treated, 40 h SB-12 dialyzed CcO complex (*top*) and the native CcO complex (*bottom*) at 80 K (average of four scans). (B) The EPR spectra of the same two samples at 10 K. Spectra are scaled to protein concentration based on the pyridine hemochrome method and the buffer is 25 mM Tris, 0.1% DDM, pH 8.0. Spectrometer settings: modulation amplitude, 10 G; time constant, 32 ms; power, 1 mW; microwave frequency, 9.22 GHz; scan rate, 8.3 G/s.

Results

Development of a Type-II Copper EPR Signal

As shown in Figure 4.5A, SB-12 heat-treatment of the CcO complex results in the development of a type-II signal. The appearance of this type-II copper EPR signal is accompanied by a high-spin heme signal in the $g = 6$ (~ 1100 G) region of the spectrum. This high-spin heme signal is best seen at low temperature (Figure 4.5B) where line-broadening is less of a problem. Curiously, the development of this type-II EPR signal is critically dependent on the length of the first dialysis step (see Experimental

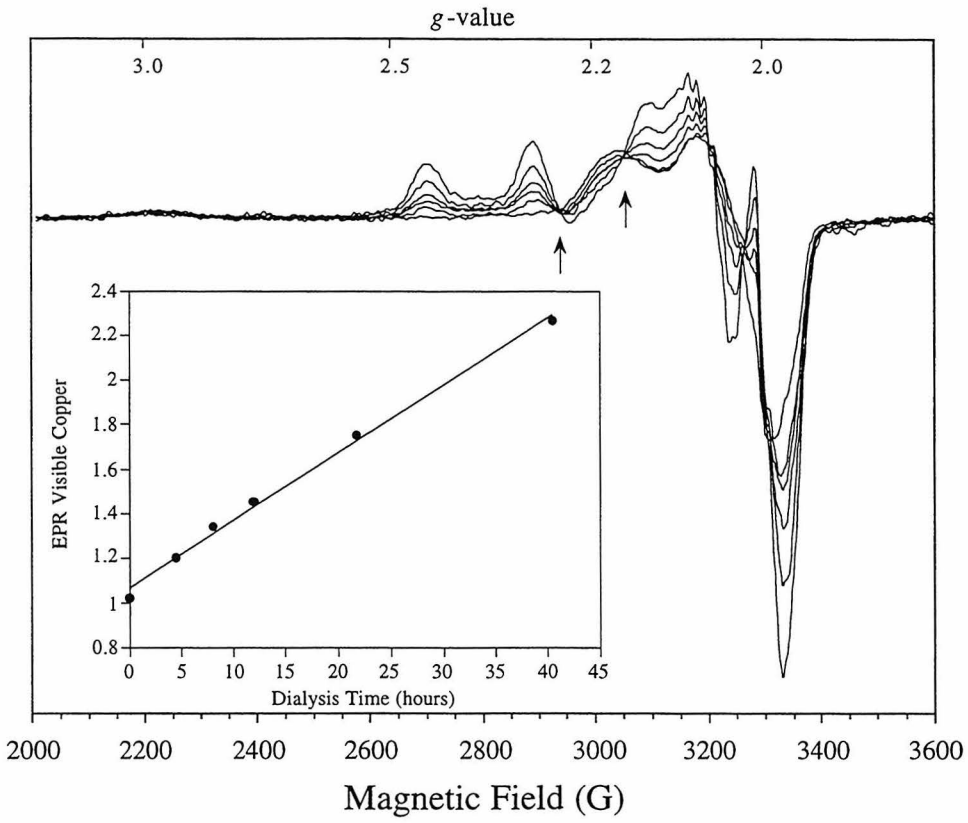

Figure 4.6 Development of the type-II EPR signal (77 K) as a function of dialysis time after SB-12 heat-treatment. The inset shows the linear dependence of integrated intensity on dialysis time (see text for details). Spectrometer settings are the same as in Figure 4.5 except for a time constant of 128 ms (average of five scans).

Procedures) as shown in Figure 4.6. Double integration and correction for spectrometer gain and enzyme concentration as determined by the pyridine hemochrome technique reveals that the amount of EPR visible copper approximately doubles after 40 h of dialysis (Figure 4.6 inset). The integration error is estimated to be in the range of 10-20%; this error arises from the protein concentration estimate, the baseline correction routine, and the fact that there are small heme signals in the $g = 2$ region even at 80 K. Copper standards were used to estimate the EPR visible copper in the native enzyme. As expected, the ratio of EPR visible copper to enzyme complex is approximately unity for native enzyme; therefore, this was assumed to be the case and the integration of modified enzyme was standarized to this value. There appear to be two "isosbestic points" (at 2938 and 3059 G - denoted by arrows in Figure 4.6); these isosbestic points suggest that a

single process occurs to produce the type-II signal.

Various attempts were made to determine what step of the SB-12 heat-treatment procedure is responsible for the perturbations to the EPR spectrum of the enzyme. Gel electrophoresis reveals that subunit III is lost during the SB-12 heat-treatment procedure. Subunit III can be removed by high salt and detergent concentration (see Experimental Procedures). In and of itself, it is found that subunit III depletion is insufficient to yield the large type-II copper signal shown in Figure 4.5. However, a small amount of type-II copper signal is sometimes apparent in the EPR spectrum of the subunit III-depleted CcO complex; this signal intensifies upon 40 h dialysis against 10 mM Tris, 0.1% DDM, pH 8.0 at 8°C. Dialysis of the native enzyme itself against this same buffer results in the

Table 4.1 EPR Visible Copper Resulting from Various Treatments of the CcO Complex

	subunit III present?[a]	K_m (μM)	k_{cat} (s^{-1})	EPR visible copper (80K)
native	yes	47	230	1.00
subunit III-depleted[b]	no	56	165	1.11
40 h DDM dialyzed[c]	yes	52	182	1.25
40 h DDM dialyzed,[c] subunit III-depleted[b]	no	49	152	1.49
40 h SB-12 dialyzed	no	49	128	1.81
SB-12 heat-treated, 40 h SB-12 dialyzed	no	60	47	2.25

[a] An entry of "no" implies that greater than 90% of subunit III is missing as determined by SDS-PAGE.
[b] The phrase "subunit III-depleted" refers to the high detergent, high salt treatment described in Experimental Procedures.
[c] The phrase "DDM dialyzed" denotes dialysis against 10 mM Tris, 0.1% DDM, pH 8.0 at 8°C followed by the short DE-52 column treatment described for the SB-12 heat-treated enzyme.

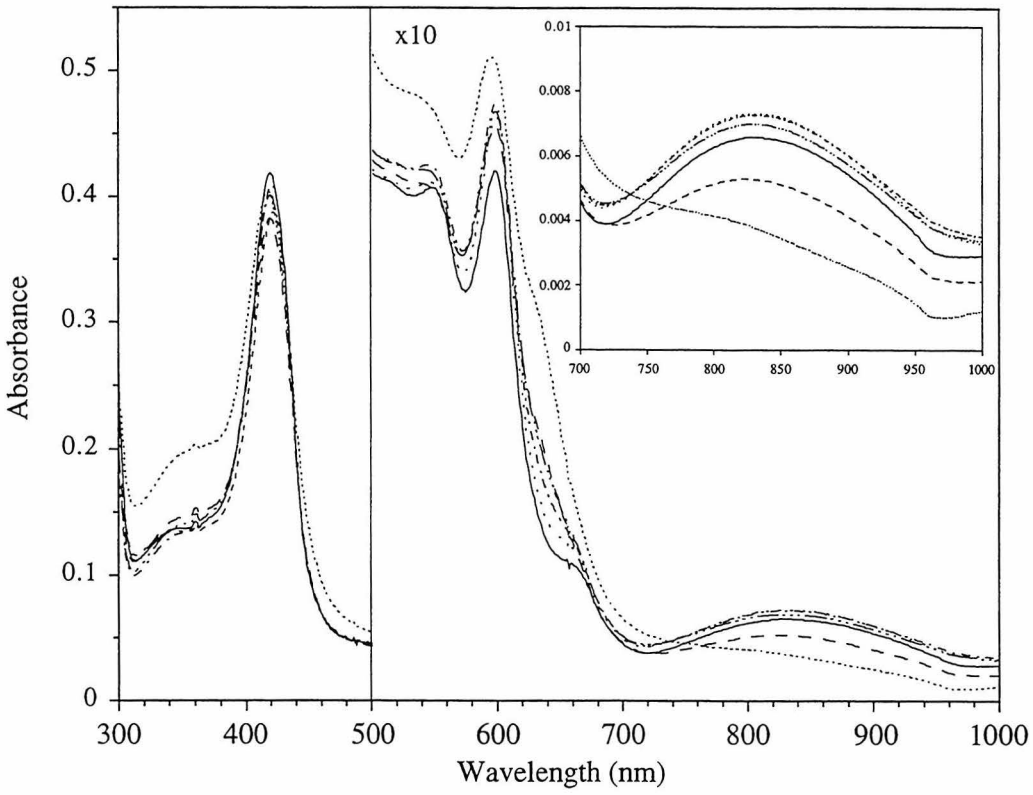

Figure 4.7 UV-Visible absorption spectra of the six samples listed in Table 4.1: native (———); subunit III-depleted (- · - · -); 40 h DDM dialyzed (- - - -); subunit III-depleted, 40 h DDM dialyzed (— · · ·); 40 h SB-12 dialyzed (— — — —); SB-12 heat-treated, 40 h SB-12 dialyzed (·····). The protein concentration in each case is 2.5 μM in 25 mM Tris, 0.1% DDM, pH 8.0.

appearance of a small amount of the type-II signal. A substantial type-II copper signal develops upon 40 h dialysis of the CcO complex in SB-12 buffer *without* a 15 min heat-treatment. Typical results of these experiments are tabulated in Table 4.1. The optical spectra shown in Figure 4.7 reveal that there is very little perturbation to the 830 nm absorption band except in the case of the SB-12 treated samples. In general, the 830 nm absorption intensity diminishes roughly according to time in contact with SB-12. No correlation is found, however, between the 830 nm absorption intensity and the appearance of the type-II copper signal. In fact, a substantial type-II copper signal is seen for the subunit III-depleted, 40 h DDM dialyzed enzyme yet no diminution of the 830 nm absorption intensity is apparent. As shown in Figure 4.8, the type-II copper signal is

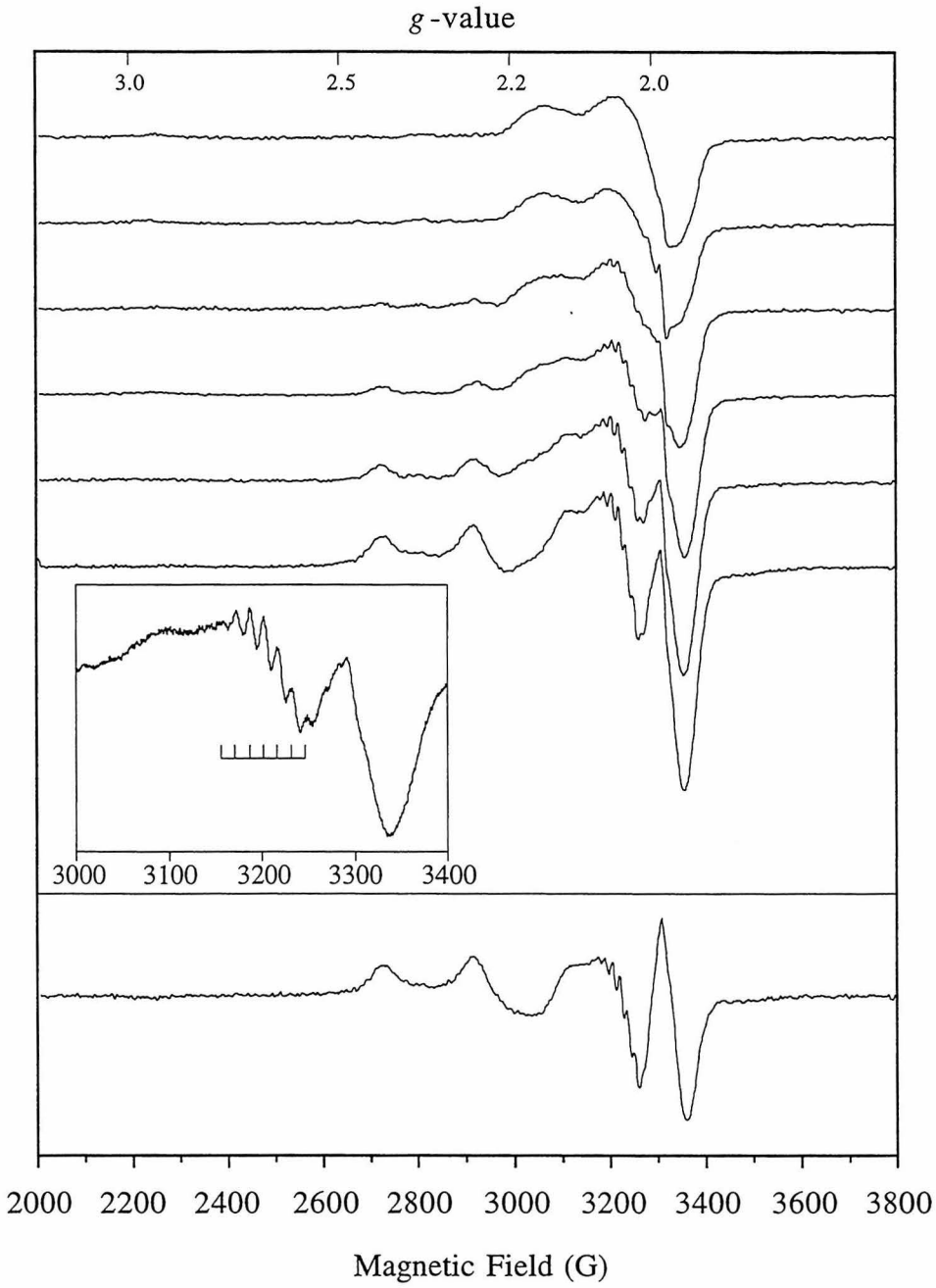

Figure 4.8 The EPR spectra at 80 K of the six samples listed in Table 4.1. From top to bottom: native; subunit III-depleted; 40 h DDM dialyzed; subunit III-depleted, 40 h DDM dialyzed; 40 h SB-12 dialyzed; SB-12 heat-treated, 40 h SB-12 dialyzed. Spectra are scaled to protein concentration based on the pyridine hemochrome method. The inset shows the seven-line hyperfine pattern for the SB-12 heat-treated, 40 h SB-12 dialyzed enzyme. The bottom panel shows the difference spectrum between the SB-12 heat-treated, 40 h SB-12 dialyzed and the native samples. Spectrometer settings are the same as in Figure 4.5 except for a modulation amplitude of 5 G for the inset spectrum (average of two scans).

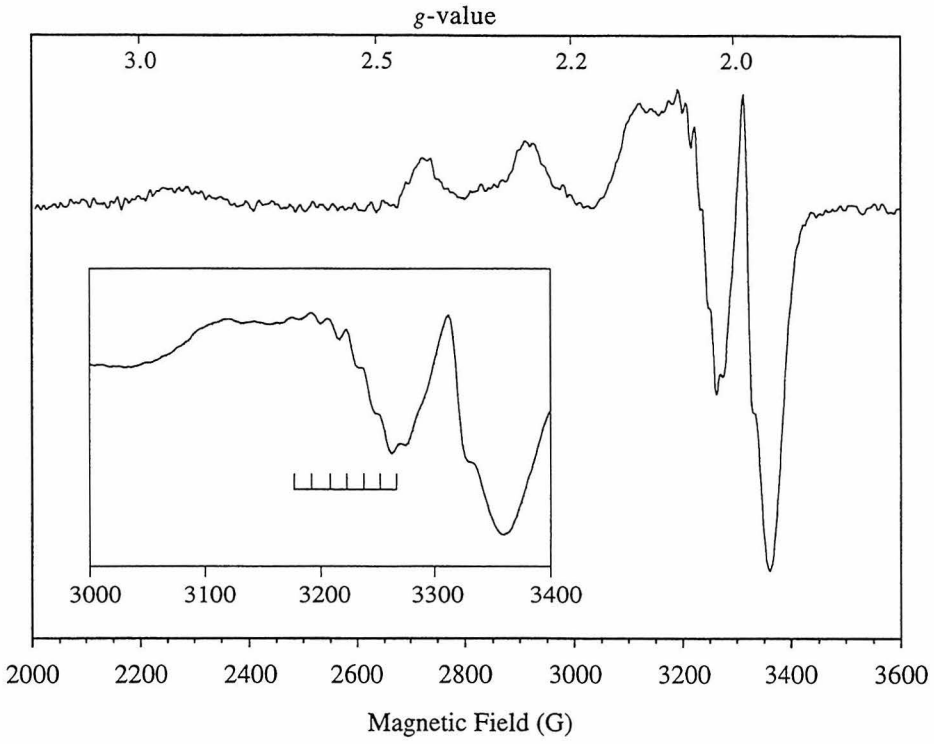

Figure 4.9 The EPR spectrum at 80 K of the as-isolated cytochrome bo_3 complex. Spectrometer settings are the same as in Figure 4.5 except for a time constant of 64 ms (average of 16 scans). Compare with Figure 4.8.

characterized by a $g_{||}$ of about 2.19, an $A_{||}$ of about 190 G and a seven-line hyperfine pattern at $g_{\perp} = 2.06$ with a splitting of about 15 G.

Figure 4.9 shows the EPR spectrum of the as-isolated UQO complex. The type-II copper signal in this spectrum is characterized by a $g_{||}$ of 2.19, an $A_{||}$ of about 190 G, and a seven-line hyperfine pattern at $g_{\perp} = 2.04$ with a splitting of about 15 G. At liquid helium temperatures, substantial high-spin heme signal is present (data not shown) indicating that the heme o_3-Cu_B binuclear center is magnetically uncoupled.

^{1}H ENDOR

The 35 GHz continuous-wave (CW) ^{1}H ENDOR spectrum of the SB-12 heat-treated, 40.5 h SB-12 dialyzed CcO complex taken in the $g_{||}$ region of the type-II copper center shows a doublet centered at the proton Larmor frequency ($\nu_H \approx 46.3$ MHz) and split by a

hyperfine coupling constant ($A_{\|}$) of about 10 MHz (Figure 4.10A) as predicted by equation 4.2. This proton, which is not seen for the native enzyme (Figure 4.4), is not associated with the hemes because the hyperfine-split doublet vanishes when the spectrum is taken outside the type-II copper EPR envelope. In addition, the proton ENDOR signals associated with the Cu_A center are still present and remain unperturbed throughout the Cu_A EPR envelope indicating this site remains intact under the experimental conditions (data not shown). The proton ENDOR spectrum is very similar to that reported by Fann and coworkers[249] for the Cu_B site of the cytochrome aa_3-600 ubiquinol oxidase complex isolated from *Bacillus subtilis* (Figure 4.10B). In the case of the *Bacillus* enzyme, this strongly coupled proton ($A_{\|} \approx 10$ MHz) is solvent exchangeable and is consistent with a bound hydroxide anion.

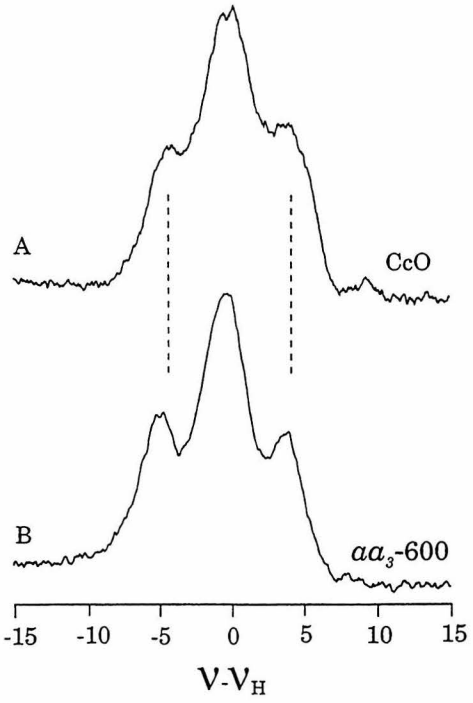

Figure 4.10 Comparison of ^{1}H ENDOR spectra of the CcO complex (*top*, 35.04 GHz, $g_{\|} \approx 2.20$) and the *B. subtilis* cytochrome aa_3-600 ubiquinol oxidase complex (*bottom*, 35 GHz, $g_{\|} \approx 2.23$). Both spectra show a hyperfine-split doublet centered at the proton Larmor frequency. Experimental conditions: modulation amplitude, 0.6 G; scan rate, 1 MHz/s; temperature, 2K (average of 50 scans). The aa_3-600 ubiquinol oxidase spectrum is reproduced from Fann and coworkers.[249]

^{14}N ENDOR

Figure 4.11 shows the ENDOR spectra of the SB-12 heat-treated, 40.5 h SB-12 dialyzed CcO complex taken in the $g_{\|}$ and $g_{\perp}$ regions with the frequency range expected for ^{14}N ligands coordinated to copper. Each ^{14}N ligand should give ENDOR patterns as described in equation 4.1. In the $g_{\|}$ spectrum (Figure 4.11, top), ENDOR peaks with frequencies greater than 10 MHz can be assigned to ν_+ branches of three ^{14}N ligands,

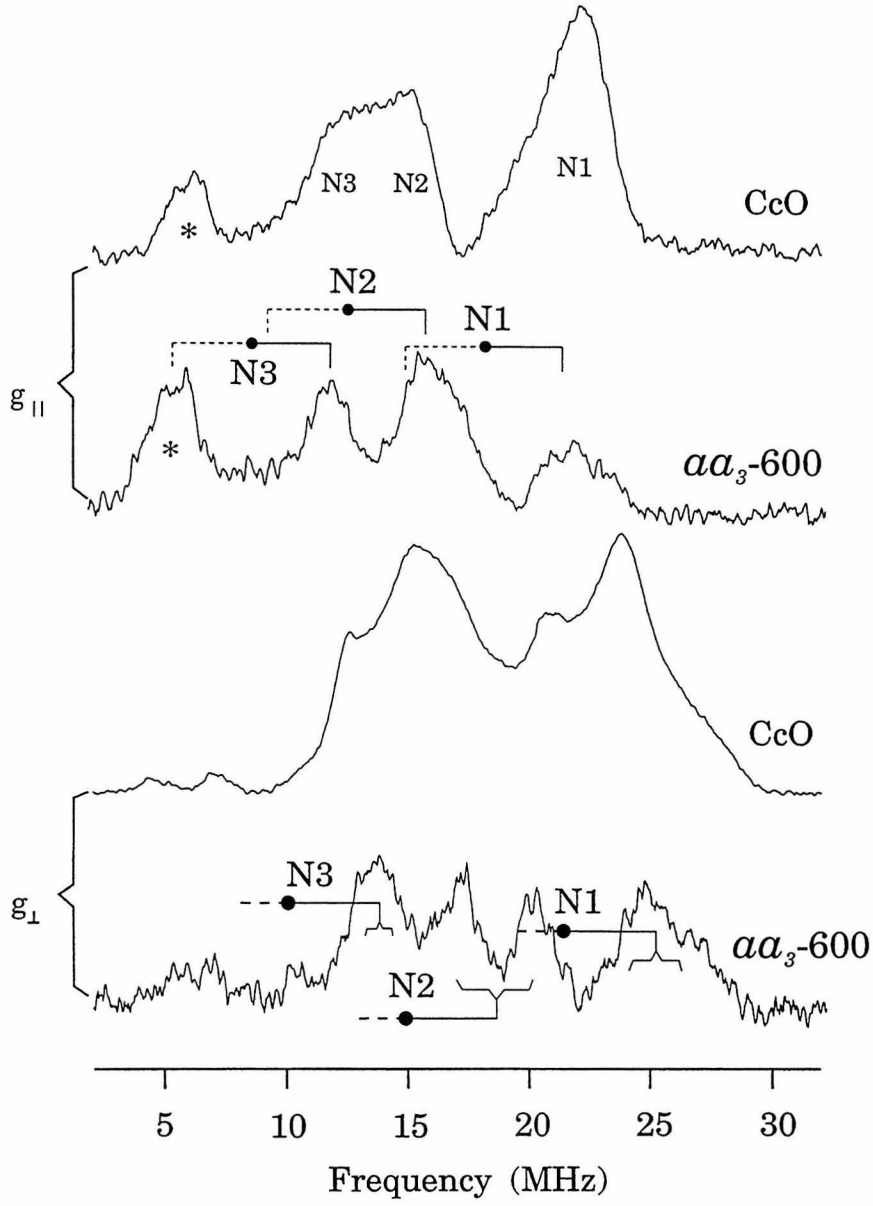

Figure 4.11 Comparison of ^{14}N ENDOR spectra of the CcO complex (35.04 GHz, $g_{\|} \approx 2.22$, $g_{\perp} = 2.04$) and *B. subtilis* cytochrome aa_3-600 ubiquinol oxidase complex (35.2 GHz, $g_{\|} \approx 2.23$, $g_{\perp} = 2.05$). Experimental conditions are the same as for Figure 4.10 except: modulation amplitude 2.5 G (CcO)/1.25 G (aa_3-600); scan rate, 2 MHz/s. The aa_3-600 ubiquinol oxidase spectra are reproduced from Fann and coworkers.[249]

denoted as N1, N2, and N3, with hyperfine couplings ($A_{||}$) of 38, 24, and 17 MHz, respectively. No quadrupole splittings were resolved. The resonance at 7 MHz (marked with a *) is associated with heme nitrogens as the signal persists outside the type-II copper EPR envelope. As the field increases from $g_{||}$ into the Cu_A region ($2.2 < g < 1.94$), the ^{14}N ENDOR pattern becomes more complicated as the ^{14}N signals observed arise from both the native Cu_A center as well the type-II copper site (Figure 4.11, bottom). However, the ^{14}N ENDOR taken at $g_{||}$ clearly shows three peaks from three distinct nitrogens and these ^{14}N ENDOR signals can be unambiguosly tracked in the field-dependent ENDOR spectra taken across the EPR envelope of the type-II copper center. Hyperfine couplings ($A_{\perp}$) of 40, 32, and 24 MHz are estimated for the three nitrogen ligands denoted N1, N2, and N3, respectively. The ^{14}N ENDOR spectra acquired in both the $g_{||}$ and $g_{\perp}$ regions yield very similar hyperfine coupling constants to those observed for the Cu_B center of the *B. subtilis* cytochrome aa_3-600 ubiquinol oxidase complex.[249] The ^{14}N ENDOR spectra from this ubiquinol oxidase and those

Table 4.2 ^{14}N Hyperfine Coupling Constants (in MHz) for the Type-II Copper Center in the SB-12 Heat-treated CcO Complex and for Cu_B of the *B. subtilis* Cytochrome aa_3-600 Ubiquinol Oxidase Complex*

		N1	N2	N3
cytochrome *c* oxidase complex	$A_{||}$	38	24	17
	$A_{\perp}$	40	32	24[a]
cytochrome aa_3-600 complex	$A_{||}$	37	25	17
	$A_{\perp}$	42	31	20

* Uncertainty in A: ± 3 MHz. Values for the cytochrome aa_3-600 ubiquinol oxidase complex were originally reported by Fann and coworkers.[249]

[a] This value is estimated since the signal overlaps with nitrogens of the Cu_A site.

reported here for the SB-12 heat-treated CcO complex are compared in Figure 4.11. Table 4.2 summarizes the hyperfine coupling constants.

Discussion

The appearance of a type-II copper species as a consequence of SB-12 heat-treatment of the CcO complex has been reported previously by Nilsson and coworkers.[240] In addition, *p*-HMB treatment or incubation with $AgNO_3$ has been found to cause the appearance of this type-II species.[242,243,250] In terms of EPR characterization, the type-II copper species reported here appears to be identical to the one described by these authors. As discussed earlier, this type-II species has been interpreted to result from modification of a mononuclear Cu_A site (Figure 4.1).

The explanation for the appearance of the type-II signal upon SB-12 heat-treatment must be re-evaluated in light of the binuclear nature of the Cu_A center and the data presented here. Two possibilities are considered feasible. The first is that the SB-12 heat-treatment procedure causes disruption of the Cu_A site; the approximate doubling of the copper EPR intensity arises from full oxidation of the two copper ions. The second possibility is that the Cu_A site remains in a native configuration and the magnetic coupling of the heme a_3-Cu_B binuclear center is broken making Cu_B EPR visible. In this scenario, the extra EPR visible copper, all of which appears to be in a type-II configuration, is Cu_B. The strongest evidence in support of the first explanation is the diminution in the 830 nm absorption intensity, which is believed to arise predominantly from the Cu_A center,[55] upon SB-12 heat-treatment of the enzyme. It has been found here, however, that the type-II EPR signal can be created without any apparent loss in the 830 nm absorption intensity (Figure 4.7). In addition, ^1H and ^{14}N ENDOR spectroscopy reveals that the Cu_A resonances are present when a stoichiometric amount of the type-II copper species is EPR detectable. Instead, three additional ^{14}N ENDOR resonances are detected (Figure 4.11). The seven-line hyperfine pattern in the $g_\perp$ region of the EPR

spectrum (Figure 4.8) is consistent with three approximately equivalent nitrogen ligands. The excellent agreement between the hyperfine coupling constants of the type-II center described here and those for the Cu_B center of the *B. subtilis* cytochrome aa_3-600 ubiquinol oxidase complex (Table 4.2), which does not contain a Cu_A center, allows confident assignment of the three new nitrogen ENDOR resonances as Cu_B histidines. Finally, the EPR spectrum of the as-isolated UQO complex contains the identical type-II copper species that results upon SB-12 heat-treatment of the CcO complex. As this enzyme also does not contain a Cu_A center but is otherwise structurally similar to the CcO complex (Chapter 1), and, in this particular sample, the heme o_3-Cu_B binuclear center is magnetically uncoupled, these data provide strong confirmation that the type-II signals that appear as a result of the various CcO treatments discussed here do indeed arise from Cu_B. The changes in the resonance Raman spectrum of heme a_3 when the type-II copper signal is apparent in the CcO EPR spectrum are now more easily understood.[240,251] The perturbations that uncouple the heme a_3-Cu_B binuclear center and make Cu_B EPR detectable also disrupt the heme a_3 pocket. The approximate isosbestic points (Figure 4.6) as the type-II signal grows in provide a good indication that there is only one process occurring during the SB-12 heat-treatment procedure, namely, the uncoupling of the heme a_3-Cu_B binuclear center (In the $g = 2$ region, there is no clear isosbestic point most likely due to the sensitive nature of the high spin heme contributions).

Given that the type-II EPR signal seen arises predominantly from Cu_B, it is important to ask to what extent the structural integrity of the Cu_B redox site is preserved. Cline and coworkers[37] report an EPR spectrum of Cu_B obtained by full reduction of the enzyme, flushing with O_2 and quick freezing in liquid N_2. This spectrum is characterized by a $g_{||}$ of about 2.28, and an $A_{||}$ of about 100 G. Photolysis and freezing of the fully-reduced CO-bound CcO complex in the presence of oxygen has been found to yield a type-II copper signal with a $g_{||}$ of 2.28 and an $A_{||}$ of 102 G.[244] High pH causes the appearance of

a type-II species with a $g_{\|}$ of 2.30 and and $A_{\|}$ of 136 G.[245] Addition of cyanide to the *Thermus thermophilus* cytochrome ba_3 complex produces a type-II copper species with a $g_{\|}$ of 2.28 and an $A_{\|}$ of about 140 G.[252,253] These spectra contrast with the type-II signal obtained by SB-12 heat-treatment which has a larger $A_{\|}$ (~ 190 G) and a smaller $g_{\|}$ (~ 2.19). As harsher treatments tend to result in larger $A_{\|}$ values, the indication is that the structural integrity of the Cu_B site has been perturbed in the experiments described here. A small perturbation to the heme a_3-Cu_B site clearly must have occurred to break the magnetic coupling in this binuclear center. The structural perturbations likely explain, at least in part, the lower dioxygen reduction activity of the enzyme when the type-II signal is observed. Both the SB-12 heat-treated CcO complex and the cytochrome aa_3-600 complex have a strongly coupled proton with an $A_{\|}$ of about 10 MHz (Figure 4.10). In the case of the cytochrome aa_3-600 complex, this proton is solvent exchangeable and has been tentatively assigned as arising from a bound hydroxide anion.[249] A hydroxide anion could certainly be the fourth ligand for the type-II copper site reported here.

The finding that SB-12 heat-treatment makes Cu_B EPR detectable raises the issue of which copper ions give rise to the type-II signals seen upon $AgNO_3$ or *p*-HMB treatment.[242,243,250] Since ENDOR experiments have not been attempted on such enzyme samples, a definitive conclusion cannot be made here. It is certainly possible that these treatments affect the Cu_A site exclusively since they are thiol specific reagents. Gelles and Chan[250] observed an approximate 40% increase in copper EPR intensity upon *p*-HMB treatment of the enzyme. This observation is consistent with a scenario where the type-II copper signals arise from Cu_B due to perturbations similar to those caused by SB-12 heat-treatment. On the other hand, disruption of the Cu_A center and oxidation of the cuprous copper would also result in a similar increase in the integrated EPR intensity.

While the ENDOR data reveal the presence of native Cu_A resonances in the presence of stoichiometric amounts of type-II copper, the possibility that a substoichiometric population of Cu_A sites have been perturbed cannot be ruled out. The creation of a small

amount of a type-II copper species from severe disruption of the Cu_A ligation structure would be undetectable in the EPR and ENDOR spectra due to the strong signals arising from the Cu_B center. The diminution in the 830 nm absorption intensity and the slightly larger than stoichiometric increase in the integrated intensity of the copper EPR signals are consistent with this possibility.

On the other hand, less drastic perturbations to the Cu_A site could occur. Li and coworkers[241] found that heat-treatment in DDM results in substoichiometric populations of both type-I and type-II copper species. Zickermann and colleagues[254] have recently found that mutation of the weakly coordinating methionine of the binuclear Cu_A center (Figure 1.5) to isoleucine results in a type-I copper EPR spectrum ($g_{\|} = 2.18$, $A_{\|} = 61$ G) and loss of 830 nm absorption intensity. These data suggest that a type-I species could result in the native enzyme through dissociation of the weak Met-Cu bond and upon lengthening of one of the Cu-S bonds as shown in Figure 4.12. As a result of this conformational rearrangement, one of the copper atoms would have a type-I structure (one His, one Cys, one carbonyl and a long Cu-S bond). The other copper atom would have a high reduction potential due to the two strongly coordinating cysteines, and therefore, would become completely reduced with the electron initially shared by the two atoms. As only the type-I-like copper would be EPR visible, the EPR integration would remain constant. The loss in 830 nm absorption intensity reported here for some samples may result from a Cu_A rearrangement of this type. The associated type-I EPR signals are likely to be difficult to detect in the presence of

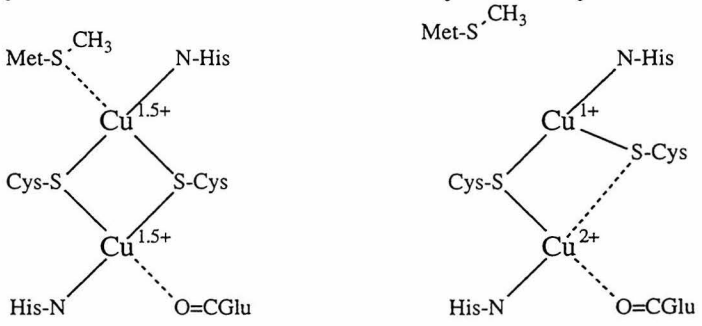

Figure 4.12 (*left*) Schematic of the binuclear nature of the Cu_A site as revealed by X-ray crystallography.[13,14] The fourth ligand for the lower copper is the main chain carbonyl of a glutamic acid residue. (*right*) Possible perturbation to the Cu_A site that results in the appearance of a type-I EPR signal (lower copper atom) and loss in 830 nm absorption intensity. See text for details. Solid lines denote strong bonds; dashed lines denote weak ligation.

strong type-II signals and need not be identical to those resulting from the methionine mutation structure.[254] The well-known interaction potentials in the CcO complex[6] implies conformational interaction between redox centers. Therefore, the disruption of the heme a_3-Cu_B binuclear site that produces a type-II signal could potentially, under some conditions, perturb the methionine of the Cu_A center resulting in loss of 830 nm absorption intensity. In fact, during enzyme turnover, the Cu_A reduction potential could be modulated through allosteric interactions between the heme a_3-Cu_B binuclear site and the Cu_A methionine.

To summarize, the Cu_B center undergoes a small structural modification and becomes EPR detectable upon SB-12 heat-treatment. It is *not* assumed that the thiol specific reagents $AgNO_3$ and *p*-HMB, both of which cause the appearance of a type-II copper species, affect the CcO complex in the same manner. However, it is feasible that the type-II species resulting from treatment with these reagents is a perturbed Cu_B site and not a modified Cu_A site. It is possible that SB-12 heat-treatment perturbs a small population of Cu_A sites since this procedure results in a decrease in the 830 nm absorption intensity of the enzyme, perhaps through allosteric interactions with the methionine of the Cu_A site. It has been demonstrated, however, that under some conditions, Cu_B of the fully-oxidized CcO complex is EPR detectable in the form of a type-II copper center.

Concluding Remarks

As mentioned at the beginning of this chapter, the appearance of a type-II copper species in the EPR spectrum of the CcO complex is correlated with loss of proton pumping activity of the enzyme. The goal of the work described here was to more explictly correlate the presumed structural changes at the Cu_A site with loss of this activity. At least in the case of SB-12 heat-treatment, the appearance of a type-II copper center is a result of perturbations to the heme a_3-Cu_B binuclear center. This finding raises

the question of whether it is this disruption of the heme a_3-Cu_B binuclear center structure that results in the decreased proton pumping ability. As heat and high detergent concentrations are very non-specific means by which to modify proteins, the protocols utilized here can certainly result in a number of modifications to the CcO complex that would be undetectable by the methods applied thus far. If the thiol specific reagents *p*-HMB and Ag^+ do indeed disrupt the magnetic coupling of the heme a_3-Cu_B binuclear center much like heat-treatment, they certainly react peculiarly with the CcO complex. Unfortunately, then, at this juncture, little can be concluded about the implication of these modification experiments on the role of the Cu_A site in the proton pumping reactions. However, it is clear that the Cu_A site is not as structurally labile as had been previously thought. As the tight coupling between ET and the proton pumping reactions implies that very minor structural changes would be sufficient to completely uncouple the proton pump, it is certainly possibly that minor, undetectable (at least by the methods utilized) structural perturbations to the Cu_A site or in the vicinity of this site are allosteric linked to the appearance of the Cu_B type-II EPR signal. Alternatively, the structural modifications that cause the appearance of the type-II copper signal may be linked to the allosteric coupling between the dioxygen binding site and the linkage site. These possibilities are reasonable since, as discussed in Chapter 2, there must be allosteric communication between the dioxygen binding site and the linkage site for the coupled electron transfer steps.

Chapter 5

The Role of Subunit III in Proton Translocation

It is well established that the CcO complex pumps up to four protons for each molecule of dioxygen reduced resulting in an average stoichiometry of about 1 H^+/e^- (Table 2.1). As a consequence of the thermodynamics of dioxygen reduction, however, proton translocation can only result from the last two electron transfers to the dioxygen binding site (Chapter 2). As a result, the H^+/e^- stoichiometry for these last two electrons is 2. In an attempt to decipher the proton pumping machinery, investigators have modified the CcO complex by various means and determined the functional and structural properties of these altered enzymes. In general, it is found that the average H^+/e^- ratio can vary anywhere from zero to unity (Note that this finding is the strongest experimental argument in favor of a redox-linked proton pump mechanism rather than a redox loop mechanism – see Chapter 2.). Not surprisingly, a number of chemical models of redox linkage have been proposed. These models differ dramatically in the manner in which the exergonic ET is proposed to couple to the endergonic proton pumping reactions. In direct coupling, the ligands of a redox center become protonated and subsequently deprotonated at some point during the oxidation-reduction cycle of the metal. Each of the four metal centers has been proposed to be the site of redox linkage.[44,129,189,190,192,255] A discussion of one of these models will be used to illustrate the important principles of electron and proton gating in the next chapter. Models of indirect coupling have been proposed also.[204,256-258] In indirect coupling, the redox state of the metal centers influences the conformational state of the proton translocating elements at some distant location in the protein. The H^+/e^- ratio of 2 for the pumping electron transfers presents a dilemma with regards to directly coupled models of redox linkage because it is difficult to construct chemically reasonable scenarios in which uptake of two protons at a redox site is required to balance a one-electron reduction reaction. A scenario in which protons are pumped by two different mechanisms, one directly and one indirectly coupled, provides a simple solution to this dilemma.[6]

A number of investigators have raised the possibility that some indirectly coupled

proton translocating elements of the proton pump reside in subunit III.[259-262] It has been known for some time that reaction of the enzyme with dicyclohexylcarbodiimide (DCCD), which modifies Glu^{90} of subunit III (bovine numbering), or removal of subunit III by a variety of methods results in inhibited proton translocation (Table 5.1). There are at least two possible interpretations of these observations. One explanation is that part or

Table 5.1 Inhibited Proton Pumping Activity for Various Modified Forms of the CcO Complex

Cytochrome *c* Oxidase Sample	*maximal % inhibition of proton pumping activity*	Reference(s)
Subunit III-Depleted Enzyme:		
reconstituted beef heart enzyme	30% 40% 45% 50-60% 75% 100%	241 263 264 265 260 266
reconstituted ox heart enzyme	35-90%	267
reconstituted rat liver enzyme	50-85%	262
P. denitrificans enzyme: spheroplasts (deletion mutant)	0%	268
reconstituted two-subunit enzyme	50%	158,195,203
DCCD Modified Enzyme:		
reconstituted beef heart enzyme	45% 60% 65% 75%	269 195,259 194 270,271
rat liver mitochondria	90%	194
reconstituted two-subunit enzyme (*P. denitrificans*)	20%	195

all of the proton translocating elements of the proton pump are located in subunit III. Alternatively, it is possible that all the proton translocating elements of the pump are located in subunits I and II but subunit III plays a role in modulating the allosteric interactions between subunits I and II in order to accomplish the redox linkage and to vary the proton to electron stoichiometry. Haltia and coworkers[268] have prepared mutants of the Glu^{90} residue in subunit III of the *P. denitrificans* CcO complex and have measured the proton pumping activity of these mutants in spheroplasts. These investigators found that the ET and proton pumping activity were unaffected by mutation of Glu^{90} to Gln, Ala, Asp, and Lys. In addition, deletion of the entire subunit III gene resulted in a lower ET activity (5-15% of wildtype) yet the same apparent proton translocation activity. Unfortunately, these investigators were unaware of the complexity of the *Paracoccus* respiratory chain and the fact that there is an alternative cytochrome *b*-containing terminal oxidase complex which translocates protons when operating in conjunction with the cytochrome bc_1 complex.[272] This alternative terminal oxidase complex is likely responsible for the high proton translocation activity observed for the CcO subunit III deletion mutant in light of the low ET activity for this mutant. However, the conclusion that Glu^{90} is not an *intrinsic* element of the CcO proton pump based on the wildtype-like activities of various mutations of this residue is still considered valid. Note, however, that Wu and coworkers[273] recently found that the CcO-dependent ATP synthesis of a few of these Glu^{90} mutants is attenuated therefore indicating that subunit III does play *some* role in energy coupling. It is apparent that further biophysical and biochemical studies are required to decipher the role of subunit III in enzyme turnover, despite the recent crystal structures.

Chadwick and Thomas[274] demonstrated that N-cyclohexyl-N'-(4-dimethylamino-α-napthyl)carbodiimide (NCD-4) can be used as a fluorescent probe for DCCD binding sites in proteins with their work on the sarcoplasmic reticulum (Ca^{2+}+Mg^{2+})-ATPase complex. NCD-4 is a useful probe in that the starting material is non-fluorescent, yet

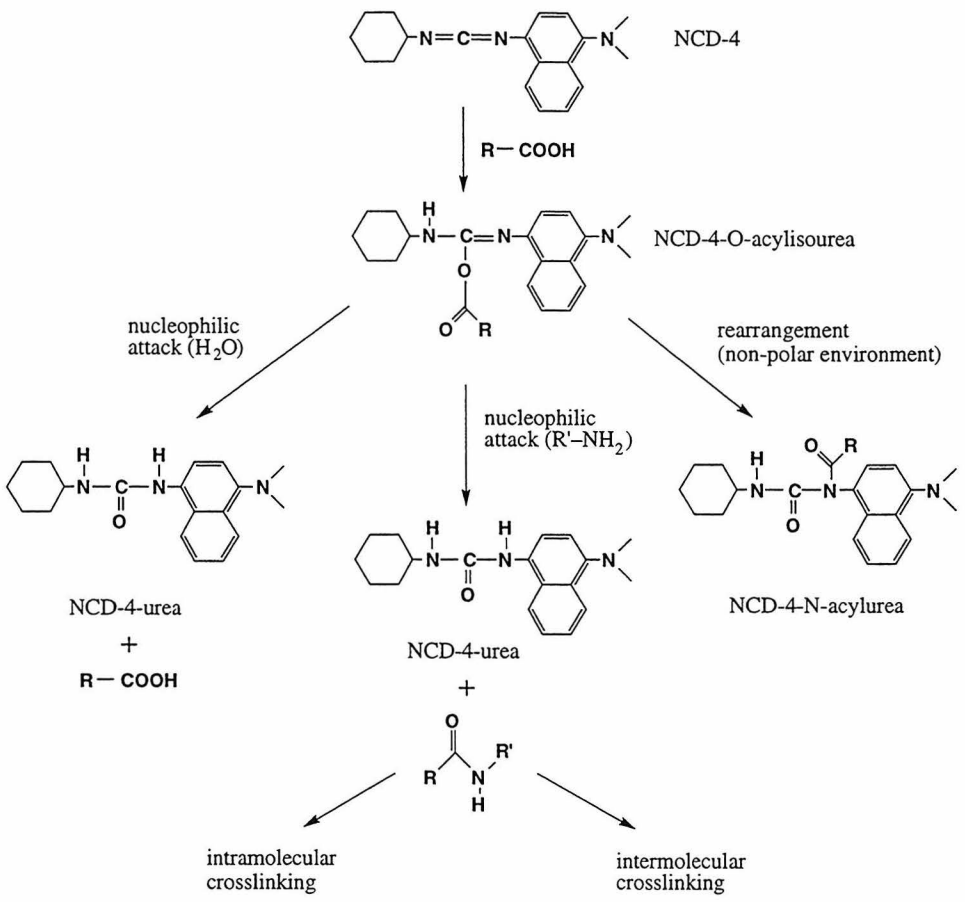

Figure 5.1 Schematic representation of the possible reactions following an initial modification of a single carboxyl group in a protein by NCD-4. Reproduced from Musser and coworkers.[275]

both the protein adduct (an acylurea) and the sideproduct of the reaction (a urea) are fluorescent. These two potential products (Figure 5.1) are readily distinguished by different fluorescent maxima (Table 5.2). Pringle and Taber[276] have used NCD-4 and a series of spin-labeled stearic acids to show that the major carbodiimide binding site on the mitochondrial proton channel of the bovine F_0F_1-ATPase complex is fairly deeply buried within the membrane. In this work, Pringle and Taber assumed a 4-6 Å interaction distance for nitroxide quenching of fluorophores.[277] More recent data by Abrams and London[278] indicate, however, an interaction distance of 11-15 Å for the quenching of fluorophores by spin-labeled lipids. In support of the larger interaction, others have shown that in the case of covalent fluorophore-nitroxide conjugates, the interaction

distance for nitroxide quenching is as large as 12 Å and significant quenching occurs over a separation distance of up to 20 Å.[279,280] Any appreciable quenching of fluorophore-labeled protein complexes by spin-labeled lipids or fatty acids indicates that the fluorescent label is on or near the protein-lipid interface of the membrane spanning region of the enzyme. Since the cross-section of transmembrane helices including the sidechains is on the order of 10 Å, a protein-bound fluorophore quenched by hydrophobic spin-labels could be at most about one transmembrane helix away from this interface.

The goal of the work described below was to apply the Pringle and Taber

Table 5.2 Fluorescence Emission Maxima of NCD-4 Derivatives in Various Solvents at 23°C*

	Emission wavelength (nm)[a]		
NCD-4 derivative	Hexane	Ethanol	Ethanol/H_2O (1:1, v/v)
NCD-4-acetylurea[b]	398	425 (430)[c] $\phi = 0.06$[d]	440
NCD-4-urea	—[e]	460 (467)[c] $\phi = 0.58$[d]	473
O-Phenylisourea[f]	435	452	465

* Adapted from Chadwick and Thomas.[274]
[a] Excitation was at 330 nm.
[b] NCD-4-acylurea is the adduct with the protein (Figure 5.1); NCD-4-acetylurea is the model compound formed by reaction of NCD-4 with acetic acid.
[c] Values in parentheses represent corrected emission maxima.
[d] ϕ = quantum yield.
[e] NCD-4 urea proved too insoluble in hexane for spectral measurements.
[f] Formed by reaction of NCD-4 with phenol.

methodology to locate Glu^{90} of subunit III with respect to the membrane bilayer and the surface of the protein. In order to better delineate the possibility of subunit III as an allosteric effector, it is certainly necessary to obtain some idea of the location of Glu^{90} within the protein as a whole. As the location of Glu^{90} determined by these fluorescence studies was confirmed by the recent crystal structures, the description of these experiments will be brief (this work is described in full by Musser and coworkers[275]). Instead, the focus of this discussion will be the possible function of subunit III in light of the data now in hand.

Experimental Procedures

Materials

The beef heart CcO complex was isolated by the method of Hartzell and Beinert.[247] Enzyme concentrations were determined by using the reduced-minus-oxidized difference spectrum at 605 nm ($\Delta\varepsilon_{605}^{red\text{-}ox}$ = 24 mM^{-1} cm^{-1}) using sodium dithionite as the reductant. Enzyme preparations were stored at -80°C in 25 mM K-phos, pH 7.8 and 0.5 or 0.1% Brij-35 until ready for use. The native CcO complex had a turnover number (turnover number = $\upsilon/[E_{total}]$) of 390 s^{-1} in 10 mM K-phos, 100 mM KCl, 0.05% DDM, pH 6.0 with an initial ferrocytochrome *c* concentration of 50 μM.

Unless otherwise described below, chemicals were reagent grade, were obtained from commercial suppliers and were used without further purification. NCD-4 and 5-, 7-, and 12-DOXYL-stearic acids were obtained from Molecular Probes; 10-DOXYL-stearic acid and TEMPO were from Aldrich; and 16-DOXYL-stearic acid was from Molecular Probes or Aldrich. Carbonyl cyanide, *m*-chlorophenyl hydrozone (CCCP) was obtained from Calbiochem; cytochrome *c* (type VI), and 4-amino-TEMPO were from Sigma; valinomycin was from Sigma or Calbiochem. Lipids from Sigma were as follows: bovine heart cardiolipin (CL); synthetic dioleoyl L-α-phosphatidyl-choline (PC), approximately 99% pure; and synthetic dioleoyl L-α-phosphatidylethanolamine (PE),

approximately 99% pure. Cholic acid (Sigma) was twice recrystallized from water:ethanol (1:1, v/v) and stored at 8°C and pH 7.6 as a 20% stock solution of the potassium salt. DEAE Bio-gel was from Bio-rad; DE-52 beads were from Whatman; and Sephadex G-25 and G-100 were from Sigma.

Spectroscopic Methods

Optical absorption spectra and kinetic measurements were obtained with a Hewlett-Packard 8452 diode array UV/Vis spectrophotometer. X-band EPR spectra were recorded using the Varian E-line Century Series spectrometer described in Chapter 4; protein samples were at liquid nitrogen temperature (finger dewar) and spin-labels were at room temperature. Steady-state fluorescence spectra were recorded on an SLM 4800 spectrofluorimeter equipped with a SMC-210 monochromater controller and SE-480-485 electronics (SLM Instruments) which were interfaced to an IBM XT computer. Scattering data was obtained at 90° to a Spectra-Physics series 2000 Argon laser beam (488 nm) using a Malvern System 4700c sub-micron particle analyser interfaced to a Malvern PC 6300.

NCD-4 Modification of the CcO Complex

The NCD-4 modified CcO (NCD-4-CcO) complex was prepared as follows. To a 5 μM solution of the CcO complex in 10 mM K-phos, 0.1% Brij-35, pH 7.4 was added a 100-fold molar excess of NCD-4 from a 100 mM ethanol stock solution. The mixture was incubated at 8°C for 18 or 24 h and then centrifuged at 20,000 × *g* for 10 min to remove the precipitated urea. The supernatant was concentrated to about 100 μM using Centricon-100s (Amicon). The concentrated NCD-4-labeled protein was then applied to a DEAE or DE-52 column equilibrated with 10 mM K-phos, 0.1% Brij-35, pH 7.4 (low salt). After washing with this buffer (to remove the NCD-4-urea), the salt concentration was increased to 100 mM KCl (high salt) for elution of the protein. The protein was

concentrated (as above), diluted to remove 90% of the KCl, and concentrated again, the final concentration being accurately determined using $\Delta\varepsilon_{605}^{red\text{-}ox} = 24\ mM^{-1}\ cm^{-1}$. For the DCCD inhibition experiments, the enzyme was first incubated with a 100- or 500-fold molar excess of DCCD (from a 100 mM ethanol stock solution) for 18 h at 8°C; after the addition of a 100-fold molar excess of NCD-4, the incubation was continued for another 18 h. Removal of dicyclohexylurea and NCD-4-urea was accomplished by anion exchange chromatography as described above.

NCD-4 labeled subunits were determined by SDS-PAGE as described in Chapter 4 except that an LKB2001 vertical electrophoresis unit was used. Gels were first photographed under UV illumination to observe the NCD-4 fluorescence; staining with Coomassie Blue allowed identification of the subunits.

Reconstitution of the CcO Complex

CcO vesicles (COVs) were formed by the cholate dialysis technique.[281] PC:PE:CL lipid mixtures (2:2:1, w/w) were brought to near dryness under a stream of nitrogen and residual solvent was removed by vacuum desiccation overnight. The dried lipids were made to a concentration of 25 mg/ml in 93 mM K-phos, 1.5% K-cholate, pH 7.4 and sonicated to clarity using a model W-375 tip sonicator from Heat Systems-Ultrasonics, Inc. After cooling for 10 min, 3.5 ml of the sonicated lipids were mixed with the CcO complex and 100 mM K-phos, pH 7.4 to a final volume of 5.0 ml and a CcO concentration of 2 μM. The protein-lipid solution was then incubated on ice for 15 min and thereafter centrifuged at 20,000 × *g* for 30 min at 8°C. The supernatant was dialyzed (Spectra/Por 4 dialysis tubing; 12-14 kDa cutoff) for at least 22 h at 8°C against 75 volumes of 100 mM K-phos, pH 7.4 with three changes of buffer. After dialysis, the vesicles were centrifuged at 20,000 × *g* for 40 min at 8°C, and the supernatant was stored at 8°C until use.

Respiratory control ratios (RCRs) of the COVs were determined as follows.

Cytochrome *c* stock freshly reduced with sodium dithionite was passed through a 1.5 × 16 cm Sephadex G-25 column equilibrated with 1 mM K-phos, pH 7.4 to remove the excess dithionite. The activity of the COVs was monitored by following the cytochrome *c* absorption at 550 nm as a function of time after the addition of 4 µl vesicles to a 2 ml solution of 40 µM ferrocytochrome *c*, 8 µM CCCP, 7 µM valinomycin and 1 mM K-phos, pH 7.4 in a stirred cuvette. The initial slope was determined and compared with that of an equivalent kinetics run with no ionophores to give the RCR. Typical RCRs for the COVs were between 2 and 3; respiratory control was almost completely lost in the case of the NCD-4-CcO vesicles (NCD-4-COVs). Such low respiratory control was most likely due to leaky vesicles. Light scattering experiments indicate that the vesicles had an average diameter of 40 to 70 nm. No evidence for particles in the 4.5-20 nm range was found thus indicating the absence of enzyme in a micellar phase. While respiratory control was poor for these vesicles, it was found necessary to utilize purified synthetic lipids to reduce contaminating fluorescence from impurities found in a more conventional vesicular system. Using semi-purified phosphatidylcholine, RCRs greater than 5 have been obtained using the identical reconstitution procedure.

Fluorescence Quenching

Fluorescence emission spectra of the NCD-4-COVs and COVs were obtained by exciting the sample at 320 nm and scanning from 350-550 nm. All bandwidths were 8 nm. Vesicles (50-200 µl) were brought to 1 ml with 100 mM K-phos, pH 7.4 and the emission spectra were recorded. Quenchers were added from a stock solution and emission spectra were recorded about 30 s after the addition of quencher. Difference spectra were computed from the fluorescence of NCD-4-COVs and COVs observed under identical conditions to obtain the NCD-4-CcO fluorescence spectra in the absence or presence of quencher. For comparison of NCD-4 quenching efficiencies, spectra were

integrated from 400-550 nm.

Spin-labeled stearic acid stock solutions were made approximately 100 mM in ethanol. First derivative EPR spectroscopy was used to determine the relative concentrations of spin-labels in these stock solutions as follows. First derivative EPR spectra were taken of three different aliquots of all stock solutions. Peak to trough heights of the middle band were assumed to be proportional to the concentration of spin-label and an average height was determined for each of the stearic acid stock solutions. The average height over all spin-labels was assumed to correspond to 100 mM, and this intensity was used to determine the concentration of each spin-label stock solution. In ethanol solution, all of the DOXYL nitroxides used should have similar EPR linewidths so the spin concentration can be determined from the height of the central line. The concentration of the 4-amino-TEMPO stock solution was determined by comparison of its EPR signal with that of an accurately made TEMPO stock solution. All spin label solutions were stored at -80°C until use. Potassium iodide solutions were prepared immediately before use. The NCD-4-acetylurea model compound was synthesized by reaction of NCD-4 with acetic acid as described by Chadwick and Thomas.[274]

Results

NCD-4 Labeling of the CcO Complex

Incubation of NCD-4 with the CcO complex can potentially yield two fluorescent products with overlapping fluorescence spectra, an NCD-4-acylurea and NCD-4-urea (Figure 5.1). According to Chadwick and Thomas,[274] the quantum yield of fluorescence of NCD-4-urea is about ten times greater than that of NCD-4-acylurea, the adduct formed with the protein (Table 5.2). The NCD-4-urea therefore interferes with attempts to monitor quenching of the fluorescence from the labeled protein. This problem is accentuated by the fact that a 100-fold molar excess of NCD-4 is required to obtain

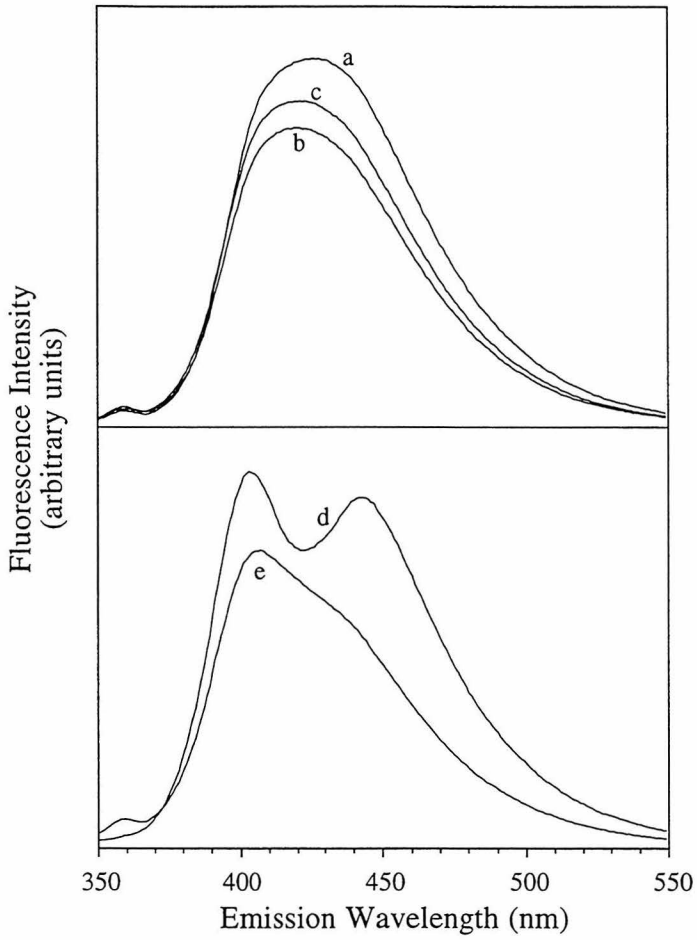

Figure 5.2 Fluorescence spectra of the NCD-4-CcO complex following various levels of purification: (a) after a 1.5 × 15 cm G-100 column; (b) after a 1.5 × 15 cm G-100 column and 16 hr dialysis; (c) after two 1.5 × 15 cm G-100 columns and 16 hr dialysis; (d) after a 50 ml wash on a DEAE column; and (e) after a 200 ml wash on a DEAE column. The fluorescence maximum of the NCD-4-protein adduct occurs at about 405 nm and the NCD-4-urea has an emission maximum at about 445 nm. All emission spectra were obtained in 10 mM K-phos, 0.1% Brij-35, pH 7.4 with an excitation wavelength of 320 nm. The small peak at about 360 nm is a Raman band of water. Reproduced in modified format from Musser and coworkers.[275]

sufficient labeling of the protein and this excess results in a great deal of the undesired urea. Some of this NCD-4-urea is easily removed since it has a low solubility and precipitates out of solution. The remaining NCD-4-urea seems tightly associated with the protein as evidenced by the fact that the residual NCD-4-urea was not removed upon passing the sample through a 1.5 × 15 cm G-100 size-exclusion column. Likewise, there was virtually no loss of NCD-4-urea upon 16 hr dialysis against a 100-fold excess of

detergent-buffer (Figure 5.2A).

On the other hand, almost all of the NCD-4-urea can be removed by applying the modified protein to a DE-52 or DEAE column and washing with about 200 ml of buffer (low salt) before elution (high salt). However, EPR spectroscopy reveals the presence of a type-II copper species as result of this purification procedure (EPR data not shown). This type-II copper species most likely results from perturbations to the heme a_3-Cu_B binuclear center that make Cu_B EPR visible in a manner similar to the modifications discussed in Chapter 4. Decreasing the volume of the wash buffer to about 50 ml limits the amount of this type-II copper species; however, the removal of the NCD-4-urea is incomplete (Figure 5.2B). Interestingly, this remaining NCD-4-urea is lost during the formation of vesicles by cholate dialysis. Reconstitution of the NCD-4-CcO complex without any removal of NCD-4-urea by anion exchange chromatography also yields vesicles devoid of the NCD-4-urea impurity. Thus, the anion exchange chromatography step was either omitted or the NCD-4-CcO complex was washed with only 50 ml buffer on a DEAE column before reconstitution for use in the fluorescence quenching experiments.

SDS-PAGE indicates that NCD-4 labels predominantly subunit III of the CcO complex (Figure 5.3). A small amount of fluorescence from subunits I and IV was sometimes observed; this phenomenon depended on preparation of enzyme and was not investigated further. The fluorescence from subunit III always appeared much bluer than that from subunits I and IV which was yellowish; this yellowish fluorescence was similar in color to the tryptophan fluorescence observed from the native subunit I. The modification of subunits I and IV by NCD-4 thus appears minimal.

DCCD Inhibition of NCD-4 Labeling of the CcO Complex

Reaction of the CcO complex with DCCD before incubation with NCD-4 results in reduced NCD-4-acylurea fluorescence per mole of protein. Using samples treated

identically except for the amount of DCCD added to the solutions, it was determined that a 100-fold excess of DCCD inhibited NCD-4 labeling by about 53%; a 500-fold excess of DCCD inhibited labeling by about 70%. In order to reduce the interfering NCD-4-urea fluorescence, these samples were washed on a DE-52 column with about 200 ml of low salt buffer before elution and the fluorescence spectra were integrated from 400 to 410 nm. SDS-PAGE reveals that NCD-4 labeling of subunit III is inhibited by DCCD (Figure 5.3). A comparison of the fluorescence of subunit III when NCD-4 is reacted with native protein (Figure 5.3 - lane 2) with the subunit III fluorescence resulting from incubation of NCD-4 with DCCD-incubated enzyme (lanes 3 and 4) indicates that DCCD almost completely inhibits NCD-4 labeling of the CcO complex. These DCCD inhibition results strongly suggest that NCD-4 and DCCD modify the identical site on the CcO complex; thus, NCD-4 should be effective as a fluorescence probe of the Glu^{90} DCCD binding site.

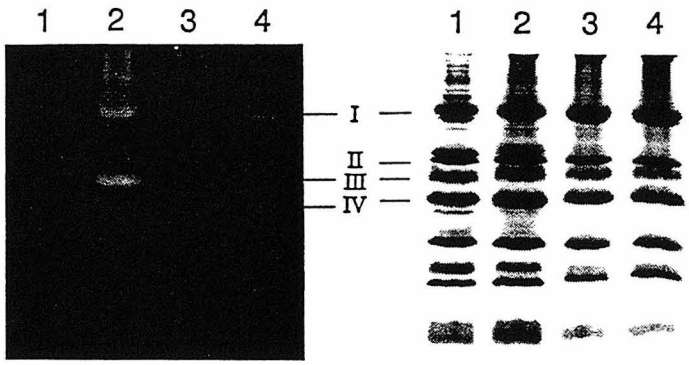

Figure 5.3 SDS-PAGE of NCD-4-CcO: (*left*) fluorescence, (*right*) Coomassie Blue stain. Lane 1, native enzyme; lane 2, enzyme treated with a 100-fold molar excess of NCD-4; lane 3, enzyme treated with a 100-fold molar excess of DCCD before reaction with a 100-fold molar excess of NCD-4; lane 4, enzyme treated with a 500-fold molar excess of DCCD before reaction with a 100-fold molar excess of NCD-4. All samples were depleted of NCD-4-urea before electrophoresis by washing with about 200 ml of low salt buffer on a DE-52 column before elution as described in Experimental Procedures (i.e. fluorescence emission spectra of samples like that of Figure 5.2e). In each case, there is 168 μg total protein per lane. Reproduced from Musser and coworkers.[275]

Fluorescence Quenching of NCD-4-COVs

The lipids used for the formation of vesicles were not completely devoid of fluorescent impurities; however, the subtraction of a COV spectrum from an NCD-4-COV spectrum obtained under identical conditions should correct for the

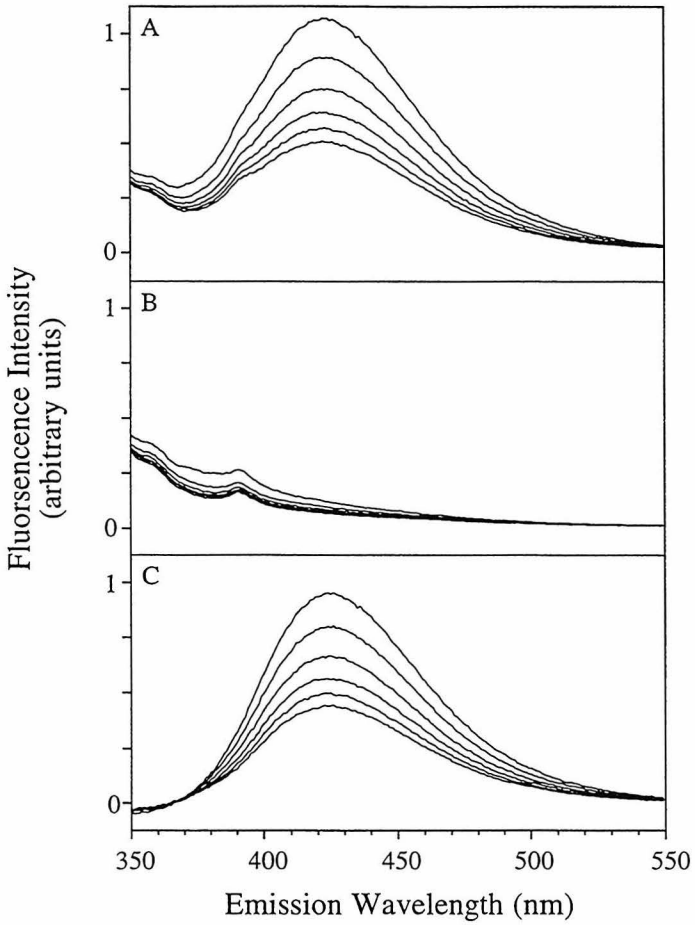

Figure 5.4 Typical fluorescence titration curves of (A) NCD-4-COVs and (B) COVs with the quencher 12-DOXYL-stearic acid (0-716 μM). The lipid concentration was 2.19 mg/ml. (C) depicts the set of difference spectra (A – B), assumed to be the pure NCD-4-CcO fluorescence spectra, used to calculate the quenching efficiencies at the various quencher concentrations. Reproduced in modified format from Musser and coworkers.[275]

contribution of these impurities to the emission spectrum resulting in a pure NCD-4-CcO spectrum (Figure 5.4). The fluorescence of the reconstituted NCD-4-CcO complex is quenched by 12-DOXYL-stearic acid, TEMPO and 4-amino-TEMPO as shown in Figure 5.5. The chemical structures of these quenchers are shown in Figure 5.6. As 12-DOXYL-stearic acid partitions preferentially into the membrane bilayer (the partition coefficient is 10^3-10^4)[275] and 4-amino-TEMPO is highly water soluble, these data dramatically indicate that the NCD-4 probe is bound to the membrane spanning portion

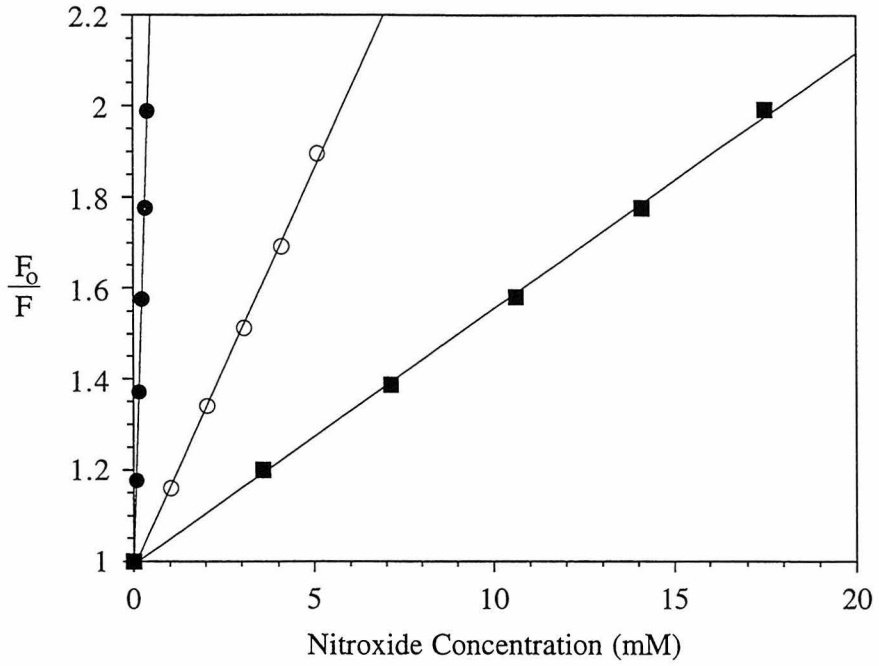

Figure 5.5 Quenching of the NCD-4-CcO complex by 12-DOXYL-stearic acid (filled circles), TEMPO (open circles), and 4-amino-TEMPO (filled squares). The data are fitted according to the Stern-Volmar equation, $F_0/F = (1 + K_{sv}[Q])$, where F_0 is the fluorescence in the absence of quencher, and F is the fluorescence at a given quencher concentration, [Q]. Reproduced in modified format from Musser and coworkers.[275]

of the CcO complex.

Discussion

N-(2,2,6,6-tetramethylpiperidyl-1-oxyl)-N'-cyclohexylcarbodiimide (NCCD), a spin-label analog of DCCD, has been used previously to probe the DCCD binding site[270,282] on subunit III of the CcO complex suggesting that NCD-4 would label also at this site. The inhibition of NCD-4 labeling of the enzyme by DCCD confirmed this expectation. The NCCD labeling studies indicated that Glu^{90} is located in a fairly apolar environment. This finding is confirmed by two different lines of evidence from the data reported here. Firstly, the λ_{max} of the fluorescence emission by NCD-4-CcO (~ 425 nm) is consistent with the idea that the NCD-4 probe is located in a hydrophobic environment (Table 5.2). Secondly, the use of nitroxide quenchers of dramatically differing

hydrophobicities dramatically demonstrates that the NCD-4 probe is located in a hydrophobic location (Figure 5.5). However, there is additional information gained from use of the NCD-4 probe. Since the interaction distance for fluorophore quenching by nitroxides is at most 15-20 Å,[278-280] the fluorescence quenching data reveal that Glu^{90} is fairly close to the surface of the protein. While a scenario in which Glu^{90} is on the interior face of a transmembrane helix (diameter in excess of 10 Å) in contact with the lipid bilayer is consistent with this data, there is no evidence for major disruption of the helix-helix packing and/or reorientation of the membrane helices to accommodate the bulky label. Thus, these fluorescence quenching data reveal that Glu^{90} is most likely exposed to the lipid milieu. Although no data is presented here, a series of DOXYL-stearic acids was used to further delineate the depth in the membrane at which the NCD-4 probe is located.[275] The assumption made when using this approach is that the stearic acids align themselves with respect to the bilayer so that the position at which the stearic acid chain is labeled can be correlated with the quenching data to yield an estimated depth. In this way, it was estimated that the NCD-4 probe is located about one quarter of the way through the lipid bilayer.

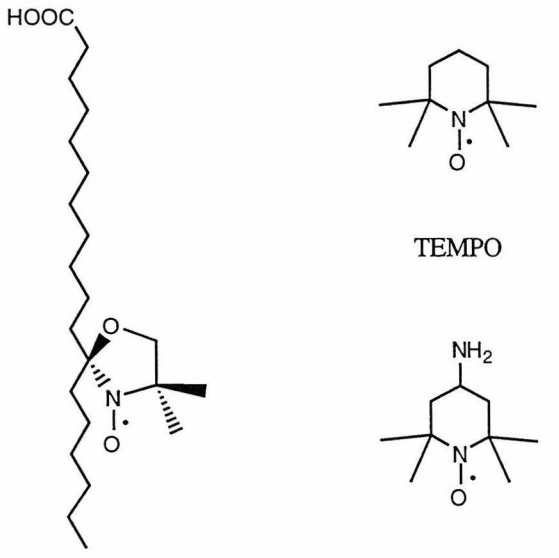

Figure 5.6 Chemical structures of the spin-label quenchers used in the experiments summarized in Figure 5.5.

The appearance of crystal structures[13,14] of the CcO complex provides the rare opportunity to evaluate the accuracy of the methods used to predict the location of the Glu^{90} residue and the subunit III topology as a whole. The location of transmembrane helices are typically predicted using one of a number

of hydrophobicity scales. Musser and coworkers[6] used the Kyte and Doolittle[283] hydrophobicity scale and a window length of 9 residues to predict the transmembrane topology of a "consensus sequence" of subunit III determined from 35 different sequences (Figure 5.7). The seven predicted transmembrane helices are indeed found in the crystal structures and the "register" (i.e. the residues in the helices which are found at the two membrane-aqueous interfaces) of all the predicted helices was surprisingly accurate. In the crystal structures, however, a number of the transmembrane helices are found to extend beyond the transmembrane spanning segments. The Glu^{90} residue is located in the approximate center of helix III in the crystal structures, as predicted on the

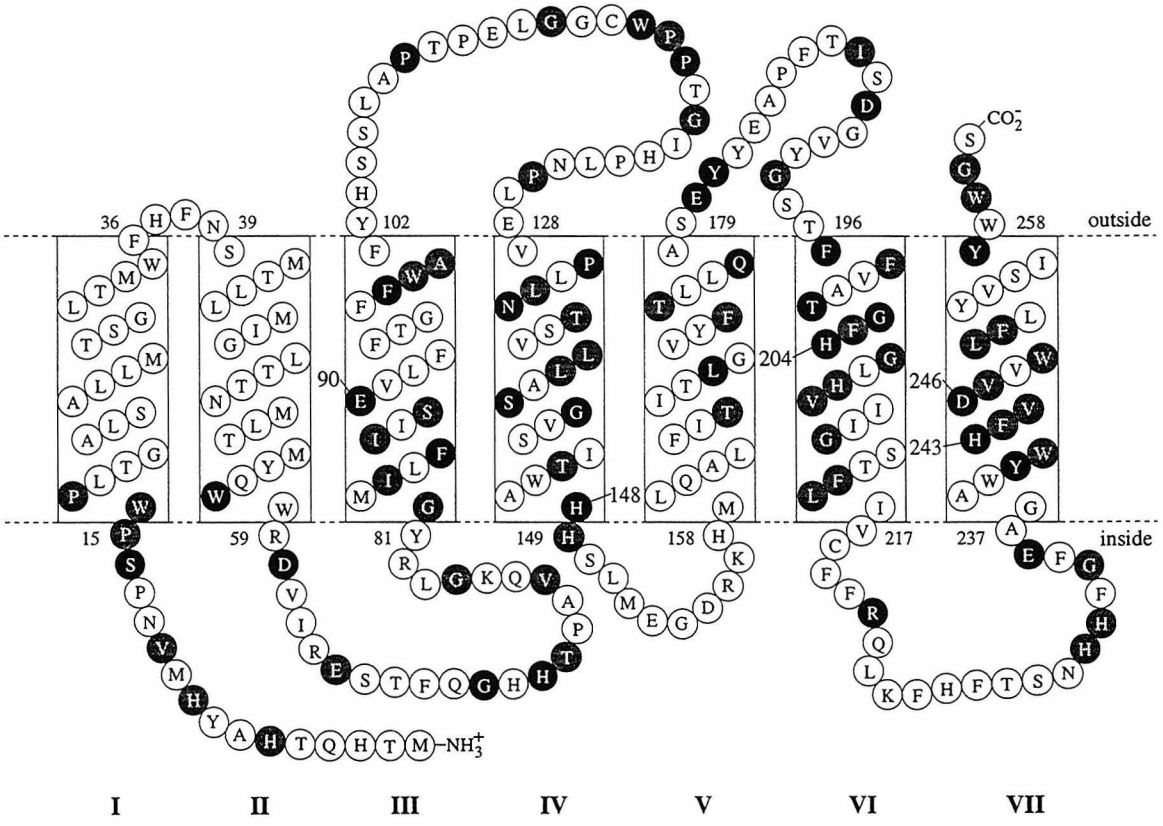

Figure 5.7 Subunit III sequence of the bovine CcO complex showing the seven transmembrane helices predicted on the basis of the hydrophobicity of a consensus sequence. Blackened residues are strictly conserved in 35 species whereas the shaded residues are highly conserved (conserved in > 90% of the 35 species). The residues participating in the seven transmembrane helices according to the *P. denitrificans* crystal structure are 15-35, 41-69, 73-108, 129-155, 159-185, 194-227 and 235-261, respectively.[13] Reproduced from Musser and coworkers.[6]

basis of hydrophobicity calculations. In the DOXYL-stearic acid quenching experiments mentioned above, however, it was found that Glu^{90} was closer to a membrane-aqueous interface. The explanation for this slight error is not understood but may arise from differential binding affinities of the different DOXYL-stearic acids. When the location of Glu^{90} was confirmed to be located in a transmembrane segment of subunit III and was most likely expected to be exposed to the lipid milieu on the basis of the fluorescence quenching results reported here, it was recognized that this is a thermodynamically unfavorable position for an acidic residue. Therefore, it was postulated that Glu^{90} salt-bridges to one of the highly conserved histidines in the transmembrane spanning segments of subunit III.[275] His^{204} and His^{207} were considered to be the most likely candidates for such a salt-bridge partner.[6] The *Paracoccus* crystal structure confirmed that Glu^{90} does indeed salt-bridge to His^{207} (helix VI). Clearly, the fluorophore–spin-label quencher technique is a useful method for investigating the structure and function of specific residues in proteins.

The fluorescence experiments on the NCD-4-CcO complex provided a few puzzles that cannot be answered by the present CcO crystal structures. In these experiments, the fluorescence maximum of NCD-4-CcO never exceeded 425 nm. Chadwick and Thomas[274] reported the fluorescence maximum for the N-acetylurea model compound as about 398 nm in hexane, 425 nm in ethanol, and 440 nm in 50% ethanol (Table 5.2). Under the conditions of the above experiments, the NCD-4-acetylurea model compound was found to have a fluorescence maximum of about 420 nm in DDM micelles and 440 nm in 20% ethanol (data not shown). Clearly, the fluorescence maximum of the NCD-4 probe is a sensitive indicator of local dielectric. Interestingly, the detergent (Brij-35) solubilized NCD-4-CcO complex exhibits a fluorescence maximum at about 405 nm (Figure 5.2), though the emission maximum is around 425 nm (Figure 5.4) in the reconstituted protein. This difference in λ_{max} of the emission spectrum reflects the different environments surrounding the NCD-4 probe in the detergent solubilized and

reconstituted proteins. Whether these different environments are simply a result of different interactions of detergent and lipid with the protein complex or whether such different interactions induce a protein conformational change in the vicinity of the NCD-4 probe cannot be concluded at this point. Interestingly, there is a large V-shaped cleft between helices II and III of subunit III which can easily accomodate the bulky NCD-4 probe.[13] It is possible that the width and shape of this cleft varies when the CcO complex is transferred from a detergent to a lipid environment. The NCD-4 probe, then, could certainly report such a conformational change by a shift in its fluorescence maximum.

In the course of the above fluorescence experiments, it was found that extensive washing on an anion exchange column (which tended to modify the CcO complex) was necessary to completely isolate the NCD-4-labeled protein from the NCD-4-urea sideproduct. The fluorescence maximum of NCD-4-urea is also an effective indicator of the solvent dielectric as it has a fluorescence maximum at about 460 nm in pure ethanol and at about 473 nm in 50% ethanol (Table 5.2). The λ_{max} of 445 nm observed for the fluorescence emission of the bound NCD-4-urea (Figure 5.2(d)) indicates that the bound NCD-4-urea must be located in a fairly hydrophobic environment ($\varepsilon < 10$). Thus, the NCD-4-urea appears to bind also to the transmembrane spanning regions of the CcO complex. But, since the NCD-4-urea is not covalently bound like the NCD-4-acylurea adduct, it can be removed by extensive washing on an anion exchange column. The binding of NCD-4-urea certainly can affect the function of the CcO complex, specifically, the proton pumping activity (perhaps through disruption of the helix-helix packing of the transmembrane helices). Thus, there is the possibility that the inhibition of proton pumping activity by DCCD results from the hydrophobic binding of this reagent to the enzyme. The work of Lehninger and coworkers[284] supports this hypothesis. These investigators found that the proton pumping activity of the CcO complex is partially inhibited *immediately* after addition of DCCD presumably before the enzyme is modified by DCCD. As mutagenesis experiments[268] strongly suggest that the covalent

modification of Glu^{90} by DCCD does not explain the inhibition of proton pumping activity by this reagent, if it is not the hydrophobic binding of DCCD/DCCD-urea to the enzyme that inhibits the proton pump, the only other option is that DCCD introduces an inter- or intramolecular crosslink (Figure 5.1). Whatever the explanation for the inhibitory effects of DCCD, the answer is sure to yield information about the CcO proton pump.

Concluding Remarks

It is apparent from the many conflicting reports over the involvement of subunit III in proton pumping activity that this subunit plays a very subtle role in the function of the CcO complex. At the very least, it is likely that subunit III is required to maintain the structural integrity of the CcO complex, that is, it is required for stabilization of the enzyme core, subunits I and II. In addition, subunit III may be required for the *functional* integrity of the CcO complex. For example, subunit III could serve as an allosteric effector and modulate the allosteric interactions between subunits I and II that are expected to be obligatory for redox linkage. In this scenario, the salt-bridge between Glu^{90} (helix III) and His^{207} (helix VI) may be required for conformational communication between transmembrane segments – if one of these residues is mutated, this communication link is broken. Note that a salt-bridge located in the low dielectric of the lipid bilayer serves to satisfy the hydrogen bonding requirements of the involved residues. Through the second Wien effect,[285,286] the carboxylate-imidizolium ion-pair will become stabilized in the presence of the electric field of a transmembrane electrostatic potential. If so, this salt-bridge may be an electrically sensitive molecular switch (which "opens" at high membrane potential) that could be used to fine tune the conformational linkage among the three hydrophobic subunits (I, II, and III) of the enzyme. In this manner, Glu^{90} may be part of a (gear-shift) mechanism that could be utilized to disengage part of the proton pumping machinery. The idea that the proton

pump is regulated is fairly new and it certainly is not obvious why such regulation is desirable or necessary. Insight into this possibility requires further examination of the thermodynamics of redox linkage and will be addressed in the next chapter. However, the strict conservation of Glu^{90} and the high conservation of His^{207} argues for a functional purpose to the salt-bridge between these two residues. Clearly, Nature is not satisfied with two hydrophobic residues in these lipid exposed locations.

Chapter 6

Further Insights into the Thermodynamics of Redox Linkage

In this chapter, the theoretical framework of redox linkage is further developed. Conceptually, redox linkage is simply the coupling of redox energy to thermodynamically unfavorable proton transport across a membrane. However, from a mechanistic standpoint, redox linkage is poorly understood. The thermodynamic description presented in Chapter 2 incomplete because it does not explicitly take into account the pmf which dramatically affects the potentials of the conformational states of the protein. In addition, extending the model to encompass a more realistic situation and expanding the discussion within the framework of a specific chemical model of redox linkage allows a more thorough understanding of electron leaks and proton slips. Unfortunately, there is neither consensus regarding which redox center of the CcO complex is the linkage site nor is it known which polypeptide elements are most directly involved in the proton pump machinery. As a result, many chemical models of redox linkage have been presented over the years (the more detailed ones are reviewed by Musser and coworkers[6]). These models are variously successful in incorporating the four requirements of a redox-linked proton pump (a sufficiently exergonic ET, redox linkage, electron gating, and proton gating – see Chapter 2) although they all have flaws. However, each of these models is informative; they all reveal principles that allow a greater understanding of how the proton pump functions. A few chemical models are therefore used here to illustrate the connection between the theory and chemistry of redox linkage. This exercise leads to considerable insight into the coupling between the electron and proton transfer reactions.

An important question that must be addressed regarding the CcO proton pump is which redox center is the linkage site. When the structural similarity of the ubiquinol and cytochrome *c* terminal oxidase complexes and the lack of a Cu_A site in the former family were first observed and it was learned that the proton translocation stoichiometry is the same for both families of enzymes, it was natural to ask whether this superfamily of enzymes were related by similar proton translocation mechanisms. Since the low-spin

heme varies in this superfamily and the only chemical model of redox linkage that relies on this heme requires the formyl group found only on heme A,[189] attention focused on the high-spin heme and Cu_B as candidates for the linkage site. However, as was discussed at the end of Chapter 2, it is difficult to construct a scenario in which the very rapid ET from the high-spin heme or Cu_B to the dioxygen adduct is slowed sufficiently so that the ET can be coupled to the slow conformational relaxations of the proton pump machinery (lack of electron gating). In addition, the discussion in Chapter 3 makes it clear that it is possible, in fact, highly probable, that the ubiquinol and cytochrome *c* terminal oxidase complexes have completely different methods of proton translocation.

The first electron input to the CcO complex is rapidly transferred from the Cu_A site to cytochrome *a* (Chapter 1). Upon input of a second electron, the first electron is presumably transferred from cytochrome *a* to the heme a_3-Cu_B binuclear site. Thus, the first electron apparently follows a cytochrome $c \rightarrow Cu_A \rightarrow$ cytochrome $a \rightarrow$ dioxygen binding site ET pathway. Little data are available which directly address electron input for the third and fourth electrons (the pumping electrons), however. The same ET pathway may be utilized for the third and fourth electrons; on the other hand, the ET pathway cytochrome $c \rightarrow Cu_A \rightarrow$ dioxygen binding site is more likely since the reduction potential of cytochrome *a* drops dramatically relative to Cu_A when dioxygen binds to the enzyme.[209] The available ET data is actually quite confusing most likely due to the fact that ET between any two pairs of redox centers is possible under appropriate conditions. This apparent lack of control of ET between redox centers likely results from the fact that the *physiologically relevant* ET pathways, for the most part, are controlled kinetically under situations that are difficult to reproduce in the laboratory. Note that if the role of the Cu_A site were to simply transfer electrons into the hydrophobic core of the enzyme, there is no reason for Nature to utilize a binuclear copper site; a simple type-I copper site used so frequently as an electron transfer motif (e.g. plastocyanin, azurin, stellacyanin, amicyanin, etc.[287]) would suffice. Because of its structure, it is much easier to envision

reduction/oxidation-induced conformational changes (a requirement for the linkage site) at the Cu_A site than at cytochrome *a*. Thus, it is certainly possible that the Cu_A site of the cytochrome *c* oxidase complexes is a crucial component of the proton pumping machinery of these enzymes. In this discussion, then, the Cu_A center is assumed to be the electron donor to the dioxygen intermediates for the coupled electron transfer steps.

The Chan Cu_A Model

The Chan Cu_A model of redox linkage as originally described by Gelles and coworkers[44] contains all of the elements essential for an efficient proton pump. The postulated ligand exchange reactions of this model are summarized in Figure 6.1. A single copper ion, Cu_A^{2+}, is assumed to be ligated by two histidines and two cysteine residues in a distorted tetrahedral arrangement; this is the electron input state (**A**). Upon reduction by ET from ferrocytochrome *c*, the Cu_A center becomes thermodynamically unstable (**B**). This thermodynamic instability results in a lengthening of one of the Cu-Cys bonds, and concurrently, a shortening of the distance between the copper ion and another ligand which is proposed to be a tyrosine (**C**). Eventually, full ligand exchange occurs via an "SN_2-like" mechanism and the phenolic proton from the tyrosine is transferred to the dissociated thiolate anion (**D**). The ligand geometry is now roughly trigonal planar, the tyrosine pulling the copper slightly out of the plane formed by the other three ligands. ET to the activated dioxygen binding site again results in an thermodynamically unstable conformation (**E**) prompting the reverse ligand exchange back to the original ligand structure. However, due to the greater charge on the Cu_A ion in **E** than in **C**, transfer of the thiol proton back to the tyrosinate anion is inhibited, and instead, this proton is released into a proton channel leading to the cytosolic side of the membrane (**F**). The tyrosine residue is reprotonated via a proton from a water or proton channel leading from the matrix (**G**). The loss of the thiol proton and the reprotonation of the tyrosinate anion may not occur simultaneously; hence, the two individual steps **F** and

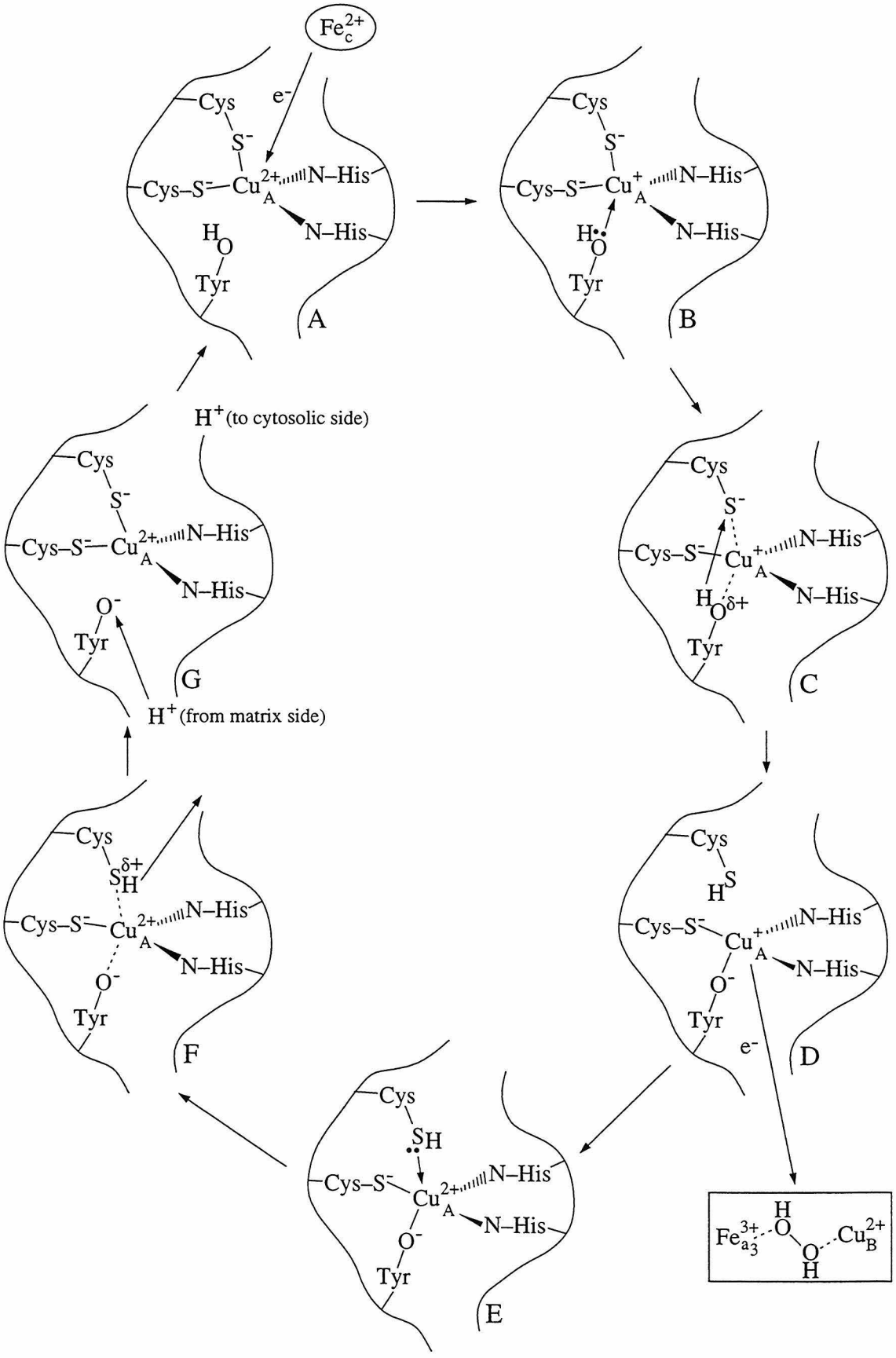

Figure 6.1 Chan Cu_A model of redox linkage. Reproduced from Musser and Chan.[218]

G.

Electron and proton gating mechanisms are incorporated in this model. ET from ferrocytochrome *c* to Cu_A^{2+} is faster in **A** than in **E**. Likewise, ET from Cu_A^{1+} to the activated dioxygen binding site is faster in **D** than in **B**. Gelles and coworkers[44] estimated that the Cu_A ion moves by a minimum of 3 Å, thus favoring the coupled ET over the uncoupled ET by a factor of at least 66. This motion of the Cu_A ion allows for control of the desired ET by distance. There is another manner in which ET rates can be controlled in this model, however. By assuming that the major electron input pathway proceeds through the cysteine sulfur that dissociates from the Cu_A site (**B** $\rightarrow$ **D**) and the major electron output pathway proceeds through the oxygen of the tyrosine, efficient electron gating is achieved by the creation and destruction of ET pathways. It is a little more difficult to envision how gating of proton flow occurs during this ligand exchange process since the transition state (approximately trigonal bipyramidal) appears identical in both the forward and reverse ligand exchange reactions. The transition states are not exactly identical, however, since the oxidation state of the redox site is different. Gelles and coworkers[44] postulate that the greater charge on the Cu_A ion in the **E** $\rightarrow$ **A** transition prevents transfer of the thiol proton back to the tyrosinate anion due to electrostatic repulsion but no insight into exactly how this occurs is provided. Musser and Chan[218] suggested that the greater charge of the redox site directly affects the *orientation* of the incoming thiol ligand. This orientational effect has been incorporated into the model in Figure 6.1; whereas the thiol proton is on the left side of the sulfur atom in **D**, it is on the right side in **E**.

An Indirectly-coupled Cu_A Model

The Chan Cu_A model described above is clearly wrong as described since the crystal structures show that the Cu_A site is actually binuclear. The model illustrates some important principles, however. A redox-linked proton pump requires that

reduction/oxidation of a redox site initiates a sequence of conformational changes that result from the instability of the metal-ligand complex following the ET. Hemes are quite stable structurally upon reduction/oxidation although they may have dramatically different functional properties (therefore arguing against the reduction/oxidation cycle of cytochrome *a* as driving the proton pumping reactions). On the other hand, the ligand field preferred by Cu(I) and Cu(II) is dramatically different (tetrahedral and square planar, respectively). It is this ligand field preference that is the basis for the conformational changes of the Cu_A model. Note that a *sequence* of conformational changes is induced by reduction/oxidation of the copper ion in this model. This feature is expected to be true of any chemical model of redox linkage and implies that the simple four-state thermodynamic model presented in Chapter 2 is an oversimplification. Because of the very local nature of the conformational changes in this directly-coupled model, it is straight-forward to postulate electron and proton gating mechanisms. These control mechanisms can clearly be quite subtle (e.g. the formation of one or two hydrogen bonds or the orientation of a residue based on local charge), but they are required in order for the desired sequence of reactions to occur and so that the process remains directional.

The fact that the Chan Cu_A model is incorrect does not by any means imply that the Cu_A site does not participate in coupling ET to the proton pumping reactions. The Cu-Cu distance in binuclear copper complexes with two bridging sulfur or oxygen ligands varies dramatically (2.7-3.4 Å) based on ligand coordination structure.[288-293] It is certainly possible that the Cu-Cu distance in the Cu_A structure changes significantly upon reduction. For example, the addition of an electron makes the Cu_A center electron rich possibly resulting in a weakening of the Cu-Met and Cu-carbonyl bonds and a more trigonal planar ligation structure. As the Cu-Cu distance is 2.7 Å and the S-S distance is 3.8 Å in the oxidized Cu_A center,[14] this structural rearrangement would result in an increase in the Cu-Cu distance and a decrease in the S-S distance. Upon reoxidation, conformational relaxation back to the original coordination structure would occur. This

conformational cycling would be sufficient to drive the CcO proton pumping machinery in an indirectly-coupled mechanism of redox linkage. In fact, the Mn EPR signal of the *Paracoccus* CcO complex changes upon reduction of the Cu_A site.[294,295] As the *Paracoccus* Mn site is analogous to the Mg site in the mitochondrial CcO complex[295,296] and is thus close to the Cu_A site (Chapter 1), these data support the conformational cycling of the Cu_A site proposed here. A model of redox linkage based on this reaction cycle is given in Figure 6.2. In this model, ET from cytochrome *c* to the oxidized Cu_A site (**A**) yields a reduced Cu_A site with an unstable configuration (**B**). Upon structural stabilization, the two cysteine ligands are pulled closer together (**C**). This structural rearrangement of the Cu_A ligation structure is transferred to a proton channel some distance away (could be anywhere in subunits I, II and III) in two discrete steps (**C** $\rightarrow$ **D** $\rightarrow$ **E**). After ET to the peroxidic or oxyferryl dioxygen intermediate (**E** $\rightarrow$ **F**), the Cu_A center relaxes back to its original ligation structure (**F** $\rightarrow$ **G**) and two more discrete rearrangements within the proton channel (**G** $\rightarrow$ **H** $\rightarrow$ **A**) lead to the net transfer of one proton to the cytosolic side of the membrane. While the conversions **C** $\rightarrow$ **E** and **G** $\rightarrow$ **A** have been broken into two distinguishable steps and it is certainly debatable how any real representation should be drawn, this has been done for illustrative purposes. The proton pump machinery clearly operates by achieving a series of conformationally connected configurations of progressively lower free energy.

This model of redox linkage is intentionally short on details. It is presented only to illustrate the discussion to follow. The point intended, however, is that structural instability at the Cu_A site can be used to drive the proton pumping machinery. In this model, redox linkage occurs through allosteric interactions mediated by one of the cysteine ligands (heavy dashed line). Note that similar allosteric interactions can be mediated by the other cysteine so that the 2 H^+/e^- ratio experimentally observed for the pumping electrons is realized. Electron and proton gating mechanisms have not been incorporated explicitly into the model although they are most certainly required for

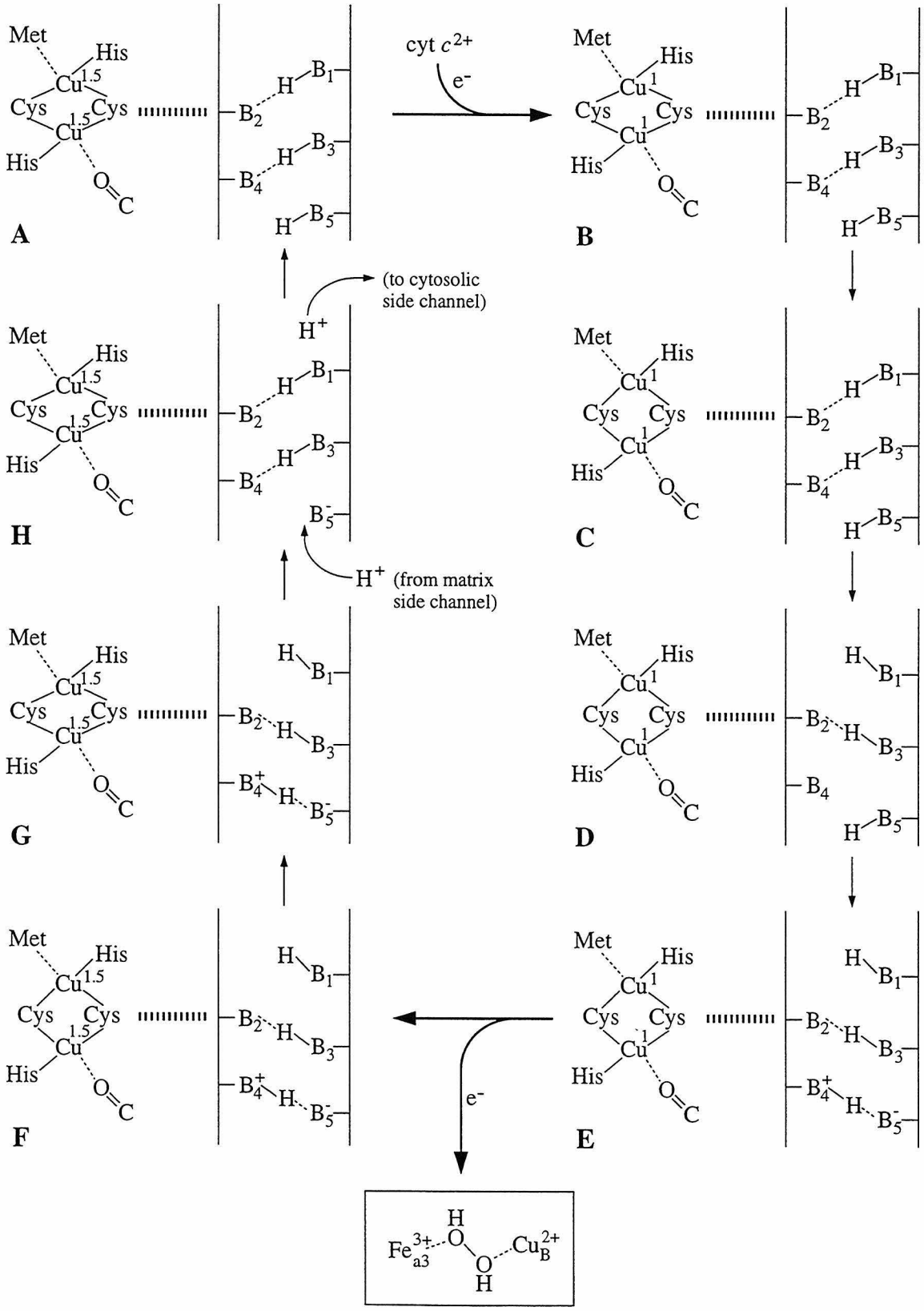

Figure 6.2 Schematic of an indirectly-coupled proton pump mechanism based on structural rearrangments at the Cu_A site.

successful proton pumping. The breaking/forming of hydrogen bonds and the perturbations in local charge distributions that cause reorientation of polypeptide residues are expected means by which these gating mechanisms can be effected.

The CcO Complex as a Faraday Box

In order to incorporate the pmf and the additional conformations required for any postulated proton pump mechanism into an expanded model of the thermodynamics of redox linkage, it is necessary to predict how the potential of the various conformational states is affected by the components of the pmf (pmf = $\Delta\psi$ – 2.303(RT/F)ΔpH).[211,212] Reliable estimates of perturbations to these potentials clearly depends on an accurate assessment of how these electrostatic and pH potential gradients vary within the protein matrix. While it is tempting to assume that an electrostatic potential difference across a membrane gives rise to a potential gradient with a simple linear dependence on distance across the membrane, this picture is only a first approximation. The higher static dielectric constant in the region of the lipid head groups relative to the center of the lipid bilayer results in a compression of the potential energy surfaces in the head group regions of the membrane. The result is that a substantial $\Delta\psi$ exists over the head group regions of the lipid bilayer. A similar compression of the potential energy surfaces is expected to occur near the surface of integral membrane proteins such as the CcO complex since the dielectric constant near the aqueous interfaces of these proteins is expected to be larger than that in the hydrophobic core. The Cu_A site is located about 10 Å from the surface of the CcO complex. Thus, in the presence of a transmembrane potential, an electron transferred from cytochrome *c* to the Cu_A site likely experiences a greater potential difference than an electron transferred over a distance of 10 Å in the interior of the enzyme complex. Similarly, the energetics of proton transfers are different in various locations within the protein matrix. In this manner, the protein acts somewhat as a Faraday box shielding the hydrophobic core from external fields (clearly, the protein does

not act as a true Faraday box since the surface is not a perfect conductor). It is thus expected that electron and proton transfers across the inner and outer protein surfaces of the CcO complex require a substantial driving force so that the desired reaction occurs even in the presence of a pmf.

Thermodynamics of the Indirectly-coupled Cu_A Model

In the indirectly-coupled Cu_A model of redox linkage introduced above, each of the states **A**-**H** denotes the conformation of the protein as a whole; in Figure 6.2, attention is focused on the conformation of the linkage site and a section of a proton channel through the protein. Each of these eight different conformational states has a different oxidation potential.* In the absence of a pmf, the final state, (c^{3+}**A**), is assumed to have an oxidation potential of -1060 mV as discussed earlier (Chapter 2), that is, the oxidation potential of the oxyferryl and hydroxyl intermediates is about -1060 mV. The initial state, (c^{2+}**A**), has an oxidation potential of -250 mV. In this notation, (c^{3+}**A**) denotes a later dioxygen intermediate than (c^{2+}**A**). The 810 mV potential difference between these two states is the redox energy converted largely into heat upon input of the third and fourth electrons to the enzyme. This energy is lost in eight sequential steps according to the indirectly-coupled model in Figure 6.2. In order to estimate the oxidation potentials of the other seven states of this model (the two possibilities involving **A** are discussed above), it is useful to first estimate the perturbing effect of a pmf on these potentials. The rationale for this exercise will become clear later.

For purposes of this discussion, it is assumed that a 50 mV electrostatic potential gradient exists within the first 10 Å of the inner and outer surfaces of the CcO complex under fully energized conditions (pmf = 200 mV; $\Delta\psi$ = 150 mV; -2.303(RT/F)ΔpH = 50 mV). Thus, the remaining 20-30 Å between the electron input and output surfaces is spanned by the remaining 50 mV of the electrostatic potential. These assumptions are

* It is more convenient to use oxidation potentials rather than reduction potentials in the context of the present discussion: oxidation potential = - reduction potential.

consistent with the above view of the CcO complex acting somewhat as a Faraday box. Since the Cu_A site is located about 10 Å from the surface of the protein, the conversion $(c^{2+}\mathbf{A}) \rightarrow \mathbf{B}$ must combat a 50 mV potential gradient under fully energized conditions according to these assumptions. The electron output step, $\mathbf{E} \rightarrow \mathbf{F}$, must therefore be inhibited by 100 mV under these conditions. Note that this value assumes uptake of a matrix proton by the dioxygen binding site upon ET to this site (as part of the dioxygen chemistry) by either a one step or two step process (concomitant with or subsequent to the ET). These effects of a $\Delta\psi$ on the energetics of this indirectly-coupled model of redox linkage are summarized in Table 6.1 (column 2).

So far, only the effect of a pmf on the movement of electrons through the enzyme complex has been considered. The energetics of proton transfers are also perturbed by a pmf, although both $\Delta\psi$ and the pH gradient inhibit these transfer reactions. For simplicity, it is assumed that the structural rearrangements that result from reduction/oxidation of the Cu_A site drive proton pumping reactions through two different channels within the protein complex and that each of these channels is responsible for pumping 1 H^+/e^-. Thus, the net 2 H^+/e^- stoichiometry experimentally observed for the third and fourth electrons is accounted for in this discussion. In addition, it is assumed that both protons are similarly affected by a pmf at each step in the proton pump cycle. This latter assumption is most likely untrue but does not affect the arguments made below and the model developed can be easily modified to incorporate any differences between the energetics of these two proton pumping channels. The first proton transfer reaction occurs in the $\mathbf{C} \rightarrow \mathbf{D}$ conversion. The rearrangment of the two hydrogen bonds shown is assumed to require 40 meV in the presence of a 200 mV pmf. The $\mathbf{D} \rightarrow \mathbf{E}$ conversion is assumed to require only about 20 meV under these conditions as only one proton moves against the pmf in each channel. The $\mathbf{G} \rightarrow \mathbf{H}$ and $\mathbf{H} \rightarrow (c^{3+}\mathbf{A})$ conversions are expected to be the most endergonic because they follow the highly exergonic ET to the binuclear site. Therefore, it is assumed that the proton ejection step ($\mathbf{G} \rightarrow \mathbf{H}$) requires 60 meV and

Table 6.1 Estimated Oxidation Potentials of Intermediates in the Indirectly-coupled Model of Redox Linkage in Figure 6.2*

	Energetic requirement for movement in presence of $\Delta\psi$ = 150 mV (in meV):		Total energetic requirement for movement in presence of pmf = 200 mV (in meV):		Effective oxidation potentials of intermediates (in mV):					
Step	e^-	H^+	1 H^+/e^-	2 H^+/e^-	pmf = 0		pmf = 200 mV 1 H^+/e^-		pmf = 200 mV 2 H^+/e^-	
					(c^{2+}**A**)	-250	(c^{2+}**A**)'	-250	(c^{2+}**A**)"	-250
(c^{2+}**A**) → **B**	50		50	50	**B**	-320	**B'**	-270	**B"**	-270
B → **C**					**C**	-350	**C'**	-300	**C"**	-300
C → **D**		20	20	40	**D**	-410	**D'**	-340	**D"**	-320
D → **E**		10	10	20	**E**	-450	**E'**	-370	**E"**	-340
E → **F**	100		100	100	**F**	-650	**F'**	-470	**F"**	-440
F → **G**					**G**	-680	**G'**	-500	**G"**	-470
G → **H**		60	60	120	**H**	-820	**H'**	-580	**H"**	-490
H → (c^{3+}**A**)		110	110	220	(c^{3+}**A**)	-1060	(c^{3+}**A**)'	-710	(c^{3+}**A**)"	-510
total:	150	200 per H^+	350	550	ΔE:	-810		-460		-260

* Columns 2 and 3 summarize the approximate energetic requirements of electron and proton movement, respectively, for the conversions in column 1 (see Figure 6.2) in the presence of a 200 mV pmf ($\Delta\psi$ = 150 mV, -2.303(RT/F)ΔpH = 50 mV). Columns 4 and 5 are the estimated total energetic requirements for each step assuming a 1 and a 2 H^+/e^- stoichiometry, respectively. The total energetic requirement for a 2 H^+/e^- stoichiometry is used to estimate the effective oxidation potential of the various intermediates by assuming that each step is spontaneous under these conditions (column 11); the oxidation potentials of the various intermediates for non-pumping conditions or a 1 H^+/e^- stoichiometry are obtained by back calculation as described within the text (columns 7 and 9). Constructed following the example of Musser and coworkers.[218]

filling the proton hole ($\mathbf{H} \rightarrow (c^{3+}\mathbf{A})$) requires 110 meV. These effects of a pmf on the energetics of this indirectly-coupled model of redox linkage are also summarized in Table 6.1 (column 3). In addition, the total effect of a pmf on both the electron and proton transfer reactions is calculated for both a 1 and a 2 H^+/e^- stoichiometry (columns 4 and 5).

The oxidation potentials of the various intermediates in this indirectly-coupled model of redox linkage can now be estimated. Since the electron input step, $(c^{2+}\mathbf{A}) \rightarrow \mathbf{B}$, is assumed to be inhibited by a 50 mV potential gradient under fully energized conditions, the oxidation potential of **B** must be less than -300 mV [= -250 mV + (-50 mV)]. It is reasonable to expect at least about 20 mV of driving force for this reaction under fully energized conditions so the oxidation potential of **B** is assigned as -320 mV. The $\mathbf{B} \rightarrow \mathbf{C}$ conversion is not affected by a pmf. A driving force of 30 mV is assigned to this conversion in the absence of a pmf to yield an oxidation potential for **C** of -350 mV [= -320 mV + (-30 mV)]. The remaining oxidation potentials in this redox linkage cycle are estimated in a similar manner assuming a driving force of 20-30 mV under fully energized conditions for each step and are tabulated in Table 6.1 (column 7). The one exception is the ET step, $\mathbf{E} \rightarrow \mathbf{F}$. In order to enforce irreversibility, the ET to the dioxygen binding site is expected to be governed by a substantially larger driving force (here assumed to be 100 mV under fully energized conditions). Note that the ET reaction is expected to occur faster than the major conformational changes of the proton pumping elements making irreversibility of this ET necessary for efficient proton pumping. The effective oxidation potentials for the various states of this indirectly-coupled model under fully energized conditions can be calculated by accounting for the additional energy required for ET across the membrane bilayer and that required to pump 1 or 2 H^+/e^-. These effective oxidation potentials are also tabulated in Table 6.1 (columns 9 and 11). The conformations of the protein may be different in the presence of a pmf; this possibility is denoted by the use of primed and double-primed states (the 1 H^+/e^-

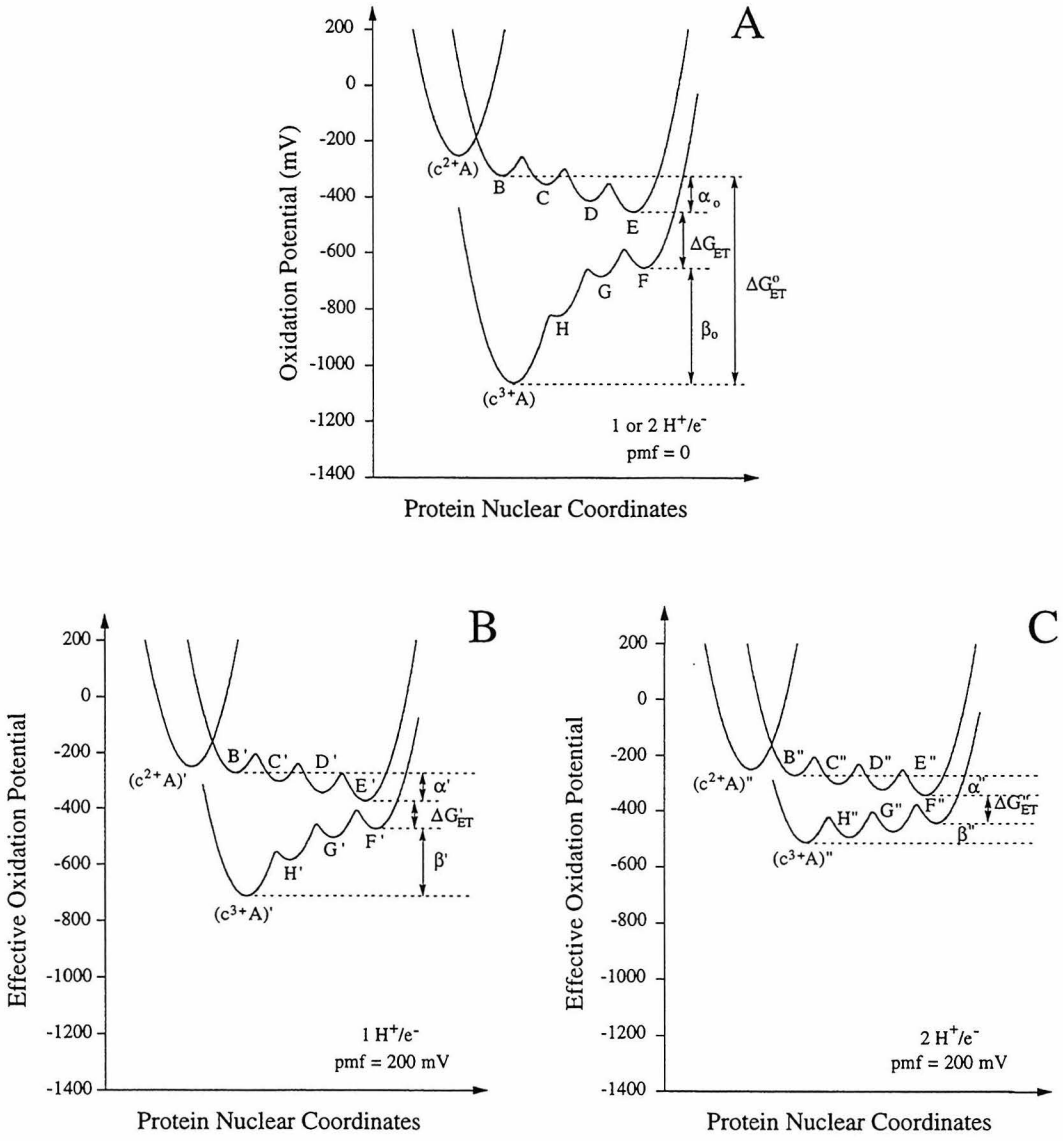

Figure 6.3 Thermodynamics of the indirectly-coupled model of redox linkage in Figure 6.2. (A) depicts the energetics of the ETs and conformational changes in the absence of a membrane potential for the third and fourth electrons of the dioxygen turnover cycle. The conformational nomenclature is used loosely since (c^{3+} **A**) is not identical for 1 and 2 H^+/e^- stoichiometries (likewise for the other eight states). The *energy* of a given conformation is the same, however, for both a 1 and a 2 H^+/e^- stoichiometry since the pmf = 0. (B) and (C) reveal how these energetics are modified in the presence of a 200 mV pmf ($\Delta\psi$ = 150 mV and -2.303(RT/F)ΔpH = 50 mV) assuming a 1 H^+/e^- and 2 H^+/e^- stoichiometry, respectively. The values in Table 6.1 were used to construct these schematics. Note that in the calculation of the various potentials for these schematics, the entropic contribution to free energy, which could be substantial in some steps, has been ignored. The overall picture is expected to remain the same, however, when this entropic contribution is included.

conformations are *certainly* different than the 2 H^+/e^- conformations).

These estimated effective oxidation potentials can be used to construct an expanded potential energy model of redox linkage. This model is summarized in Figure 6.3 and depicts the thermodynamics of the proton pump in the absence of a pmf and under fully energized conditions where a 1 or 2 H^+/e^- stoichiometry is assumed. Note that the energy stored during enzyme turnover is, for example, given by $(c^{3+}\mathbf{A})'' - (c^{3+}\mathbf{A}) = 550$ meV. While this number may seem strangely high for the 2 H^+/e^- ratio, it must be remembered that energy is stored by transfer of a negative charge-equivalent across $\Delta\psi$. It is thermodynamically possible for water oxidation to occur by reverse transfer of electrons across this $\Delta\psi$ (as has been shown by Wikström and coworkers[87,88,213]). An alternative manner of interpreting this energy storage process is that ET across the membrane dielectric increases $\Delta\psi$, thereby increasing the pmf. This 550 meV of stored energy can be used for ATP synthesis; namely, the F_0F_1-ATP synthase complex couples the conversion $(c^{3+}\mathbf{A})'' \rightarrow (c^{3+}\mathbf{A})$ to ATP synthesis. The system can only be recharged by input of reactants, that is, by addition of a reductant (ferrocytochrome *c*) and an oxidant (dioxygen). It is simple to see from this theoretical framework that a pmf is a prerequisite for the storage of energy by enzyme turnover.

Implications of this Thermodynamic Model

It should be emphasized that the effective oxidation potentials in this model should not be taken too seriously. The large number of assumptions involved in calculation of these potentials reveals our ignorance of the detailed energetics of the proton pump. In addition, the $H_2O_2/H_2O_2^-$ and $H_2O_2^-/H_2O$ redox couples are expected to function at different potentials.[87,88] There are, however, a few general features that are expected to hold true for any refined model. The energies of $(c^{2+}\mathbf{A})$ and $(c^{3+}\mathbf{A})$ as well as of the respective primed and double-primed conformations are expected to be valid whenever $\Delta\psi = 150$ mV and $-2.303(RT/F)\Delta pH = 50$ mV and regardless of whether **A** corresponds

to this indirectly-coupled model or any other model of redox linkage. From this B-type model of redox linkage, it is clear that $|\alpha_0 + \beta_0| > 400$ meV ($|\alpha_0 + \beta_0| = 540$ meV), the minimum energy needed for the pumping of 2 H^+/e^- to be spontaneous under fully energized conditions. Of course, this *must* be the case since energy is necessary to drive the conformational changes of the proton pump. The driving energies for the 1 and 2 H^+/e^- pumping stoichiometries are shown as α'/α'' and β'/β'' in Figure 6.3.

This model allows an informative discussion of electron leaks and proton slips. An electron leak exists, for example, if an ET from **B**" to a (c^{3+}**A**)-like state occurs (implying inefficient electron gating) instead of the desired **B**" $\rightarrow$ **C**" $\rightarrow$ **D**" $\rightarrow$ **E**" conformational change. Note that ET cannot occur from **B**" to (c^{3+}**A**) because the latter state implies that (a) proton(s) have been translocated. *This is a subtle, but important, point.* Proton slippage occurs, for example, when conversion from **F**" to a (c^{3+}**A**)-like state occurs via the reverse of the forward reactions. The astute reader will note that an electron leak or a proton slip *always* occurs by conversion to a state of lower energy than the desired state. This is a *very* important point. The proton pump is successful only if a specified sequence of events occurs. Once a leak or slip occurs, the next desired conformational state is almost impossible to achieve for thermodynamic as well as kinetic reasons. For example, it is virtually impossible for conversion from an **H'**-like state to the **H**" state to occur; the former state is the one of lower energy, and, mechanistically, it is straight-forward to understand why this conversion does not occur. Since both electron leaks and proton slips occur by conversion to a state of lower energy than the desired state, it may be somewhat difficult to understand the difference between a leak and a slip. The difference is more than just semantic because a leak occurs predominantly along the NCET while a slip occurs along the NCPP. This directionality of the undesired conformational rearrangements or transitions is considered to define leaks and slips.

It is important to understand why electron leaks and proton slips are more likely to occur when the pmf is large rather than when it is small. The reason for the occurrence of

these undesirable reactions is that the barrier heights impeding conformational conversions in the presence of a pmf are higher than in the absence of a pmf. This fact results from the simple vertical displacement of the vibronic energy wells for a given state in the presence of a pmf. The implication of these increased barrier heights is that the turnover rate of the enzyme is necessarily slower in the presence of a pmf. This prediction agrees well with experiment (e.g., the respiratory control ratio compares the turnover rate in the absence and presence of a transmembrane potential and is typically 4-8).[105,241,297-299] However, the states that give rise to leak and slip pathways are always of lower energy than those of the proton pump cycle indicating that the barrier heights for transition to these states is almost always lower (when an electron leak is governed by a driving force in the inverted region, the barrier height for the leak may be higher than for the desired reaction). Thus, the leak and slip pathways are expected to become more favored in the presence of a pmf. This argument is not meant to imply that the proton pump does not function in the presence of a 200 mV pmf but rather that the probability that the proton pump cycle is *completed* is lower. Note, as discussed above, once a leak or slip has occurred, it is virtually impossible to complete the proton pump cycle. From this analysis, it is postulated that the average H^+/e^- stoichiometry is lower in the presence of a pmf. Also, the turnover rate assuming a 1 H^+/e^- stoichiometry is expected to be faster than the case for a 2 H^+/e^- stoichiometry due to the lower barrier heights for the required conformational conversions in the former case. In addition, there is a lower probability for leakage and slippage in the case of a 1 H^+/e^- stoichiometry. The enzyme may in fact be designed to utilize this 1 H^+/e^- stoichiometry pathway and mitigate the lower H^+/e^- stoichiometry via a more rapid turnover. It is here where the Glu^{90} salt-bridge of subunit III may be important (Chapter 5). An electrically sensitive molecular switch in subunit III would allow the enzyme to alter the coupling between ET and the proton pump and vary the efficiency of the proton pump to suit the present conditions.

It is clear that the proton pump is coupled to the ETs to the dioxygen binding site. It is also evident that only two of the four such ETs are exergonic enough to drive the proton pump, namely the third and fourth electrons of the dioxygen reduction cycle. This fact leads to the following theoretical argument and is expected to hold for any model of the complete turnover cycle of the CcO complex: the CcO complex must have a mechanism preventing itself from becoming locked in a potential well of the proton pump cycle. For the first and second electrons of the dioxygen reduction cycle, the lower curves in Figure 6.3 are displaced to higher energy by about 560 mV (the difference between the O_2/H_2O_2 and the H_2O_2/H_2O redox couples which function at about 500 mV and 1060 mV, respectively - see Chapter 2). This displacement is pictorially represented for the indirectly-coupled model of Figure 6.2 under conditions where the pmf = 0 in Figure 6.4. In this representation, it is clear that the conversion **B** $\rightarrow$ **E** can occur; however, the conversion **E** $\rightarrow$ (c^{3+}**A**) cannot occur via the normal sequence of conformational conversions (explaining why pumping does not occur). This **E** $\rightarrow$ (c^{3+}**A**) conversion most likely cannot occur directly either (at least in a kinetically facile manner) since the reorganizational energy (λ) for ET is so high (here, λ would include a large reorganization energy along the NCPP). The situation is even worse in the presence of a $\Delta\psi$ = 150 mV since conversion from a **E**-like to a (c^{3+}**A**)-like state actually becomes

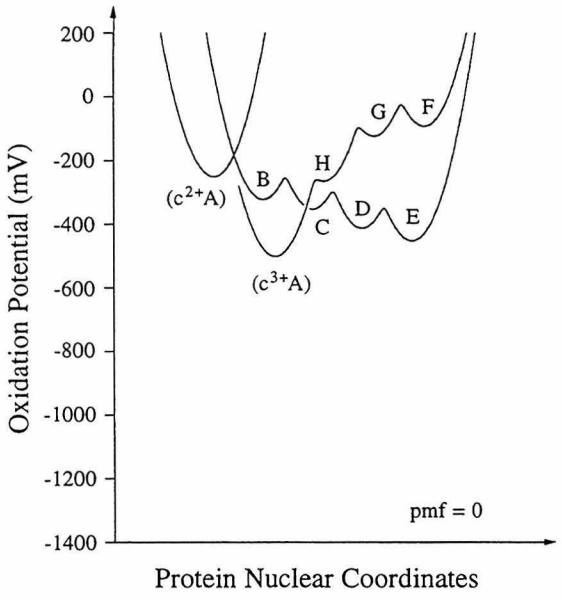

Figure 6.4 Thermodynamics of the indirectly-coupled redox linkage model in Figure 6.2 for the first and second electrons of the dioxygen turnover cycle in the absence of a transmembrane potential. This scheme is intended to be compared with Figure 6.3A.

endergonic and λ is even greater. These arguments apply even to the simple four-state models of redox linkage in Figure 2.1. Under these conditions, then, once the enzyme achieves the **E**-like configuration, turnover is essentially halted, that is, the enzyme is stuck in a potential well. The conclusion drawn from this analysis is that the enzyme must never achieve the **E**-like conformation for the first and second electrons of the dioxygen turnover cycle. Two scenarios exist which would allow the enzyme to avoid becoming locked in a potential well: 1) the enzyme must be able to inform the linkage site as to the pumping or non-pumping nature of the incoming electrons; or 2) only pumping electrons pass through the linkage site.

The Complete Turnover Cycle

The available ET studies (Chapter 1) suggest that the Cu_A center is the initial electron acceptor for all four electrons of the dioxygen reduction cycle. The extramembranous location of the Cu_A site as shown by the crystal structures lend strong support to these data. If the Cu_A site is indeed the linkage site, then, scenario (2) at the end of the last section *cannot* be true. Thus, the enzyme *must* be able to inform the Cu_A site *before* it is reduced whether the incoming electron will be a pumping electron or not. In this section, a mechanism explaining how this allosteric communication between the Cu_A site and the heme a_3-Cu_B binuclear site could be mediated is discussed.

Since it is the dioxygen intermediate present at the heme a_3-Cu_B binuclear site that determines the energetics of the internal ET and thus whether the incoming electron is a pumping or nonpumping electron, it is reasonable to assume that conformational changes occurring at the binuclear site relay the pumping or nonpumping nature of the incoming electron to the rest of the enzyme. It is noteworthy that heme a_3 is six-coordinate for the pumping ETs (input of the third and fourth electrons), yet five-coordinate for the nonpumping ETs (input of the first and second electrons).* Thus, the conformational

* It has been assumed here that in the "pulsed" enzyme, heme a_3 behaves as a five-coordinate heme (Fe_{a3}

change that allows the enzyme to distinguish the pumping from the nonpumping ETs may result from the change in coordination of heme a_3.[300] The five- to six-coordinate transition is accompanied by a movement of the iron atom into the plane of the porphyrin macrocycle. This motion of the iron atom is transferred to the proximal histidine ligand, a phenomenon that has the potential for effecting a global conformational change. Note that the binding of dioxygen to hemoglobin and the resulting motion of the proximal histidine is responsible for the cooperativity of dioxygen binding.[301] Thus, it is postulated that the out-of-plane–in-plane transition of Fe_{a3} is responsible for engaging the proton pump; conversely, the in-plane–out-of-plane transition results in the reverse conformational change thereby disengaging the proton pump. This scenario is consistent with the "closed" to "open" transition discussed in Chapter 1. The simplest means of disengaging the proton pump is by small perturbations to the ligation structure of the Cu_A site. This full catalytic cycle is summarized in Figure 6.5.

By presenting this model of the full turnover cycle of the CcO complex, the intention is not to imply that the discussed ETs are the only ones that can occur during turnover. Rather, this model postulates ET events that are consistent with a greal deal of experimental data and that provide for efficient dioxygen turnover and proton pumping (see Musser and coworkers[6] for a review). There are electron leaks in the full turnover cycle similar to the electron leaks discussed earlier for the proton pump. For example, dioxygen certainly can bind following slow ET of the first electron to the heme a_3-Cu_B binuclear center from cytochrome *a*. Since the proton pump engages at this point, the second electron will become trapped at the Cu_A site in a potential well of the proton pump cycle. Eventually, the protein will be able to work its way out of this dead-end conformation, but this may not occur before compound A degrades to the free superoxide anion. Thus, this model postulates that cytochrome *a* is an electron trap used to ensure that there are at least two electrons available when dioxygen binds so that loss

---

out-of-plane) since histidine is a much stronger ligand than HO^-/H_2O.

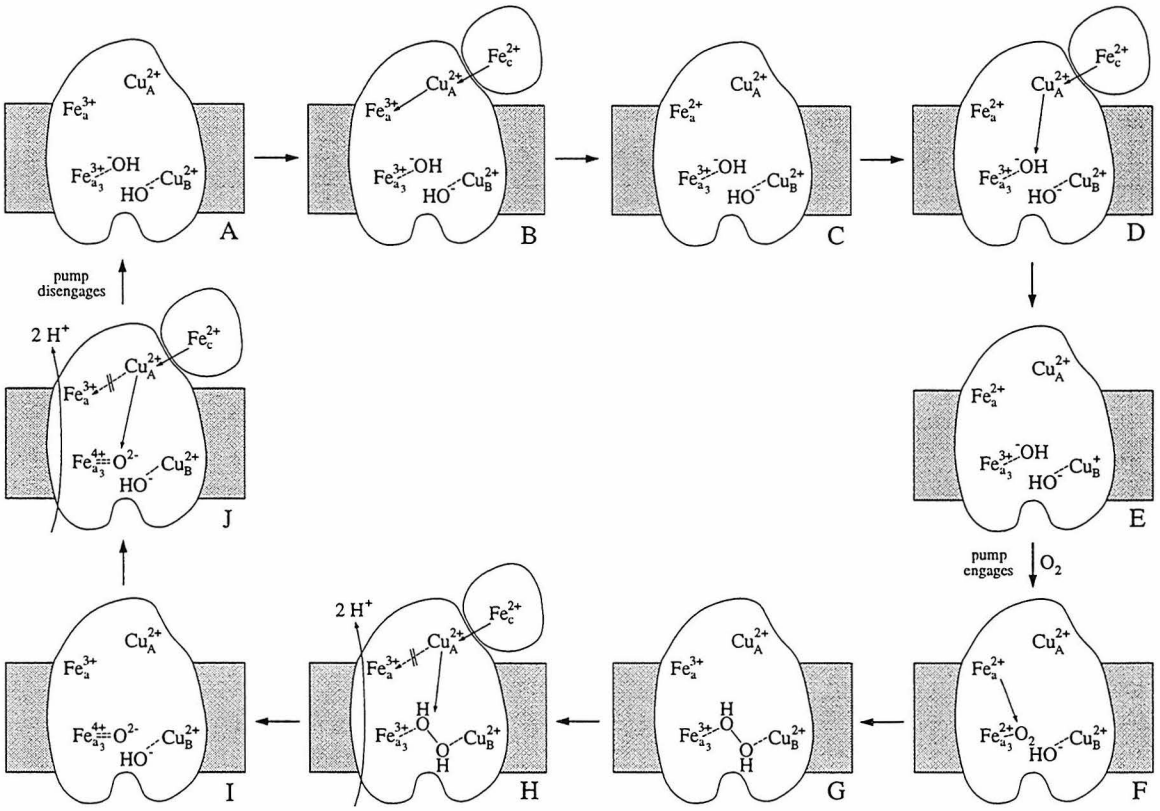

Figure 6.5 Model of the complete turnover cycle of the CcO complex. Solid arrows indicate viable ET pathways and dashed arrows signify kinetically inviable ET pathways. The Cu_A site is assumed to be the linkage site (D in the nomenclature introduced in Figure 2.1), yet no particular chemical model of redox linkage is assumed. See text for details. Reproduced from Musser and coworkers[6] with minor modifications.

of the toxic superoxide anion is minimized. In addition, if the third or fourth electron is rapidly transferred from the Cu_A site to cytochrome *a*, the proton pump is bypassed.

Concluding Remarks

The proton pump function of the CcO complex dictates that this enzyme must be conformationally flexible. Specifically, reduction or oxidation of the linkage site commences a conformational relaxation process. The energy released by adoption of a more stable protein conformation is used to translocate protons against a transmembrane electrochemical gradient. As a result of this conformational cycling, the free energy of the internal ET between the linkage site and the activated dioxygen binding site (ΔG_{ET}) is

much less than that predicted from a simple difference of reduction potentials. Unfortunately, there are many undesirable configurations the enzyme could adopt in its conformational cycling which are lower in energy than the next desired conformation. Clearly, to accomplish the desired result, kinetic barriers must be introduced to inhibit the uncoupling reactions from occurring. Thus, the existence of efficient electron and proton gating mechanisms is crucial for preventing electron leaks and proton slips from occurring during turnover. In the context of the model presented herein, electron gating mechanisms favor conformational relaxation along the NCPP until the appropriate time in the proton pump cycle for ET to occur. Proton slips occur along the NCPP but they are always more exergonic than the desired reaction. Thus, highly effective proton gating mechanisms are required for completion of the desired result with high probability. Since efficient electron and proton gating mechanisms are so vital to the success of the proton pump, they are expected to be important features of any detailed model of the proton pumping process in the CcO complex. The analysis indicates that at high pmf enzyme turnover is expected to decrease due to the higher energetic barriers for ET and protein conformational changes. Therefore, it is unnecessary to invoke pmf-induced conformational changes to explain the slower experimentally observed turnover under these conditions. It is possible that a high pmf stretches the electron and proton gating mechanisms to the limit of their effectiveness leading to the increased occurrence of the more energetically favorable electron leak and proton slip reactions, and thus, a reduced H^+/e^- stoichiometry. It is important to point out that the CcO complex acts as a cooperative unit such that conformational changes occurring at a given redox center do not a priori identify that site as the site of linkage. Finally, the concepts that have developed here are completely general and are applicable to any molecular model of redox linkage proposed for the CcO complex.

Chapter 7

Evolution of the Cytochrome *c* Oxidase Proton Pump

In this chapter, attention is focused on the evolutionary relationship between the ubiquinol and cytochrome *c* terminal oxidase complexes. In Chapter 1, it was noted that the UQO complex combines the oxidation/reduction chemistry mediated by the cytochrome bc_1 and CcO complexes. However, a price is paid. The UQO complex catalyzes the net translocation of 8 H^+/4 e^-:

$$\begin{aligned} &4\ QH_2\,(Q_A\ \text{site}) + 4\ H^+\,(\text{scalar}) + O_2 + 4\ H^+\,(Q_B\ \text{site}) + 2\ Q(Q_B\ \text{site}) \\ &\quad \rightarrow 4\ Q(Q_A\ \text{site}) + 8\ H^+\,(Q_A\ \text{site}) + 2\ H_2O + 2\ QH_2\,(Q_B\ \text{site}) \end{aligned} \qquad (7.1)$$

whereas the combination of the cytochrome bc_1 and CcO complexes results in the net translocation of 12 H^+/4 e^-:

$$\begin{aligned} &4\ QH_2\,(Q_P\ \text{site}) + 4\ H^+\,(Q_N\ \text{site}) + 2\ Q(Q_N\ \text{site}) + 4\ \ \text{cyt}\,c^{3+} \\ &\quad \rightarrow 4\ Q(Q_P\ \text{site}) + 8\ H^+\,(Q_P\ \text{site}) + 2\ QH_2\,(Q_N\ \text{site}) + 4\ \ \text{cyt}\,c^{2+} \end{aligned} \qquad (\text{cyt } bc_1) \quad (7.2a)$$

$$\begin{aligned} &4\ \ \text{cyt}\,c^{2+} + 4\ H^+\,(\text{scalar}) + O_2 + 4\ H^+\,(\text{inside}) \\ &\quad \rightarrow 4\ \ \text{cyt}\,c^{3+} + 2\ H_2O + 4\ H^+\,(\text{outside}) \end{aligned} \qquad (\text{CcO}) \quad (7.2b)$$

$$2\ QH_2 + 12\ H^+\,(\text{inside}) + O_2 \rightarrow 2\ Q + 12\ H^+\,(\text{outside}) + 2\ H_2O \qquad (\text{net}) \quad (7.2c)$$

Clearly, a respiratory chain which contains the latter two enzymes is more efficient in energy transduction. However, a number of bacteria encode both ubiquinol and cytochrome *c* terminal oxidase complexes in their genome. Presumably, in this manner, these bacteria are able to regulate the energy conversion efficiency of their respiratory chain at the genomic level. This regulatory capability is advantageous because, for example, when the energy supply is high, ATP synthesis is unnecessary but elimination of excess reducing equivalents - e.g. regeneration of NAD^+ from NADH - may be required so that other cellular functions may proceed. Regulation of the cytochrome *c* oxidase proton pump through the many nuclear-encoded subunits found in eukaryotes

therefore obviates the need for a ubiquinol oxidase complex. It is typically assumed that the bo_3-type ubiquinol oxidase complex evolved from a cytochrome *c* oxidase complex that lost its Cu_A site.[50,179,302,303] It is difficult to rationalize, however, why a primitive bacterium such as *E. coli* would contain this ubiquinol terminal oxidase complex yet no cytochrome *c* oxidase complex[221] if the former enzyme evolved later. The respiratory efficiency of an organism that contains cytochrome bc_1 and cytochrome *c* oxidase complexes in its respiratory chain can be reduced by a number of means (e.g. by uncoupling the cytochrome *c* oxidase proton pump or by increasing the proton permeability of the membrane with fatty acids or an uncoupling protein like that found in brown adipocytes[304,305]); however, an organism which contains only a ubiquinol oxidase complex cannot *increase* its respiratory efficiency. This argument suggests that an organism would be at a severe selective disadvantage if it had a ubiquinol terminal oxidase complex in addition to cytochrome bc_1 and cytochrome *c* oxidase complexes but somehow lost the function of one of the latter two complexes. On the other hand, it makes evolutionary sense that the cytochrome bc_1 and cytochrome *c* oxidase complexes arose from a primitive ubiquinol terminal oxidase complex via a series of beneficial mutations. Although this idea has been objected to because of the similarities between the cytochrome *c* oxidase complexes and a number of denitrifying enzymes[306] and the assumption that nitrogenic respiration existed before dioxygen was plentiful enough to support oxygenic respiration,[307] one of the general rules of evolutionary tree construction is that simplicity leads to complexity. It is this basic rule that suggests that the cytochrome bc_1 and cytochrome *c* oxidase complexes evolved from a primitive ubiquinol terminal oxidase complex. The following discussion attempts to rationalize how this might have happened.

The Beginning of Life

The conditions during the first billion years of Earth's 4.5 billion year existence were

violent times to be sure with horrific impact events (comets and meteorites), volcanic erruptions, lightning and torrential rains. There was little if any free oxygen and no layer of ozone to shield the surface from the Sun's UV irradiation. Initially, only simple molecules were present (H_2O, CH_4, NH_3, H_2, H_2S, CO_2, CO, HCN, H_2CO, etc.), but the four major classes of small organic molecules found in cells - amino acids, nucleotides, sugars, and fatty acids - accumulated over time as a result of these extreme conditions. Polymers of nucleic acids that formed were able to act as templates for polymerization of new polynucleotides and were able to catalyze novel chemical transformations. In this primordial soup, primitive membranes formed from long chain hydrocarbons giving rise to vesicles. Initially, of course, the solutions on each side of these membranes were identical, yet the semipermeability of these membranes played a very crucial role. Gases could freely diffuse through the membranes, yet ions must have diffused much slower as a result of their ionic charge. As chemistry progressed in the vesicles, then, asymmetric distributions of ions must have resulted.[1,308] While these vesicles could not be called life, the beginnings were certainly there. They contained energy rich molecules, polymers that could act as templates for their own reproduction, and primitive enzymes, and the solution composition inside was different than that found outside.

While ATP (and PP_i) was likely made initially by UV irradiation of the prebiotic soup,[308,309] the conversion of glucose to ethanol via the glycolytic reactions could have been the first catabolic reaction sequence of primitive cells:[1]

$$\text{glucose} + 2\ P_i + 2\ ADP + H^+ \rightarrow 2\ \text{ethanol} + 2\ CO_2 + 2\ ATP + 2\ H_2O \qquad (7.3)$$

Note that dioxygen, which was present in only low concentrations (at best) in the early atmosphere,[310] is not required in this metabolic pathway. In this reaction sequence, the reactant (glucose) and the products (ethanol, CO_2 and H_2O) are all neutral and so could have exchanged relatively easily through primitive membranes. All other species of the overall reaction are charged (and therefore would have been easily retained within

primitive cells) and would have been recycled during the cells' energy requiring reactions. The genetic code (most likely RNA-based originally) and a primitive translation machinery (also RNA-based as evidenced by the high percentage of RNA in ribosomes today) likely developed at about the time glycolysis developed. While the first enzymes are thought to have been RNA molecules that were randomly generated in the prebiotic soup, the clear superiority of proteins as catalysts led to their dominance as biological catalysts.[308] With the genetic code in place, random polypeptide synthesis from the many RNA polymers in the early biotic soup most likely led to a boom in polypeptide synthesis. Clearly, the synthesis of proteins places a high demand on energy production, and therefore, the stage was set for the evolution of the citric acid cycle.

The Advent of Respiration

The hydride transfer acceptor NAD^+ is crucially important in the glycolytic reactions and it was again found useful in the citric acid cycle. However, whereas the conversion of glucose to ethanol uses up as much NADH as it produces, the full oxidation of glucose via the citric acid cycle produces excess NADH:[2]

$$\begin{aligned} &\text{glucose} + 4\ P_i + 2\ ADP + 2\ GDP + 10\ NAD^+ + 2\ FAD + 2\ H_2O \\ &\quad \rightarrow 6\ CO_2 + 2\ ATP + 2\ GTP + 10\ NADH + 2\ FADH_2 + 6\ H^+ \end{aligned} \tag{7.4}$$

Therefore, for the citric acid cycle to have been useful for primitive cells, a way to regenerate NAD^+ was required. The many iron-sulfur clusters present in the organic soup likely played a role here as they are still utilized extensively by NADH dehydrogenase complexes today.[311] These iron-sulfur clusters may have been in solution or adhered to the membrane surface. The acceptor of electrons from the NADH oxidation chemistry was probably a quinone (by analogy with the present-day NADH dehydrogenase complexes), most likely a small water soluble benzoquinone. Similarily, the succinate $\rightarrow$ fumarate step of the citric acid cycle probably utilized this same quinone

as an acceptor of electrons (by analogy with the present-day succinate dehydrogenase complexes). As a primitive succinate dehydrogenase complex is likely to have been water soluble[312] (like the other enzymes of the citric acid cycle), a water soluble quinone acceptor would have been required. Electron acceptors such as SO_4^{2-} and NO_3^- have complicated enzymatic pathways to full reduction in present day organisms.[3,313,314] In addition, their charge would have inhibited uptake from the external medium through primitive membranes and therefore these ions are not considered good candidates for the terminal electron acceptor of early cells.[311] However, oxides of nitrogen (e.g. NO and N_2O) are electron acceptors that were present in the acidic biotic soup that can easily diffuse through membranes.[308] It should also be observed, though, that a ubiquinol terminal oxidase complex (which could certainly have been water soluble) would satisfy early cells' need to regenerate quinone. While dioxygen (which can also easily diffuse through membranes) was not available in high concentrations in the atmosphere until much later (after the advent of the water-splitting enzyme of photosystem II about 2 billion years ago),[307,308] it was certainly present in low concentrations as a result of water and CO_2 photolysis by UV irradiation.[310,315] It was this same UV irradiation present at the Earth's surface (due to the lack of an ozone shield) that was presumably instrumental in the early production of ATP.[309] The presence of oxygen in a number of the early gases (e.g. CO_2, H_2O, NO_2, SO_3) and ions (e.g. CO_2^-, NO_3^-, SO_4^-) certainly argues for a minor presence of dioxygen in the atmosphere. More importantly, though, while the atmospheric dioxygen level likely was low, oxidizing conditions could have been maintained throughout entire lakes or ocean basins forming localized "oxygen oases" with dissolved O_2 levels possibly as high as 10% of present day levels.[310] Therefore, it is clearly possible that dioxygen was the terminal acceptor of electrons from quinol molecules in early cells.

It is not known when the first membrane protein evolved. However, it is likely that the first membrane proteins were antiporter/symporter-type exchange proteins required

for the passage of ions, food, and waste. It is very probable that one of the early ionic gradients across the cell membrane was a proton gradient. Such proton gradients could have formed, for example, by membrane-bound dye sensitized reactions.[308] There was clearly a selective advantage to those early cells that could advantageously utilize such gradients. The F_0 component of the F_0F_1-ATPase complex probably developed as a way to control the proton gradient and the $\Delta\psi$ across the membrane. The complexity of the motor part of the F_0F_1-ATPase complex suggests that it was still some time yet before the enzyme realized its present activity. In fact, it is likely that the related, but simpler, PP_i synthase developed first.[316] It is also possible that a primitive ubiquinol oxidase complex was able to translocate protons before the F_1 motor developed; this scenario assumes, of course, that oxidative phosphorylation had become a membrane-associated process by this time. Certainly, by the time that the $Q(H_2)$-loop proton translocation mechanism evolved, the time was ripe for evolution of the F_1 motor if it did not already exist. Therefore, as imagined here, the first real respiratory chain contained NADH dehydrogenase, succinate dehydrogenase and ubiquinol oxidase complexes, at least one of which translocated protons, and a PP_i synthase or F_0F_1-ATPase complex (all of these enzyme complexes could have been significantly different than the present day enzymes). Certainly, if bacteriorhodopsin-based photosynthesis did not exist yet, it developed soon after the F_0F_1-ATPase (or PP_i synthase) complex resulting in ATP (or PP_i) generation much like it occurs in *Halobacter halobium* today.[2]

Evolution of the Cytochrome c *Oxidase Complex*

After the usefulness of a proton gradient for generation of ATP and for the transport of small molecules across the cell membrane had been firmly established, evolutionary pressures were responsible for diversification and improvements in the efficiency of these processes. There are a number of indications that a primitive ubiquinol oxidase complex present in the primitive cell slowly became more complicated structurally and

functionally and eventually split into two enzyme complexes.

Sulfolobus acidocaldarius is a typical sulfur-dependent archaebacterium which grows at 70-80°C and at pH 2.0-3.5 and thus appears to be a living fossil of the early biotic soup.[317] This bacterium contains an NADH dehydrogenase complex,[318] a succinate dehydrogenase complex,[319] and a two similar caldariellaquinol terminal oxidase complexes of mysterious composition. One of these ubiquinol oxidase complexes contains three different polypeptides. These polypeptides are homologous to cytochrome *b* (of the cytochrome bc_1 complex) and to cytochrome *c* oxidase subunits I and II, respectively.[165] The four hemes of this enzyme are all hemes A_s (modified hemes A).[5] This enzyme has been postulated to translocate protons via a $Q(H_2)$-loop[165] similar (in principle) to that described in Chapter 3 for the *E. coli* cytochrome bo_3 complex. The other ubiquinol oxidase complex contains at least three polypeptides. One of these polypeptides is homologous to a fusion between cytochrome *c* oxidase subunits I and III, one polypeptide is apparently the same cytochrome *b* homolog found in the previously described *Sulfolobus* enzyme, and a third polypeptide contains a Rieske-type iron-sulfur center. This enzyme also contains four hemes: three hemes A_s and one heme B.[320] The ET pathways in these enzymes have not been worked out, especially with regards to the extra hemes and the iron-sulfur center. However, it is quite apparent that these caldariellaquinol terminal oxidase complexes are more complicated structurally and functionally than the cytochrome bo_3 complex and contain essential structural features of both the mitochondrial cytochrome bc_1 and cytochrome *c* oxidase complexes.

An ubiquinol supercomplex containing both the cytochrome bc_1 and cytochrome *c* oxidase complexes have been isolated from *P. denitrificans* and the thermophilic bacterium PS3. The *Paracoccus* enzyme consists of normal mitochondrial-type cytochrome bc_1 and cytochrome *c* oxidase complexes as well as an extra membrane-bound cytochrome *c* (cytochrome c_{552}) sandwiched between the two larger complexes.[321] *Paracoccus* also contains a soluble cytochrome *c* (cytochrome c_{550}) that is

analogous to the mitochondrial cytochrome *c*. The ET path from cytochrome c_{552} to the cytochrome *c* oxidase complex is apparently different than that for the soluble cytochrome c_{550} indicating an important role for both of these cytochromes *c*.[112] The ubiquinol supercomplex isolated from PS3 is very similar to the *Paracoccus* supercomplex; the major difference is the presence of a cytochrome *c* domain at the C-terminus of the cytochrome *c* oxidase subunit II.[322] These supercomplexes are clearly highly advanced versions of a primitive ubiquinol oxidase complex as they contain all of the redox centers found in the mitochondrial respiratory chain. Analogous membrane-bound cytochromes *c* have been found in *Bacillus subtilis* and *Nitrobacter winogradskyi* as well.[323,324] The membrane-bound cytochromes *c* were possibly initially necessary for efficient ET chemistry. Since a soluble cytochrome *c* was only feasible after bacteria acquired a second membrane, if this membrane had not been acquired at the time these supercomplexes evolved, the cytochrome *c* mediating ET between the cytochrome bc_1 and cytochrome *c* oxidase complexes had to have remained membrane-bound.

A number of cytochrome caa_3 complexes have been found in bacteria. All of these complexes are similar to the PS3 cytochrome caa_3 complex mentioned above - the cytochrome *c* domain is a C-terminal extension on subunit II of the enzyme - although they have been isolated without attached cytochrome bc_1 polypeptides (see Table 1.1). All of these bacteria have a soluble cytochrome *c* that serves to shuttle electrons from the cytochrome bc_1 complex to the cytochrome caa_3 complex. The functional role of the covalently attached cytochrome *c* is a mystery as it appears to serve as an intermediate electron transfer site between the soluble cytochrome *c* and the Cu_A site. As the mitochondrial cytochrome *c* oxidase complex exemplifies, however, this extra ET site is clearly not necessary. This extra cytochrome *c* domain was most likely lost when mitochondria evolved and mitochondrial genes were transferred to the nuclear genome.

Denitrification Enzymes

There is one class of cytochrome *c* oxidase complexes found in a number of bacteria (*Bradyrhizobium japonicum*, *P. denitrificans*, *Rhodobacter sphaeroides*, and *Rhodobacter capsulatus*) that must have arisen within a different evolutionary branch than that which gave rise to the mitochondrial cytochrome *c* oxidase complex. This class of enzymes contains a low-spin heme and a high-spin heme-Cu_B binuclear center in subunit I of the enzyme as is common to all cytochrome *c* oxidase complexes. However, electron input from a soluble cytochrome *c* occurs through a series of three hemes in extramembranous domains of two other subunits. Notably, none of these enzymes has a Cu_A center.[176-178,325,326] The nitric oxide reductase (NOR) complex from *Pseudomonas stutzeri* (which catalyzes the reduction of two molecules of NO to N_2O) is clearly related to these cytochrome *c* oxidase complexes. The largest subunit of this NOR complex is homologous to subunit I of the cytochrome *c* oxidase family and the two hemes and copper ion in this subunit are ligated by the six invariant histidines common to this family of enzymes. In addition to the two hemes B in this subunit, this NOR complex contains a heme C in an associated subunit (hence, this enzyme is termed a cytochrome *bc*-type NOR complex) which appears to be the primary acceptor of electrons from a soluble cytochrome *c*.[306,327] *P. stutzeri* also contains a nitrous oxide reductase (N_2OR) complex (which catalyzes the reduction of N_2O to N_2). This enzyme contains a binuclear copper site that is very similar structurally to the Cu_A site of the cytochrome *c* oxidase complexes.[46,47,328,329]

Construction of an Evolutionary Tree

As Nature very rarely builds a new protein but rather builds with the material at hand already, it is quite unlikely that the NOR and N_2OR complexes and the cytochrome *c* oxidase complexes evolved independently to yield very similar structures. Thus, the clear homology between these nitrogenic respiratory enzymes and the cytochrome *c*

oxidase complexes implies that these proteins have a common ancestor. However, it is not so simple to decipher which group of enzymes evolved first as arguments support both possibilities. The notion that denitrifying and sulfur-reducing bacteria were present on the early earth when the availablity of atmospheric dioxygen was low is an attractive one. The average temperature of the early earth was much hotter to be sure[308] and the many bacteria found only in hot springs or near deep sea thermal vents today do appear to be living fossils. However, quite a few thermophilic bacteria have ubiquinol and/or cytochrome *c* oxidase complexes in their respiratory chains (e.g. *S. acidocaldarius*, PS3, *Thermus thermophilus*)[152,165,166,173,320,330,331] suggesting that dioxygen was indeed sufficiently abundant wherever and whenever life began. It is considered unlikely that these bacteria obtained oxygenic respiratory chains when dioxygen became plentiful in the atmosphere through separate major gene transfer events.[332] While NO was likely present in the early atmosphere,[315] it is by no means certain that its concentration was that much higher than the free O_2 concentration.[308] In fact, it is considered possible that localized "oxygen oases" existed on the early earth despite an anoxic atmosphere as a result of water and CO_2 photolysis in aqueous basins with low concentrations of reduced substances (such as H_2, CO, H_2S and Fe^{2+}).[310,315] The appearance of superoxide dismutases in prokaryotes more primitive than cyanobacteria argues for an early presence of relatively high dioxygen concentrations for "it is difficult to understand the evolution of an enzyme designed to protect an organism from something that supposedly did not exist."[308] The many ubiquinol and cytochrome *c* oxidase complexes expressed only under conditions of low oxygen tension indicate that high concentrations of dioxygen are not required for these enzymes to function efficiently.[303] Thus, the argument that denitrifying enzymes evolved before terminal oxidase complexes because dioxygen was essentially unavailable on the early earth is not very convincing.

Natural selection works quite fast to eliminate mutant organisms that cannot compete or enzymes that do not provide a selective advantage. An organism that has both

cytochrome bc_1 and cytochrome *c* oxidase complexes as well as a ubiquinol terminal oxidase complex is not expected to be able to compete successfully with other members of its species if it loses the function of one of the former complexes (e.g. due to a single-site mutation or gene deletion). The loss in respiratory efficiency will quite powerfully select against the mutant organism. On the other hand, a cell that is able to split its ubiquinol oxidase activity into two complexes that yield a better respiratory efficiency can certainly father the take-over of its niche by a new species. *E. coli* do not contain cytochrome bc_1 or cyochrome *c* oxidase complexes, or anything resembling these complexes, and yet this species does contain the cytochrome bo_3 ubiquinol oxidase complex.[179] Because of this fact and the argument that natural selection would strongly select against an organism that loses cytochrome bc_1/cytochrome *c* oxidase respiratory activity, it is quite certain, in my opinion, that a ubiquinol terminal oxidase complex existed before a cytochrome *c* oxidase complex. In this discussion, there has been no mention of the cytochrome *bd* complex, an alternative but structurally unrelated ubiquinol oxidase complex also found in *E. coli*.[221] The most likely explanation for these two ubiquinol terminal oxidase complexes in *E. coli* is convergent evolution. These enzymes probably evolved approximately simultaneously in two physically-separated primitive cell populations. Most likely, a gene transfer event between the two populations resulted in a species with greater adaptability (The cytochrome *bd* complex has a higher oxygen affinity and is preferentially expressed under low oxygen tension whereas the cytochrome bo_3 complex translocates twice as many protons and is preferentially expressed under high oxygen tension[221]).

If it is accepted that the ancestral bo_3-type ubiquinol oxidase complex was the progenitor of the cytochrome *c* oxidase complexes, the cytochrome *bc*-type NOR complex must have evolved after oxygenic respiration. This evolution scenario makes sense from the standpoint of complexity. Clearly, when a cytochrome *c* oxidase complex existed, a cytochrome bc_1 complex must also have existed. As the ferrocytochrome *c*

arising from cytochrome bc_1 turnover is required for membrane-bound nitrous oxide reductase activity,[302,333] it is a relatively simple evolutionary step to convert a cytochrome *c* oxidase complex into a *P. stutzeri*-type nitrous oxide reductase complex; in fact, the present-day mitochondrial cytochrome *c* oxidase complex has a low nitric oxide reductase activity.[16] Once a cytochrome *bc*-type nitrous oxide reductase complex existed, the other enzymes involved in nitrate/nitrite respiration (nitrite and nitric oxide reductase complexes) could evolve. In this scenario, the Cu_A site of the cytochrome *c* oxidase complexes was found useful for the *P. stutzeri* N_2OR complex. Note that there exists a nitrate reductase in *E. coli* but the nitrite produced is excreted by a nitrate/nitrite antiporter. And attempts to find a nitric oxide reductase complex in *E. coli* have been unsuccessful.[334] In the context of this discussion, the absence of a nitric oxide reductase complex in *E. coli* is not surprising as its progenitor - a cytochrome *c* oxidase complex - is also absent from this species. Thus, the increase in respiratory complexity according to this discussion proceeded from a ubiquinol terminal oxidase complex (one enzyme) to cytochrome bc_1 and cytochrome *c* oxidase complexes (two enzymes) and eventually to cytochrome bc_1, nitrite reductase, nitric oxide reductase and nitrous oxide reductase complexes (four enzymes) (note that the electron carriers between the various complexes also contribute to increased complexity). The electron donor remains the same (ubiquinol) although the resultant reduced species changes (at first, H_2O; at the end of one evolutionary branch, N_2) in this evolutionary progression. At each step in this progression, many pieces of the new enzymes clearly arise from structural motifs already present.

The increase in respiratory complexity throughout evolution as discussed in this chapter is summarized in Figure 7.1. It is important to point out that *every* enzyme observed today is the result of 4.5 billion years of evolution. Thus, it is incorrect to state, for example, that the *E. coli* cytochrome bo_3 complex evolved to yield the mitochondrial cytochrome bc_1 and cytochrome *c* oxidase complexes. Therefore, each of the complexes

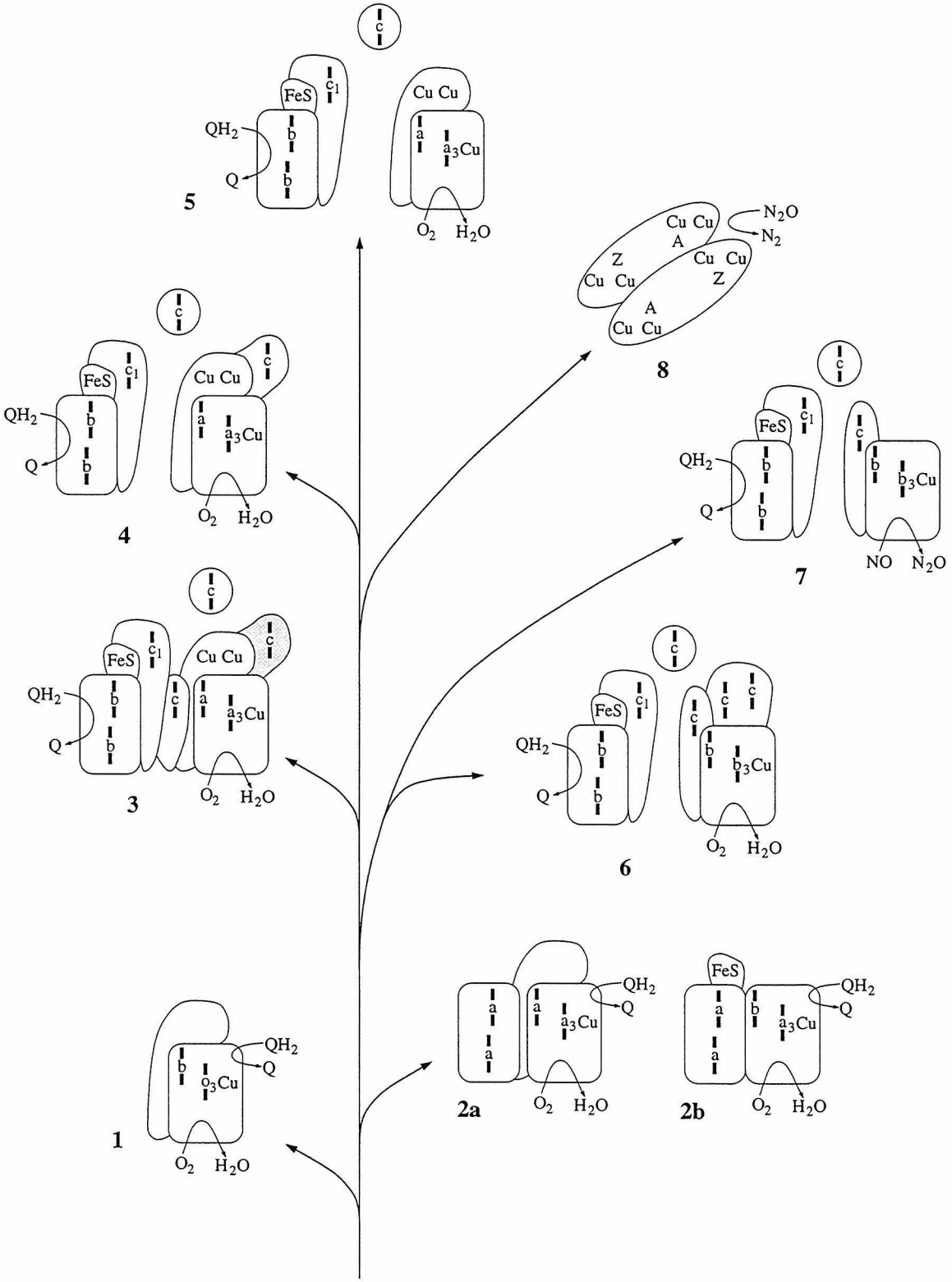
c
FeS
c1
QH2
b
Q
Cu Cu
a
a3Cu
O2
H2O
5
N2O
N2
Cu Cu
A
Z
Cu Cu
Cu Cu
Z
A
Cu Cu
8
4
3
6
7
b3Cu
NO
N2O
1
2a
2b
primitive ubiquinol oxidase

in Figure 7.1 is shown at the end of a branch. However, the present-day enzymes certainly yield clues as to the common ancestor for all the enzymes included in this scheme: a primitive ubiquinol oxidase complex. It has not been settled whether the cytochrome cbb_3 complexes (**6**) are proton pumps but the experimental evidence favors this possibility.[325] On the other hand, there are no indications that the *P. stutzeri* NOR complex (**7**) pumps protons despite sufficient redox energy to support this function.[302] From the standpoint of this evolutionary tree, however, it is unlikely that the cytochrome cbb_3 complexes are proton pumps and the *P. stutzeri* NOR complex is not. Based on this thesis, it is postulated that neither of these complexes are proton pumps because both lack a Cu_A site. The proton pump data on the cytochrome cbb_3 complex was collected using whole cells, and therefore, the observed proton pumping could certainly arise from unidentified enzymes.

Concluding Remarks

In this thesis, the argument has been made that despite the high structural similarities

---

Figure 7.1 An evolutionary tree depicting the increase in complexity of respiratory proteins as evidenced by present-day enzyme complexes. Length of branches are *not* scaled to evolutionary distance. (1) The *E. coli* cytochrome bo_3 ubiquinol oxidase complex. Subunit II contains the same cupredoxin fold found in the Cu_A-binding domain of cytochrome *c* oxidase and nitrous oxide reductase complexes. Protons are translocated via a $Q(H_2)$-loop mechanism (Chapter 3). (2a) *S. acidocaldarius* caldariellaquinol terminal oxidase complex containing homologs of cytochrome *b* (of the cytochrome bc_1 complex) and cytochrome *c* oxidase subunits I and II. Proton translocation is postulated to occur via a $Q(H_2)$-loop mechanism. (2b) *S. acidocaldarius* caldariellaquinol terminal oxidase complex containing homologs of cytochrome *b* (of the cytochrome bc_1 complex) and a fusion protein of cytochrome *c* oxidase subunits I and III. A third subunit contains a Rieske-type iron-sulfur center. (3) Cytochrome bc_1/cytochrome *c*/cytochrome *c* oxidase supercomplex found in *P. denitrificans* and the thermophilic bacterium PS3. The C-terminal extension on subunit II of the cytochrome *c* oxidase complex (shaded) is found in the PS3 enzyme. (4) A cytochrome caa_3 complex has been found in a number of bacteria. It is not known if a cytochrome bc_1/cytochrome *c*/cytochrome *c* oxidase supercomplex exists under physiological conditions in all cases. An active cytochrome *c* oxidase complex from *P. denitrificans* and the thermophilic bacterium PS3 can be isolated alone or as part of a supercomplex as in (4). (5) The mitochondrial cytochrome bc_1 and cytochrome aa_3 (cytochrome *c* oxidase) complexes. In (3), (4) and (5), proton translocation occurs via a $Q(H_2)$-loop mechanism (cytochrome bc_1 complex) and the cytochome *c* oxidase proton pump. (6) The cytochrome bc_1 and cytochrome cbb_3 complexes found in *B. japonicum*, *P. denitrificans*, *R. sphaeroides*, and *R. capsulatus*. The general belief is that the cytochrome cbb_3 complexes pump protons (but see text). (7) The cytochrome bc_1 and nitric oxide reductase complexes found in *P. stutzeri* . The nitric oxide reductase complex has not been found to catalyze proton translocation. (8) The periplasmic nitrous oxide reductase complex found in *P. stutzeri* contains two binuclear copper centers: a Cu_A-type center, thought to function as an electron transfer site, and the Z center, thought to be the catalytic site. See text for references and further details.

of the UQO and the CcO complexes, these enzymes are very different functionally. The UQO complex utilizes a relatively simple mechanism to catalyze proton translocation: a $Q(H_2)$-loop. The simplicity of this mechanism is apparent because electron gating, but not proton gating, is required for successful proton translocation: protons are simply released into/taken up from the most accessible aqueous phase in order to balance electron output/input reactions. On the other hand, the CcO complex is a redox-linked proton pump. Very efficient proton gating mechanisms are required in order to alternate accessibility of a transmembrane proton channel to the opposing sides of the membrane at the appropriate steps during turnover. The redox-energy is carefully transferred to the polypeptide matrix in discrete steps in order to accomplish this proton gating and move protons stepwise through the proton channel. An understanding of how the CcO proton pump functions on a molecular level is still far from complete, but the recently solved crystal structures promise to aid tremendously in solving this problem. The greater functional complexity of the cytochrome bc_1/cytochrome *c* oxidase segment of the mitochondrial respiratory chain relative to the UQO complex strongly argues that the common ancestor of these enzymes was a ubiquinol oxidase complex and an attempt has been made here to rationalize how the evolutionary process might have occurred. The basic assumption that an organism with a ubiquinol terminal oxidase complex as well as cytochrome bc_1 and cytochrome *c* oxidase complexes in its respiratory chain would never be able to successfully compete with other members of its species if it lost the function of one of the latter enzymes can be experimentally tested by integrating the required genes for cytochrome bc_1/cytochrome *c* oxidase respiration into the *E. coli* genome and determining if wild-type *E. coli* can still survive in the presence of this mutant. From this discussion, it is apparent that oxygenic respiration is quite an old process, and, in fact, predates nitrogenic respiration as well as reaction center photosynthesis since both of these processes require the cytochrome bc_1 complex which arose in the later stages of oxygenic respiratory evolution.

Literature Citations

(1) Alberts, B., D. Bray, J. Lewis, M. Raff, K. Roberts and J. D. Watson. **1989**. Molecular biology of the cell. Garland Publishing, Inc., New York.

(2) Stryer, L. **1988**. Biochemistry. W. H. Freeman and Co., New York.

(3) Brittain, T., R. Blackmore, C. Greenwood and A. J. Thompson. **1992**. Bacterial nitrite-reducing enzymes. *Eur. J. Biochem.* 209:793-802.

(4) Schauder, R. and A. Kröger. **1993**. Bacterial sulfur respiration. *Arch. Microbiol.* 159:491-497.

(5) Lübben, M. and K. Morand. **1994**. Novel prenylated hemes as cofactors of cytochrome oxidases: archaea have modified hemes A and O. *J. Biol. Chem.* 269:21473-21479.

(6) Musser, S. M., M. H. B. Stowell and S. I. Chan. **1995**. Cytochrome *c* oxidase: chemistry of a molecular machine. *In* Advances in Enzymology and Related Areas of Molecular Biology, vol. 71. A. Meister, ed. John Wiley and Sons, Inc., New York. pp. 79-208.

(7) Mogi, T., K. Saiki and Y. Anraku. **1994**. Biosynthesis and functional role of haem O and haem A. *Mol. Microbio*. 14:391-398.

(8) Hakvoort, T. B. M., K. M. C. Sinjorgo, B. F. van Gelder and A. O. Muijsers. **1985**. Separation of enzymatically active bovine cytochrome *c* oxidase monomers and dimers by high performance liquid chromatography. *J. Inorg. Biochem.* 23:381-388.

(9) Robinson, N. C. and L. Talbert. **1986**. Triton X-100 induced dissociation of beef heart cytochrome *c* oxidase into monomers. *Biochemistry*. 25:2328-2335.

(10) Sone, N. and T. Kosako. **1986**. Evidence for dimer structure of proton-pumping cytochrome *c* oxidase, an analysis by radiation inactivation. *EMBO J*. 5:1515-1519.

(11) Hakvoort, T. B. M., K. Moolenaar, A. H. M. Lankvelt, K. M. C. Sinjorgo, H. L. Dekker and A. O. Muijsers. **1987**. Separation, stability and kinetics of monomeric and dimeric bovine heart cytochrome *c* oxidase. *Biochim. Biophys. Acta*. 894:347-354.

(12) Antonini, G., M. Brunori, F. Malatesta, P. Sarti and M. T. Wilson. **1987**. Reconstitution of monomeric cytochrome *c* oxidase into phospholipid vesicles yields functionally interacting cytochrome aa_3 units. *J. Biol. Chem*. 262:10077-10079.

(13) Iwata, S., C. Ostermeier, B. Ludwig and H. Michel. **1995**. Structure at 2.8 Å resolution of cytochrome *c* oxidase from *Paracoccus denitrificans*. *Nature*. 376:660-669.

(14) Tsukihara, T., H. Aoyama, E. Yamashita, T. Tomizaki, H. Yamaguchi, K. Shinzawa-Itoh, R. Nakashima, R. Yaono and S. Yoshikawa. **1995**. Structure of metal sites of oxidized bovine heart cytochrome *c* oxidase at 2.8 Å. *Science*. 269:1069-1974.

(15) Blair, D. F., C. T. Martin, J. Gelles, H. Wang, G. W. Brudvig, T. H. Stevens and S. I. Chan. **1983**. The metal centers of cytochrome *c* oxidase: structures and interactions. *Chemica Scripta*. 21:43-53.

(16) Brudvig, G. W., T. H. Stevens and S. I. Chan. **1980**. Reactions of nitric oxide with cytochrome *c* oxidase. *Biochemistry*. 19:5275-5285.

(17) Powers, L., B. Chance, Y. Ching and P. Angiolillo. **1981**. Structural features and the reaction mechanism of cytochrome oxidase. *Biophysical J*. 34:465-498.

(18) Scott, R. A. **1989**. X-ray absorption spectroscopic investigations of cytochrome *c* oxidase structure and function. *Ann. Rev. Biophys. Biophys. Chem*. 18:137-158.

(19) Scott, R. A., J. R. Schwartz and S. P. Cramer. **1986**. Structural aspects of the copper sites in cytochrome *c* oxidase. An X-ray absorption spectroscopic investigation of the resting-state enzyme. *Biochemistry*. 25:5546-5555.

(20) Chance, B. and L. Powers. **1985**. Structure of cytochrome oxidase redox centers in native and modified forms: an EXAFS study. *Curr. Top. Bioenerg*. 14:1-19.

(21) Day, E. P., J. Peterson, M. S. Sendova, J. Schoonover and G. Palmer. **1993**. Magnetization of fast and slow oxidized cytochrome *c* oxidase. *Biochemistry*. 32:7855-7860.

(22) Mascarenhas, R., Y.-H. Wei, C. P. Scholes and T. E. King. **1983**. Interaction in cytochrome *c* oxidase between cytochrome a_3 ligated with nitric oxide and cytochrome *a*. *J. Biol. Chem*. 258:5348-5351.

(23) Ohnishi, T., R. LoBrutto, J. C. Salerno, R. C. Bruckner and T. G. Frey. **1982**. Spatial relationship between cytochrome *a* and a_3. *J. Biol. Chem*. 257:14821-14825.

(24) Scholes, C. P., R. Janakisaman, H. Taylor and T. E. King. **1984**. Temperature dependence of the electron spin-lattice relaxation rate from pulsed EPR of Cu_A and heme *a* in cytochrome *c* oxidase. *Biophysical J*. 45:1027-1030.

(25) Brudvig, G. W., D. F. Blair and S. I. Chan. **1984**. Electron spin relaxation of Cu_A and cytochrome *a* in cytochrome *c* oxidase: comparison to heme, copper, and sulfur radical complexes. *J. Biol. Chem*. 259:11001-11009.

(26) Gelles, J., D. F. Blair, C. T. Martin, H. Wang and S. I. Chan. **1983**. Structural studies on the metal centers of cytochrome *c* oxidase. *In* Frontiers in Biochemical and Biophysical Studies of Proteins and Membranes. T.-Y. Liu, S. Sakakibara, A. N. Schechter, K. Yagi, H. Yajima and K. T. Yasunobu, eds. Elsevier, New York. pp. 259-277.

(27) Goodman, G. and J. S. Leigh Jr. **1985**. Distance between the visible copper and cytochrome *a* in bovine heart cytochrome oxidase. *Biochemistry*. 24:2310-2317.

(28) Ohnishi, T., H. Blum, J. S. Leigh Jr and J. C. Salerno. **1979**. Location of cytochrome oxidase EPR active centers. *In* Membrane Bioenergetics. C. P. Lee, G. Schatz and L. Ernster, eds. Addison-Wesley, Massachusetts. pp. 21-30.

(29) Kent, T. A., L. J. Young, G. Palmer, J. A. Fee and E. Münck. **1983**. Mössbauer study of beef heart cytochrome oxidase: comparative study of the bovine enzyme and cytochrome c_1aa_3 from *Thermus thermophilus*. *J. Biol. Chem*. 258:8543-8546.

(30) Wang, H., T. Sauke, P. G. Cebrunner and S. I. Chan. **1988**. The CO adduct of yeast cytochrome *c* oxidase. *J. Biol. Chem*. 263:15260-15263.

(31) Martin, C. T., C. P. Scholes and S. I. Chan. **1985**. The identification of histidine ligands to cytochrome *a* in cytochrome *c* oxidase. *J. Biol. Chem*. 260:2857-2861.

(32) Blokzijl-Homan, M. F. J. and B. F. van Gelder. **1971**. Biochemical and biophysical studies on cytochrome aa_3 III. The EPR spectrum of NO-ferrocytochrome a_3. *Biochim. Biophys. Acta*. 234:493-498.

(33) Stevens, T. H. and S. I. Chan. **1981**. Histidine is the axial ligand to cytochrome a_3 in cytochrome *c* oxidase. *J. Biol. Chem*. 256:1069-1071.

(34) Ogura, T., K. Hon-nami, T. Oshima, S. Yoshikawa and T. Kitagawa. **1983**. *J. Am. Chem. Soc*. 105:7781-7783.

(35) Kitagawa, T. **1988**. The heme protein structure and iron histidine stretching mode. *In* Biological Applications of Raman Spectroscopy, vol. 3. T. G. Spiro, ed. Wiley, New York. pp. 97-131.

(36) Li, P. M., J. Gelles, S. I. Chan, R. J. Sullivan and R. A. Scott. **1987**. Extended X-ray absorption fine structure of copper in Cu_A-depleted, *p*-(hydroxymercuri)benzoate-modified, and native cytochrome *c* oxidase. *Biochemistry*. 26:2091-2095.

(37) Cline, J., B. Reinhammer, P. Jensen, R. Venters and B. M. Hoffman. **1983**. Coordination environment for the type III copper center of tree laccase and Cu_B of cytochrome *c* oxidase as determined by electron nuclear double resonance. *J. Biol. Chem*. 258:5124-5128.

(38) Shapleigh, J. P., J. P. Hosler, M. M. J. Tecklenburg, Y. Kim, G. T. Babcock, R. B.

Gennis and S. Ferguson-Miller. **1992**. Definition of the catalytic site of cytochrome *c* oxidase: specific ligands of heme *a* and the heme a_3-Cu_B center. *Proc. Natl. Acad. Sci. USA*. 89:4786-4790.

(39) Hosler, J. P., S. Ferguson-Miller, M. W. Calhoun, J. W. Thomas, J. Hill, L. Lemieux, J. Ma, C. Georgiou, J. Fetter, J. Shapleigh, M. M. J. Tecklenburg, G. T. Babcock and R. B. Gennis. **1993**. Insight into the active-site structure and function of cytochrome oxidase by analysis of site-directed mutants of cytochrome aa_3 and cytochrome *bo*. *J. Bioenerg. Biomemb*. 25:121-136.

(40) Greenwood, C., A. J. Thomson, C. P. Barrett, J. Peterson, G. N. George, J. A. Fee and J. Reichardt. **1988**. Some spectroscopic views of the Cu_A site in cytochrome *c* oxidase preparations. *Ann. N. Y. Acad. Sci.* 550:47-52.

(41) Stevens, T. H., C. T. Martin, H. Wang, G. W. Brudvig, C. P. Scholes and S. I. Chan. **1982**. The nature of Cu_A in cytochrome *c* oxidase. *J. Biol. Chem.* 257:12106-12113.

(42) Gurbiel, R. J., Y.-C. Fann, K. K. Surerus, M. M. Werst, S. M. Musser, P. E. Doan, S. I. Chan, J. A. Fee and B. M. Hoffman. **1993**. Detection of two histidyl ligands to Cu_A of cytochrome oxidase by 35 GHz ENDOR: $^{14,15}N$ and $^{63,65}Cu$ ENDOR studies of the Cu_A site in bovine heart cytochrome aa_3 and cytochromes caa_3 and ba_3 from *Thermus thermophilus*. *J. Am. Chem. Soc.* 115:10888-10894.

(43) Martin, C. T., C. P. Scholes and S. I. Chan. **1988**. On the nature of cysteine coordination to Cu_A in cytochrome *c* oxidase. *J. Biol. Chem.* 263:8420-8429.

(44) Gelles, J., D. F. Blair and S. I. Chan. **1986**. The proton-pumping site of cytochrome *c* oxidase: a model of its structure and mechanism. *Biochim. Biophys. Acta*. 853:205-236.

(45) Kroneck, P. M. H., W. A. Antholine, J. Reister and W. G. Zumft. **1988**. The cupric site in nitrous oxide reductase contains a mixed-valence [Cu(II),Cu(I)] binuclear center: a multifrequency electron paramagnetic resonance investigation.

FEBS Lett. 242:70-74.

(46) Scott, R. A., W. G. Zumft, C. L. Coyle and D. M. Dooley. **1989**. *Pseudomonas stutzeri* N_2O reductase contains Cu_A-type sites. *Proc. Natl. Acad. Sci. USA*. 86:4082-4086.

(47) Antholine, W. E., D. H. W. Kastrau, G. C. M. Steffens, G. Büse, W. G. Zumft and P. M. H. Kroneck. **1992**. A comparative EPR investigation of the multicopper proteins nitrous-oxide reductase and cytochrome *c* oxidase. *Eur. J. Biochem.* 209:875-881.

(48) Fee, J. A., D. Sanders, C. E. Slutter, P. E. Doan, R. Aasa, M. Karpefors and T. Vänngård. **1995**. Multifrequency EPR evidence for a binuclear Cu_A center in cytochrome *c* oxidase: studies with a ^{63}Cu- and ^{65}Cu-enriched, soluble domain of the cytochrome ba_3 subunit II from *Thermus thermophilus*. *Biochem. Biophys. Res. Comm*. 212:77-83.

(49) Lappalainen, P., R. Aasa, B. G. Malmström and M. Saraste. **1993**. Soluble Cu_A-binding domain from the *Paracoccus* cytochrome *c* oxidase. *J. Biol. Chem.* 268:26416-26421.

(50) van der Oost, J., P. Lappalainen, A. Musacchio, A. Warne, L. Lemieux, J. Rumbley, R. B. Gennis, R. Aasa, T. Pascher, B. G. Malmström and M. Saraste. **1992**. Restoration of a lost metal-binding site: construction of two different copper sites into a subunit of the *E. coli* cytochrome *o* quinol oxidase complex. *EMBO J*. 11:3209-3217.

(51) Kelly, M., P. Lappalainen, G. Talbo, T. Haltia, J. van der Oost and M. Saraste. **1993**. Two cysteines, two histidines, and one methionine are ligands of a binuclear purple copper center. *J. Biol. Chem*. 268:16781-16787.

(52) Zumft, W. G., A. Dreasch, S. Löchelt, H. Cuypers, B. Friedrich and B. Schneider. **1992**. Derived amino acid sequences of the *nosZ* gene (respiratory N_2O reductase) from *Alcaligenes eutrophus*, *Pseudomonas aeruginosa* and *Pseudomonas stutzer*i

reveal potential copper–binding residues: implications for the Cu_A site of N_2O reductase and cytochrome *c* oxidase. *Eur. J. Biochem*. 208:31-40.

(53) Thomson, A. J., C. Greenwood, J. Peterson and C. P. Barrett. **1986**. Determination of the optical properties of Cu_A(II) in bovine cytochrome *c* oxidase using magnetic circular dichroism as an optical detector of paramagnetic resonance. *J. Inorg. Biochem*. 28:195-205.

(54) Kroneck, P. M. H., W. E. Antholine, D. H. W. Kastrau, G. Buse, G. C. M. Steffens and W. G. Zumft. **1990**. Multifrequency EPR evidence for a bimetallic center at the Cu_A site in cytochrome *c* oxidase. *FEBS Lett.* 268:274-276.

(55) Beinert, H., R. W. Shaw, R. E. Hansen and C. R. Hartzell. **1980**. Studies on the origin of the near-infrared (800-900 nm) absorption of cytochrome *c* oxidase. *Biochim. Biophys. Acta*. 591:458-470.

(56) Steffens, G. C. M., T. Soulimane, G. Wolff and G. Buse. **1993**. Stoichiometry and redox behavior of metals in cytochrome *c* oxidase. *Eur. J. Biochem*. 213:1149-1157.

(57) Lappalainen, P. and M. Saraste. **1994**. The binuclear Cu_A center of cytochrome oxidase. *Biochim. Biophys. Acta.* 1187:222-225.

(58) Blackburn, N. J., M. E. Barr, W. H. Woodruff, J. van der Oost and S. de Vries. **1994**. Metal-metal bonding in biology: EXAFS evidence for a 2.5 Å copper-copper bond in the Cu_A center of cytochrome oxidase. *Biochemistry*. 33:10401-10407.

(59) Hansen, A. P., R. D. Britt, M. P. Klein, C. J. Bendes and G. T. Babcock. **1993**. ENDOR and ESEEM studies of cytochrome *c* oxidase: evidence for exchangeable protons at the Cu_A site. *Biochemistry*. 32:13718-13724.

(60) Taha, T. S. M. and S. Ferguson-Miller. **1992**. Interaction of cytochrome *c* with cytochrome *c* oxidase studied by monoclonal antibodies and a protein modifying reagent. *Biochemistry*. 31:9090-9097.

(61) Bisson, R. and C. Montecucco. **1982**. Different polypeptides of bovine heart cytochrome *c* oxidase are in contact with cytochrome *c*. *FEBS Lett.* 150:49-53.

(62) Bisson, R., G. C. M. Steffens, R. A. Capaldi and G. Buse. **1982**. Mapping of the cytochrome *c* binding site on cytochrome *c* oxidase. *FEBS Lett*. 144:359-363.

(63) Millett, F., C. de Jong, L. Paulson and R. A. Capaldi. **1983**. Identification of the specific carboxylate groups on cytochrome *c* oxidase that are involved in binding cytochrome *c*. *Biochemistry*. 22:546-552.

(64) Millett, F., V. Darley-Usmar and R. A. Capaldi. **1982**. Cytochrome *c* is cross-linked to subunit II of cytochrome *c* oxidase by a water-soluble carbodiimide. *Biochemistry*. 21:3857-3862.

(65) Yewey, G. L. and W. S. Caughey. **1988**. Metals of the bovine heart cytochrome *c* oxidase. *Ann. N. Y. Acad. Sci*. 550:22-32.

(66) Yewey, G. L. and W. S. Caughey. **1987**. Metals and activity of bovine heart cytochome *c* oxidase are independent of polypeptide subunit III, subunit VII, subunit A and subunit B. *Biochem. Biophys. Res. Commun*. 148:1520-1526.

(67) Lin, J., L.-P. Pan and S. I. Chan. **1993**. The subunit location of magnesium in cytochrome *c* oxidase. *J. Biol. Chem*. 268:22210-22214.

(68) Babcock, G. T. and M. Wikström. **1992**. Oxygen activation and the conservation of energy in cell respiration. *Nature*. 356:301-309.

(69) Chan, S. I., S. N. Witt and D. F. Blair. **1988**. The dioxygen chemistry of cytochrome *c* oxidase. *Chemica Scripta*. 28A:51-56.

(70) Hill, B. C., C. Greenwood and P. Nicholls. **1986**. Intermediate steps in the reaction of cytochrome oxidase with molecular oxygen. *Biochim. Biophys. Acta*. 853:91-113.

(71) Naqui, A., B. Chance and E. Cadenas. **1986**. Reactive oxygen intermediates in biochemistry. *Ann. Rev. Biochem*. 55:137-166.

(72) Weng, L. and G. M. Baker. **1991**. Reaction of hydrogen peroxide with the rapid

form of resting cytochrome oxidase. *Biochemistry*. 30:5727-5733.

(73) Blair, D. F., S. N. Witt and S. I. Chan. **1985**. Mechanism of cytochrome *c* oxidase-catalyzed dioxygen reduction at low temperatures. Evidence for two intermediates at the three-electron level and entropic promotion of the bond-breaking step. *J. Am. Chem. Soc*. 107:7389-7399.

(74) Witt, S. N. and S. I. Chan. **1987**. Evidence for a ferryl Fe_{a3} in oxygenated cytochrome *c* oxidase. *J. Biol. Chem.* 262:1446-1448.

(75) Witt, S. N., D. F. Blair and S. I. Chan. **1986**. Chemical and spectroscopic evidence for the formation of a ferryl Fe_{a3} intermediate during turnover of cytochrome *c* oxidase. *J. Biol. Chem.* 261:8104-8107.

(76) Ogura, T., S. Takahashi, K. Shinzawa-Itoh, S. Yoshikawa and T. Kitagawa. **1990**. Observation of the Fe^{4+}=O stretching Raman band for cytochrome oxidase compound B at ambient temperature. *J. Biol. Chem*. 265:14721-14723.

(77) Varotsis, C. and G. T. Babcock. **1990**. Appearance of the $\nu(Fe^{IV}=O)$ vibration from a ferryl-oxo intermediate in the cytochrome oxidase/dioxygen reaction. *Biochemistry*. 29:7357-7362.

(78) Larsen, R. W., W. Li, R. A. Copeland, S. N. Witt, B.-S. Lou, S. I. Chan and M. R. Ondrias. **1990**. Room temperature characterization of the dioxygen intermediates of cytochrome *c* oxidase by resonance Raman spectroscopy. *Biochemistry*. 29:10135-10140.

(79) Han, S., Y. Ching and D. L. Rousseau. **1990**. Ferryl and hydroxyl intermediates in the reaction of oxygen with reduced cytochrome *c* oxidase. *Nature*. 348:89-90.

(80) Fee, J. A., B. H. Zimmerman, C. I. Nitsche, F. Rusnak and E. Münck. **1988**. The cytochrome caa_3 from *Thermus thermophilus*. *Chemica Scripta*. 28A:75-78.

(81) Kumar, C., A. Naqui, L. Powers, Y. Ching and B. Chance. **1988**. Does the peroxide compound of cytochrome oxidase contain ferryl iron? *J. Biol. Chem.* 263:7159-7163.

(82) Wikström, M. **1988**. Protonic sidedness of the binuclear iron-copper center in cytochrome oxidase. *FEBS Lett*. 231:247-252.

(83) Ksenzenko, M. Y., T. V. Vygodina, V. Berka, E. K. Ruuge and A. A. Konstantinov. **1992**. Cytochrome oxidase-catalyzed superoxide generation from hydrogen peroxide. *FEBS Lett*. 297:63-66.

(84) Vygodina, T. V. and A. A. Konstantinov. **1988**. H_2O_2-induced conversion of cytochrome *c* oxidase peroxy complex to the oxoferryl state. *Ann. N. Y. Acad. Sci.* 550:124-138.

(85) Wikström, M. **1981**. Energy-dependent reversal of the cytochrome oxidase reaction. *Proc. Natl. Acad. Sci. USA*. 78:4051-4054.

(86) Wikström, M. **1987**. Insight into the mechanism of cellular respiration from its partial reversal in mitochondria. *Chemica Scripta*. 27B:53-58.

(87) Wikström, M. **1988**. Mechanism of cell respiration. *Chemica Scripta*. 28A:71-74.

(88) Wikström, M. and J. Morgan. **1992**. The dioxygen cycle: spectral, kinetic, and thermodynamic characteristics of ferryl and peroxy intermediates observed by reversal of the cytochrome oxidase reaction. *J. Biol. Chem*. 267:10266-10273.

(89) Ogura, T., S. Yoshikawa and T. Kitagawa. **1989**. Raman/absorption simultaneous measurements for cytochrome oxidase compound A. *Biochemistry*. 28:8022-8027.

(90) Ogura, T., S. Takahashi, K. Shinzawa-Itoh, S. Yoshikawa and T. Kitagawa. **1990**. Observation of the Fe^{II}–O_2 stretching Raman band for cytochrome oxidase compound A at ambient temperature. *J. Am. Chem. Soc*. 112:5630-5631.

(91) Orii, Y. **1984**. Formation and decay of the primary oxygen compound of cytochrome oxidase at room temperature as observed by stopped flow, laser flash photolysis and rapid scanning. *J. Biol. Chem*. 259:7187-7190.

(92) Varotsis, C., W. H. Woodruff and G. T. Babcock. **1989**. Time-resolved Raman detection of ν(Fe–O) in an early intermediate in the reduction of O_2 by cytochrome oxidase. *J. Am. Chem. Soc*. 111:6439-6440.

(93) Babcock, G. T., J. M. Jean, L. N. Johnston, W. H. Woodruff and G. Palmer. **1985.** Flow-flash, time-resolved resonance Raman spectroscopy of the oxidation of reduced and of mixed valence cytochrome oxidase by dioxygen. *J. Inorg. Biochem*. 23:243-251.

(94) Han, S., Y. Ching and D. L. Rousseau. **1990.** Primary intermediate in the reaction of mixed-valence cytochrome *c* oxidase with oxygen. *Biochemistry*. 29:1380-1384.

(95) Han, S., Y. Ching and D. L. Rousseau. **1990.** Primary intermediate in the reaction of oxygen with fully reduced cytochrome *c* oxidase. *Proc. Natl. Acad. Sci. USA*. 87:2491-2495.

(96) Hill, B. C. and C. Greenwood. **1983.** Spectroscopic evidence for the participation of compound A (Fe_{a3}^{2+}–O_2) in the reaction of mixed-valence cytochrome *c* oxidase with dioxygen at room temperature. *Biochem. J.* 215:659-667.

(97) Han, S., Y. Ching and D. L. Rousseau. **1990.** Time evolution of the intermediates formed in the reaction of oxygen with mixed-valence cytochrome *c* oxidase. *J. Am. Chem. Soc*. 112:9445-9451.

(98) Varotsis, C., W. H. Woodruff and G. T. Babcock. **1990.** Direct detection of a dioxygen adduct of cytochrome a_3 in the mixed valence cytochrome oxidase/dioxygen reaction. *J. Biol. Chem*. 265:11131-11136.

(99) Hazzard, J. T., S. Rong and G. Tollin. **1991.** Ionic strength dependence of the kinetics of electron transfer from bovine mitochondrial cytochrome *c* to bovine cytochrome *c* oxidase. *Biochemistry*. 30:213-222.

(100) Larsen, R. W., J. R. Winkler and S. I. Chan. **1992.** Photoinitiated electron transfer between cytochrome *c* and cytochrome *c* oxidase using a novel uroporphyrin/NADH reducing system. *J. Phys. Chem*. 96:8023-8027.

(101) Pan, L.-P., J. T. Hazzard, J. Lin, G. Tollin and S. I. Chan. **1991.** The electron input to cytochrome *c* oxidase from cytochrome *c*. *J. Amer. Chem. Soc*. 113:5908-

5910.

(102) van Kuilenburg, A. B. P., H. L. Dekker, C. van den Bogert, P. Nieboer, B. F. van Gelder and A. O. Muijsers. **1991**. Isoforms of human cytochrome *c* oxidase: subunit composition and steady-state kinetic properties. *Eur. J. Biochem.* 199:615-622.

(103) Büge, U. and B. Kadenbach. **1986**. Influence of buffer composition, membrane lipids and proteases on the kinetics of reconstituted cytochrome *c* oxidase from bovine liver and heart. *Eur. J. Biochem.* 161:383-390.

(104) Thörnström, P.-E., P. Brzezinski, P.-O. Fredriksson and B. Malmström. **1988**. Cytochrome *c* oxidase as an electron-transport-driven proton pump: pH dependence of the reduction levels of the redox centers during turnover. *Biochemistry*. 27:5441-5447.

(105) Antonini, G., F. Malatesta, P. Sarti and M. Brunori. **1991**. Control of cytochrome oxidase activity. *J. Biol. Chem.* 266:13193-13202.

(106) Chan, S. I., G. W. Brudvig, C. T. Martin and T. H. Stevens. **1982**. The nature and the distribution of the metal centers in cytochrome *c* oxidase. *In* Interaction Between Iron and Proteins in Oxygen and Electron Transport. C. Ho, ed. Elsevier, Amsterdam. pp. 171-177.

(107) Malmström, B. G. **1989**. The mechanism of proton translocation in respiration and photosynthesis. *FEBS Lett*. 250:9-21.

(108) Oliveberg, M. and B. G. Malmström. **1991**. Internal electron transfer in cytochrome *c* oxidase: evidence for a rapid equilibrium between cytochrome *a* and the bimetallic site. *Biochemistry*. 30:7053-7057.

(109) Hill, B. C. **1991**. The reaction of the electrostatic cytochrome *c*-cytochrome *c* oxidase complex with oxygen. *J. Biol. Chem.* 266:2219-2226.

(110) Hill, B. C. **1994**. Modeling the sequence of electron transfer reactions in the single turnover of reduced, mammalian cytochrome *c* oxidase with oxygen. *J. Biol.*

Chem. 269:2419-2425.

(111) Einarsdóttir, Ó., T. D. Dawes and K. E. Georgiadis. **1992**. New transients in the electron-transfer dynamics of photolyzed mixed-valence CO-cytochrome *c* oxidase. *Proc. Natl. Acad. Sci. USA*. 89:6934-6937.

(112) Stowell, M. H. B., R. W. Larsen, J. R. Winkler, D. C. Rees and S. I. Chan. **1993**. Transient electron-transfer studies on the two-subunit cytochrome *c* oxidase from *Paracoccus denitrificans*. *J. Phys. Chem*. 97:3054-3057.

(113) Kobayashi, K., H. Une and K. Hayashi. **1989**. Electron transfer process in cytochrome oxidase after pulse-radiolysis. *J. Biol. Chem*. 264:7976-7980.

(114) Nilsson, T. **1992**. Photoinduced electron transfer from tris(2,2'-bipyridyl)ruthenium to cytochrome *c* oxidase. *Proc. Natl. Acad. Sci. USA*. 89:6497-6501.

(115) Morgan, J. E., P. M. Li, D. J. Jang, M. A. El-Sayed and S. I. Chan. **1989**. Electron transfer between cytochrome *a* and copper A in cytochrome *c* oxidase: a perturbed equilibrium study. *Biochemistry*. 28:6975-6983.

(116) Oliveberg, M. and B. G. Malmstrom. **1992**. Reaction of dioxygen with cytochrome *c* oxidase reduced to different degrees: indications of a transient dioxygen complex with copper B. *Biochemistry*. 31:3560-3563.

(117) Fabian, M., P.-E. Thörnström, P. Brezezinski and B. G. Malmström. **1987**. Two-electron reduction is required for rapid internal electron transfer in resting, pulsed and oxygenated cytochrome *c* oxidase. *FEBS Lett*. 213:396-400.

(118) Moody, A. J., U. Brandt and P. R. Rich. **1991**. Single electron reduction of 'slow' and 'fast' cytochrome *c* oxidase. *FEBS Lett*. 293:101-105.

(119) Malatesta, F., P. Sarti, G. Antonini, B. Vallone and M. Brunori. **1990**. Electron transfer to the binuclear center in cytochrome oxidase: catalytic significance and evidence for an additional intermediate. *Proc. Natl. Acad. Sci. USA*. 87:7410-7413.

(120) Jensen, P., M. T. Wilson, R. Aasa and B. G. Malmström. **1984**. Cyanide inhibition of cytochrome *c* oxidase: a rapid freeze EPR investigation. *Biochem. J.* 224:829-837.

(121) Jones, M. G., D. Bickar, M. T. Wilson, M. Brunori, A. Colosimo and P. Sarti. **1984**. A re-examination of the reactions of cyanide with cytochrome *c* oxidase. *Biochem. J.* 220:57-66.

(122) Scholes, C. P. and B. G. Malmström. **1986**. Two-electron reduction of cytochrome *c* oxidase triggers a conformational transition. *FEBS Lett.* 198:125-129.

(123) Brezezinski, P. and B. G. Malmström. **1987**. The mechanism of electron gating in proton pumping cytochrome *c* oxidase: the effect of pH and temperature on internal electron transfer. *Biochim. Biophys. Acta*. 894:29-38.

(124) Wilson, M. T., G. Antonini, F. Malatesta, P. Sarti and M. Brunori. **1994**. Probing the oxygen binding site of cytochrome *c* oxidase by cyanide. *J. Biol. Chem.* 269:24114-24119.

(125) Hill, B. C. **1988**. Electron transfer from cytochrome *c* to O_2. *Ann. N. Y. Acad. Sci.* 550:98-104.

(126) Oliveberg, M., P. Brzezinski and B. G. Malmström. **1989**. The effect of pH and temperature on the reaction of fully reduced and mixed-valence cytochrome *c* oxidase with dioxygen. *Biochim. Biophys. Acta*. 977:322-328.

(127) Verkhovsky, M. I., J. E. Morgan and M. Wikström. **1994**. Oxygen binding and activation: early steps in the reaction of oxygen with cytochrome *c* oxidase. *Biochemistry*. 33:3079-3086.

(128) Einarsdóttir, Ó., P. M. Killough, J. A. Fee and W. H. Woodruff. **1989**. An infrared study of the binding and photodissociation of carbon monoxide in cytochrome ba_3 from *Thermus thermophilus*. *J. Biol. Chem.* 264:2405-2408.

(129) Woodruff, W. H. **1993**. Coordination dynamics of heme-copper oxidases: the

ligand shuttle and the control and coupling of electron transfer and proton translocation. *J. Bioenerg. Biomemb*. 25:177-188.

(130) Woodruff, W. H., Ó. Einarsdóttir, R. B. Dyer, K. A. Bagley, G. Palmer, S. J. Atherton, R. A. Goldbeck, T. D. Dawes and D. S. Kliger. **1991**. Nature and functional implications of the cytochrome a_3 transients after photodissociation of CO–cytochrome oxidase. *Proc. Natl. Acad. Sci. USA*. 88:2588-2592.

(131) Dyer, R. B., Ó. Einarsdóttir, P. M. Killough, J. J. López-Garriga and W. H. Woodruff. **1989**. Transient binding of photodissociated CO to Cu_B^+ of eukaryotic cytochrome oxidase at ambient temperature. Direct evidence from time-resolved infrared spectroscopy. *J. Am. Chem. Soc.* 111:7657-7659.

(132) Einarsdóttir, Ó., R. B. Dyer, P. M. Killough, D. D. Lemon, P. M. Killough, S. M. Hubig, S. J. Atherton, J. J. López-Garriga, G. Palmer and W. H. Woodruff. **1993**. Photodissociation and recombination of carbonmonoxy cytochrome oxidase: dynamics from picoseconds to kiloseconds. *Biochemistry*. 32:12013-12024.

(133) Song, S., S. Han, Y.-C. Ching and D. L. Rousseau. **1992**. Reaction of cytochrome *c* oxidase with oxygen: different end products in rapid mixing and flow, flash, probe experiments. *Biophysical J*. 61:A202.

(134) Rousseau, D. L., S. Han, S. Song and Y. Ching. **1992**. *J. Raman Spectroscopy*. 23:551-556.

(135) Brunori, M., A. Colosimo, G. Rainoni, M. T. Wilson and E. Antonini. **1979**. Functional intermediates of cytochrome oxidase: role of "pulsed" oxidase in the pre–steady state and steady state reactions of the beef enzyme. *J. Biol. Chem.* 254:10769-10775.

(136) Takahashi, S., Y. Ching, J. Wang and D. L. Rousseau. **1995**. Microsecond generation of oxygen-bound cytochrome *c* oxidase by rapid solution mixing. *J. Biol. Chem*. 270:8405-8407.

(137) Anraku, Y. **1988**. Bacterial electron transport chains. *Ann. Rev. Biochem.* 57:101-

132.

(138) Anraku, Y. and R. B. Gennis. **1987**. The aerobic respiratory chain of *Escherichia coli*. *Trends Biochem. Sci*. 12:262-266.

(139) Chepuri, V., L. Lemieux, D. C.-T. Au and R. B. Gennis. **1990**. The sequence of the *cyo* operon indicates substantial structural similarities between the cytochrome *o* ubiquinol oxidase of *Escherichia coli* and the aa_3-type family of cytochrome *c* oxidases. *J. Biol. Chem*. 265:11185-11192.

(140) Puustinen, A., M. Finel, M. Virkki and M. K. F. Wikström. **1989**. Cytochrome *o* (*bo*) is a proton pump in *Paracoccus denitrificans* and *Escherichi coli*. *FEBS Lett.* 249:163-167.

(141) Puustinen, A., M. Finel, T. Haltia, R. B. Gennis and M. Wikström. **1991**. Properties of the two terminal oxidases of *Escherichia coli*. *Biochemistry*. 30:3936-3942.

(142) Hata, A., Y. Kirino, K. Matsuura, S. Itoh, T. Hiyama, K. Konishi, K. Kita and Y. Anraku. **1985**. Assignment of ESR signals of *Escherichia coli* terminal oxidase complexes. *Biochim. Biophys. Acta*. 810:62-72.

(143) Uno, T., Y. Nishimura, M. Tsuboi, K. Kita and Y. Anraku. **1985**. Resonance Raman study of cytochrome b_{562}-*o* complex, a terminal oxidase of *Escherichia coli* in its ferric, ferrous, and CO-ligated states. *J. Biol. Chem*. 260:6755-6760.

(144) Ingledew, W. J. and M. Bacon. **1991**. A comparative review of the structure and function of cytochrome *o* from *Escherichia coli* and cytochrome aa_3. *Biochem. Soc. Trans*. 19:613-616.

(145) Salerno, J. C., B. Bolgiano, R. K. Poole, R. B. Gennis and W. J. Ingledew. **1990**. Heme-copper and heme-heme interactions in the cytochrome *bo*-containing quinol oxidse of *Escherichia coli*. *J. Biol. Chem*. 265:4364-4368.

(146) Salerno, J. C. and W. J. Ingledew. **1991**. Orientation of the haems of the ubiquinol oxidase:O_2 reductase, cytochrome *bo* of *Escherichia coli*. *Eur. J. Biochem.*

198:789-792.

(147) Puustinen, A., J. E. Morgan, M. Verkhovsky, J. M. Thomas, R. B. Gennis and M. Wikström. **1992**. The low-spin heme site of cytochrome *o* from *Echerichia coli* is promiscuous with respect to heme type. *Biochemistry*. 31:10363-10369.

(148) Minghetti, K. C., V. C. Goswitz, N. E. Gabriel, J. J. Hill, C. A. Barassi, C. D. Georgiou, S. I. Chan and R. B. Gennis. **1992**. Modified, large-scale purification of the cytochrome *o* complex (*bo*-type oxidase) of *Escherichia coli* yields a two heme/one copper terminal oxidase with high specific activity. *Biochemistry*. 31:6917-6924.

(149) Lemieux, L. J., M. W. Calhoun, J. W. Thomas, W. J. Ingledew and R. B. Gennis. **1992**. Determination of the ligands of the low spin heme of the cytochrome *o* ubiquinol oxidase complex using site-directed mutagenesis. *J. Biol. Chem*. 267:2105-2113.

(150) Minagawa, J., T. Mogi, R. B. Gennis and Y. Anraku. **1992**. Identification of heme and copper ligands in subunit I of the cytochrome *bo* complex in *Escherichia coli*. *J. Biol. Chem*. 267:2096-2104.

(151) Uno, T., T. Mogi, M. Tsubaki, Y. Nishimura and Y. Anraku. **1994**. Resonance Raman and Fourier transform infrared studies on the subunit I histidine mutants of the cytochrome *bo* complex in *Escherichia coli*. *J. Biol. Chem*. 269:11912-11920.

(152) Mather, M. W., P. Springer, S. Hensel, G. Buse and J. A. Fee. **1993**. Cytochrome oxidase genes from *Thermus thermophilus*: nucleotide sequence of the fused gene and analysis of the deduced primary structure for subunits I and II of cytochrome caa_3. *J. Biol. Chem*. 268:5395-5408.

(153) Gennis, R. B. **1992**. Site-directed mutagenesis studies on subunit I of the aa_3-type cytochrome *c* oxidase of *Rhodobacter sphaeroides*: a brief review of progress to date. *Biochim. Biophys. Acta*. 1101:184-187.

(154) Hallén, S., M. Svensson and T. Nilsson. **1993**. Cytochrome *bo* from *E. coli* does

not exhibit the same proton transfer characteristics as the bovine cytochrome *c* oxidase during oxygen reduction. *FEBS Lett.* 325:299-302.

(155) Ma, J., L. Lemieux and R. B. Gennis. **1993**. Genetic fusion of subunits I, II, and III of the cytochrome *bo* ubiquinol oxidase from *Escherichia coli* results in a fully assembled and active enzyme. *Biochemistry*. 32:7692-7697.

(156) Fukaya, M., K. Tayama, T. Tamaki, H. Egisuya, Y. Okumura, Y. Kawamura, S. Horinouchi and T. Beppu. **1993**. Characterization of a cytochrome a_1 that functions as a ubiquinol oxidase in *Acetobacter aceti*. *J. Bacteriol.* 175:4307-4314.

(157) Matsushita, K., E. Shinagawa, O. Adachi and M. Ameyama. **1990**. Cytochrome a_1 of *Acetobacter aceti* is a cytochrome *ba* functioning as ubiquinol oxidase. *Proc. Natl. Acad. Sci. USA*. 87:9863-9867.

(158) Solioz, M., E. Carafoli and B. Ludwig. **1982**. The cytochrome *c* oxidase of *Paracoccus denitrificans* pumps protons in a reconstituted system. *J. Biol. Chem.* 257:1579-1582.

(159) van der Oost, J., T. Haltia, M. Raitio and M. Saraste. **1991**. Genes coding for cytochrome *c* oxidase in *Paracoccus denitrificans*. *J. Bioenerg. Biomemb.* 23:257-267.

(160) Lauraeus, M., T. Haltia, M. Saraste and M. Wikström. **1991**. *Bacillus subtilis* expresses two kinds of haem A-containing terminal oxidases. *Eur. J. Biochem.* 197:699-705.

(161) Santana, M., F. Kunst, M. F. Hullo, G. Rapoport, A. Danchin and P. Glaser. **1992**. Molecular cloning, sequencing, and physiological characterization of the *qox* operon from *Bacillus subtilis* encoding the aa_3-600 quinol oxidase. *J. Biol. Chem.* 267:10225-10231.

(162) Anemüller, S., E. Bill, G. Schäfer, A. X. Trautwein and M. Teixeira. **1992**. EPR studies of cytochrome aa_3 from *Sulfolobus acidocaldarius*. *Eur. J. Biochem.*

210:133-138.

(163) Anemüller, S. and G. Schäfer. **1989**. Cytochrome aa_3 from the thermoacidophile archaebacterium *Sulfolobus acidocaldarius*. *FEBS Lett*. 244:451-455.

(164) Anemüller, S. and G. Schäfer. **1990**. Cytochrome aa_3 from *Sulfolobus acidocaldarius*: a single-subunit, quinol-oxidizing archaebacterial terminal oxidase. *Eur. J. Biochem.* 191:297-305.

(165) Lübben, M., B. Kolmerer and M. Saraste. **1992**. An archaebacterial terminal oxidase combines core structures of two mitochondrial respiratory complexes. *EMBO J*. 11:805-812.

(166) Zimmerman, B. H., C. I. Nitsche, J. A. Fee, F. Rusnak and E. Münck. **1988**. Properties of a copper-containing cytochrome ba_3: a second terminal oxidase from the extreme thermophile *Thermus thermophilus*. *Proc. Natl. Acad. Sci. USA*. 85:5779-5783.

(167) Büse, G., S. Hensel and J. A. Fee. **1989**. Evidence for cyochrome oxidase subunit I and a cytochrome *c*-subunit II fused protein in the cyochrome 'c_1aa_3' of *Thermus thermophilus*. *Eur. J. Biochem*. 181:261-268.

(168) de Vrij, W., R. I. R. Heyne and W. N. Konings. **1989**. Characterization and application of a thermostable primary transport system: cytochrome *c* oxidase from *Bacillus stearothermophilus*. *Eur. J. Biochem.* 178:763-770.

(169) Sone, N. and Y. Fujiwara. **1991**. Effects of aeration during growth of *Bacillus stearothermophilus* on proton pumping activity and change of terminal oxidases. *J. Biochem.* 110:1016-1021.

(170) Sone, N. and Y. Yanagita. **1982**. A cytochrome aa_3-type terminal oxidase of a thermophilic bacterium: purification, properties and proton pumping. *Biochim. Biophys. Acta*. 682:216-226.

(171) Sone, N. and Y. Yanagita. **1984**. High vectorial proton stoichiometry by cytochrome *c* oxidase from the thermophilic bacterium PS3 reconstituted in

liposomes. *J. Biol. Chem.* 259:1405-1408.

(172) Sone, N., F. Yokoi, T. Fu, S. Ohta, T. Metso, M. Raitio and M. Saraste. **1988**. Nucleotide sequence of the gene coding for cytochrome oxidase subunit I from the thermophilic bacterium PS3. *J. Biochem*. 103:606-610.

(173) Ishizuka, M., K. Machida, S. Shimada, A. Mogi, T. Tsuchiza, T. Ohmori, Y. Souma, M. Gonda and N. Sone. **1990**. Nucleotide sequence of the gene coding for four subunits of cytochrome *c* oxidase from the thermophilic bacterium PS3. *J. Biochem*. 108:866-873.

(174) Saraste, M., T. Metso, T. Nakari, T. Jalli, M. Lauraeus and J. van der Oost. **1991**. The *Bacillus subtilis* cytochrome *c* oxidase. Variations on a conserved protein theme. *Eur. J. Biochem*. 195:517-525.

(175) van der Oost, J., C. von Wachenfeld, L. Hederstedt and M. Saraste. **1991**. *Bacillus subtilis* cytochrome oxidase mutants: biochemical analysis and genetic evidence for two aa_3-type oxidases. *Mol. Microbiol.* 5:2063-2072.

(176) Gray, K. A., M. Grooms, H. Myllykallio, C. Moomaw, C. Slaughter and F. Daldal. **1994**. *Rhodobacter capsulatus* contains a novel *cb*-type cytochrome *c* oxidase without a Cu_A center. *Biochemistry*. 33:3120-3127.

(177) Thöny-Meyer, L., C. Beck, O. Preisig and H. Hennecke. **1994**. The *cccNOQP* gene cluster codes for a *cb*-type cytochrome oxidase that functions in aerobic respiration of *Rhodobacter capsulatus*. *Mol. Microbiol.* 14:705-716.

(178) Garcia-Horsmann, J. A., E. Berry, J. P. Shapleigh, J. O. Alben and R. B. Gennis. **1994**. A novel cytochrome *c* oxidase from *Rhodobacter sphaeroides* that lacks Cu_A. *Biochemistry*. 33:3113-3119.

(179) García-Horsman, J. A., B. Barquera, J. Rumbley, J. Ma and R. B. Gennis. **1994**. The superfamily of heme-copper respiratory oxidases. *J. Bacteriol*. 176:5587-5600.

(180) Sone, N. and Y. Fujiwara. **1991**. Haem O can replace haem A in the active site of

cytochrome *c* oxidase from thermophilic bacterium PS3. *FEBS Lett.* 288:154-158.

(181) Sone, N., T. Ogura, S. Noguchi and T. Kitagawa. **1994**. Proton pumping activity and visible absorption and resonance Raman spectra of a *cao*-type cytochrome *c* oxidase isolated from the thermophilic bacterium PS3. *Biochemistry*. 33:849-855.

(182) Musser, S. M., M. H. B. Stowell and S. I. Chan. **1993**. Comparison of ubiquinol and cytochrome *c* terminal oxidases. *FEBS Lett.* 327:131-136.

(183) Trumpower, B. L. **1990**. The protonmotive Q cycle. *J. Biol. Chem*. 265:11409-11412.

(184) Suzuki, H. and T. E. King. **1983**. Evidence of an ubisemiquinone radical(s) from the NADH-ubiquinone reductase of the mitochondrial respiratory chain. *J. Biol. Chem*. 258:352-358.

(185) Kotlyar, A. B., V. D. Sled, D. S. Burbaev, I. A. Moroz and A. D. Vinogradov. **1990**. Coupling site I and the rotenone-sensitive ubisemiquinone in tightly coupled submitochondrial particles. *FEBS Lett.* 264:17-20.

(186) Westenberg, D. J., R. P. Gunsalus, B. A. C. Ackrell, H. Sices and G. Cecchini. **1993**. *Escherichia coli* fumarate reductase FRDC and FRDD mutants: identification of amino acid residues involved in catalytic activity with quinones. *J. Biol. Chem.* 268:815-822.

(187) Miki, T., L. Yu and C.-A. Yu. **1992**. Characterization of ubisemiquinone radicals in succinate-ubiquinone reductase. *Arch. Biochem. Biophys*. 293:61-66.

(188) Sato-Watanabe, M., T. Mogi, T. Ogura, T. Kitagawa, H. Miyoshi, H. Iwamura and Y. Anraku. **1994**. Identification of a novel quinone-binding site in the cytochrome *bo* complex from *Escherichia coli*. *J. Biol. Chem.* 269:28908-28912.

(189) Babcock, G. T. and P. M. Callahan. **1983**. Redox-linked hydrogen bond strength changes in cytochrome *a*: implications for a cytochrome oxidase proton pump. *Biochemistry*. 22:2314-2319.

(190) Larsen, R. W., L.-P. Pan, S. M. Musser, Z. Li and S. I. Chan. **1992**. Could Cu_B be

the site of redox linkage in cytochrome *c* oxidase? *Proc. Natl. Acad. Sci. USA.* 89:723-727.

(191) Rousseau, D. L., Y.-C. Ching and J. Wang. **1993**. Proton translocation in cytochrome *c* oxidase: redox linkage through proximal ligand exchange on cytochrome a_3. *J. Bioenerg. Biomemb*. 25:165-176.

(192) Wikström, M., A. Bogachev, M. Finel, J. E. Morgan, A. Puustinen, M. Raitio, M. Verkhovskaya and M. I. Verkhovsky. **1994**. Mechanism of proton translocation by the respiratory oxidases: the histidine cycle. *Biochim. Biophys. Acta.* 1187:106-111.

(193) Hatefi, Y. **1985**. The mitochondrial electron transport and oxidative phosphorylation system. *Ann. Rev. Biochem*. 54:1015-1069.

(194) Casey, R. P., M. Thelen and A. Azzi. **1979**. Dicyclohexylcarbodiimide inhibits proton translocation by cytochrome *c* oxidase. *Biochem. Biophys. Res. Commun.* 87:1044-1051.

(195) Püttner, I., M. Solioz, E. Carafoli and B. Ludwig. **1983**. Dicyclohexylcarbodiimide does not inhibit proton pumping by cytochrome *c* oxidase of *Paracoccus denitrificans*. *Eur. J. Biochem.* 134:33-37.

(196) Proteau, G., J. M. Wrigglesworth and P. Nicholls. **1983**. Protonmotive functions of cytochrome *c* oxidase in reconstituted vesicles. *Biochem. J.* 210:199-205.

(197) Sigel, E. and E. Carafoli. **1979**. The charge stoichiometry of cytochrome *c* oxidase in the reconstituted system. *J. Biol. Chem*. 254:10572-10574.

(198) Sigel, E. and E. Carafoli. **1980**. Quantitative analysis of the proton and charge stoichiometry of cytochrome *c* oxidase from beef heart reconstituted into phospholipid vesicles. *Eur. J. Biochem.* 111:299-306.

(199) Wikström, M. K. F. and H. T. Saari. **1977**. The mechanism of energy conservation and transduction by mitochondrial cytochrome *c* oxidase. *Biochim. Biophys. Acta.* 462:347-361.

(200) Wikström, M., K. F. **1977**. Proton pump coupled to cytochrome *c* oxidase in mitochondria. *Nature*. 266:271-273.

(201) Antonini, G., F. Malatesta, P. Sarti and M. Brunori. **1993**. Proton pumping by cytochrome oxidase as studied by time-resolved stopped-flow spectrophotometry. *Proc. Natl. Acad. Sci. USA*. 90:5949-5953.

(202) Wikström, M. K. F. and K. Krab. **1978**. Cytochrome *c* oxidase is a proton pump: a rejoinder to recent criticism. *FEBS Lett*. 91:8-14.

(203) van Verseveld, H. W., K. Krab and A. H. Stouthamer. **1981**. Proton pump coupled to cytochrome *c* oxidase in *Paracoccus denitrificans*. *Biochim. Biophys. Acta*. 635:525-534.

(204) Mitchell, P., R. Mitchell, A. J. Moody, I. C. West, H. Baum and J. M. Wrigglesworth. **1985**. Chemiosmotic coupling in cytochrome oxidase: possible protonmotive O loop and O cycle mechanisms. *FEBS Lett*. 188:1-7.

(205) Murphy, M. P. and M. D. Brand. **1988**. The stoichiometry of charge translocation by cytochrome oxidase and the cytochrome bc_1 complex of mitochondria at high membrane potential. *Eur. J. Biochem*. 173:645-651.

(206) Murphy, M. P. and M. D. Brand. **1988**. Membrane-potential-dependent changes in the stoichiometry of charge translocation by the mitochondrial electron transport chain. *Eur. J. Biochem*. 173:637-644.

(207) Blair, D. F., W. R. Ellis Jr., H. Wang, H. B. Gray and S. I. Chan. **1986**. Spectroelectrochemical study of cytochrome *c* oxidase: pH and temperature dependences of the cytochrome potentials. *J. Biol. Chem*. 261:11524-11537.

(208) Wang, H., D. F. Blair, W. R. Ellis Jr., H. B. Gray and S. I. Chan. **1986**. Temperature dependence of the reduction potential of Cu_A in carbon monoxide inhibited cytochrome *c* oxidase. *Biochemistry*. 25:167-171.

(209) Brunori, M., G. Antonini, F. Malatesta, P. Sarti and M. T. Wilson. **1987**. Structure and function of cytochrome oxidase: a second look. *Adv. Inorg. Biochem*. 7:93-

154.

(210) Rodkey, F. L. and E. G. Ball. **1950**. Oxidation-reduction potentials of the cytochrome *c* system. *J. Biol. Chem*. 182:17-28.

(211) Rottenberg, H. **1979**. The measurement of membrane potential and ΔpH in cells, organelles, and vesicles. *Meth. Enzymol*. 55:547-569.

(212) Wikström, M. and M. Saraste. **1984**. The mitochondrial respiratory chain. *In* Bioenergetics, vol. 9. L. Ernster, ed. Elsevier, Amsterdam. pp. 49-94.

(213) Wikström, M. **1989**. Identification of the electron transfers in cytochrome oxidase that are coupled to proton-pumping. *Nature*. 338:776-778.

(214) Myslovatyi, B. S., D. L. Zairov, A. A. Chebotarev and É. L. Muzykantskii. **1982**. Partial pressure of oxygen in different organs and tissues and some hemodynamic parameters in tourniquet shock. *Bull. Expt. Biol. Med*. 94:872-875.

(215) Chan, S. I. and P. M. Li. **1990**. Cytochrome *c* oxidase: understanding nature's design of a proton pump. *Biochemistry*. 29:1-12.

(216) Williams, R. J. P. **1990**. Overview of biological electron-transfer. *In* Electron Transfer in Biology and the Solid State, vol. 226. M. K. Johnson, R. B. King, D. M. Kurtz Jr., C. Kurtal, M. L. Norton and R. A. Scott, eds. American Chemical Society, Washington, D. C. pp. 3-23.

(217) Malmström, B. G. **1994**. Rack-induced bonding in blue-copper proteins. *Eur. J. Biochem*. 223:711-718.

(218) Musser, S. M. and S. I. Chan. **1995**. Understanding the cytochrome *c* oxidase proton pump: the thermodynamics of redox linkage. *Biophysical J*. 68:2543-2555.

(219) Bowler, B., A. L. Raphael and H. B. Gray. **1990**. Long-range electron transfer in donor (spacer) acceptor molecules and proteins. *In* Progress in Inorganic Chemistry: Bioinorganic Chemistry, vol. 38. S. J. Lippard, ed. John Wiley and Sons, Inc., New York. pp. 259-319.

(220) Marcus, R. A. and N. Sutin. **1985**. Electrons transfers in chemistry and biology. *Biochim. Biophys. Acta*. 811:265-322.

(221) Trumpower, B. L. and R. B. Gennis. **1994**. Energy transduction by cytochrome complexes in mitochondrial and bacterial respiration: the enzymology of coupling electron transfer reactions to transmembrane proton translocation. *Ann. Rev. Biochem*. 63:675-716.

(222) Brunori, M. and M. T. Wilson. **1995**. Electron transfer and proton pumping in cytochrome oxidase. *Biochimie*. 77:668-676.

(223) Puustinen, A., M. I. Verkhovsky, J. E. Morgan, N. P. Belevich and M. Wikström. **1996**. Reaction of the *E. coli* quinol oxidase cytochrome bo_3 with dioxygen – the role of a bound ubiquinone molecule. *Proc. Natl. Acad. Sci. USA*. 93:1545-1548.

(224) Selwood, D. L. and K. S. Jandu. **1988**. A new, efficient synthesis of 5-undecyl-6-hydroxy-4,7-dioxobenzothiazole (UHDBT), a potent electron transport inhibitor. *Heterocycles*. 27:1191-1196.

(225) Trumpower, B. L. and J. G. Haggerty. **1980**. Inhibition of electron transfer in the cytochrome bc_1 segment of the mitochondrial respiratory chain by a synthetic analog of ubiquinone. *J. Bioenerg. Biomembr*. 12:151-164.

(226) Ksenzhek, O. S., S. A. Petrova and M. V. Kolodyazhny. **1982**. Redox properties of ubiquinones in aqueous solutions. *Bioelectr. Bioenerg*. 9:167-174.

(227) Morgan, J. E., M. I. Verkhovsky, A. Puustinen and M. Wikström. **1995**. Identification of a "peroxy" intermediate in cytochrome bo_3 of *Escherichia coli*. *Biochemistry*. 34:15633-15637.

(228) van Ark, G. and J. A. Berden. **1977**. Binding of HQNO to beef-heart sub-mitochondrial particles. *Biochim. Biophys. Acta*. 459:119-137.

(229) Rich, P. R. **1984**. Electron and proton transfers through quinones and cytochrome *bc* complexes. *Biochim. Biophys. Acta*. 768:53-79.

(230) Berry, E. A. and B. L. Trumpower. **1987**. Simultaneous determination of hemes *a*,

b, and *c* from pyridine hemochrome spectra. *Anal. Biochem.* 161:1-15.

(231) Puustinen, A. and M. Wikström. **1991**. The heme groups of cytochrome *o* from *Escherichia coli*. *Proc. Natl. Acad. Sci. USA*. 88:6122-6126.

(232) Rich, P. R. and R. Harper. **1990**. Partition coefficients of quinones and hydroquinones and their relation to biochemical reactivity. *FEBS Lett*. 269:139-144.

(233) Ts'o, P. O. and S. I. Chan. **1964**. Interaction and association of bases and nucleosides in aqueous solutions. II. Association of 6-methylpurine and 5-bromouridine and treatment of multiple equilibria. *J. Am. Chem. Soc*. 86:4176-4181.

(234) Matsushita, K., L. Patel and H. R. Kaback. **1984**. Cytochrome *o* type oxidase from *Escherichia coli*. Characterization of the enzyme and mechanism of electrochemical proton gradient generation. *Biochemistry*. 23:4703-4714.

(235) Sato-Watanabe, M., T. Mogi, H. Miyoshi, H. Iwamura, K. Matsushita, O. Adachi and Y. Anraku. **1994**. Structure-function studies on the ubiquinol oxidation site of the cytochrome *bo* complex from *Escherichia coli* using *p*-benzoquinones and substituted phenols. *J. Biol. Chem*. 269:28899-28907.

(236) Welter, R., L.-Q. Gu, L. Yu, C.-A. Yu, J. Rumbley and R. B. Gennis. **1994**. Identification of the ubiquinol-binding site in the cytochrome bo_3-ubiquinol oxidase of *Escherichia coli*. *J. Biol. Chem*. 269:28834-28838.

(237) Sato-Watanabe, M., S. Itoh, T. Mogi, M. K., H. Miyoshi and Y. Anraku. **1995**. Stabilization of a semiquinone radical at the high-affinity binding site (Q_H) of the *Escherichia coli bo*-type ubiquinol oxidase. *FEBS Lett*. 374:265-269.

(238) Ingledew, W. J., T. Ohnishi and J. C. Salerno. **1995**. Studies on a stabilization of ubisemiquinone by *Escherichia coli* quinol oxidase, cytochrome *bo*. *Eur. J. Biochem*. 227:903-908.

(239) Nilsson, T., J. Gelles, P. M. Li and S. I. Chan. **1988**. Chemical modification of the

Cu_A site affects the proton pumping activity of cytochrome *c* oxidase. *Biochemistry*. 27:296-301.

(240) Nilsson, T., R. A. Copeland, P. A. Smith and S. I. Chan. **1988**. Conversion of Cu_A to a type II copper in cytochrome *c* oxidase. *Biochemistry*. 27:8254-8260.

(241) Li, P. M., J. E. Morgan, T. Nilsson, M. Ma and S. I. Chan. **1988**. Heat treatment of cytochrome *c* oxidase perturbs the Cu_A site and affects proton pumping behavior. *Biochemistry*. 27:7538-7546.

(242) Chan, S. I., D. F. Bocian, G. W. Brudvig, R. H. Morse and T. H. Stevens. **1978**. A model for the "visible " copper in cytochrome *c* oxidase. *In* Frontiers of Biological Energetics, vol. 2. P. L. Dutton, J. S. Leigh Jr. and A. Scarpa, eds. Academic, New York. pp. 883-888.

(243) Chan, S. I., D. F. Bocian, G. W. Brudvig, R. H. Morse and T. H. Stevens. **1979**. The nature of the "visible" copper in cytochrome *c* oxidase. *In* Cytochrome Oxidase. T. E. King, Y. Orii, B. Chance and K. Okunuki, eds. Elsevier, New York. pp. 177-188.

(244) Reinhammer, B., R. Malkin, P. Jensen, B. Karlsson, L.-E. Andréasson, R. Aasa, T. Vänngård and B. G. Malmström. **1980**. A new copper(II) electron paramagnetic resonance signal in two laccases and in cytochrome *c* oxidase. *J. Biol. Chem*. 255:5000-5003.

(245) Carithers, R. P. and G. Palmer. **1981**. Characterization of the potentiometric behavior of soluble cytochrome oxidase by magnetic circular dichroism. *J. Biol. Chem*. 256:7967-7976.

(246) Hoffman, B. M., V. J. Derose, P. E. Doan, R. J. Gurbiel, A. L. P. Houseman and J. Telser. **1993**. Metalloenzyme active-site structure and function through multifrequency CW and pulsed ENDOR. *In* Biological Magnetic Resonance: EMR of Paramagnetic Molecules (vol. 13). L. J. Berliner and J. Reuban, eds. Plenum Press, New York. pp. 151-218.

(247) Hartzell, C. R. and H. Beinert. **1974**. Components of cytochrome *c* oxidase detectable by EPR spectroscopy. *Biochim. Biophys. Acta*. 368:318-338.

(248) Werst, M. M., C. E. Davoust and B. M. Hoffman. **1991**. Ligand spin-densities in blue copper proteins by Q-band ^{1}H and ^{14}N ENDOR spectroscopy. *J. Am. Chem. Soc.* 113:1533-1538.

(249) Fann, Y. C., I. Ahmed, N. J. Blackburn, J. S. Boswell, M. L. Verkhovskaya, B. M. Hoffman and M. Wikström. **1995**. Structure of Cu_B in the binuclear heme-copper center of the cytochrome aa_3-type quinol oxidase from *Bacillus subtilis*: an ENDOR and EXAFS study. *Biochemistry*. 34:10245-10255.

(250) Gelles, J. and S. I. Chan. **1985**. Chemical modification of the Cu_A center in cytochrome *c* oxidase by sodium *p*-(hydroxymercuri)benzoate. *Biochemistry*. 24:3963-3972.

(251) Larsen, R. W., M. R. Ondrias, R. A. Copeland, P. M. Li and S. I. Chan. **1989**. Resonance Raman studies of Cu_A-modified cytochrome *c* oxidase. *Biochemistry*. 28:6418-6422.

(252) Surerus, K. K., W. A. Oertling, C. Fan, R. J. Gurbiel, Ó. Einarsdóttir, W. E. Antholine, R. B. Dyer, B. M. Hoffman, W. H. Woodruff and J. A. Fee. **1992**. Reaction of cyanide with cytochrome ba_3 from *Thermus thermophilus*: spectroscopic characterization of the $Fe(II)_{a3}$-CN•$Cu(II)_B$-CN complex suggests four ^{14}N atoms are coordinated to Cu_B. *Proc. Natl. Acad. Sci. USA*. 89:3195-3199.

(253) Oertling, W. A., K. K. Surerus, Ó. Einarsdóttir, J. A. Fee, R. B. Dyer and W. H. Woodruff. **1994**. Spectroscopic characterization of cytochrome ba_3, a terminal oxidase from *Thermus thermophilus*: comparison of the a_3/Cu_B site to that of bovine cytochrome aa_3. *Biochemistry*. 33:3128-3141.

(254) Zickermann, V., M. Verkhovsky, J. Morgan, M. Wikström, S. Anemüller, E. Bill, G. C. M. Steffens and B. Ludwig. **1995**. Perturbation of the Cu_A site in

cytochrome *c* oxidase of *Paracoccus denitrificans* by replacement of Met227 with isoleucine. *Eur. J. Biochem.* 234:686-693.

(255) Morgan, J. E., M. I. Verkovsky and M. Wikström. **1994**. The histidine cycle: a new model for proton translocation in the respiratory heme-copper oxidases. *J. Bioenerg. Biomemb.* 26:599-608.

(256) Wikström, M. **1988**. How does cytochrome oxidase pump protons? *Ann. NY Acad. Sci.* 550:199-206.

(257) Mitchell, P. **1987**. A new redox loop formality involving metal-catalysed hydroxide-ion translocation: a hypothetical Cu loop mechanism for cytochrome oxidase. *FEBS Lett.* 222:235-245.

(258) Mitchell, P. **1988**. Possible protonmotive osmochemistry in cytochrome oxidase. *Ann. N. Y. Acad. Sci.* 550:185-198.

(259) Casey, R. P., M. Thelen and A. Azzi. **1980**. Dicyclohexylcarbodiimide binds specifically and covalently to cytochrome *c* oxidase while inhibiting its H^+-translocating activity. *J. Biol. Chem.* 255:3994-4000.

(260) Prochaska, L. J. and K. A. Reynolds. **1986**. Characterization of electron-transfer and proton-translocation activities in bovine heart mitochondrial cytochrome *c* oxidase deficient in subunit III. *Biochemistry*. 25:781-787.

(261) Prochaska, L. J. and P. S. Fink. **1987**. On the role of subunit III in proton translocation in cytochrome *c* oxidase. *J. Bioenerg. Biomembr.* 19:143-166.

(262) Thompson, D. A., L. Gregory and S. Ferguson-Miller. **1985**. Cytochrome *c* oxidase depleted of subunit III: proton-pumping, respiratory control, and pH dependence of the midpoint potential of cytochrome *a*. *J. Inorg. Chem*. 23:357-364.

(263) Püttner, I., E. Carafoli and F. Malatesta. **1985**. Spectroscopic and functional properties of subunit III-depleted cytochrome oxidase. *J. Biol. Chem*. 260:3719-3723.

(264) Brunori, M., P. Sarti, A. Colosimo, G. Antonini, F. Malatesta, M. G. Jones and M. T. Wilson. **1985**. Mechanism of control of cytochrome oxidase activity by the electrochemical-potential gradient. *EMBO J*. 4:2365-2368.

(265) Finel, M. and M. K. F. Wikström. **1986**. Studies on the role of the oligomeric state and subunit III of cytochrome oxidase in proton translocation. *Biochim. Biophys. Acta*. 851:99-108.

(266) Thelen, M., P. O'Shea, G. Petrone and A. Azzi. **1985**. Proton translocation by a native and subunit III-depleted cytochrome *c* oxidase reconstituted into phospholipid vesicles: use of fluorescein-phosphatidylethanolamine as an intravesicular pH indicator. *J. Biol. Chem*. 260:*3626-3631*.

(267) Sarti, P., M. G. Jones, G. Antonini, F. Malatesta, A. Colosimo, M. T. Wilson and M. Brunori. **1985**. Kinetics of redox-linked proton pumping activity of native and subunit III-depleted cytochrome *c* oxidase: a stopped-flow investigation. *Proc. Natl. Acad. Sci. USA*. 82:4876-4880.

(268) Haltia, T., M. Saraste and M. Wikström. **1991**. Subunit III of cytochrome *c* oxidase is not involved in proton translocation: a site-directed mutagenesis study. *EMBO J*. 10:2015-2021.

(269) Prochaska, L. J., R. Bisson, R. A. Capaldi, G. C. M. Steffens and G. Buse. **1981**. Inhibition of cytochrome *c* oxidase function by cyclohexylcarbodiimide. *Biochim. Biophys. Acta*. 637:360-373.

(270) Casey, R. P., C. Broger, M. Thelen and A. Azzi. **1981**. Studies on the molecular basis of H^+ translocation by cytochrome *c* oxidase. *J. Bioenerg. Biomemb*. 13:219-228.

(271) Azzi, A., R. Bisson, R. P. Casey, H. Gutweniger, C. Montecucco and M. Thelen. **1979**. Hydrophobic interactions, proton movements and dicyclohexylcarbodiimide labeling in cytochrome *c* oxidase. *In* Membrane Bioenergetics. C. P. Lee, G. Schatz and L. Ernster, eds. Addison-Wesley,

Reading, MA. pp. 13-20.

(272) Raitio, M. and M. Wikström. **1994**. An alternative cytochrome oxidase of *Paracoccus denitrificans* functions as a proton pump. *Biochim. Biophys. Acta.* 1186:100-106.

(273) Wu, S., R. Moreno-Sanchez and H. Rottenberg. **1995**. Involvement of cytochrome *c* oxidase subunit III in energy coupling. *Biochemistry*. 34:16298-16305.

(274) Chadwick, C. C. and E. W. Thomas. **1983**. Inactivation of sarcoplasmic reticulum (Ca^{2+}+Mg^{2+})-ATPase by N-cyclohexyl-N'(4-dimethylamino-α-napthyl)carbo-diimide. *Biochim. Biophys. Acta.* 730:201-206.

(275) Musser, S. M., R. W. Larsen and S. I. Chan. **1993**. Fluorescence quenching of reconstituted NCD-4-labeled cytochrome *c* oxidase by DOXYL-stearic acids. *Biophysical J*. 65:2348-2359.

(276) Pringle, M. J. and M. Taber. **1985**. Fluorescent analogs of N,N'-dicyclohexylcarbodiimide as structural probes of the bovine mitochondrial proton channel. *Biochemistry*. 24:7366-7371.

(277) Green II, J. A., L. A. Singer and J. H. Parks. **1973**. Fluorescence quenching by the stable free radical di-*t*-butylnitroxide. *J. Chem. Phys*. 58:2690-2695.

(278) Abrams, F. S. and E. London. **1992**. Calibrating the parallax fluorescence quenching method for determination of membrane penetration depth: refinement and comparison of quenching by spin-labeled and brominated lipids. *Biochemistry*. 5312-5322.

(279) Green, S. A., D. J. Simpson, G. Zhou, P. S. Ho and N. V. Blough. **1990**. Intramolecular quenching of excited singlet states by stable nitroxide radicals. *J. Am. Chem. Soc*. 112:7337-7346.

(280) Matko, J., K. Ohki and M. Edidin. **1992**. Luminescence quenching by nitroxide spin labels in aqueous solution: studies on the mechanism of quenching. *Biochemistry*. 31:703-711.

(281) Hinkle, P. C., J. J. Kim and E. Racker. **1972**. Ion transport and respiratory control in vesicles formed from cytochrome oxidase and phospholipids. *J. Biol. Chem.* 247:1338-1342.

(282) Casey, R. P., C. Broger and A. Azzi. **1981**. Structural studies on the cytochrome *c* oxidase proton pump using a spin-label probe. *Biochim. Biophys. Acta*. 638:86-93.

(283) Kyte, J. and R. F. Doolittle. **1982**. A simple method for displaying the hydropathic character of a protein. *J. Mol. Biol*. 157:105-132.

(284) Lehninger, A. L., B. Reynafarje and L. Costa. **1985**. Action of DCCD on the H^+/O stoichiometry of mitoplast cytochrome *c* oxidase. *J. Inorg. Chem*. 23:335-340.

(285) Eckstrom, H. C. and C. Schmelzer. **1939**. The Wien effect: deviations of electrolytic solutions from Ohm's law under high field strength. *Chem. Rev.* 24:367-414.

(286) Onsager, L. **1934**. Deviations from Ohm's law in weak electrolytes. *J. Chem. Phys*. 2:599-615.

(287) Solomon, E. I., M. J. Baldwin and M. D. Lowery. **1992**. Electronic structures of active sites in copper proteins: contributions to reactivity. *Chem. Rev*. 92:521-542.

(288) Aslanidis, P., S. K. Hadjikakou and P. Karagiannidis. **1994**. Preparation and spectral studies of dinuclear mixed-ligand copper(I) complexes. The crystal structure of bis[μ-S(pyridine-2-thione)(tmtp) copper(I) bromide]. *Polyhedron*. 13:3119-3125.

(289) Karlin, K. D., J. Shi, J. C. Hayes, J. W. McKown, J. P. Hutchinson and J. Zubieta. **1984**. Cu(I)-dioxygen reactivity: structural characterization of a bridged-binuclear Cu(II) complex formed by oxidation of a new binuclear Cu(I) compound. *Inorg. Chim. Acta*. 91:L3-L7.

(290) Butcher, R. J., G. Diven, G. Erickson, J. Jasinski, G. M. Mockler, R. Y.

Pozdniakov and E. Sinn. **1995**. Binuclear copper(II) complexes containing phenols and catechols. *Inorg. Chim. Acta*. 239:107-116.

(291) Karlin, K. D., J. C. Hayes, Y. Gultneh, R. W. Cruse, J. W. McKown, J. P. Hutchinson and J. Zubieta. **1984**. Copper-mediated hydroxylation of an arene: model system for the action of copper monooxygenases. Structures of a binuclear copper(I) complex and its oxygenated product. *J. Am. Chem. Soc.* 106:2121-2128.

(292) Houser, R. P., J. A. Halfen, V. J. Young Jr., N. J. Blackburn and W. B. Tolman. **1995**. Structural characterization of the first example of a bis(μ-thiolato)dicopper(II) complex. Relevance to proposals for the electron transfer sites in cytochrome *c* oxidase and nitrous oxide reductase. *J. Am. Chem. Soc.* 117:10745-10746.

(293) Houser, R. P., V. G. Young Jr. and W. B. Tolman. **1996**. A thiolate-bridged, fully-delocalized mixed-valence dicopper (I,II) complex that models the Cu_A biological electron-transfer site. *J. Am. Chem. Soc*. 118:2101-2102.

(294) Haltia, T. **1992**. Reduction of Cu_A induces a conformational changes in cytochrome *c* oxidase from *Paracoccus denitrificans*. *Biochim. Biophys. Acta*. 1098:343-350.

(295) Espe, M. P., J. P. Hosler, S. Ferguson-Miller, G. T. Babcock and J. McCracken. **1995**. A continuous wave and pulsed EPR characterization of the Mn^{2+} binding site in *Rhodobacter sphaeroides* cytochrome *c* oxidase. *Biochemistry*. 34:7593-7602.

(296) Hosler, J. P., M. P. Espe, Y. Zhen, G. T. Babcock and S. Ferguson-Miller. **1995**. Analysis of site-directed mutants locates a non-redox-active metal near the active site of cytochrome *c* oxidase of *Rhodobacter sphaeroides*. *Biochemistry*. 34:7586-7592.

(297) Brunori, M., G. Antonini, A. Colosimo, F. Malatesta, P. Sarti, M. G. Jones and M. T. Wilson. **1985**. Stopped-flow studies of cytochrome oxidase reconstituted into

liposomes: proton pumping and control of activity. *J. Inorg. Chem*. 23:373-379.

(298) DiBiase, V. A. and L. J. Prochaska. **1985**. Characterization of electron-transfer and proton translocation activities in trypsin-treated bovine heart michondrial cytochrome *c* oxidase. *Arch. Biochem. Biophys*. 243:668-677.

(299) Steverding, D., B. Kadenbach, N. Capitanio and S. Papa. **1990**. Effect of chemical modification of lysine amino-groups on redox and proton motive activity of bovine heart cytochrome *c* oxidase reconstituted in phospholipid-membranes. *Biochemistry*. 29:2945-2950.

(300) Baum, H., M. F. Grahn, J. Elsden and J. M. Wrigglesworth. **1987**. How does cytochrome oxidase pump protons? *In* Bioenergetics: Structure and Function of Energy Transducing Systems. T. Ozawa and S. Papa, eds. Japan Sci. Soc. Press, Tokyo. pp. 263-278.

(301) Baldwin, J. and C. Chothia. **1979**. Haemoglobin: the structural changes related to ligand binding and its allosteric mechanism. *J. Mol. Biol*. 129:175-220.

(302) van der Oost, J., A. P. N. de Boer, J.-W. L. de Gier, W. G. Zumft, A. H. Stouthamer and R. J. M. van Spanning. **1994**. The heme-copper oxidase family consists of three distinct types of terminal oxidases and is related to nitric oxide reductase. *FEMS Micro. Biol. Lett*. 121:1-10.

(303) Castresana, J., M. Lübben, M. Saraste and D. G. Higgens. **1994**. Evolution of cytochrome oxidase, an enzyme older than atmospheric oxygen. *EMBO J*. 13:2516-2525.

(304) Rehnmark, S., A. C. Bianco, J. D. Kieffer and J. E. Silva. **1992**. transcriptional and posttranscriptional mechanisms in uncoupling protein mRNA response to cold. *Am. J. Physl*. 262:E58-E67.

(305) Ricquier, D., L. Casteilla and F. Bouillaud. **1991**. Molecular studies of the uncoupling protein. *FASEB J*. 5:2237-2242.

(306) Saraste, M. and J. Castresana. **1994**. Cytochrome oxidase evolved by tinkering

with denitrification enzymes. *FEBS Lett*. 341:1-4.

(307) Castresana, J. and M. Saraste. **1995**. Evolution of energetic metabolism: the respiration-early hypothesis. *Trends Biochem. Sci*. 20:443-448.

(308) Bengston, S., ed. **1994**. Early Life on Earth. Columbia University Press, New York.

(309) Skulachev, V. P. **1994**. Bioenergetics: the evolution of molecular mechanisms and the development of bioenergetic concepts. *Anton. van Leewen*. 65:271-284.

(310) Schopf, J. W. and C. Klein, eds. **1992**. The Proterozoic Biosphere: A Multidisciplinary Approach. Cambridge University Press, New York.

(311) Koch, A. L. and T. M. Schmidt. **1991**. The first cellular bioenergetic process: primitive generation of a proton-motive force. *J. Mol. Evol*. 33:297-304.

(312) Ackrell, B. A. C., M. K. Johnson, R. P. Gunsalus and G. Cecchini. **1991**. Structure and function of succinate dehydrogenase and fumarate reductase. *In* Chemistry and Biochemistry of Flavoenzymes, vol. 3. F. Müller, ed. CRC Press, Boca Raton. pp. 229-297.

(313) Hansen, T. A. **1994**. Metabolism of sulfate-reducing prokaryotes. *Anton. van Leeuwen*. 66:165-185.

(314) Hochstein, L. I. and G. A. Tomlinson. **1988**. The enzymes associated with denitrification. *Ann. Rev. Microbiol*. 42:231-261.

(315) Kasting, J. F. **1993**. Earth's early atmosphere. *Science*. 259:920-926.

(316) Baltscheffsky, M. and H. Baltscheffsky. **1995**. Alternative photophosphorylation, inorganic pyrophosphate synthase and inorganic pyrophosphate. *Photosyn. Res*. 46:87-91.

(317) Brock, T. D., K. M. Brock, R. T. Belly and R. L. Weiss. **1972**. *Sulfolobus*: a new genus of sulfur-oxidizing bacteria living at low pH and high temperature. *Arch. Mikrobiol*. 84:54-68.

(318) Wakao, H., T. Wakagi and T. Oshima. **1987**. Purification and properties of

NADH dehydrogenase from a thermoacidophilic archaebacterium, *Sulfolobus acidocaldarius*. *J. Biochem.* 102:255-262.

(319) Moll, R. and G. Schäfer. **1991**. Purification and characterization of an archaebacterial succinate dehydrogenase complex from the plasma membrane of the thermoacidophile *Sulfolobus acidocaldarius*. *Eur. J. Biochem*. 201:593-600.

(320) Lübben, M., S. Arnaud, J. Castresana, A. Warne, S. P. J. Albracht and M. Saraste. **1994**. A second terminal oxidase in *Sulfolobus acidocaldarius*. *Eur. J. Biochem.* 224:151-159.

(321) Berry, E. A. and B. L. Trumpower. **1985**. Isolation of ubiquinol oxidase from *Paracoccus denitrificans* and resolution into the cytochrome bc_1 and cytochrome c-aa_3 complexes. *J. Biol. Chem*. 260:2458-2467.

(322) Sone, N., M. Sekimachi and E. Kutoh. **1987**. Identification and properties of a quinol oxidase super-complex composed of a bc_1 complex and cytochrome oxidase in the thermophilic bacterium PS3. *J. Biol. Chem*. 262:15386-15391.

(323) von Wachenfeldt, C. and L. Hederstedt. **1990**. *Bacillus subtilis* 13-kilodalton cytochrome *c*-550 encoded by *cccA* consists of a membrane-anchor and a heme domain. *J. Biol. Chem.* 265:13939-13948.

(324) Nomoto, T., Y. Fukumori and T. Yamanaka. **1993**. Membrane-bound cytochrome *c* is an alternative electron donor for cytochrome aa_3 in *Nitrobacter winogradskyi*. *J. Bacteriol*. 175:4400-4404.

(325) de Gier, J.-W. L., M. Lübben, W. N. M. Reijnders, C. A. Tipker, D.-J. Slotboom, R. J. M. van Spanning, A. H. Stouthamer and J. van der Oost. **1994**. The terminal oxidases of *Paracoccus denitrificans*. *Mol. Microbiol.* 13:183-196.

(326) Preisig, O., D. Anthamatten and H. Hennecke. **1993**. Genes for a microaerobically induced oxidase complex in *Bradyrhizobium japonicum* are essential for a nitrogen-fixing endosymbiosis. *Proc. Natl. Acad. Sci. USA*. 90:3309-3313.

(327) Zumft, W. G., C. Braun and H. Cuypers. **1994**. Nitric oxide reductase from

Pseudomonas stutzeri: primary structure and gene organization of a novel bacterial cytochrome *bc* complex. *Eur. J. Biochem.* 219:481-490.

(328) Jin, H., H. Thomann, C. L. Coyle and W. G. Zumft. **1989**. Copper coordination in nitrous oxide reductase from *Pseudomonas stutzeri*. *J. Am. Chem. Soc*. 111:4262-4269.

(329) Farrar, J. A., A. J. Thompson, M. R. Cheesman, D. M. Dooley and W. G. Zumft. **1991**. A model of the copper centers of nitrous oxide reductase (*Pseudomonas stutzeri*): evidence from optical, EPR and MCD spectroscopy. *FEBS Lett.* 294:11-15.

(330) Baines, B. S., J. A. M. Hubbard and R. K. Poole. **1984**. Purification and partial characterization of two cytochrome oxidases (caa_3 and *o*) from the thermophilic bacterium PS3. *Biochim. Biophys. Acta*. 766:438-445.

(331) Mather, M. W., P. Springer and J. A. Fee. **1991**. Cytochrome oxidase genes from *Thermus thermophilus*: nucleotide sequence and analysis of the deduced primary structure of subunit IIc of cytochrome caa_3. *J. Biol. Chem.* 266:5025-5035.

(332) Stouthamer, A. H. **1992**. Metabolic pathways in *Paracoccus denitrificans* and closely related bacteria in relation to the phylogeny of prokaryotes. *Anton. van Leeuwen*. 61:1-33.

(333) Ferguson, S. J. **1994**. Denitrification and its control. *Anton. van Leeuwen*. 66:89-110.

(334) Kaldorf, M., K.-H. L. von Berg, U. Meier, U. Servos and H. Bothe. **1993**. The reduction of nitrous oxide to dinitrogen by *Escherichia coli*. *Arch. Microbiol.* 160:432-439.